Dipl.-Ing. Johannes Rumetshofer, BSc

Model-based Control of
Dedicated Hybrid Drivetrains

DOCTORAL THESIS
to achieve the university degree of
Doktor der technischen Wissenschaften
submitted to

Graz University of Technology

Supervisor

Univ.-Prof. Dipl.-Ing. Dr.techn. Martin Horn

Institute of Automation and Control
Faculty of Electrical and Information Engineering

Graz, May 2019

STATUTORY DECLARATION

I declare that I have authored this thesis independently, that I have not used other than the declared sources/resources, and that I have explicitly indicated all material which has been quoted either literally or by content from the sources used.

....
               date   signature

Abstract

Dedicated hybrid drivetrains are expected to be a major mid-term competitor to zero-emission drivetrain concepts, considering the trends in automotive emission regulations. This work addresses potential for further improvement of drivability and efficiency of dedicated hybrid drivetrains with a single electric machine in gear shifting. A concept for smooth and lossless gear shifting is proposed, which resolves the trade-off between dissipation in clutches and propulsion torque interruptions. A model-based control strategy, which applies this concept in a drivetrain control system, is investigated. An exemplary implementation of this control strategy is validated in model-in-the-loop and software-in-the-loop simulations as wells as vehicle tests. In order to support usability of this model-based strategy a generic and modular modeling approach for drivetrain mechanics, applicable to all common geared drivetrains, including combined planetary gear sets, is presented. In combination with a proposed model-based drivetrain analysis method this work supports the development process of automotive drivetrains in general and dedicated hybrid drivetrains in particular.

Keywords: dedicated hybrid drivetrain, generic modeling, model-based analysis, model-based control, smooth and lossless gear shifting

Kurzfassung

Unter der Berücksichtigung der Trends der automobilen Abgasvorschriften wird erwartet, dass dedizierte Hybrid-Antriebsstränge mittelfristig ein wichtiger Konkurrent zu emissionsfreien Antriebskonzepten sein werden. Diese Arbeit befasst sich mit dem Potenzial zur weiteren Verbesserung der Fahrbarkeit und Effizienz von dedizierten Hybrid-Antriebssträngen mit einer einzigen elektrischen Maschine bei Schaltvorgängen. Es wird ein Konzept für ein ruck- und verlustfreies Schalten vorgeschlagen, das den Kompromiss zwischen der Verlustleistung in Kupplungen und den Unterbrechungen des Antriebsmoments auflöst. Eine modellbasierte Regelstrategie, die dieses Konzept in einem Steuerungssystem für Antriebsstränge anwendet, wird untersucht. Eine exemplarische Umsetzung dieser Regelstrategie wird in Model-in-the-Loop und Software-in-the-Loop Simulationen, sowie in Fahrzeugtests validiert. Um die Verwendbarkeit dieser modellbasierten Strategie zu unterstützen, wird ein generischer und modularer Modellierungsansatz für die Mechanik von Antriebssträngen vorgestellt, der für alle gängigen Getriebeantriebe, einschließlich kombinierter Planetenradsätze, anwendbar ist. In Kombination mit einer vorgeschlagenen modellbasierten Antriebsstrang-Analysemethode unterstützt diese Arbeit den Entwicklungsprozess von Fahrzeugantrieben im Allgemeinen und dedizierten Hybridantrieben im Speziellen.

Schlagwörter: Dedizierte Hybrid-Antriebsstränge, generische Modellierung, modellbasierte Analyse, modellbasierte Regelung, ruck- und verlustfreie Schaltvorgänge

Acknowledgments

It is also a special concern to me to thank Prof. Martin Horn for the scientific support and the supervision of the entire development process of this thesis. Furthermore, I would like to thank my colleagues at VIRTUAL VEHICLE Research Center and AVL List GmbH, in particular Markus Bachinger, Wolfgang Ebner, Georg Stettinger and Michael Stolz, for their technical guidance, for many technical discussions and for encouraging me to finalize this thesis.

Apart from my occupational environment I would like to show my gratitude to my parents, Maria and Konrad, for their unconditional support and to my brother, Michael, for the continuous exchange of ideas and views.

Finally, I would like to cite my colleague and PhD companion Zlatan Ajanović, who once rightly surmised in our coffee break on a working Sunday: "It must be quite hard to be in a relationship with someone, who is writing a PhD-Thesis." – Thank you, Katrin, for your endless patience and mental support during the last three years.

Graz, May 2019

Johannes Rumetshofer

Contents

1

Introduction

At the beginning of this thesis its background and motivation shall be considered. Therefore, it is necessary to make a step back from the technical scope and to take a short excursus into the area of conflict between automotive transportation and environmental sustainability controlled by emission regulations. The conclusion of this excursus will lead back to the technical scope of this thesis. An actual scientific gap is identified, which the presented research contributes to fill. Finally, a short summary of the main contributions and a general overview of the thesis are presented followed by a list of non-goals.

1.1 Background and Motivation

In the last decade the automotive industry is facing disruptive changes: The key words automation, electrification and digitalization are omnipresent and corresponding technologies are transferred from vision into daily business. Whereas in past the economic progress was maintained by advancement of established technologies and by breaking into new markets, this transformation forces many traditional Original Equipment Manufacturers (OEMs) to reinvent and reorganize their expertise and Unique Selling Propositions (USPs). This process also pushes research. The main driver of the research presented in this thesis is the electrification trend encouraged respectively compelled by emission regulations. These regulations for road transportation pressurized conventional automotive driving concepts and hence already applied significantly changes to the product portfolio of most OEMs. The regulations reflect society's raising awareness of environmental sustainability, which is nowadays more crucial than ever to avoid impending grave consequences – key word climate change. To do so, however, the current emission regulations are not sufficient. The following section lists the most important and on the long term inevitable changes for future road transportation emissions. Some of them are already in implementation, others may yet seem very ambitious or even unrealistic.

1.1.1 Vehicle emission trends

- Both Greenhouse Gas (GHG) fleet emissions, e.g. Carbon Dioxide (CO_2), and toxic vehicle emissions, e.g. Nitrogen Oxides (NO_x) and carbon monoxide (CO), have to be decreased constantly. This is already planned and announced in regulations for example in European Union (EU): 95g CO_2/km (see [1]) and Euro 6d limits (see [2]) in 2021.

- The computational basis of emissions has to be tightened in order to reflect the actual emissions. Therefore, on the one hand in addition to classical driving cycles, like for example New European Driving Cycle (NEDC) and Worldwide harmonized Light vehicles Test Procedure (WLTP), Real Driving Emissions (RDE) have to be considered, as already announced (see [1] and [2]). On the other hand this requires the abolishment of distortive privileges, for example so-called Super Credits in fleet fuel consumption computation and the unconsidered consumption of electric energy stored in batteries of Hybrid Electric Vehicles (HEVs), when applying driving cycles.

- Furthermore, new regulations are necessary:
  - local emission prohibition, for example urban access restrictions, as already valid or in discussion in several European cities,
  - GHG limits for single vehicle (China, for example, already banned production of 553 car models due to high fuel consumption in January 2018[1]),
  - and life-cycle emission and Cumulative Energy Demand (CED) considerations.

Historically, the implementation of such arrangements is considered to be a political issue to avoid competitive disadvantages for industry. This approach requires trust between politics and automotive industry, which suffered from serious damage in the last years caused by populist short-term regulations and intervention into technological aspects, e.g. diesel ban discussions, on the one side, and criminal software manipulations to meet emission limits on the other side. For sure the rebuild of this trust and hence a transparent, coordinated, predictive and predictable implementation of emission regulation limits requires huge effort from both sides. The alternative approach for automotive industry is to take on responsibility for the provision of clean technologies on their own. The risk of temporarily competitive disadvantage, may be compensated by a technological advance, if the upcoming regulations meet the expected trends.

1.1.2 Long-term winner – ZEV

Considering the summation of the above postulations and today's transportation technologies, the long-term winner of the competition of driving concepts are Zero Emission Vehicles (ZEVs), most likely Battery Electric Vehicles (BEVs) and Fuel Cell Electric Vehicles (FCEVs). However, both are still facing some problems:

---

[1]https://www.nytimes.com/2018/01/02/climate/china-cars-pollution.html

- **Battery technology:** Although, tremendous research progress in battery technology has been reached, their capacity and hence the driving range as well as the charging time is not yet competitive to conventional vehicles, which gain their energy by burning fossil fuel. A summary of the most common battery types and their evaluation is presented in [3], [4] and [5]. Furthermore, the environmental aspects of battery production and disposal affect CED consideration in a negative way.

- **Hydrogen storage:** One of the main limitations to the wide spread usage of hydrogen as energy carrier for road transportation is its mobile storage. In [6] a state-of-the-art summary to this topic is presented.

- **Infrastructure:** For both, BEV and FCEV, the existing infrastructure is not capable to supply full ZEV traffic at the moment.

- **Well-to-Wheel:** The term ZEV considers only tank-to-wheel emissions. However, especially in case of full ZEV traffic also well-to-tank emissions have to be considered, i.e. including the entire energy supply chain.

The fact that the above list contains non-technological issues (infrastructure and well-to-wheel), complicates a prediction when the final breakthrough of ZEVs will occur. This brings the back traditional ICE into business.

1.1.3 The main competitor of ZEVs

Although the ICE is not competitive implemented in conventional drivetrains from emission point of view, it turns out to be a good complementation to the Electrical Machine (EM) in order to overcome the present weak points of ZEVs. This fusion of ICE and EM into one single drivetrain is called hybridization, which is the special case of electrification, not aiming the total removal of the ICE. The emission trends considered in Section 1.1.1 challenges also the development of hybrid vehicle concepts. Urban access restrictions, for example, are the category killer of micro and mild HEVs. The most serious mid-term competitor to ZEV is a full hybrid DT with optimized synergy between ICE and EM: the so-called dedicated hybrid DT, featuring a Dedicated Hybrid Transmission (DHT). This category of complex drivetrains (for details see Section 2.2.3) tries to optimally fuse the benefits and compensate the drawbacks of ICE and EM in every driving situation, by application of diverse hybrid modes. Consequently, a high level of efficiency and drivability is reached. In dedicated hybrid DTs one or more EMs operate functional transmission tasks. Therefore, the removal of the EMs results in a transmission without (full) functionality and hence drivability. The term DHT was first officially introduced in 2015 at the CTI Symposium[2] in Berlin (see [7]), as a new category of transmission. Within the next years the concept and various applications have been proposed and discussed in several special conference sessions. The necessary development effort of dedicated hybrid DTs requires production units, which are not meet yet by most OEMs, to ensure economy. However, due to their huge

---

[2]The CTI Symposia World Series (`http://drivetrain-symposium.world`) is an annual series of three conferences in Novi/Michigan, Shanghai and Berlin/Germany assembling the world's leading experts on the development and production automotive drivetrains.

potential in fuel efficiency, experts expect dedicated hybrid DTs to hit the market from 2020[3] (see [8]). Considering today's technologies, the dedicated hybrid DT is going to be the last remaining competitor to ZEVs. This expected success resurrects the ICE although its nature will change significantly, featuring reduced dynamics, components, size and weight.

1.2 Gap

Although the general concept for the future hybrid DT is well defined, its detailed implementation offers a huge range of possibilities and is an ongoing research topic. The development process of dedicated hybrid DTs in general includes three consecutive and interacting stages (cf. [9]): The first stage is the synthesis of the DT topology, including the arrangement and sizing of the components. This stage can also be referred to as the hardware development stage. In contrast to this stage the next two stages concern the software development: The second stage is the Energy Management Strategy (EMS) development, which defines the operation strategy of the hybrid DT. Thirdly, a DT control system has to be developed, which is responsible for application of the operation strategy. All these three stages are facing the high complexity of dedicated hybrid DTs and impact to the resulting overall drivability and efficiency (see Figure 1.1). Consequently, an optimized DT has to provide optimal solutions in each stage. The order of these three stages furthermore reflects the size of the single impacts on drivability and efficiency. Therefore, a poor DT topology design, caused for example by a wrong component sizing (power of ICE and EM) or matching of ICE and transmission, can not be compensated by applying an excellent EMS and DT control. Furthermore, the best DT control concept is not able to compensate a weak EMS.
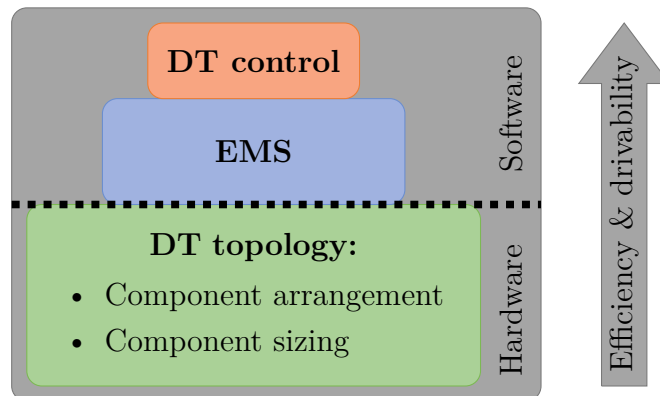
Figure 1.1: *Three main stages of dedicated hybrid DT development*

Although extensive research has been done on the synthesis of different topologies, see for example [10, 11, 12], and on EMS development, see for example [13, 14], so far no

---

[3]`www.iav.com/us/automotion-magazine/automotion-2017-issue-01/`
`dedicated-hybrid-transmission-plug-vehicles`

proved superior dedicated hybrid DT topology has been developed. In fact, even the number of EMs in an optimized topology is still under discussion.

Therefore, at the moment many promising special solutions are developed and produced with each high development cost. An investigation of the EMS and DT control development stage separated from the topology design would contribute to the reduction of this cost and hence further strengthen the position of dedicated hybrid DTs in the competition of DT concepts. However, this requires a general and generic consideration of these two stages, which is a big challenge due to the complexity and diversity of dedicated hybrid DTs.

1.3 Contribution

Contributing to this overall target, this thesis proposes a generic model-based control approach for single-EM dedicated hybrid DTs focusing on drivability and fuel efficiency. In particular the contribution is:

- the general concept of smooth and lossless gear shifting in single-EM dedicated hybrid DTs to reduce fuel efficiency and improve drivability,
- a generic and modular modeling approach for geared DTs,
- a model-based DT analysis method including the potential for smooth and lossless gear shifting for single-EM dedicated hybrid DTs,
- and the integration of the concept of smooth and lossless gear shifting for single-EM dedicated hybrid DTs into a model-based DT control system.

Although these single contributions focus on the DT control stage, they support the whole development process of dedicated hybrid DTs, as illustrated in Figure 1.2. For example, accurate DT models can be used for simulation centered testing and driving cycle simulations. In combination with a model-based analysis this enables a fast evaluation of topologies and hence the opportunity for optimization in an early development stage.
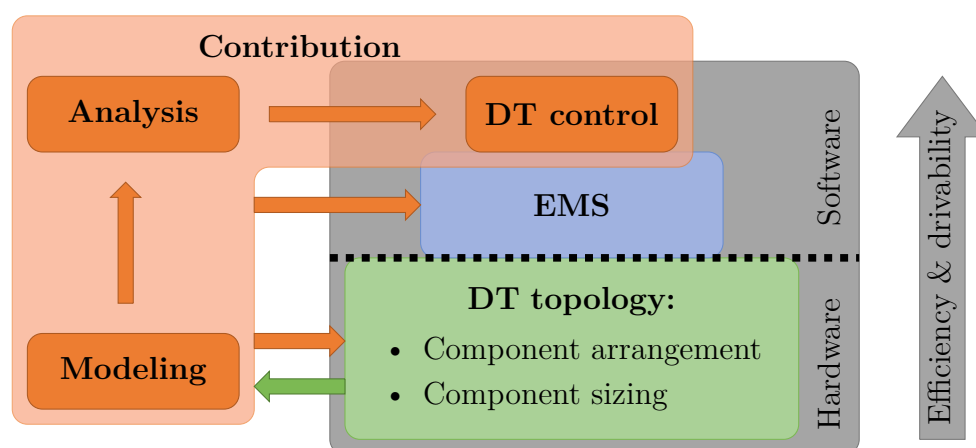
Figure 1.2: *Thesis contribution to the development process of single-EM dedicated hybrid DTs*

An additional focus of this thesis is on reusability, which shall enable the application of the modeling approach and the analysis method in general automotive DT development.

1.4 Overview

After stating the motivation and contribution of the thesis this section shall give a rough overview of its content.

Chapter 2 assembles important general definitions about conventional and hybrid DTs including terminology, classifications and components and their functionality. Based on these preliminary definitions the object of research in this thesis – the single-EM dedicated hybrid DT – is presented. Subsequently, the focus is moved to DT control starting again with the conventional drivetrain and ending up with the control tasks and requirements for single-EM dedicated hybrid DTs. Furthermore, the general concept of smooth and lossless gear shifts is introduced, which plays an essential role throughout this thesis. At the end of this chapter the general problem statement to this thesis is given and its contribution is specified in more detail.

In Chapter 3 a generic and modular modeling approach is presented, which forms the basis to the model-based methods presented in the next chapters. The modeling approach is applied to an exemplary single-EM dedicated hybrid DTs. A switched LTI model with reasonable control outputs is proposed for the later control of dedicated hybrid DTs in general and the control of smooth and lossless gear shifts in particular.

Based on the generic DT model investigated in Chapter 3, Chapter 4 states the opportunities to automate computation of drivetrain characteristics and design evaluation criteria with respect to drivability and shiftability. Finally, decoupling theory is used to state a mathematical condition to evaluate a DT's potential for smooth and lossless gear shifting. The approach is applied to the exemplary DT, which has already been considered in Chapter 3.

Chapter 5 combines the outcomes of Chapter 3 and Chapter 4 and proposes a model-based control concept for single-EM dedicated hybrid DTs focusing on the control of smooth and lossless gear shifts. An exemplary implementation of this concept is applied to an exemplary single-EM dedicated hybrid DT. The implementation consists of a feedforward control, which is extended to an Internal Model Control (IMC) structure with polynomial trajectory generation. Finally, the chapter considers the discretization of the presented control concept.

Chapter 6 concludes the technical part of this thesis. The exemplary implementation, and hence the control concept, is validated on different levels of a classical software-to-vehicle process, including MiL simulations, SiL simulations and vehicle testing in a demonstrator car.

1.5 Non-Goals

To conclude this introduction furthermore the non-goals of this thesis shall be stated:

- The modeling, analysis and control approaches presented in this thesis focuses on the DT and not the entire powertrain (PT). Therefore, the generation of torque in ICE and EM is not considered (cf. Section 2.1).
- This thesis concerns fundamental research, although usability is considered and also practical implementations and integrations are presented. Consequently, it does not target the development of a Start of Production (SOP)-control software.
- The thesis focuses on the DT control system development stage (cf. Figure 1.2) of dedicated hybrid DTs. It does not consider the hardware synthesis and the development of an EMS.

2

Object of Research

This preliminary chapter specifies the basic terminology and the technical background of this thesis. First, the general functionality and components of conventional automotive DTs are considered (Section 2.1). Subsequently, these considerations are extended to hybrid DTs, with respect to two common classifications (Section 2.2). This context is used to introduce the actual object of research in this thesis – the single-EM dedicated hybrid DT. A comprehensive overview on its operation modes is presented in Section 2.3. The last part of this chapter considers a general, torque-based, control structure of conventional PTs and its adaption for single-EM dedicated hybrid PTs (Section 2.4 and Section 2.5). A special approach of gear shifting in single-EM dedicated hybrid DTs – so-called smooth and lossless shifting – is introduced. The model-based control of these shifts is one of the main contribution of this thesis. Furthermore, the DT control tasks are summarized in a general way. The chapter concludes with the general problem statement, which motivates the research presented in this thesis, and a specification of the thesis contributions.

2.1 The conventional drivetrain

In general, the term DT, or synonymously driveline, means the aggregation of all components in a vehicle, which transfer propulsion from a power source for torque generation to the driving wheels. While in some literature, e.g. in [15], the power source is considered a component of the DT, others, like in [16, p. 193] and [17, p. 373], explicitly exclude the power source from the DT. For the combination of power source and DT the term PT is used. This thesis follows the second definition. Therefore, it does *not* cover the detailed modeling of power sources as well as their control.

In conventional DTs the power source is assumed to be an ICE supplied with fossil fuel. It is coupled to the transmission by a coupling element, i.e. a clutch or a hydrodynamic torque converter, see for example [18, pp. 148]. The modeling and control of a torque converter is investigated for example in [19] and will not be considered in this thesis. The general task of the coupling element is to handle the torque transfer at high differential rotational speeds when launching the vehicle and to optionally disconnect
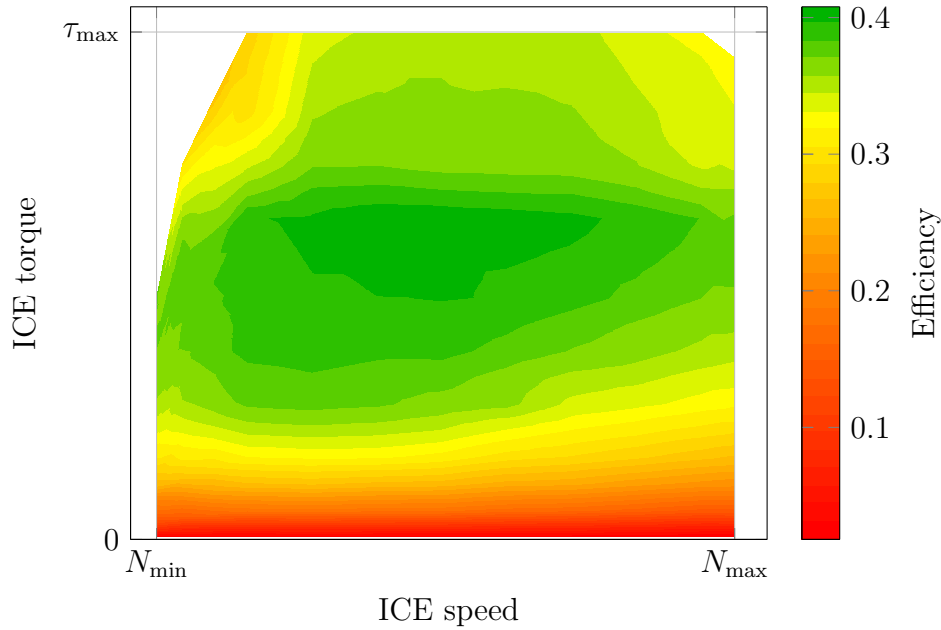
Figure 2.1: *Exemplary ICE characteristic (Turbocharged Gasoline Direct Injection)*

the ICE from the DT.

The core of a DT is the transmission. Its task is to adapt rotational speeds and torques of the power source to enable on the one hand sufficient acceleration of the vehicle and on the other hand an efficient operation of the ICE and hence decreasing fuel consumption and emissions in all driving situations. These two aspects – so-called drivability and efficiency – represent the central requirements to the operation of a DT and hence will be of essential importance throughout this thesis. In order to reach an acceptable level of both drivability and efficiency an optimized matching of the ICE and the transmissions is essential, see [18, pp. 1-47]. To do so, the transmission consists of several different gear ratios, which can temporarily connect its input and output. These gear ratios transform the ICE torque and speed to a reasonable level at the wheels. Consequently, they are matched on the ICE characteristics and the required vehicle dynamics. These dynamics are defined considering for example gradability and maximum vehicle speed of the vehicle (see [18, pp. 39]). Figure 2.1 shows the available torque levels and the corresponding efficiencies of an exemplary ICE depending on the rotational speed. Figure 2.2 shows the resulting traction forces at the wheels in combination with an exemplary transmission featuring five different gear ratios.

Gear shifting is the general process of switching from one gear ratio to another gear ratio. To do so either gear wheels and shafts are displaced mechanically by a gear lever or additional rigid connections are locked or released by engaging or disengaging clutches. These clutches are actuated electro-hydraulically, employing an electrical or mechanical pump and electro-magnetic valves, which control the pressure of a transmission fluid. This hydraulic pressure is used to displace the clutch plates. The transmission fluid is simultaneously used for lubrication and cooling. For details to the actuation of electro-hydraulic systems of a vehicle see [20]. Although gear shifting
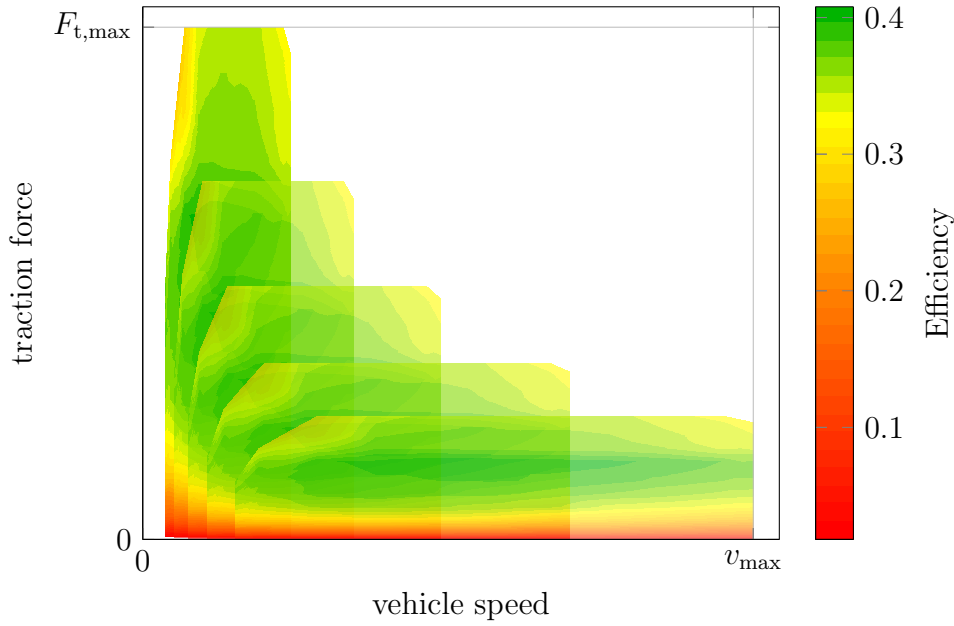
Figure 2.2: *Traction force resulting of a combination of the exemplary ICE (see 2.1) and an exemplary transmission with five gear ratios*

is necessary to ensure overall drivability and efficiency in conventional DTs it temporarily affects both requirements, depending on the different mechanical concepts of transmissions and their grade of automation: In Manual Transmissions (MTs) the driver decouples the ICE from the DT using a pedal for gear shifting, resulting in both propulsion torque interruption and friction losses in the clutch. In Automated Manual Transmissions (AMTs), the clutch actuation is automated, which generally improves both drivability and efficiency. In Dual Clutch Transmissions (DCTs) and Automatic Transmissions (ATs) torque interruption is avoided by temporarily operating two gear ratios at the same time using two slipping clutches. While DCTs consist of different spur gear sets mounted on two shafts, ATs use planetary gear sets. Whereas DCTs feature a higher overall efficiency, ATs feature a more compact design. For more details according different types of automotive transmissions see for example [18, pp. 229-272]. The driveshaft connects the output of the transmission – the final drive – to the differential, in the center of the driving axle. The implementation of the driveshaft differs depending on the placing and size of the transmission and the ICE. The task of the differential is the torque distribution to the wheels and the compensation of different wheel speeds in cornering. The axle shafts connect the differential and the driving wheels. Finally, the driving wheels convert the rotational motion of the axle shafts into a translatory motion of the vehicle using traction. Figure 2.3 shows the position of all the mentioned DT components in a conventional PT.
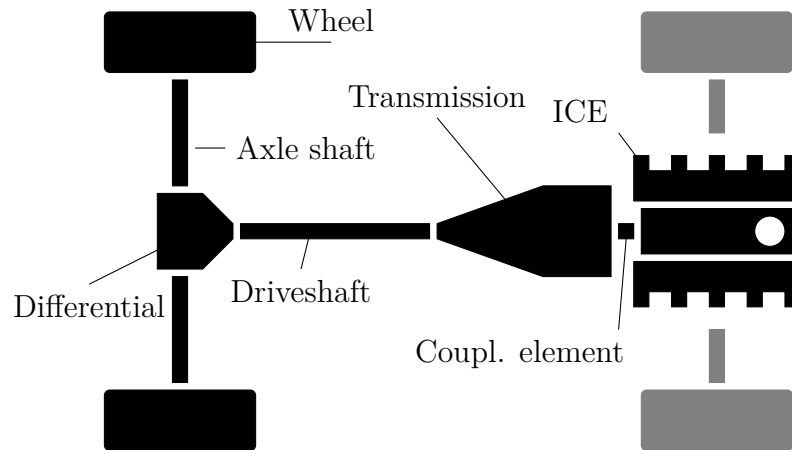
Figure 2.3: *Components of a conventional PT*

2.2 The hybrid drivetrains

In hybrid DTs the energy of two different power sources from different physical domains is converted into mechanical power to drive the vehicle. In addition to the ICE the most common converting devices are EMs, fuel cells, flywheels, hydraulic motors and pneumatic motors. This work considers the combination of ICE and EM. Therefore, the term hybrid means hybrid-electric. For automotive application asynchronous and permanently excited synchronous machines are the most used EMs ([18, p. 265]). They are powered by electrical energy stored in batteries. For details on battery technologies see [3], [4] and [5]. As already discussed in Chapter 1 the basic intention of hybridization is to decrease emissions. In hybrid DTs this is achieved by using several effects:

Opportunities of hybridization to decrease emissions:

- The EM can support the engine start.
- The electrical energy gained from the grid may be used to support vehicle propulsion in plug-in hybrid DTs. This enables downsizing of the ICE and hence decreased emissions.
- Since it is possible to operate one single EM as motor and generator, the braking energy can be partially reused – so-called recuperation or regenerative braking – which improves the overall efficiency.
- The EM may increase ICE efficiency by shifting its operation point, similar to gear shifting.
- Especially in low speed and stop-and-go scenarios, e.g. in city driving, the ICE suffers from low efficiency. The EM can drive the vehicle in such scenarios.

Beside these effects on efficiency the hybridization furthermore effects drivability in a positive way:

Opportunities of hybridization to improve drivability:

- An EM features a high initial torque, i.e. torque at zero and low rotational speeds. This enables fast vehicle launching without heat losses in coupling elements.
- The fast torque build-up of an EM offers high accelerations by electrical boosting, which is of special interest for example in overtaking scenarios.

The various possibilities to apply hybridization results in extensive and sometimes also ambiguous nomenclature, for different hybrid DTs. The following sections try to clarify this nomenclature by considering the two most common classifications of hybrid DTs according to the degree of hybridization and the hybrid topology.

2.2.1 Classification I – degree of hybridization

The degree of hybridization (see [17, p. 48]) considers the ratio between maximum available power of the ICE and the EM. The increase of the EM power enables all the opportunities for enhanced efficiency step by step. The lowest possible degree of hybridization is applied in so-called micro hybrid DTs: A small EM implements an automated start-stop system for the ICE. Although indicated by its name, a micro hybrid DT actually is no hybrid DTs in the narrow sense, since the electrical energy is not used for propulsion. In contrast mild hybrid DTs feature an EM of increased size in order to offer additionally recuperation and modest power support for propulsion. If the power of the EM is high enough to drive the vehicle fully electrically in some driving situations, the DT is classified as a full hybrid. If a full hybrid DT offers the possibility to charge the battery directly from the electricity grid, it is considered as plug-in hybrid. The highest possible degree of hybridization is achieved by full electrification of the DT. However, since full electric DTs do not use a ICE for propulsion, they are no hybrid DTs in the narrow sense, similar to the micro hybrid DT on the other side of the scale. Figure 2.4 illustrates the classification based on the degree of hybridization.

2.2.2 Classification II – hybrid topology

The second classification considers the hybrid topology, i.e. the arrangement of the components in a hybrid DT, which defines the power flow (cf. [18, pp. 285-288], [17, p. 49] and [21]).

Series hybrid drivetrains

In series hybrid DTs the ICE powers a first EM, which is operated exclusively in generator mode and charges a battery. A second EM sources the power from the battery for vehicle propulsion. Series hybrid DTs are sometimes also referred to as
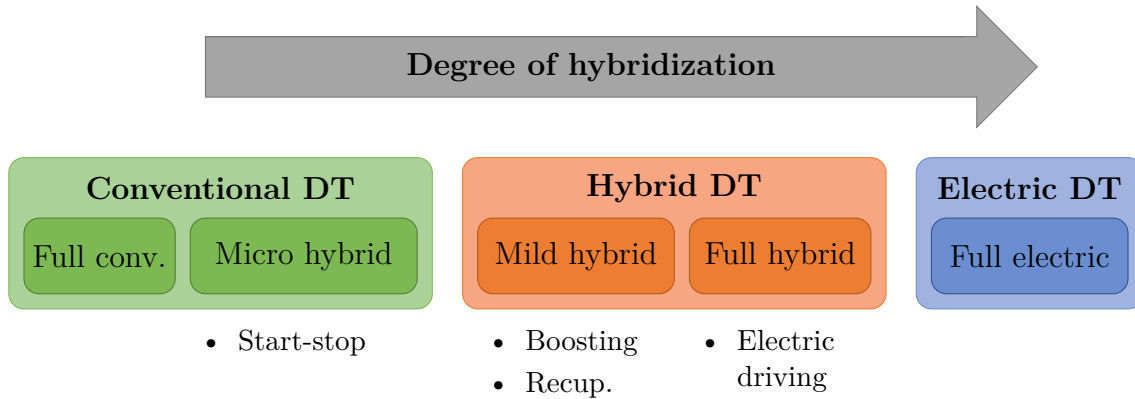
Figure 2.4: *Classification of hybrid DTs according their degree of hybridization*

range extended electric DT. On the one hand, this ambiguous term utilizes common association of electric DT with the absence of ICE for image and marketing reasons. On the other hand, it emphasizes that the used ICE differs from classical ICEs, which are primarily used for propulsion: In series hybrid DTs the ICE operates at a specific speed and load torque level for optimal combustion efficiency – the so-called sweet spot. According the first classification, based on the degree of hybridization, the series hybrid DT is a full hybrid DT, in which the EM permanently drives the vehicle. This indicates one major drawback of this architecture: The ICE and both EM are converting the whole propulsion power. This results in a high overall weight and low overall efficiency compared to other hybrid DTs, due to the losses in every energy conversion (fossil to mechanical, mechanical to electric, electric to mechanical).

Parallel hybrid drivetrains

In parallel hybrid DTs the final propulsion power is the sum of the powers provided by ICE and EM. This architecture results, if an EM is connected to a conventional DT at any position. The major benefit of the power summation is that it enables downsizing and down-speeding of the ICE, see [18, p. 273], in order to decrease emissions. If this benefit is not utilized by adapting the original conventional DT and the ICE, the hybridization is called add-on solution. On the one hand, such add-on solutions do not require extensive development cost, but on the other hand, the production cost is inevitably higher than the one of the original conventional DT, which challenges the long-term economy of such solutions.

According to the position of the EM in the DT the configuration codes P0-P4 are common practice (see for example [22]). The code P0 hybrid is synonymously used for an automated start-stop system, i.e. micro hybrid. In P1 architecture the EM is connected to the ICE's crank shaft and in P2 to the transmission input. P1 and P2 hybrid DTs are usually implemented as mild hybrid DTs. In P3 architecture the EM is connected to the transmission output and P4 at driving axle. P3 and P4 hybrid DTs are implemented as both mild and full hybrid DTs. In parallel mild hybrid DTs the EM is used for recuperation and boosting. Parallel full hybrid DTs usually use the EM additionally for vehicle launching and for electric driving at low vehicle speeds,

e.g. in stop-and-go city driving.

A special parallel hybrid topology is the split-parallel hybrid DT, also known as e-axle, through-the-road hybrid or split axle DT. In such a hybrid topology the ICE power is provided at one drive axle, and the EM is attached to the second drive axle. This results in a four-wheel-drive. In [23] the configuration code P4 is used for this parallel topology.

Power split drivetrains

Generally, the term power split concerns the presence of a mechanical splitting device: a planetary gear set. In contrast to the possible power split in parallel hybrid DTs, splitting with a planetary gear set features two mechanical degrees of freedom (DoFs). For sake of consistency the possible power split in parallel hybrid DTs is considered a 1-DoF power split (see [12]). The second mechanical DoF can be used to operate the ICE at a specific speed level independently of the current vehicle speed. Similar to the series hybrid architecture this enables increased ICE efficiency. In accordance with the belt driven Continuous Variable Transmission (CVT) this operation is referred as Electric Variable Transmission (EVT), or Electric Continuously Variable Transmission (ECVT). There are two possibilities to implement a power split device into a functional drivetrain topology: The first, rarely used, is a plug-in variant featuring the ICE and one EM. The second one is an optional plug-in variant with an additional, second EM. In this implementation the power provided by the ICE is split into a mechanical and an electrical path. Via power summation both paths contribute to vehicle propulsion (see [18, p. 273]). Since this implementation is actually a combination of series and parallel topology it is called series-parallel hybrid DT. Series-parallel DTs are already sold quite successfully: Since more then 20 years one OEM is dominating hybrid vehicle market with suchlike hybrid topologies[1]. According the position of the power split device(s), the dual-EM power split hybrid topology is further subdivided into input-split, output-split and compound split (see [9] and [24]).

Multi-mode drivetrains

The development of multi-mode DTs targets on the combination of the above topologies' advantages, in order to optimize synergy between ICE and EM. Rigid connections are locked and released by the engagement and disengagement of clutches, similar to ATs in conventional DTs. Depending on the engagement of clutches different hybrid topologies, which are referred as operation modes, can be applied according the driving situation and the battery's State-of-Charge (SoC). In addition to the modes presented as hybrid topologies in the above sections, some implementations feature additionally a mode for purely conventional driving for high but constant vehicle velocities (see for example [18, p. 274]) and a mode for purely electric driving. Exemplary multi-mode DTs are presented in [25] (series and parallel) and [26] (series and power split).

---

[1]`http://media.toyota.co.uk/2013/08/toyotas-hybrid-success-story/`

2.2.3 The dedicated hybrid drivetrain

Since several years a specific class of hybrid DTs gathered huge interest (cf. Section 1.1.3): the dedicated hybrid DT, featuring a DHT. Per definition the EM(s) operate functional transmission tasks in a DHT. To emphasize the central role of the EM(s), also the terms motor-integrated hybrid transmission (see [27]) and active transmissions (see [28]) are used. Hence, the DT loses its drivability if the EM(s) are removed. Consequently, the dedicated hybrid DT can be considered as a counterpart to add-on solutions (see Section 2.2.2). Although this nonspecific definition would also assign series hybrid DT as dedicated hybrid DT, they are implemented either in 2-DoF power split topology with two EMs, or in multi-mode topology with one or two EM. The classification dedicated hybrid considers both topologies, with the focus on an optimized synergy between the ICE and the EM(s).

While the potential and future role of this DT concept seems to be clarified (cf. Section 1.1.3), the implementation details are still investigated and optimized, for example according to the number of EMs with respect to efficiency and economy. In [10, 11, 12, 27, 29, 30] different dedicated hybrid DTs with one or two EMs are proposed.
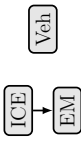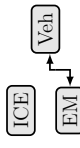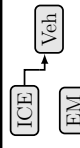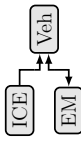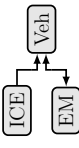
Summary of the properties of a dedicated hybrid DT:

- No add-on hybridization
- EM operates functional transmission tasks
- Focused on optimized synergy between ICE and EMs for high level of drivability and efficiency
- Two possible topological implementations:
  - dual-EM 2-DoF power split hybrid DT
  - single-EM or dual-EM multi-mode hybrid DT

2.3 Operation modes of a single-EM dedicated hybrid drivetrain

This thesis focuses on single-EM dedicated hybrid DTs. According to the last section this implies a multi-mode hybrid topology. The motivation to develop single-EM dedicated hybrid DTs is to save cost, weight, size and losses of a second EM and its power electronics (see [29]). A restriction to single-EM concepts excludes a series and series-parallel hybrid operation mode, since the EM can not operate as motor and generator at the same time. Further drawbacks are possible performance limitations and a more challenging power flow management, i.e. selection of operation mode, compared to dual-EM 2-DoF power split topologies. Similar to ATs in single-EM dedicated hybrid DTs planetary gear sets are used to implement diverse gear ratios and combinations of the ICE and EM powers in a compact design. This results in several different operation modes according to the classification presented in Section 2.2.2. Table 2.1 specifies all possible operation modes in single-EM dedicated hybrid DTs. The following list of remarks summarizes the statements of Table 2.1 and gives important interpretation

Table 2.1: *Operation modes of a single-EM dedicate hybrid DT. The torque split factor μ is defined in equation 2.2. To abbreviate notation, the index letters E for engine (ICE) and M for motor (EM) are introduced. P_P denotes the propulsion power.*

mode	power flow	DoF	P_P	P_E	P_M	λ	submode	
neutral	0	v, ω_E, ω_M	0	0	0	ω_E, ω_M		0
charge	0	$\omega_E, (v)$	0	>0	$-P_E$	ω_E, τ_E		1
electric	P_M	$v, (\omega_E)$	>0	0	P_P	(ω_E)	electric drive	2.1
			<0				recuperation	2.2
conv.	P_E	$v, (\omega_M)$	>0	P_P	0	(ω_M)		3
hybrid (parallel)	$P_E + P_M$	v	>0	$<P_P$	$P_P - P_E$	$0 < \mu < 1$	compound drive	4.1
			>0	$>P_P$	$P_P - P_E$	$\mu > 1$	conv. drive + charge	4.2
			>0	P_P	0	$\mu = 1$	conv. drive + EM idle	4.3
			>0	0	P_P	$\mu = 0$	electric drive + ICE idle	4.4
			<0	0	P_P	$\mu = 0$	recuperation +ICE idle	4.5
			<0	P_E	$P_P - P_E$	$\mu < 0$	recuperation + charge	4.6
hybrid (CVT)	$P_E + P_M$	v, ω_E	>0	P_E	$P_P - P_E$	ω_E	generator/motor	5

details:

- According to the two power sources (ICE and EM), a single-EM dedicated hybrid DT features five different modes: neutral (0), charge (1), electric (2), conventional (3) and hybrid. According to the different hybrid topologies the hybrid mode is separated into hybrid-parallel mode (4) and hybrid-CVT (5) mode.

- The modes decompose into non-drivable (0 and 1) and drivable modes $(2-5)$.

- Each hybrid mode features a hybrid DoF λ. A hybrid DoF is a physical parameter, which can be controlled to arbitrary values between specific limits (see equation 2.1) without affecting the propulsion power requested by the driver.

$$\omega_{E,min} \leqslant \omega_E \leqslant \omega_{E,max}$$
$$\tau_E = f(\omega_E) \leqslant \tau_{E,max} \qquad\qquad (2.1)$$
$$|\omega_M| \leqslant \omega_{M,max}$$

The hybrid DoFs can be either actual mechanical DoFs (rotational speeds ω), torques (τ) or a so-called torque split factor μ, which is related to the ratio between the ICE and EM power in parallel hybrid mode:

$$\mu := \frac{P_E}{P_E + P_M} \qquad\qquad (2.2)$$

In some literature, e.g. [31], this factor is defined differently: $\mu = \frac{P_M}{P_E + P_M}$. According to the fixed speeds of the ICE and the EM with respect to the vehicle speed, the term power-split factor is used synonymously (c.f. Section 2.2.2).

- The number of mechanical DoFs is not unique for modes $1-3$, since additionally some shafts can be blocked without influencing the principle mode functionality. This reduction of mechanical DoFs, however, possibly fixes the mode's hybrid DoFs.

- Modes 2 and 4 are divided into submodes. The electric mode splits into the submodes electric drive (2.1) and recuperation (2.2), according to the sign of the requested propulsion power P_P. In hybrid-parallel mode (4) a further division into submodes is applied according to the value of the hybrid DoF μ.

- Except for mode 1, transitions between submodes of one mode, do not require a gear shift, i.e. any clutch engagement or disengagement. These transitions are initiated either by a change of the driving situation (sign of P_P) or the control of the hybrid DoF.

- The submodes $4.3-4.5$ of parallel hybrid mode, offer similar functionality as the submodes of electric mode 2.1 and 2.2, and conventional mode 3. The efficiency in submode 2.1 is higher than the one of 4.4 due to the drag losses of the ICE. However, submode 4.4 enables transition into all submodes of parallel mode without gear shifting. The same consideration applies for conventional mode 3 and submode 4.3 due to the drag losses of the EM.

- The implementation of a reverse gear is possible in modes $2-5$. In most configurations, however, reverse driving is covered in electrical mode 2, since the EM

can be operated at reverse speed without any implementation of an additional negative gear ratio, which would be necessary for reverse driving in modes $3 - 5$.

- In hybrid-CVT mode (5) the required propulsion power P_P, the vehicle speed and the ICE speed (hybrid DoF) define whether the EM operates in generator or motor mode.

- The list of modes in Table 2.1 does not consider EM-supported ICE-start as well as breaking scenarios involving either a mechanical break or ICE break. Furthermore, expect for mode 1, no modes with blocked transmission output shafts, used for example for parking, are considered.

The basic differentiation between the modes of hybrid DTs, like presented above, is well established, although many different notations are used (see for example [29], [10], [11] and [12]). The classical single-EM dedicated hybrid DT features, multiple implementations of different modes with different ratios. In order to avoid ambiguity of the term mode, within this thesis the term gear is used for the actual mechanical implementation of a mode with certain gear ratios. The term mode specifies the basic hybrid topology of a gear. This nomenclature emphasizes that a conventional DT featuring several gears of the same, conventional, mode is not a multi-mode DT. Each gear is uniquely identified by the state of engagement of the clutches. This binary information per clutch can be assembled in a vector $\boldsymbol{\kappa}$, the so-called clutch state vector. The length of this vector is equivalent the number of clutches. Given a number of n_c clutches, hence, the maximum number of gears is 2^{n_c}. The closer the number of actual gears provided by a specific DT topology comes to this limit the more compact is the resulting design, which correlates with its production cost. This is a general challenge in the hardware design synthesis (arrangement and sizing of DT components and its optimization), which is a key stage in the development of dedicated hybrid DTs, as already indicated in Section 1.2. However, more important than the actual number of gears is, if the provided gears can cover all driving situation in order to provide sufficient overall drivability and efficiency. Due to the huge range of possibilities spanned by the selection, arrangement and dimensioning of components this is a nontrivial problem and hence an on-going research topic, investigated for example in [10], [11] and [12]). So far no specific single-EM dedicated hybrid DT design turned out to be superior. This fact is the main motivation to investigate the control of single-EM dedicated hybrid DTs in a modular and general way, instead of developing special control systems solution for special designs.

2.4 Control of conventional powertrains

Based on the basic explanations in the last sections the next two sections focus on the control aspects of automotive DTs in general and of single-EM dedicated hybrid DTs in particular.

The DT control system controls the action and interaction of all DT components and it is part of the superordinate PT control system. The overall task of the PT control system is to control a specific wheel torque or traction force to provide the vehicle propulsion required by the driver via the accelerator and breaking pedals. While this

task historically has been handled directly by the driver, increasing permeation of technology transferred this task step by step from the driver to an electrical control unit. The control system of conventional PTs typically includes an interpretation of the driver inputs, the DT control and the control of the ICE handled by the Engine Control Unit (ECU). Figure 2.5 shows a simplified, torque-based PT control structure as presented in [17, p. 53].
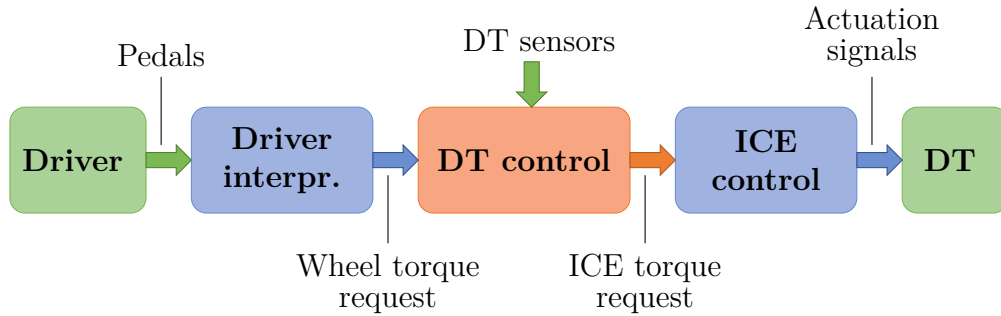
Figure 2.5: *Simple torque-based PT control structure*

The separation into several systems ensures modularity, required by the diversity of DTs, with respect to different types and sizes of ICEs and transmissions for different vehicle classes. The overall performance is defined by the performances of the single systems and their coordination. Figure 2.5 illustrates the central task of DT control: computation of an engine torque request to control a specific wheel torque according to the current gear. The complexity of DT control systems is defined by the complexity of the considered DT model and ranges from simple linear relations or look-up-tables to high order nonlinear dynamical systems.

With the automation of gear shifts (in AMTs, DCTs and ATs) the PT control system takes responsibility of both drivability and efficiency. The process of choosing a gear in the current driving situation (vehicle velocity and pedal positions) – the gear selection – is not handle directly by the driver anymore. Depending on the PT control structure the gear selection is either part of the DT control system itself or of the driver interpretation. Another common term for the gear selection is shift strategy and it is usually implemented as a simple evaluation of static look-up tables (see for example [18, pp. 213]). The automation of gear shifting extends the tasks for DT control by the actuation of clutches. To do so specific clutch torques request have to be computed in order to engage the requested gear. According to these torque request the clutch control system applies electric currents to the coils of hydraulic valves. The interpretation of the trade-off between dissipation in clutches (efficiency) and torque interruptions (drivability) in different types of transmissions during a gear shift has already be mentioned in Section 2.1. Actually, the design and calibration of the DT control system defines this interpretation. In some control topologies the actuation of clutches is delegated to a special Transmission Control Unit (TCU). Since avoidance of torque interruptions, torque ripples and resulting DT oscillation is an important issue during the control of gear shifts, it is indeed reasonable to embed the control of gear sifting into the DT control system.

To reach acceptable control performance beside the reference input signals, several sensor signals are available. These are provided either by physical rotational speed sensors, see [18, p. 195], or by various virtual sensors computed in DT models and observers like presented in [15].

2.5 Control of dedicated hybrid powertrains

Considering hybrid PTs, several additional control systems extend the conventional PT control system, while the basic structure is unchanged. The Motor Control Unit (MCU) controls the operation of the EM. The battery, which powers the EM, is controlled by a Battery Management System (BMS), operating basically two tasks: control of the battery's SoC and of its temperature, cf. [18, p. 269]. The biggest adaption is probably the need for an EMS. The EMS is the generalization of the gear selection system (shift strategy). Hence, similar to the shift strategy the EMS is the key component to exploit the DT's potential for drivability and efficiency. In dedicated hybrid PTs the EMS handles two tasks subject to the current driving situation, the efficiency maps of ICE and EM and battery's state (SoC and temperature):

EMS tasks

- Selection of a gear (gear request) with respect to its mode and ratio as well as the current driving situation
- Computation of reference values of the gear's hybrid DoF

Due to the mechanical complexity of multi-mode DTs in general and dedicated hybrid DTs in particular the complexity of the necessary EMS is considerable: The EMS has to provide a solution to a multi-objective optimization problem. This problem is an ongoing research topic and is not considered in this thesis. In general, the development of EMSs is based on a specific hybrid topology and drive cycles (see [32] and [14]). In [24], [13] and [33] an overview of different optimal, suboptimal, off-line and on-line EMS approaches is given. Several publications, e.g. [29], [17, p. 59], consider the control of the DT to be part of the EMS. Hence, the output signals of the EMS are torque requests, which are handed over directly to the ECU and MCU.

In order to provide a generic approach to the DT control, this thesis proposes a clear separation of EMS and DT control as already indicated in the three stages of dedicated hybrid DT development in Section 1.2. It is reasonable to use the requested gear and reference value of the hybrid DoF as generalized interface between these two components. Based on this separation, Figure 2.6 shows a simplified, torque-based PT control structure for dedicated hybrid DTs, which extends the conventional system in Figure 2.5. According to this separation and the EMS tasks, the central DTs control tasks can be stated in a general form:
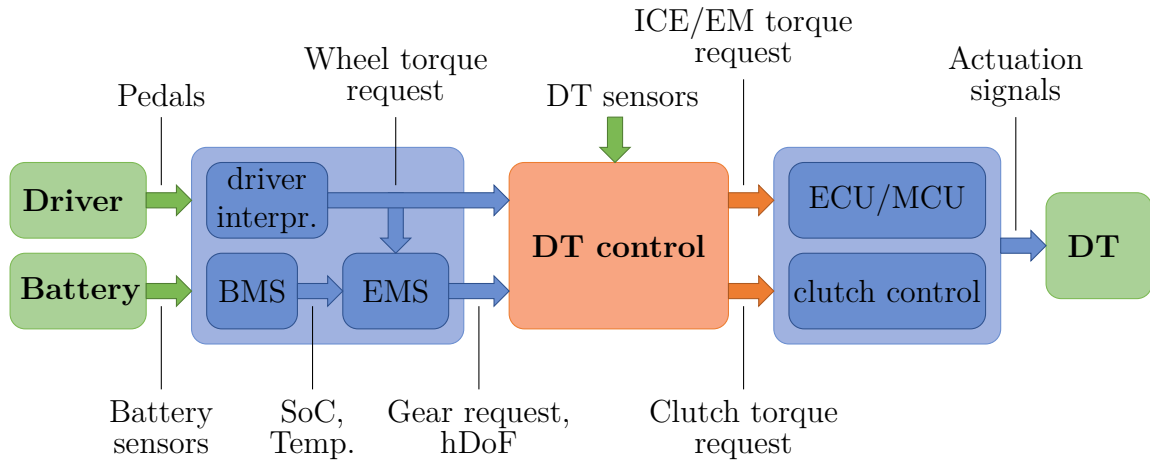
Figure 2.6: *Simplified, torque-based PT control structure for dedicated hybrid DTs*

DT control tasks

- **Mode operation:** driving in a specific gear (control of wheel torque and hybrid DoF)
- **Mode transition:** gear shifting (control of wheel torque and clutch torques)

The general requirements to these control tasks are equivalent to the overall performance indicators of the PT control system: drivability and efficiency. Whereas both control tasks – mode operation and transition – directly affect drivability, in mode operation the responsibility about efficiency is at the EMS which specifies the reference value of the hybrid DoFs. In mode transition the DT can contribute to efficiency since it is affected by dissipation in clutches.

2.5.1 Smooth and lossless gear shifting

Single-EM dedicated hybrid DTs feature significant opportunities for the control of gear shifts: The trade-off between dissipation in clutches (efficiency) torque interruptions (drivability) can be resolved for specific shifts. This is achieved by the full synchronization of the clutch before the engagement resp. full unloading before the disengagement. Simultaneously, the full wheel torque is provided according to the driver's request. To emphasize the contribution of such gear shifts to drivability and efficiency they will be called smooth and lossless gear shifts within this thesis. While contributing to an increased fuel efficiency, these gear shifts furthermore enable downsizing of friction clutches or even transition to rigid (form-fitting) coupling elements. This contributes to a reduction of component production and maintenance cost.

There are basically two approaches to implement smooth and lossless gear shifts. The first one is a passive approach: The gear shift is triggered by the EMS in a driving situation, in which the clutch plates of the clutch that has to be engaged are already fully synchronized. Hence, there is no need for an active clutch synchronization. In this

approach the DT control system, simply has to engage the clutch, whereas the ICE and the EM do not have to actively contribute to the shifting. The point of synchronization is already fixed by the mechanical design of the DT topology and the driving situation. If a hybrid DT concept fully relies on this shifting approach the complexity of the EMS decreases dramatically. Actually, it can be replaced by a gear selection based on static look-up tables as used in conventional PTs. On CTI Symposium 2017 in Berlin ([28]), for example, a DHT with form-fitting coupling elements, following this passive shifting approach, was presented.

The fixed shifting point on the other hand is at once also the major drawback of this passive shifting approach. The invariability of the shifting strategy detracts the EMS all optimization opportunities according to the current driving situation. Furthermore, the consideration of the clutches' disengagement is not as straight forward as the engagement due to the more complex relation between the load torque of a locked clutch and the current driving situation.

In contrast to the passive approach an active approach enables variability of the shifting point. Therefore, a dynamic shifting strategy, optimized by the EMS can be applied. In active smooth and lossless gear shifting the ICE and EM torques are used to control the clutch slip speed (differential angular velocity between the clutch plates) respectively the load or locking torque of the clutch to zero before the clutch engagement or disengagement is initiated. The control of these shifts in dedicated hybrid DT is one of the major topics of this thesis. The general problem is to control two tasks at the same time: the clutch synchronization resp. unloading and the wheel torque. To do so from control perspective obviously a necessary condition is the presence of two actuators. This condition is valid for hybrid DTs in general. However, it is not a sufficient condition, since the two control tasks may be in conflict to each other. The solution to this problem is part of the field of Multi-Input Multi-Output (MIMO) systems, the so-called decoupling theory. The application of this condition to a dedicated hybrid DT is investigated in detail within this thesis. It will be shown that dedicated hybrid DT indeed offer potential for active smooth and lossless shifting. Furthermore, the relations between clutch slip resp. load torque and the hybrid DoFs are investigated. Compared to the passive shifting approach the active approach features a increased shifting time. However, if there are no torque interruptions during the shifting, this turns out to be not substantial. The main challenge of the active approach is the increased complexity of the DT control system, which is responsible for gear shifting. Figure 2.7 compares the passive and active shifting approach in a qualitative manner. So far, there are no generic approaches to the model-based analysis and active control of smooth and lossless gear shifts. Such an approach is proposed in this thesis. It will be shown that it is furthermore possible to integrate this shifting concept into a general DT control concept.

2.5.2 DT control setup

According to the statements of the last sections the following list summarizes the general control setup for the control of a single-EM dedicated hybrid DT, implemented in a torque-based PT control system (see Figure 2.6).
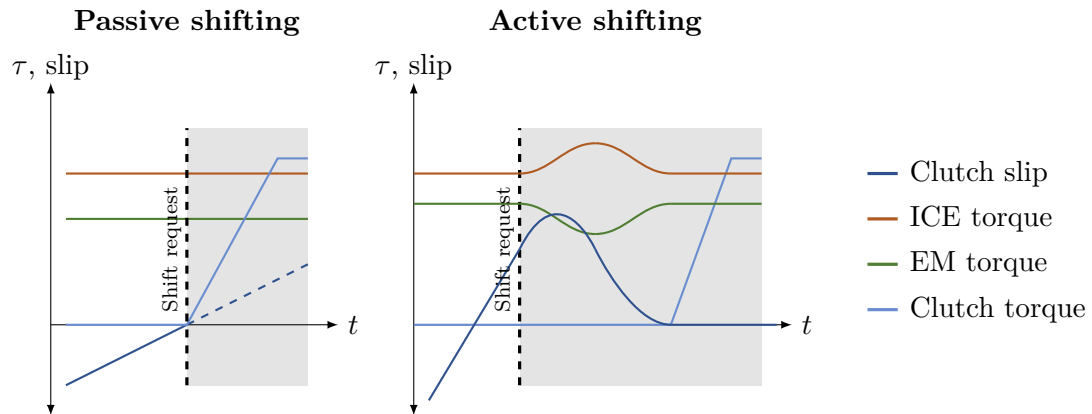
Figure 2.7: *Qualitative comparison between passive and active smooth and lossless gear shifting*

Control setup for single-EM dedicated hybrid DTs

- **Input signals:**
  - Driver interpretation: wheel torque request
  - EMS: gear request, hybrid DoF reference
  - Physical and virtual sensors: speeds, torques, clutch state
- **Control variables:**
  - Mode operation: wheel torque, hybrid DoF
  - Mode transition: wheel torque, clutch slip resp. clutch load torque
- **Outputs signals:**
  - ICE torque request
  - EM torque request
  - Clutch torque requests

2.6 Problem statement

To finalize this preliminary chapter the general problem statement, which motivates the research presented in this thesis, is stated:

Problem statement

Initial situation: The starting point of the research presented in this thesis is a given exemplary single-EM dedicated hybrid DT, implemented in a demonstrator vehicle. The PT is controlled by a state-of-the-art, torque-based PT control system.

Objective: Model-based approaches shall be investigated to improve efficiency and drivability by adaption of the current DT control system. Special attention shall be paid to gear shifting. Novel prototype software components, which enable active smooth and lossless gear shifting, shall be implemented, integrated into the current PT control software and validated in simulation and measurement.

Requirements:
- **Generalizability:** Although the investigations shall focus on the exemplary DT topology, they shall be generalized, if possible, to arbitrary single-EM dedicated hybrid DTs. Furthermore, partial results and approaches shall be applicable to other classes of automotive DTs.
- **Compatibility:** The developed software components should substitute existing components. Therefore, the torque-based control software, has to keep its present structure and no modification of the operation strategy should be necessary.
- **Usability**: The developed software components shall feature an easy and comprehensible parametrization.

Based on this problem statement an outlook on the research activities has been fixed:

Outlook:

1. DT modeling of automotive geared DTs in general and single-EM dedicated hybrid DTs in particular

2. Investigation of an evaluation criterion on the potential of smooth and lossless gear shifts

3. Design of a control concept for these shifts in the given framework

4. Implementation and integration of exemplary, prototype shifting components for validation of the concept

2.7 Specification of thesis contribution

With respect to the problem statement, presented in the last section and the explanations of this chapter, the contribution of the thesis, cf. Chapter 1, is now restated more precisely.

- A **generic and modular approach** to determine mathematical models for the dynamic behavior of geared DTs is contributed. Special attention is paid to the dynamic relation between the system inputs (propulsion torques of ICE and EM) and the control variables (wheel torque, hybrid DoF, clutch slip and load torque). Furthermore, a compact mathematical approach to consider the impact of engaged clutches on the DT model is proposed.

- The modeling of the control variables and the consideration of the impact of engaged clutches lay the basis for the model-based control of gear shifts. The opportunities to perform active **smooth and lossless gear shifting in single-EM dedicated hybrid DTs** are investigated in a general mathematical way. This is done by the statement and consideration of an equivalent decoupling problem, and hence application of decoupling theory.

- Another application of the modeling approach is the proposed **model-based DT analysis method**. It features a generic assignment of an operation mode to each possible clutch state of a given DT topology, according to Table 2.1 and the computation of some DT characteristics like gear ratios and traction forces. Furthermore, the analysis method investigates the shiftability, with respect to traction force intersections and the potential for smooth and lossless gear shifting by the evaluation of the corresponding decoupling problem.

- The relations between the control variables in mode operation and mode transition enables an **implementation of the concept of smooth and lossless gear shifting** into a general model-based control system for single-EM dedicated hybrid DTs.

3

Generic and modular drivetrain modeling

In order to apply model-based methods for analysis and control of DTs, it is necessary in a first step to investigate the modeling. The major investigations, which are presented in this chapter have been already published in [34] and [35]. A modular and generic modeling approach in state-space based on the combination of a comprehensible and compact set of elementary modeling components and a generic modeling algorithm is proposed. A coordinate-partitioning method is used to finally compute a state-space model. Expansions to the modeling algorithm are given to include a consideration of engaged clutches and virtual DT sensors. Subsequently, an implementation of the approach in a user-friendly DT modeling software is presented. This enables DT modeling of all common geared DTs for non-experts in the field of mechanics and proves the algorithms potential for full automation. For the later application of a model-based DT control system, mode specific plant models and a switched linear and time-invariant (LTI) model for gear shifting are proposed, including the appropriate control variables.

3.1 Problem statement and literature

In compliance with the problem statement in Section 2.6 the central task of this chapter is to model the dynamics of a single-EM dedicated hybrid DT with respect to the development of a model-based DT control system focused on gear shifting. Therefore, the dynamic relation between the propulsion torques applied by ICE and EM and the rotational speeds and torques of shafts are of special interest. Hence, this chapter considers exclusively DT mechanics and not the modeling of electrical (battery, power electronics, EM), hydraulic (clutch actuation and torque converter) or thermodynamical (ICE) effects.

Since the DT model shall be applicable to all possible operation modes (cf. Table 2.1), it is reasonable to extend the scope of the modeling approach to all common geared DTs. Although the investigation of a modeling approach is motivated by the develop-

ment of a model-based control system, it shall support the parametrization of various model-based software components in the DT development process, like DT observers and Hardware-in-the-Loop (HiL) simulation models (see for example [15]). In order to offer such a general interface the model shall be given in state-space representation. The comprehensible choice of rotational speeds of shafts as system states guarantees high physical insight.

From a mechanical point of view modeling of an automotive DT's mechanics is about describing the rotational motion of interconnected rigid and flexible shafts subject to external torques. This problem has to be assigned to the domain of multibody systems. Therefore, the modeling in general yields a system of Differential Algebraic Equations (DAEs) of index=3, like every mechanical system with rigidly connected masses (see [36, p. 143]).

A common approach is the usage of object-oriented modeling languages, which apply a multiport-based modeling principle. In object-oriented modeling Ordinary Differential Equations (ODEs), which describe the dynamic behavior of specific modeling components, and additional energy preserving coupling equations are assembled to a DAE system. In a second step mathematical algorithms like index reduction techniques (see for example [37]) are applied in order to reduce the index of the DAE system, finally ending up in an ODE system, if possible. A famous framework applying object-oriented modeling is Dymola/Modelica (see [38] and [39]). Specific libraries, e.g. *engine and powertrain library* in [40], offer a simple application of object-oriented modeling for DTs. Publication [41] gives a general historic overview of object-oriented modeling languages. The drawback of many object-oriented modeling tools is their specialization on analysis and simulation of the modeled system. In fact, they do not support the output of a comprehensible state-space model for model-based function development and parametrization.

In contrast to object-oriented modeling, energy-based approaches, like Lagrange formalism and Hamilton equations, utilize physical insight to cut a corner on the way to an ODE system. A well-established concept is the concept of generalized coordinates. To obtain a set of such generalized coordinates, various methods have been proposed, e.g. the coordinate partitioning method in [42], which is called separation of coordinates in [43], and QR decomposition of the constraint's nullspace in [44]. Energy-based modeling approaches feature the benefit that they end up with comprehensible model representations with comprehensible physical system states by design.

Some proposed DT modeling approaches and their limitations shall be now discussed:

In [9] an automated modeling approach for power-split hybrid DTs is presented. It proposes a rule-based determination of a DAE system and subsequently compact transition to an ODE system.

In [45] the modeling of power-split hybrid DTs directly in state-space is considered.

In [16] and [17] a generic modeling of DTs in state-space is presented. The approach restricts to a simple series structure of the DT elements and does not apply to complex DT structures with combined Planetary Gear Set (PGS).

A promising generic modeling approach is proposed in [46]. A tool-driven parametrization of the state-space kernel of a generic real-time DT model, which is proposed and

applied in [15, 47, 48, 49], is presented. The drawback of this approach is its lack of generality, due to causality problems in the state definition and the necessary special treatment of combined PGS configurations.

In summary, the above-mentioned modeling approaches and frameworks face at least one of the following limitations:

State of the art limitations

- No focus upon a comprehensible model representation
- Restriction to specific hybrid DT topologies, and hence not applicable to all modes of a single-EM dedicated hybrid DT
- Lack of generality, especially with respect to arbitrarily combined PGS

To overcome these limitations this chapter proposes a new generic modular modeling approach for geared automotive DTs. It follows an energy-based modeling principle and applies Lagrangian formalism and a common coordinate partitioning method.

Problem Statement

Initial situation: A dynamic model describing the mechanics of a single-EM dedicated hybrid DT is required. Due to the different operation modes an extension to all common geared DTs is self-evident. Limitations of existing modeling approaches substantiate the development of a new approach.

Objective: A generic and modular modeling approach shall be proposed. The computed models shall support the development and parametrization of model-based DT control systems.

Requirements:
- The approach should provide a comprehensible model representation in state-space.
- It has to be applicable to all common geared DTs.
- The approach should feature a high potential for automation.

3.2 Introducing Example

The basic idea behind the modeling approach, which will be presented in this chapter is outlined by considering a simple introducing example. Figure 3.1 shows two rigid shafts connected with two gear wheels. An external torque acts at one shaft.

parameter	
ω	angular velocity
J	inertia
d	damping
z	number of teeth
τ	external torque

Table 3.1: *Parameters of the introducing example*
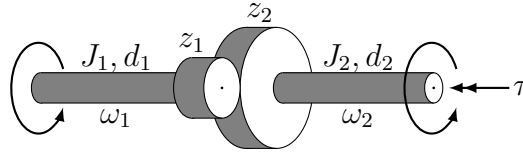
Figure 3.1: *Introducing example: two rigid shafts connected with two gear wheels. For parameters see Table 3.1.*

In order to determine a differential equation, which states the dynamics of this system, in a first step the gear ratio is neglected (see Figure 3.2).
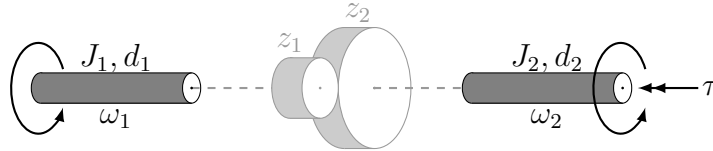
Figure 3.2: *Introducing example: modeling step I – neglect of gear wheels*

The motion of the two (decoupled) shafts is determined by a system of two linear ODEs of first order – the so-called unconstrained equations of motion:

$$\underbrace{\begin{bmatrix} J_1 & 0 \\ 0 & J_2 \end{bmatrix}}_{\tilde{\mathbf{M}}} \underbrace{\begin{bmatrix} \dot{\omega}_1 \\ \dot{\omega}_2 \end{bmatrix}}_{\dot{\mathbf{x}}} = \underbrace{\begin{bmatrix} -d_1 & 0 \\ 0 & -d_2 \end{bmatrix}}_{\tilde{\mathbf{A}}} \underbrace{\begin{bmatrix} \omega_1 \\ \omega_2 \end{bmatrix}}_{\mathbf{x}} + \underbrace{\begin{bmatrix} 0 \\ 1 \end{bmatrix}}_{\tilde{\mathbf{B}}} \underbrace{\tau}_{\mathbf{u}} \tag{3.1}$$

The consideration of the meshing gear wheels in a second step (see Figure 3.3) gives an additional algebraic equation:

$$z_1\omega_1 + z_2\omega_2 = f(\mathbf{x}) = \underbrace{\begin{bmatrix} z_1 & z_2 \end{bmatrix}}_{\mathbf{J}_{\mathrm{f}}} \mathbf{x} = 0. \tag{3.2}$$
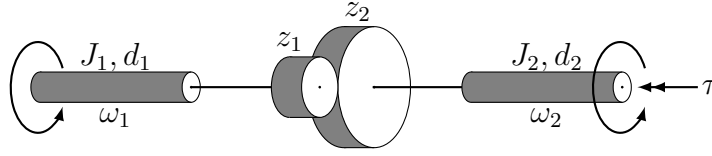
Figure 3.3: *Introducing example: modeling step II – consideration of gear wheel meshing*

This algebraic equation constrains the motion of the two shafts. Therefore, the system loses one mechanical DoF. Consequently, in this example one single ODE would be sufficient to define the final motion of both shafts. To obtain this ODE, Lagrange formalism proposes a transformation to generalized coordinates $\mathbf{q}$:

$$\mathbf{q} := \omega_2 \quad \Rightarrow \quad \mathbf{x} = \underbrace{\begin{bmatrix} -\frac{z_2}{z_1} \\ 1 \end{bmatrix}}_{\mathbf{J}_{\mathrm{x,q}}} \mathbf{q}. \tag{3.3}$$

The mapping $\mathbf{J}_{\mathrm{x,q}}$ is used to transform the system in (3.1), ending up with a single linear ODE – the so-called constrained equation of motion:

$$\underbrace{\mathbf{J}_{\mathrm{x,q}}^T \tilde{\mathbf{M}} \mathbf{J}_{\mathrm{x,q}}}_{\bar{\mathbf{M}}} \dot{\mathbf{q}} = \underbrace{\mathbf{J}_{\mathrm{x,q}}^T \tilde{\mathbf{A}} \mathbf{J}_{\mathrm{x,q}}}_{\bar{\mathbf{A}}} \mathbf{q} + \underbrace{\mathbf{J}_{\mathrm{x,q}}^T \tilde{\mathbf{B}}}_{\bar{\mathbf{B}}} \mathbf{u}, \tag{3.4}$$

$$\Downarrow \tag{3.5}$$

$$\left(J_1 \frac{z_2^2}{z_1^2} + J_2 \right) \dot{\omega}_2 = -\left(d_1 \frac{z_2^2}{z_1^2} + d_2 \right) \omega_2 + \tau. \tag{3.6}$$

The central idea of the proposed modeling approach is to generalize the two elementary modeling steps of the introducing example:

Modeling algorithm – Basic concept:

Step I: Determination of the unconstrained equations of motion, neglecting connecting elements (see (3.1))

Step II: Computation of the constrained equations of motion, considering the connecting elements (see (3.3) and (3.4))

The major questions concerning a generalization of this concept are:

- Which requirements have to be considered when defining a set of modeling components?

- What is the mathematical background of the mapping $\mathbf{J}_{\mathrm{x,q}}$? How to compute it?

- Are the constraints due to connecting elements always linear?

- How does a general form of the unconstrained equations of motions look like, including flexible shafts?
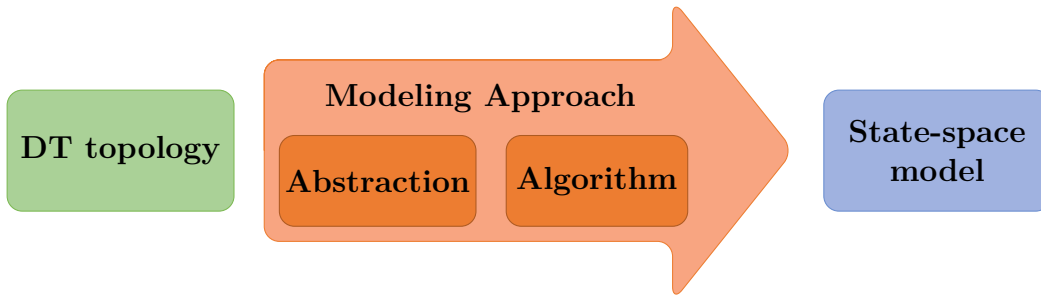
Figure 3.4: *Modeling approach: abstraction and algorithm*

The following sections address these questions and hence present the generic and modular modeling approach as it has already been published in [34]. The approach separates into an abstraction step, in which the DT topology is abstracted by using a compact set modeling components, and the actual mathematical modeling handled by a modeling algorithm, which is matched to these modeling components. This separation is illustrated in Figure 3.4.

3.3 Modeling components

In order to abstract a general geared automotive DT, first a set of elementary modeling components needs to be defined. This is a crucial point in order to lay the basis for a generic and modular modeling approach. An ill-conceived selection of components inevitably would cause serious difficulties in the modeling algorithm, especially for complex DTs. The following aspects are considered when defining a set of components:

Aspects for the choice of a set of modeling components:

- **Applicability:** The set of components should be sufficient to model all common geared DTs.
- **Non-redundancy:** The set should be compact and non-redundant in order to keep the modeling approach as concise a possible.
- **Comprehensibility:** The set should consist of comprehensible components with physical parametrization, to support the comprehensibility of the resulting DT model and to increase the usability of the approach.
- **Structure:** The structure of the set should support the applicability of the two-step algorithm (cf. 3.2).

With respect to these aspects a set of modeling components is proposed as illustrated in Figure 3.5. It is structured into shafts, inputs and connecting elements. Table 3.2 lists all properties and parameters of the single components. The rigid shaft component is the only optionally inert component. Inertia of gear wheels (spur gear set and PGS), hence, has to be modeled via the connected rigid shafts. Furthermore, rigid shafts are the only possible connection between all the other components (including flexible shafts). Losses can be modeled by the velocity dependent damping of rigid shafts or by
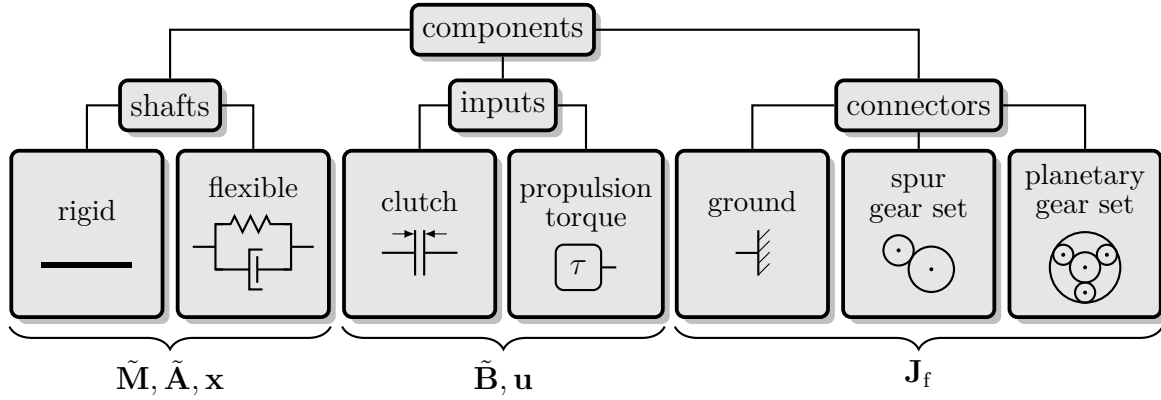
Figure 3.5: *Set of elementary DT components consisting of shafts, connectors and inputs, and their relations to the equations (3.8) and (3.21)*

Table 3.2: *Drivetrain Components and their properties*

component	ports	state	parameter
rigid shaft	2	ω (rot. speed)	J (inertia)
			d (velocity dependent damping)
flexible shaft	2	$\Delta\varphi$ (torsion)	k (stiffness)
			d (velocity dependent damping)
clutch	2	-	
torque input	1	-	
ground	1	-	
spur gear set	2	-	z_P (number of teeth on prim. side)
			z_S (number of teeth on sec. side)
planetary gear set	3 to $3+n_p$	-	z_S (number of teeth sun gear)
			z_R (number of teeth ring gear)
			z_{P_i} (number of teeth i-th planet gear)
			n_p (number planets)

defining additional torque inputs. The PGS component features a variable number of sets of planets (n_p) and possible unconnected ports, as it will be discussed in detail in Section 3.4.2. In combination with spur gear sets and grounds this enables modeling of arbitrary combined PGSs, which play an important role in the synthesis of ATs and multi-mode transmissions. The ground component can be also used to model a mechanical break (clutch with one grounded plate).

The abstraction process is the assigning of specific arrangement of shafts, inputs and connecting elements to a DT topology. The result of this abstraction can be either represented list-based or graphically and comprehends all information about the DT

topology, which shall be captured by the subsequent modeling approach.

3.4 Modeling algorithm

The basic concept of the proposed modeling algorithm follows the two-step approach of the introducing example in Section 3.2: In a first step the proposed algorithm determines the equations of free motion of all shafts, neglecting all connectors. In a second step, the algorithm applies Lagrangian formalism (see for example [50] and [51]) to obtain the constrained equations of motion, with respect to the constraints defined by the connectors. A direct determination of constrained equations of motion, using for example a Lagrangian function, would require a set of generalized coordinates. The declaration of such a set is easy for simple arrangements of components, but rather complicated, especially in the case of complex DT topologies (e.g. ATs). This fact motivates the application of a two-step approach. Both steps of the algorithm are now considered in detail in the next sections.

3.4.1 Unconstrained equations of motion

The quantities of interest in modeling automotive DTs are angular velocities (rotational speeds), torsions and torques. An explicit calculation of angular positions of shafts is not required. Therefore, the equations of free motion can be described by a system of n_x ordinary differential equations of first order, with

$$n_\mathrm{x} = n_\mathrm{rs} + n_\mathrm{fs}, \tag{3.7}$$

according to a number of n_rs rigid and n_fs flexible shafts. The restriction to linear position resp. velocity dependent torques leads to a linear system:

$$\tilde{\mathbf{M}}\dot{\mathbf{x}} = \tilde{\mathbf{A}}\mathbf{x} + \tilde{\mathbf{B}}\mathbf{u}, \tag{3.8}$$

with:

$$\mathbf{x} = \mathbf{P}^T \begin{bmatrix} \boldsymbol{\omega} \\ \Delta\boldsymbol{\varphi} \end{bmatrix}. \tag{3.9}$$

The vector $\boldsymbol{\omega}$ contains the angular velocities of all rigid shafts and $\Delta\boldsymbol{\varphi}$ the torsions of all flexible shafts. The sequence of elements in the state vector $\mathbf{x}$ is arbitrary, but effects the representation of the final model. Therefore, a permutation matrix $\mathbf{P}$ is introduced, which assigns specific angular velocities and torsions to elements in $\mathbf{x}$. The torque input vector $\mathbf{u}$ consists of n_pt propulsion torques ($\boldsymbol{\tau}_\mathrm{P}$) and n_c slipping torques ($\boldsymbol{\tau}_\mathrm{C}$) in clutches:

$$\mathbf{u} = \begin{bmatrix} \boldsymbol{\tau}_\mathrm{P} \\ \boldsymbol{\tau}_\mathrm{C} \end{bmatrix}. \tag{3.10}$$

Therefore, the vector $\mathbf{u}$ consists of $n_\mathrm{u} = n_\mathrm{pt} + n_\mathrm{c}$ entries. The generic composition of the system matrices $\tilde{\mathbf{M}}$, $\tilde{\mathbf{A}}$ and $\tilde{\mathbf{B}}$ is now considered in detail:

Inertia matrix $\tilde{\mathbf{M}}$: As defined in Section 3.3, the only optionally inert components are rigid shafts. Consequently, the inertia matrix $\tilde{\mathbf{M}}$ contains the inertia of every rigid shaft on its diagonal. For every state corresponding to the torsion of a flexible shaft, the stiffness is placed on the diagonal:

$$\tilde{\mathbf{M}} = \mathbf{P}^T \operatorname{diag}\left(\begin{bmatrix} J_1 & \dots & J_{n_{\mathrm{rs}}} & k_1 & \dots & k_{n_{\mathrm{fs}}} \end{bmatrix}\right) \mathbf{P}, \tag{3.11}$$

where J_i is the inertia of the rigid shaft i and the k_j the stiffness of the flexible shaft j.

The design of $\tilde{\mathbf{M}}$ enables compact determination of the DT's energy E, which is the sum of the kinetic energy E_{kin} of all rigid shafts and the potential energy E_{pot} of flexible shafts. According to (3.11) and (3.9) the energy results in:

$$E = E_{\mathrm{kin}} + E_{\mathrm{pot}} = \frac{1}{2}\mathbf{x}^T\tilde{\mathbf{M}}\mathbf{x}. \tag{3.12}$$

Hence, the term energy matrix would be more accurate for matrix $\tilde{\mathbf{M}}$. However, since the term inertia matrix is rather common, this thesis follows this nomenclature. Per definition the system energy is non-negative:

$$\frac{1}{2}\mathbf{x}^T\tilde{\mathbf{M}}\mathbf{x} \geqslant 0, \quad \forall \mathbf{x}. \tag{3.13}$$

This means that $\tilde{\mathbf{M}}$ is positive semidefinite (cf. [52, p. 566]):

$$\tilde{\mathbf{M}} \succeq 0. \tag{3.14}$$

Dynamic Matrix $\tilde{\mathbf{A}}$: Dynamic matrix $\tilde{\mathbf{A}}$ covers both the velocity dependent damping of all rigid shafts and their interaction over n_{fs} flexible shafts. $\tilde{\mathbf{A}}$ can be stated as sum of $n_{\mathrm{fs}} + 1$ matrices:

$$\tilde{\mathbf{A}} = \tilde{\mathbf{A}}_{\mathrm{d}} + \sum_{i=1}^{n_{\mathrm{fs}}} \tilde{\mathbf{A}}_{\mathrm{fs},i}. \tag{3.15}$$

Matrix $\tilde{\mathbf{A}}_{\mathrm{d}}$ considers damping of rigid shafts:

$$\tilde{\mathbf{A}}_{\mathrm{d}} = \mathbf{P}^T \operatorname{diag}\left(-\begin{bmatrix} d_1 & \dots & d_{n_{\mathrm{rs}}} & \mathbf{0}_{1 \times n_{\mathrm{fs}}} \end{bmatrix}\right) \mathbf{P}. \tag{3.16}$$

Parameter d_i is the damping constant for velocity dependent damping of shaft i. Since the damping constants are non-negative $d_i \geqslant 0$, matrix $\tilde{\mathbf{A}}_{\mathrm{d}}$ is negative semidefinite.

The matrices $\tilde{\mathbf{A}}_{\mathrm{fs},i}$ concern the flexible shaft i, with stiffness k_i and damping constant d_i. Let the corresponding torsion $\Delta\varphi_i$ be assigned to state x_m, and the angular velocity of the connecting rigid shafts to states x_j and x_l. The following table lists the entries $a^i_{i_1,i_2}$ for $i_1, i_2 \in \{j, m, l\}$ in $\tilde{\mathbf{A}}_{\mathrm{fs},i}$:

$$a^i_{i_1,i_2}: \quad \begin{array}{c} \\ j \\ m \\ l \end{array} \begin{array}{ccc} j & m & l \\ \begin{pmatrix} -d_i & -k_i & d_i \\ k_i & 0 & -k_i \\ d_i & k_i & -d_i \end{pmatrix} \end{array} \tag{3.17}$$

All other entries are zero:

$$a^i_{i_1,i_2} = \begin{cases} \text{see (3.17)} & \text{for} \quad i_1, i_2 \in \{j, m, l\}, \\ 0 & \text{for} \quad i_1, i_2 = 1, \ldots, n_\mathrm{x} \text{ and } i_1 \notin \{j, m, l\} \lor i_2 \notin \{j, m, l\}. \end{cases}$$
(3.18)

Note that the constant factor k_i in line m of (3.17) is related to the definition of matrix $\tilde{\mathbf{M}}$ in (3.11). Due to this definition the matrices $\tilde{\mathbf{A}}_{\mathrm{fs},i}$ decomposes into a symmetric, negative semidefinite matrix according to the damping d_i and a skew-symmetric matrix according to the stiffness k_i.

Input Matrix $\tilde{\mathbf{B}}$: According the definition of the input vector $\mathbf{u}$ in (3.10), the input matrix $\tilde{\mathbf{B}}$ structures as follows:

$$\tilde{\mathbf{B}} = \begin{bmatrix} \tilde{\mathbf{B}}_\mathrm{P} & \tilde{\mathbf{B}}_\mathrm{C} \end{bmatrix}.$$
(3.19)

$\tilde{\mathbf{B}}$ distributes input torques $\mathbf{u}$ to the states $\mathbf{x}$. For each propulsion torque $\tilde{\mathbf{B}}_\mathrm{P}$ contains an unity column vector. This unity column vector selects the angular velocity of the shaft from state vector $\mathbf{x}$, which is the contact point of the torque. A propulsion torque component can be also used to model disturbance inputs like the vehicle reaction torque due to air drag, rolling resistance and road gradient. According to Newton's third law of motion, the slipping torque of a clutch acts on both connecting rigid shafts with opposite direction. Therefore, in the corresponding column of matrix $\tilde{\mathbf{B}}_\mathrm{C}$ a (1)- resp. (-1)-entry is added in the rows assigned to the connecting rigid shafts. Note that exchanging the signs of both entries switches the arbitrarily assigned direction of the transmitted torque. The simple example in Figure 3.6 clarifies the composition of $\tilde{\mathbf{B}}$:

$$\mathbf{x} = \begin{bmatrix} x_1 \\ x_2 \end{bmatrix}, \quad \mathbf{u} = \begin{bmatrix} \tau_\mathrm{P} \\ \tau_\mathrm{C} \end{bmatrix} \quad \Rightarrow \quad \tilde{\mathbf{B}} = \begin{bmatrix} \tilde{\mathbf{B}}_\mathrm{P} & \tilde{\mathbf{B}}_\mathrm{C} \end{bmatrix} = \begin{bmatrix} 0 & -1 \\ 1 & 1 \end{bmatrix}$$
(3.20)
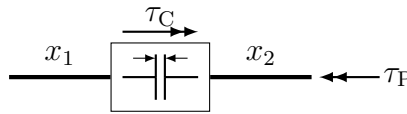
Figure 3.6: *Example for composing the input matrix* $\tilde{\mathbf{B}}$

3.4.2 Composition of constraints

The motion of shafts is constrained by several connectors. These constraints form a set of algebraic equations with respect to the state vector $\mathbf{x}$:

$$\mathbf{f}(\mathbf{x}) = \mathbf{J}_\mathrm{f}\mathbf{x} = \mathbf{0}.$$
(3.21)

$\mathbf{J}_\mathrm{f}$ is the Jacobian matrix of $\mathbf{f}(\mathbf{x})$. The set of modeling components (see Section 3.3) contains three different connecting elements: ground, spur gear set and PGS. The corresponding constraints shall now be considered in detail:

Ground: The simplest possible constraint $f_g(\mathbf{x})$ occurs, if a rigid shaft (with angular velocity x_i) is grounded:

$$f_{\mathrm{g}}(\mathbf{x}) = x_i = \mathbf{f}_{\mathrm{g}}^T \mathbf{x} = 0. \tag{3.22}$$

The constraint involves only a single shaft.

Spur gear set: A spur gear set connects two rigid shafts (angular velocities x_i and x_j) by two meshing gear wheels (number of teeth z_i and z_j). The resulting constraint $f_{\mathrm{sg}}(\mathbf{x})$ is:

$$f_{\mathrm{sg}}(\mathbf{x}) = x_i + x_j \frac{z_j}{z_i} = \mathbf{f}_{\mathrm{sg}}^T \mathbf{x} = 0. \tag{3.23}$$

The implementation of spur gear sets might include one or several intermediate gear wheels. Whereas these gear wheels do not influence the absolute value of the overall ratio $\frac{z_j}{z_i}$, they influence its sign. Therefore, a generalization of (3.23) can be made, according to a number of n_{iw} intermediate gear wheels:

$$f_{\mathrm{sg}}(\mathbf{x}) = x_i + x_j (-1)^{n_{\mathrm{iw}}} \frac{z_j}{z_i} = \mathbf{f}_{\mathrm{sg}}^T \mathbf{x} = 0. \tag{3.24}$$

Planetary gear set: PGS are a key technology in AT and DHT development. The combination of several PGSs, spur gear sets and grounds to combined PGSs (e.g. a Ravigneaux set), enables various ratios with wide spreading in a compact design. The kinematic analysis of PGSs is well-investigated (see for example [53, 54, 55]). To integrate PGSs into the presented modeling algorithm it is necessary to state the corresponding constraints in a structured and generic way.

A PGS consists of three basic elements: a sun gear (S), a planet carrier (C) and a ring gear (R) with internal gears. One or several sets of planet gears (P_i) are mounted on the planet carrier. Every set of planets consists of several planet gears, which are radially equally distributed with a constant distance to the center of the sun gear. A higher number of planets in a set increases the maximum torque, which can be transmitted, but simultaneously also increases the meshing losses. A schematic illustration of a PGS featuring one set of four planets is shown in Figure 3.7.

For the following investigations the number of planets in a single set is not important. Figure 3.8 illustrates the meshing between the gear wheels: The inner planet gear (P_1) meshes with the sun gear, the outer one (P_n) with the ring gear:

$$
\begin{aligned}
\text{S - } P_1: \quad & z_{\mathrm{S}} \left(\omega_{\mathrm{S}} - \omega_{\mathrm{C}} \right) \overset{!}{=} -z_{P_1} \omega_{P_1}, \\
\text{R - } P_{n_{\mathrm{p}}}: \quad & z_{\mathrm{R}} \left(\omega_{\mathrm{R}} - \omega_{\mathrm{C}} \right) \overset{!}{=} z_{P_{n_{\mathrm{p}}}} \omega_{P_{n_{\mathrm{p}}}}.
\end{aligned}
\tag{3.25}
$$

If a PGS consists of more than one set of planets, additionally every planet gear (P_i) meshes with its neighbor (P_{i+1}):

$$P_i \text{ - } P_{i+1}: \quad z_{P_i} \omega_{P_i} \overset{!}{=} -z_{P_{i+1}} \omega_{P_{i+1}}, \quad i = 1, \dots, n_{\mathrm{p}} - 1. \tag{3.26}$$
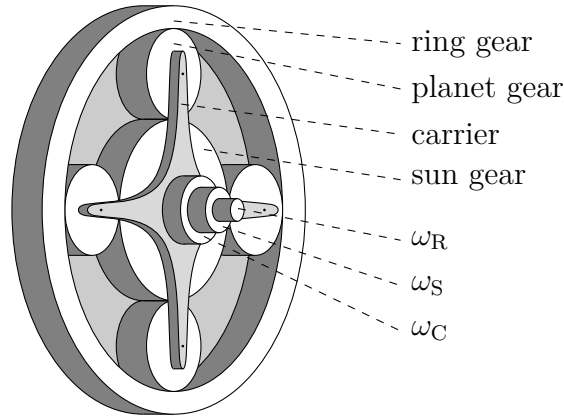
Figure 3.7: *Schematic illustration of a PGS consisting of a sun gear (ω_S), a ring gear (ω_R), a carrier (ω_C) and one set of four planets mounted on the carrier*
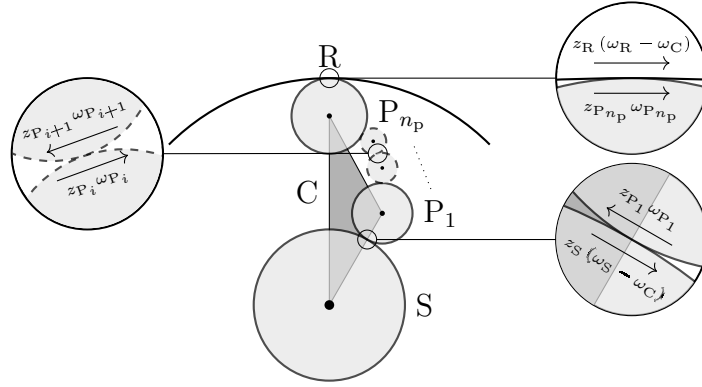
Figure 3.8: *Meshing between the gear wheels of a general PGS with n_p sets of planets*

The number of mechanical DoFs of a PGS is always two. Hence, the total number of algebraic constraints $n_{\mathrm{pg,c}_i}$ depends on the total number of connected rigid shafts $n_{\mathrm{pg,s}_i}$:

$$n_{\mathrm{pg,c}_i} = n_{\mathrm{pg,s}_i} - 2. \tag{3.27}$$

In its classical implementation three shafts are connected to the PGS: one to the sun gear, one to the ring gear and one to the carrier. A linear combination of equations 3.25 and 3.25 in this case yields the famous Willis equation (see for example [56]):

$$\omega_\mathrm{S} + \left[(-1)^{n_\mathrm{p}+1} \frac{z_\mathrm{R}}{z_\mathrm{S}} \right] \omega_\mathrm{R} - \left[1 + (-1)^{n_\mathrm{p}+1} \frac{z_\mathrm{R}}{z_\mathrm{S}} \right] \omega_\mathrm{C} = 0. \tag{3.28}$$

Noticeably, this equation depends only on the number of planet gears n_p, but it does not depend on their number of teeth $z_{\mathrm{P}_1}, \ldots, z_{\mathrm{P}_n}$. When substituting ω_S, ω_R and ω_C with states x_i, x_j and x_k representing the angular velocities of the connected shafts,

$$x_i = \omega_\mathrm{S}, \quad x_j = \omega_\mathrm{R}, \quad x_k = \omega_\mathrm{C}, \tag{3.29}$$

this yields a linear constraint:

$$f_\mathrm{pg}(\mathbf{x}) = \mathbf{f}_\mathrm{pg}^T \mathbf{x} = 0. \tag{3.30}$$

Table 3.3: *Coefficients for generalized PGS constraints (3.31)*

		k_S	k_C	k_R	$k_{\mathrm{P},i}$
$i = 1, \ldots, n_\mathrm{p}$	SCP	1	−1	0	$\frac{z_{\mathrm{P}_i}}{z_\mathrm{S}}(-1)^{i+1}$
	SPR	1	0	−1	$\frac{z_{\mathrm{P}_i}}{z_\mathrm{S}}(-1)^{i+1} + \frac{z_{\mathrm{P}_i}}{z_\mathrm{R}}(-1)^{i+n_\mathrm{P}}$
	CPR	0	−1	1	$\frac{z_{\mathrm{P}_i}}{z_\mathrm{R}}(-1)^{i+n_\mathrm{P}+1}$

In contrast to the classical implementation, in a combined implementation two or even more single PGSs share the same carrier. Additionally, either the angular velocity of planets from different PGSs are coupled or they are meshing. For modeling of these implementations the angular velocity of the planets in relation to the angular velocity of the carrier needs to be determined and connected with shafts. As stated in equation 3.27, in this case an additional constraint is needed, which involves this angular velocity. From (3.25) and (3.26) three possible linear constraints follow, which are linearly dependent in combination with (3.28), and of the type:

$$k_\mathrm{S}\omega_\mathrm{S} + k_\mathrm{R}\omega_\mathrm{R} + k_\mathrm{C}\omega_\mathrm{C} + k_{\mathrm{P},i}\omega_{\mathrm{P}_i} = 0. \tag{3.31}$$

Table 3.3 lists the coefficients $k_\mathrm{S}, k_\mathrm{R}, k_\mathrm{C}, k_{\mathrm{P},i}$ of all three possibilities. In some implementations of combined PGSs the sun or the ring gear of one PGS may not be mechanically implemented. In this case, there is only one appropriate constraint (3.31) according to Table 3.3, which does not involve the respective gear. Furthermore, in this case, according to (3.27) it is not an additional constraint, but replaces (3.28), as also the number of connected shafts is reduced.

Summary of constraints: All constraints due to n_g grounded shafts, n_sg spur gear sets and $n_\mathrm{pg,c}$ PGS constraints can be composed in three matrices $\mathbf{J}_\mathrm{f,g}$, $\mathbf{J}_\mathrm{f,sg}$ and $\mathbf{J}_\mathrm{f,pg}$, and furthermore into one matrix $\mathbf{J}_\mathrm{f}$:

$$\mathbf{J}_\mathrm{f,g}^T := \begin{bmatrix} \mathbf{f}_{\mathrm{g},1} & \ldots & \mathbf{f}_{\mathrm{g},n_\mathrm{g}} \end{bmatrix}, \tag{3.32}$$
$$\mathbf{J}_\mathrm{f,sg}^T := \begin{bmatrix} \mathbf{f}_{\mathrm{sg},1} & \ldots & \mathbf{f}_{\mathrm{sg},n_\mathrm{sg}} \end{bmatrix},$$
$$\mathbf{J}_\mathrm{f,pg}^T := \begin{bmatrix} \mathbf{f}_{\mathrm{pg},1} & \ldots & \mathbf{f}_{\mathrm{pg},n_\mathrm{pg,c}} \end{bmatrix},$$

$$\mathbf{J}_\mathrm{f} := \begin{bmatrix} \mathbf{J}_\mathrm{f,g} \\ \mathbf{J}_\mathrm{f,sg} \\ \mathbf{J}_\mathrm{f,pg} \end{bmatrix}. \tag{3.33}$$

In total this is a set of n_co constraints with:

$$n_\mathrm{co} = n_\mathrm{g} + n_\mathrm{sg} + n_\mathrm{pg,c}, \tag{3.34}$$

and

$$n_\mathrm{pg,c} = \sum_{i=1}^{n_\mathrm{pg}} n_{\mathrm{pg},c_i}. \tag{3.35}$$

At this point it is important to remark that the constraints due to all possible connecting components are indeed linear with respect to the states $\mathbf{x}$.

3.4.3 Constrained equations of motion

In order to constrain the equations of free motion in (3.8) according to (3.21), Lagrange formalism introduces the transformation to generalized coordinates $\mathbf{q}$:

$$\mathbf{x} = \mathbf{J}_{\mathrm{x,q}}\mathbf{q}. \tag{3.36}$$

Generalized coordinates $\mathbf{q}$ comply with the holonomic (linear) constraints for arbitrary values:

$$\mathbf{f}\left(\mathbf{x}(\mathbf{q})\right) = \mathbf{J}_{\mathrm{f}}\mathbf{x}(\mathbf{q}) = \mathbf{J}_{\mathrm{f}}\mathbf{J}_{\mathrm{x,q}}\mathbf{q} \equiv \mathbf{0}. \tag{3.37}$$

Equation (3.37) implies that $\mathbf{J}_{\mathrm{x,q}}$ forms a basis of $\mathbf{J}_{\mathrm{f}}$'s nullspace or kernel, denoted by $\mathcal{N}\left(\mathbf{J}_{\mathrm{f}}\right)$ (see for example [52, p. 174]):

$$\mathbf{J}_{\mathrm{f}}\mathbf{J}_{\mathrm{x,q}}\mathbf{q} \equiv \mathbf{0} \quad \Rightarrow \quad \mathbf{J}_{\mathrm{f}}\mathbf{J}_{\mathrm{x,q}} = \mathbf{0} \quad \Rightarrow \quad \mathcal{R}\left(\mathbf{J}_{\mathrm{x,q}}\right) = \mathcal{N}\left(\mathbf{J}_{\mathrm{f}}\right). \tag{3.38}$$

$\mathcal{R}\left(\mathbf{J}_{\mathrm{x,q}}\right)$ is the range or image of $\mathbf{J}_{\mathrm{x,q}}$. The rank-nullity theorem (see [52, p. 199]) determines the dimensions of $\mathbf{J}_{\mathrm{x,q}}$ and hence the number of generalized coordinates:

$$\dim \mathcal{N}\left(\mathbf{J}_{\mathrm{f}}\right) = n_{\mathrm{x}} - \dim \mathcal{R}\left(\mathbf{J}_{\mathrm{f}}\right) = n_{\mathrm{q}}. \tag{3.39}$$

This number n_{q} is equal to the number of the DT's actual mechanical DoFs. For full rank $\mathbf{J}_{\mathrm{f}}$ (no redundant constraints),

$$n_{\mathrm{q}} = n_{\mathrm{x}} - n_{\mathrm{co}} \tag{3.40}$$

holds. Equation (3.38) is only a necessary condition for $\mathbf{J}_{\mathrm{x,q}}$. Consequently, the choice of a set of generalized coordinates is not unique. This fact can be used to require the inheritance of the physical meaning of the states $\mathbf{x}$ to the generalized coordinates $\mathbf{q}$. To do so $\mathbf{J}_{\mathrm{x,q}}^{T}$ is required to be in reduced row echelon form:

> **Mapping to generalized coordinates:**
>
> $$\mathbf{J}_{\mathrm{x,q}} := \left(\mathbf{E}_{\mathcal{N}(\mathbf{J}_{\mathrm{f}})^{T}}\right)^{T} \tag{3.41}$$

The reduced row echelon from $\mathbf{E}_{\mathbf{A}}$ of a matrix $\mathbf{A}$ is unique (see [52, p. 48]). Due to the structure of $\mathbf{J}_{\mathrm{x,q}}$ according to (3.41), the generalized coordinates are a selection of n_{q} linear independent states, with respect to $\mathbf{J}_{\mathrm{f}}\mathbf{x} = \mathbf{0}$, from top to bottom of state vector $\mathbf{x}$. Consequently, the first state x_1, always becomes a generalized coordinate (q_1). In [34] this selection process is stated as optimization problem.

Although $\mathbf{J}_{\mathrm{x,q}}$ is unique according to (3.41), the order of the elements in state vector $\mathbf{x}$ influences the generalized coordinates. At this point the importance of the mapping $\mathbf{P}$ introduced in (3.9) reveals. Different mappings $\mathbf{P}$ may yield a different $\mathbf{q}$ and, hence,

lead to a different representation of the unique modeling result. State transformations can be applied afterwards to transform the state-space model to different coordinates, corresponding to a different set of $\mathbf{q}$. The transformation of the system matrices $\tilde{\mathbf{M}}$, $\tilde{\mathbf{A}}$ and $\tilde{\mathbf{B}}$ according to a state transformation is investigated in [57] and has already been applied in (3.11) and (3.16).

Due to (3.41) the coordinates $\mathbf{x}$ decompose into generalized coordinates $\mathbf{q}$ and redundant coordinates $(\bar{\mathbf{q}})$, since these coordinates are linearly dependent on $\mathbf{q}$. This decomposition is illustrated in the following artificial example:

$$\mathbf{J}_{\mathrm{f}} = \begin{bmatrix} k_1 & k_2 & 0 & 0 & 0 \\ 0 & 0 & k_3 & k_4 & k_5 \end{bmatrix} \quad \Rightarrow \quad \mathbf{J}_{\mathrm{x,q}}^{T} = \begin{bmatrix} 1 & -\frac{k_1}{k_2} & 0 & 0 & 0 \\ 0 & 0 & 1 & 0 & -\frac{k_3}{k_5} \\ 0 & 0 & 0 & 1 & -\frac{k_4}{k_5} \end{bmatrix}, \tag{3.42}$$

$$\mathbf{q}^{T} = \begin{bmatrix} x_1 & x_3 & x_4 \end{bmatrix}, \quad \bar{\mathbf{q}}^{T} = \begin{bmatrix} x_2 & x_5 \end{bmatrix}. \tag{3.43}$$

Such a decomposition is called coordinate partitioning (see for example e.g. [42] and [43]).

The mapping $\mathbf{J}_{\mathrm{x,q}}$, transforms the equations of free motion (3.8) with respect to the new coordinate system:

$$\bar{\mathbf{M}}\dot{\mathbf{q}} = \bar{\mathbf{A}}\mathbf{q} + \bar{\mathbf{B}}\mathbf{u}, \tag{3.44}$$

with:

$$\begin{aligned} \bar{\mathbf{M}} &:= \mathbf{J}_{\mathrm{x,q}}^{T}\tilde{\mathbf{M}}\mathbf{J}_{\mathrm{x,q}}, \\ \bar{\mathbf{A}} &:= \mathbf{J}_{\mathrm{x,q}}^{T}\tilde{\mathbf{A}}\mathbf{J}_{\mathrm{x,q}}, \\ \bar{\mathbf{B}} &:= \mathbf{J}_{\mathrm{x,q}}^{T}\tilde{\mathbf{B}}. \end{aligned} \tag{3.45}$$

In contrast to $\tilde{\mathbf{M}}$, see in (3.14), $\bar{\mathbf{M}}$ is required to be positive definite to ensure that the resulting model is physically reasonable:

$$E = \mathbf{q}^{T}\bar{\mathbf{M}}\mathbf{q} = 0 \quad \Leftrightarrow \quad \mathbf{q} = 0. \tag{3.46}$$

This assumption implies that $\bar{\mathbf{M}}$ is regular and therefore the corresponding state-space model can be computed as:

$$\dot{\mathbf{q}} = \underbrace{\bar{\mathbf{M}}^{-1}\bar{\mathbf{A}}}_{\mathbf{A}}\mathbf{q} + \underbrace{\bar{\mathbf{M}}^{-1}\bar{\mathbf{B}}}_{\mathbf{B}}\mathbf{u}. \tag{3.47}$$

It is remarkable that the state-space representation is not unique and hence there is no possibility to uniquely determine the system energy by considering the matrices $\mathbf{A}$ and $\mathbf{B}$.

IN summary the following computations have to be done in the two steps of the presented algorithm:

> **Modeling algorithm – Computational concept:**
>
> **Step I:** Definition of a state vector $\mathbf{x}$ and a input vector $\mathbf{u}$, and composition of matrices $\tilde{\mathbf{M}}, \tilde{\mathbf{A}}$ and $\tilde{\mathbf{B}}$
>
> **Step II:** Composition of constraint matrix $\mathbf{J}_{\mathrm{f}}$, computation of the matrix $\mathbf{J}_{\mathrm{x,q}}$ according to (3.41) and the application of a matrix transformation $\tilde{\mathbf{M}}, \tilde{\mathbf{A}}, \tilde{\mathbf{B}} \mapsto \bar{\mathbf{M}}, \bar{\mathbf{A}}, \bar{\mathbf{B}}$ according to (3.44).

Equation (3.48) summarizes the dimensions of all matrices defined in the modeling algorithm.

$$
\begin{aligned}
\tilde{\mathbf{M}}, \tilde{\mathbf{A}} &\in \mathbb{R}^{n_{\mathrm{x}} \times n_{\mathrm{x}}} = \mathbb{R}^{(n_{\mathrm{rs}}+n_{\mathrm{fs}}) \times (n_{\mathrm{rs}}+n_{\mathrm{fs}})} \\
\tilde{\mathbf{B}} &\in \mathbb{R}^{n_{\mathrm{x}} \times n_{\mathrm{u}}} = \mathbb{R}^{(n_{\mathrm{rs}}+n_{\mathrm{fs}}) \times (n_{\mathrm{pt}}+n_{\mathrm{c}})} \\
\mathbf{J}_{\mathrm{f}} &\in \mathbb{R}^{n_{\mathrm{co}} \times n_{\mathrm{x}}} = \mathbb{R}^{(n_{\mathrm{sg}}+n_{\mathrm{pg,c}}+n_{\mathrm{g}}) \times (n_{\mathrm{rs}}+n_{\mathrm{fs}})} \\
\mathbf{J}_{\mathrm{x,q}} &\in \mathbb{R}^{n_{\mathrm{q}} \times n_{\mathrm{x}}} = \mathbb{R}^{(n_{\mathrm{rs}}+n_{\mathrm{fs}}-n_{\mathrm{co}}) \times (n_{\mathrm{rs}}+n_{\mathrm{fs}})} \\
\bar{\mathbf{M}}, \bar{\mathbf{A}}, \mathbf{A} &\in \mathbb{R}^{n_{\mathrm{q}} \times n_{\mathrm{q}}} = \mathbb{R}^{(n_{\mathrm{rs}}+n_{\mathrm{fs}}-n_{\mathrm{co}}) \times (n_{\mathrm{rs}}+n_{\mathrm{fs}}-n_{\mathrm{co}})} \\
\bar{\mathbf{B}}, \mathbf{B} &\in \mathbb{R}^{n_{\mathrm{q}} \times n_{\mathrm{u}}} = \mathbb{R}^{(n_{\mathrm{rs}}+n_{\mathrm{fs}}-n_{\mathrm{co}}) \times (n_{\mathrm{pt}}+n_{\mathrm{c}})}
\end{aligned}
$$

$$(3.48)$$

Furthermore, Table 3.4 lists all used symbols.

Table 3.4: *Symbols used in the description of the modeling approach*

symbol	description
n_x	number of mechanical DoF without constraints
n_q	number of actual (i.e. with constraints) mechanical DoF
n_rs	number of rigid shafts
n_fs	number flexible shafts
n_sg	number of spur gear sets
n_pg	number of PGSs
$n_{\mathrm{pg,s}_i}$	number of shafts connected to a single PGS
$n_{\mathrm{pg,c}_i}$	number of constraints due to a single PGS
$n_\mathrm{pg,c}$	total number of constraints due to all PGSs
n_co	total number of constraints
n_g	number of grounds
n_c	number of clutches
n_pt	number of propulsion torques
n_u	number of input torques
ω_S	angular velocity sun gear
ω_R	angular velocity ring gear
ω_C	angular velocity carrier gear
ω_{P_i}	angular velocity of the i-th set of planet gears relative to the carrier
z_S	teeth count sun gear
z_R	teeth count ring gear
z_{P_i}	teeth count of the i-th set of planet gears
n_p	number of sets of planets

3.4.4 Example

The proposed two-step approach is now applied to an exemplary, simple DT topology: Figure 3.9 shows the considered (abstracted) conventional DT, including a differential.

Step I – Unconstrained equations of motion: The DT consists of 5 rigid shafts and 1 flexible shaft:

$$\boldsymbol{\omega}^T = \begin{bmatrix} \omega_1 & \ldots & \omega_5 \end{bmatrix}, \quad \Delta\boldsymbol{\varphi}^T = \begin{bmatrix} \Delta\varphi_1 \end{bmatrix}. \tag{3.49}$$
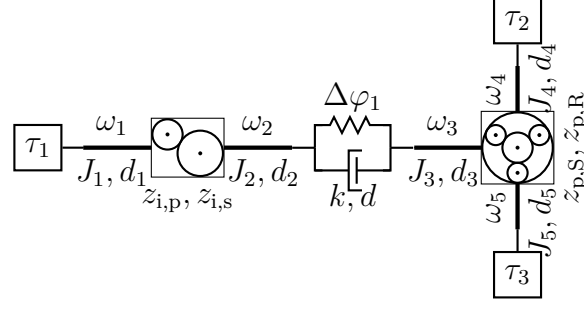
Figure 3.9: *Exemplary, conventional DT including a differential*

Permutation matrix $\mathbf{P}$ is used to give high priority to $\omega_1, \omega_4, \omega_5$, which represent the rotational speed of the engine and the wheels:

$$\mathbf{P} = \begin{bmatrix} 1 & 0 & 0 & 0 & 0 & 0 \\ 0 & 0 & 0 & 1 & 0 & 0 \\ 0 & 0 & 0 & 0 & 1 & 0 \\ 0 & 1 & 0 & 0 & 0 & 0 \\ 0 & 0 & 1 & 0 & 0 & 0 \\ 0 & 0 & 0 & 0 & 0 & 1 \end{bmatrix}. \tag{3.50}$$

Consequently, the state vector $\mathbf{x}$ is:

$$\mathbf{x} = \begin{bmatrix} \omega_1 & \omega_4 & \omega_5 & \omega_2 & \omega_3 & \Delta\varphi_1 \end{bmatrix}^T. \tag{3.51}$$

The input vector $\mathbf{u}$ consists of three propulsion torque inputs:

$$\mathbf{u} = \begin{bmatrix} \tau_1 & \tau_2 & \tau_3 \end{bmatrix}^T. \tag{3.52}$$

Torque τ_1 models the ICE propulsion, and τ_2, τ_3 the reactive torques at the driving wheels. The composition of the matrices $\tilde{\mathbf{M}}, \tilde{\mathbf{A}}, \tilde{\mathbf{B}}$ follows the procedure explained in Section 3.4:

$$\tilde{\mathbf{M}} = \mathbf{P}^T \operatorname{diag}\left(\begin{bmatrix} J_1 & J_2 & J_3 & J_4 & J_5 & k \end{bmatrix}\right) \mathbf{P}, \tag{3.53}$$

$$\tilde{\mathbf{A}}_d = \mathbf{P}^T \operatorname{diag}\left(\begin{bmatrix} d_1 & d_2 & d_3 & d_4 & d_5 & 0 \end{bmatrix}\right) \mathbf{P}, \tag{3.54}$$

$$\tilde{\mathbf{A}}_{\text{fs}} = \begin{bmatrix} 0 & 0 & 0 & 0 & 0 & 0 \\ 0 & -d & d & 0 & 0 & -k \\ 0 & d & -d & 0 & 0 & k \\ 0 & 0 & 0 & 0 & 0 & 0 \\ 0 & 0 & 0 & 0 & 0 & 0 \\ 0 & k & -k & 0 & 0 & 0 \end{bmatrix}, \quad \tilde{\mathbf{B}} = \begin{bmatrix} 1 & 0 & 0 \\ 0 & 1 & 0 \\ 0 & 0 & 1 \\ 0 & 0 & 0 \\ 0 & 0 & 0 \\ 0 & 0 & 0 \end{bmatrix}. \tag{3.55}$$

Step II – Constrained equations of motion: The considered DT features two connectors: a spur gear set and a PGS. The PGS is connected at sun gear, ring gear and carrier. Consequently, Willis equation in (3.28) is sufficient to state the kinematic relations. Matrix $\mathbf{J}_\mathrm{f}$, hence, consists of two rows:

$$\mathbf{J}_\mathrm{f} = \begin{bmatrix} 1 & 0 & 0 & \frac{z_\mathrm{i,s}}{z_\mathrm{i,p}} & 0 & 0 \\ 0 & 1 & \frac{z_\mathrm{p,R}}{z_\mathrm{p,S}} & 0 & -\left(1 + \frac{z_\mathrm{p,R}}{z_\mathrm{p,S}}\right) & 0 \end{bmatrix}. \tag{3.56}$$

A differential is a special implementation of a PGS with $z_\mathrm{p,S} = z_\mathrm{p,R}$. This further simplifies $\mathbf{J}_\mathrm{f}$:

$$\mathbf{J}_\mathrm{f} = \begin{bmatrix} 1 & 0 & 0 & \frac{z_\mathrm{i,s}}{z_\mathrm{i,p}} & 0 & 0 \\ 0 & 1 & 1 & 0 & -2 & 0 \end{bmatrix}. \tag{3.57}$$

According to 3.41 the matrix $\mathbf{J}_\mathrm{x,q}$ is:

$$\mathbf{J}_\mathrm{x,q} = \begin{bmatrix} 1 & 0 & 0 & 0 \\ 0 & 1 & 0 & 0 \\ 0 & 0 & 1 & 0 \\ -\frac{z_\mathrm{i,p}}{z_\mathrm{i,s}} & 0 & 0 & 0 \\ 0 & \frac{1}{2} & \frac{1}{2} & 0 \\ 0 & 0 & 0 & 1 \end{bmatrix}. \tag{3.58}$$

This determines the generalized coordinates,

$$\mathbf{q}^T = \begin{bmatrix} \omega_1 & \omega_4 & \omega_5 & \Delta\varphi_1 \end{bmatrix}, \tag{3.59}$$

and leads to the transformed system matrices:

$$\bar{\mathbf{M}} = \mathbf{J}_\mathrm{x,q}^T \tilde{\mathbf{M}} \mathbf{J}_\mathrm{x,q} = \begin{bmatrix} J_1 + J_2\frac{z_\mathrm{i,p}^2}{z_\mathrm{i,s}^2} & 0 & 0 & 0 \\ 0 & \frac{J_3}{4} + J_4 & \frac{J_3}{4} & 0 \\ 0 & \frac{J_3}{4} & \frac{J_3}{4} + J_5 & 0 \\ 0 & 0 & 0 & k \end{bmatrix}, \tag{3.60}$$

$$\bar{\mathbf{A}} = \mathbf{J}_\mathrm{x,q}^T \left(\tilde{\mathbf{A}}_\mathrm{d} + \tilde{\mathbf{A}}_\mathrm{fs}\right) \mathbf{J}_\mathrm{x,q} = \begin{bmatrix} \frac{-d_1 z_\mathrm{i,s}^2 - (d_2+d)z_\mathrm{i,p}^2}{z_\mathrm{i,s}^2} & -\frac{d}{2}\frac{z_\mathrm{i,p}}{z_\mathrm{i,s}} & -\frac{d}{2}\frac{z_\mathrm{i,p}}{z_\mathrm{i,s}} & k\frac{z_\mathrm{i,p}}{z_\mathrm{i,s}} \\ -\frac{d}{2}\frac{z_\mathrm{i,p}}{z_\mathrm{i,s}} & \frac{-d-d_3-4d_4}{4} & -\frac{d}{4} - \frac{d_3}{4} & \frac{k}{2} \\ -\frac{d}{2}\frac{z_\mathrm{i,p}}{z_\mathrm{i,s}} & -\frac{d}{4} - \frac{d_3}{4} & \frac{-d-d_3-4d_5}{4} & \frac{k}{2} \\ -k\frac{z_\mathrm{i,p}}{z_\mathrm{i,s}} & -\frac{k}{2} & -\frac{k}{2} & 0 \end{bmatrix},$$

$$\bar{\mathbf{B}} = \mathbf{J}_\mathrm{x,q}^T \tilde{\mathbf{B}} = \begin{bmatrix} 1 & 0 & 0 \\ 0 & 1 & 0 \\ 0 & 0 & 1 \\ 0 & 0 & 0 \end{bmatrix}. \tag{3.61}$$

The final state-space matrices $\mathbf{A}, \mathbf{B}$ are not explicitly illustrated in analytic form due to the size of the resulting symbolic expressions.

3.5 Expansions of algorithm

3.5.1 Clutch engagement

In the presented modeling approach, so far, a clutch has been considered only in slipping state as torque input, see Section 3.3. However, if the clutch is engaged by electro-hydraulic actuation (see Section 2.1), the clutch transits into locking state. In this case the two shafts, which are connected to the clutch ports, are connected rigidly. This is equivalent to adding an additional constraint, which forces the clutch slip (differential angular velocity between clutch plates) to zero. Considering the composition of the input matrix $\tilde{\mathbf{B}}_\text{C}$ in (3.19), it is obvious that the clutch slips $\Delta\boldsymbol{\omega}_\text{C}$ can be computed with:

$$\Delta\boldsymbol{\omega}_\text{C} = \tilde{\mathbf{B}}_\text{C}^T\mathbf{x}. \tag{3.62}$$

A generalization of this equation to the constrained equations of motion can be done by investigating the conservation of power. The power dissipated in the clutches is

$$P_\text{C} = \Delta\boldsymbol{\omega}_\text{C}^T\boldsymbol{\tau}_\text{C}. \tag{3.63}$$

This power has to be equal to the power in terms of the states $\mathbf{q}$:

$$P_\text{C,\mathbf{q}} = \mathbf{q}^T\bar{\mathbf{B}}_\text{C}\boldsymbol{\tau}_\text{C}. \tag{3.64}$$

The conservation of power, consequently, requires:

$$\Delta\boldsymbol{\omega}_\text{C}^T\boldsymbol{\tau}_\text{C} \overset{!}{=} \mathbf{q}^T\bar{\mathbf{B}}_\text{C}\boldsymbol{\tau}_\text{C}, \quad \forall\mathbf{q},\boldsymbol{\tau}_\text{C} \quad \Rightarrow \quad \Delta\boldsymbol{\omega}_\text{C} \overset{!}{=} \bar{\mathbf{B}}_\text{C}^T\mathbf{q}. \tag{3.65}$$

Hence, this consideration proves that it is feasible to generalize (3.62) to the constrained equations of motion. The constraint due to a locked clutch is again linear with respect to the states $\mathbf{q}$. Therefore, the second step of the modeling algorithm, which has been presented in Section 3.4, can be applied to consider the impact of one or several locked clutches. This fact has already been published in [35]. In Section 2.3 the binary clutch state vector $\boldsymbol{\kappa}$ has been introduced. For a specific clutch state $\boldsymbol{\kappa}_i$, consequently, the additional linear constraints are:

$$\mathbf{f}_\text{C}(\mathbf{q}) = \bar{\mathbf{B}}_\text{C}(\boldsymbol{\kappa}_i)^T\mathbf{q} = \mathbf{0}, \tag{3.66}$$

where the symbol $\bar{\mathbf{B}}_\text{C}(\boldsymbol{\kappa}_i)$ denotes the selection of columns of $\bar{\mathbf{B}}_\text{C}$ according $\boldsymbol{\kappa}_i$. The definition of a coordinate mapping $\mathbf{J}_{\text{q},\text{q}_i}$, cf. (3.41),

$$\mathbf{J}_{\text{q},\text{q}_i} = \left(\mathbf{E}_{\mathcal{N}\left(\bar{\mathbf{B}}_\text{C}(\boldsymbol{\kappa}_i)^T\right)^T}\right)^T, \tag{3.67}$$

and the transformation to the coordinates $\mathbf{q}_i$ according to (3.44) yields a new ODE system:

$$\underbrace{\mathbf{J}_{\text{q},\text{q}_i}^T\bar{\mathbf{M}}\mathbf{J}_{\text{q},\text{q}_i}}_{\bar{\mathbf{M}}_i}\dot{\mathbf{q}}_i = \underbrace{\mathbf{J}_{\text{q},\text{q}_i}^T\bar{\mathbf{A}}\mathbf{J}_{\text{q},\text{q}_i}}_{\bar{\mathbf{A}}_i}\mathbf{q}_i + \underbrace{\mathbf{J}_{\text{q},\text{q}_i}^T\bar{\mathbf{B}}}_{\bar{\mathbf{B}}_i}\mathbf{u}. \tag{3.68}$$

The corresponding state space model is:

$$\dot{\mathbf{q}}_i = \underbrace{\bar{\mathbf{M}}_i^{-1}\bar{\mathbf{A}}_i}_{\mathbf{A}_i}\,\mathbf{q}_i + \underbrace{\bar{\mathbf{M}}_i^{-1}\mathbf{J}_{\mathrm{q,q}_i}^T\bar{\mathbf{B}}}_{\mathbf{B}_i}\,\mathbf{u}. \tag{3.69}$$

The order of this system $(n_{\mathrm{q}} - \boldsymbol{\kappa}_i^T\boldsymbol{\kappa}_i)$, since each engaged clutch decreases the mechanical DoFs, if $\bar{\mathbf{B}}_{\mathrm{C}}(\boldsymbol{\kappa}_i)$ has full rank. Due to the fact that an engaged clutch does not transmit a slipping torque anymore, the corresponding columns in the input matrix $\bar{\mathbf{B}}_{i,\mathrm{C}}$ are zero:

$$\bar{\mathbf{B}}_{i,\mathrm{C}}(\boldsymbol{\kappa}_i) = \mathbf{0}. \tag{3.70}$$

An analytic look at equations (3.44) and (3.68) reveals that the two-step algorithm for applying a linear constraint can be done iteratively:

$$\mathbf{x} = \mathbf{J}_{\mathrm{x,q}}\mathbf{J}_{\mathrm{q,q}_i}\mathbf{q}_i. \tag{3.71}$$

Therefore, the constraint due to a locked clutch could have also been included directly into the original Jacobian matrix $\mathbf{J}_{\mathrm{f}}$. This would have led to a transformation from $\mathbf{x}$ coordinates directly to the coordinates $\mathbf{q}_i$:

$$\mathbf{x} = \mathbf{J}_{\mathrm{x,q}_i}\mathbf{q}_i, \tag{3.72}$$

with

$$\mathbf{J}_{\mathrm{x,q}_i} = \mathbf{J}_{\mathrm{x,q}}\mathbf{J}_{\mathrm{q,q}_i}. \tag{3.73}$$

The consideration of clutch engagement shows that the knowledge of state-space matrix $\mathbf{A}$ and $\mathbf{B}$ is not sufficient to apply additional constraints, since there is no unique computation of $\bar{\mathbf{M}}$ from $\mathbf{A}$ and $\mathbf{B}$. This fact has been already discussed with respect to the system energy in Section 3.4.3.

The assumption $\bar{\mathbf{M}} > 0$ enables the statement of an important property of $\bar{\mathbf{M}}_i$:

From $\bar{\mathbf{M}} > 0$ follows:

$$\mathbf{q}^T\bar{\mathbf{M}}\mathbf{q} = 0 \quad \Leftrightarrow \quad \mathbf{q} = \mathbf{0}. \tag{3.74}$$

Assuming $\mathbf{J}_{\mathrm{q,q}_i}$ has full rank, i.e. $\det\left(\mathbf{J}_{\mathrm{q,q}_i}^T\mathbf{J}_{\mathrm{q,q}_i}\right) \neq 0$, with

$$\mathbf{q} = \mathbf{J}_{\mathrm{q,q}_i}\mathbf{q}_i, \tag{3.75}$$

this yields:

$$\mathbf{q} = \mathbf{0} \quad \Leftrightarrow \quad \mathbf{q}_i = \mathbf{0}. \tag{3.76}$$

Hence,

$$\mathbf{q}_i^T\underbrace{\mathbf{J}_{\mathrm{q,q}_i}^T\bar{\mathbf{M}}\mathbf{J}_{\mathrm{q,q}_i}}_{\tilde{\mathbf{M}}_i}\,\mathbf{q}_i = 0 \quad \Leftrightarrow \quad \mathbf{q}_i = \mathbf{0}. \tag{3.77}$$

Therefore, also $\bar{\mathbf{M}}_i$ is positive definite, if

$$\det\left(\mathbf{J}_{\mathrm{q,q}_i}^T \mathbf{J}_{\mathrm{q,q}_i}\right) \neq 0. \tag{3.78}$$

This is the case if,

$$\operatorname{rank}\left(\bar{\mathbf{B}}_{\mathrm{C}}(\boldsymbol{\kappa}_i)\right) < n_{\mathrm{q}}. \tag{3.79}$$

In words this implies at least one remaining mechanical DoF with clutch state $\boldsymbol{\kappa}_i$. If this is not the case the system is static due to a fully blocked transmission.

3.5.2 Virtual DT sensors:

To use a DT model for control purpose, virtual sensors are of special interest. Virtual sensors substitute some physical sensors, which are either too expensive or not mountable at some positions in the DT. Therefore, this section presents the extension of the ODE system to a full state state-space model including a set of output equations:

$$\mathbf{y} = \tilde{\mathbf{C}}\mathbf{x} + \mathbf{D}\mathbf{u}. \tag{3.80}$$

The outputs $\mathbf{y}$ represent the virtual sensor values. The final output matrix is affected by the transformation in (3.36):

$$\mathbf{y} = \underbrace{\tilde{\mathbf{C}}\mathbf{J}_{\mathrm{x,q}}}_{\mathbf{C}} \mathbf{q} + \mathbf{D}\mathbf{u}. \tag{3.81}$$

Note that the mappings $\mathbf{J}_{\mathrm{x,q}}$ do not affect the feed-through matrix $\mathbf{D}$.

In order to control a DT virtual speed, torsion and torque sensors are beneficial. As the control of gear shift is a central topic of this thesis, virtual sensors for the differential clutch speed respectively the torque transmitted in locked clutches are of special interest. All of these virtual sensors are now considered in detail within this section.

Speed and torsion sensors: As the state vector $\mathbf{x}$ contains all rotational speeds of rigid and torsions of flexible shafts, virtual sensors of these quantities are rather simple. The corresponding output matrix $\mathbf{C}_{\mathbf{x}}$ just selects the corresponding elements of interest in $\mathbf{x}$ and is hence a selection of specific rows in the unity matrix $\mathbf{I}_{n_{\mathrm{x}} \times n_{\mathrm{x}}}$.

Clutch sensors: The basic functionality of an automotive clutch has already been discussed in Section 2.1. Further details with respect to the transition between clutch state will be investigated in Section 3.8.1. Two quantities – the clutch slip and the locking torque – will be of special interest for the control of gear shifts. In anticipation to the later control considerations, the implementation of virtual sensors to these quantities is investigated.

From (3.65) directly follows the clutch slip of all disengaged clutches:

$$\Delta\boldsymbol{\omega}_{\mathrm{C}} \overset{!}{=} \bar{\mathbf{B}}_{i,\mathrm{C}}(\bar{\boldsymbol{\kappa}}_i)^T \mathbf{q}_i. \tag{3.82}$$

With respect to the impact of a set of locked clutches (see Section 3.5.1) the clutch torques separate into the slipping torques ($\boldsymbol{\tau}_{\mathrm{C,sl}}$) of all disengaged clutches and locking torques ($\boldsymbol{\tau}_{\mathrm{C,lk}}$) of all engaged clutches:

$$\bar{\mathbf{B}}_{\mathrm{C}}\boldsymbol{\tau}_{\mathrm{C}} = \bar{\mathbf{B}}_{\mathrm{C}}(\bar{\boldsymbol{\kappa}}_i)\boldsymbol{\tau}_{\mathrm{C,sl}} + \bar{\mathbf{B}}_{\mathrm{C}}(\boldsymbol{\kappa}_i)\boldsymbol{\tau}_{\mathrm{C,lk}}. \tag{3.83}$$

The differentiation with respect to time of (3.66) yields:

$$\frac{\mathrm{d}\mathbf{f}(\mathbf{q})}{\mathrm{d}t} = \bar{\mathbf{B}}_{\mathrm{C}}(\boldsymbol{\kappa}_i)^T\dot{\mathbf{q}} \overset{!}{=} \mathbf{0}. \tag{3.84}$$

In combination with (3.44), (3.83) and (3.75) the locking torques can be computed:

$$\boldsymbol{\tau}_{\mathrm{C,lk}} = -\left[\bar{\mathbf{B}}_{\mathrm{C}}(\boldsymbol{\kappa}_i)^T\bar{\mathbf{M}}^{-1}\bar{\mathbf{B}}_{\mathrm{C}}(\boldsymbol{\kappa}_i)\right]^{-1}\dots \tag{3.85}$$
$$\bar{\mathbf{B}}_{\mathrm{C}}(\boldsymbol{\kappa}_i)^T\bar{\mathbf{M}}^{-1}\left[\bar{\mathbf{A}}\mathbf{J}_{\mathrm{q,q}_i}\mathbf{q}_i + \bar{\mathbf{B}}_{\mathrm{P}}\boldsymbol{\tau}_{\mathrm{P}} + \bar{\mathbf{B}}_{\mathrm{C}}(\bar{\boldsymbol{\kappa}}_i)\boldsymbol{\tau}_{\mathrm{C,sl}}\right].$$

The existence of $\bar{\mathbf{M}}^{-1}$ has already been postulated for every mechanically reasonable DT topology in Section 3.4.3. The existence of the inverse $\left[\bar{\mathbf{B}}_{\mathrm{C}}(\boldsymbol{\kappa}_i)^T\bar{\mathbf{M}}^{-1}\bar{\mathbf{B}}_{\mathrm{C}}(\boldsymbol{\kappa}_i)\right]^{-1}$ can be shown following the same approach as presented in Section 3.5.1 for the inverse of $\bar{\mathbf{M}}_i$.

Summarized the clutch sensor matrices are:

$$\mathbf{C}_{i,\mathrm{C}} = \begin{bmatrix} \bar{\mathbf{B}}_{i,\mathrm{C}}(\bar{\boldsymbol{\kappa}}_i)^T\mathbf{q}_i \\ -\left[\bar{\mathbf{B}}_{\mathrm{C}}(\boldsymbol{\kappa}_i)^T\bar{\mathbf{M}}^{-1}\bar{\mathbf{B}}_{\mathrm{C}}(\boldsymbol{\kappa}_i)\right]^{-1}\bar{\mathbf{B}}_{\mathrm{C}}(\boldsymbol{\kappa}_i)^T\bar{\mathbf{M}}^{-1}\bar{\mathbf{A}}\mathbf{J}_{\mathrm{q,q}_i} \end{bmatrix} \tag{3.86}$$

$$\mathbf{D}_{i,\mathrm{C}} = \begin{bmatrix} \mathbf{0} \\ -\left[\bar{\mathbf{B}}_{\mathrm{C}}(\boldsymbol{\kappa}_i)^T\bar{\mathbf{M}}^{-1}\bar{\mathbf{B}}_{\mathrm{C}}(\boldsymbol{\kappa}_i)\right]^{-1}\bar{\mathbf{B}}_{\mathrm{C}}(\boldsymbol{\kappa}_i)^T\bar{\mathbf{M}}^{-1}\bar{\mathbf{B}}_{\mathrm{C}}(\bar{\boldsymbol{\kappa}}_i). \end{bmatrix} \tag{3.87}$$

Torque sensors: In all previous investigations the distribution of inertia along a rigid shaft could be neglected. However, when computing the torque acting on a rigid shaft, this aspect has to be considered. Although a constant distribution along the shaft is assumed, the torque depends on the position of the torque sensor. In the last section the locking torque of an engaged clutch has been investigated. This investigation can be utilized by adding fictitious clutches at the position of the virtual torque sensor. The locking torque of these permanently engaged clutches is the required value of the torque sensor.

Figure 3.10 shows three possible positions of a torque sensor on a rigid shaft, abstracted by a fictitious clutch.
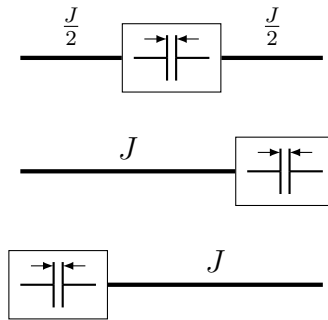
Figure 3.10: *Possible positions of a virtual torque sensor at a rigid shaft abstracted by a permanently engaged, fictitious clutch*
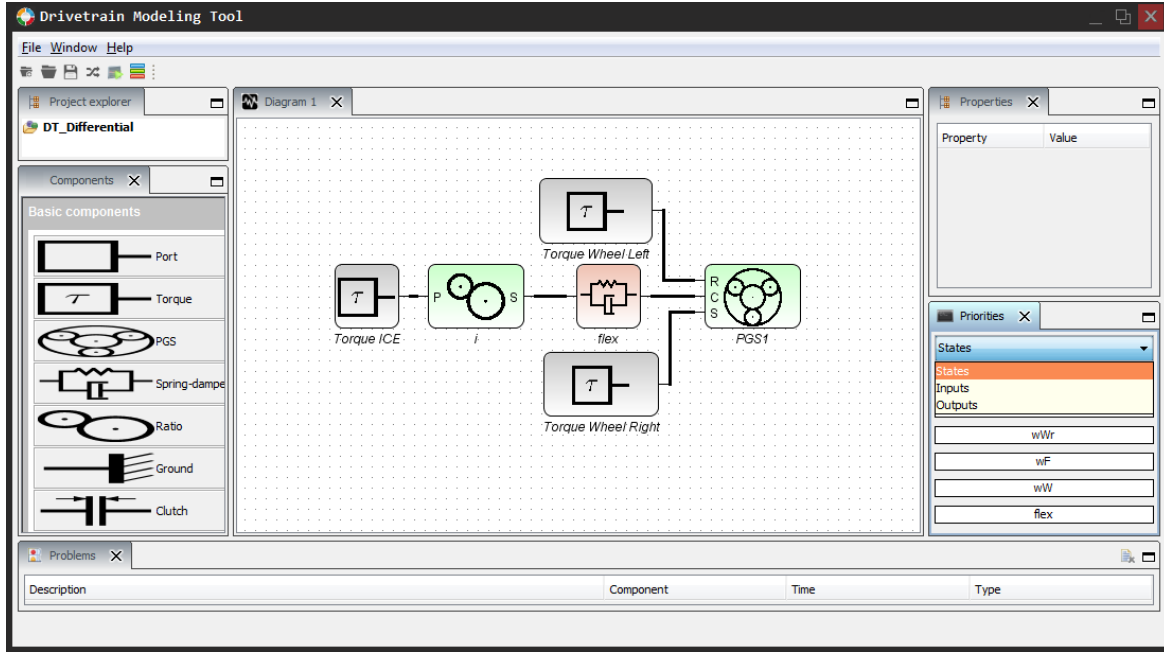
Figure 3.11: *DT modeling software with graphical user interface (**left:** modeling components, **center:** exemplary DT topology, **right top:** DT component properties, **right bottom:** priority lists)*

The mathematical consideration is already covered by (3.86), assuming that $\bar{\mathbf{M}} > 0$, which has now dimensions $(n_\mathrm{q} + n_\mathrm{ts}) \times (n_\mathrm{q} + n_\mathrm{ts})$, where n_ts is the number of torque sensors. Note that this condition may not be met although mechanical configuration is reasonable.

3.6 Automation of the modeling algorithm

Since the presented modeling approach features a modular and generic structure, its automation in a DT modeling software tool is self-evident. Therefore, a Java application has been implemented, which enables DT modeling for non-experts in the field of mechanical engineering. The implementation follows the separation of the modeling approach into abstraction and modeling algorithm (cf. Figure 3.4).

3.6.1 Graphical user interface

The abstraction step is handled by a user-friendly Graphical User Interface (GUI) (see Figure 3.11). Within this GUI the user defines the DT topology by dragging, dropping and connecting of modeling components. With respect to the set of modeling components defined in Section 3.3, it is reasonable to use the rigid shaft as connection between all the other components. Therefore, the rigid shaft is not explicitly available as modeling component (see Figure 3.11). A bold highlighting is used to illustrate the rigid shafts with inertia. The central information of this graphical abstraction process
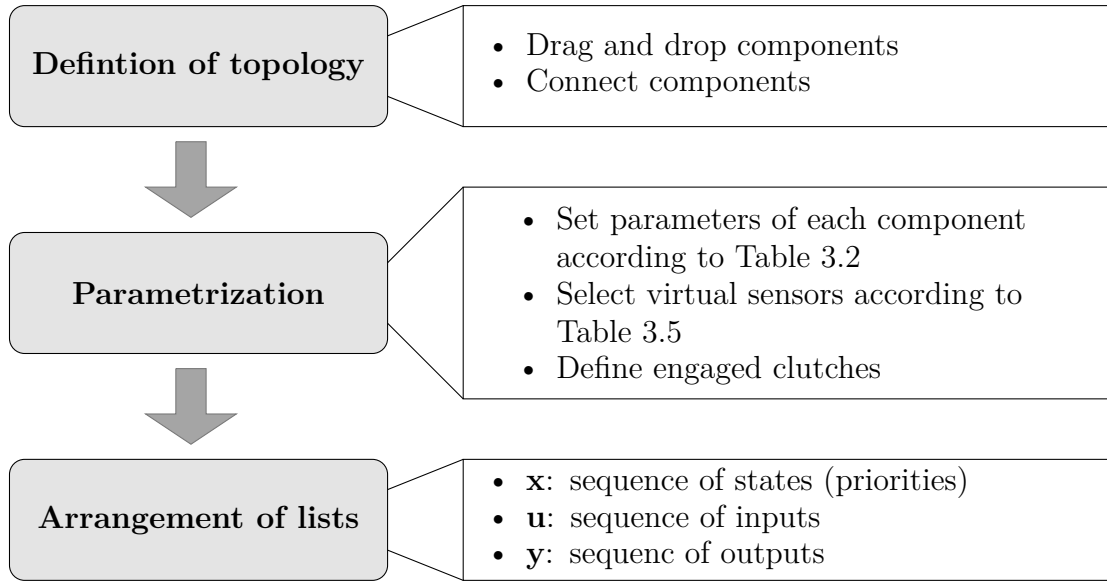
Figure 3.12: *Abstraction process of a DT in the GUI of the modeling software*

is the definition which port of which component is connected to which shaft. This information is stored in a list.

Each component or connection features specific properties, which are also listed in Table 3.2. In addition to these parameters some components provide the possibility to add specific virtual sensors according to Section 3.5.2 (see Table 3.5).

Table 3.5: *Sensors*

component	sensor
rigid shaft	rotational speed
flexible shaft	torsion
slipping clutch	differential rotational speed
locked clutch	locking torque

The component properties can be accessed and modified in a separated window of the GUI (see Figure 3.11).

The GUI provides three lists, which define the state vector **x** (state list), the input vector **u** (input list) and the output vector **y** (output list) and customize the order of elements in these vectors. While the input and output list just modify the order of columns in the matrices **B** and **D** respectively the order of rows in matrices **C** and **D**, the state list influences the final states **q** and model representation (cf. 3.4.3). Figure 3.12 summarizes the abstraction process using the GUI.

Inside the flowchart boxes and annotations:

Initialization
1) check if all ports are connected
2) initialize matrices according to (3.45)
   and the $\mathbf{x}, \mathbf{u}, \mathbf{y}$ list

Matrix composition
for each component
  if rigid shaft: $\rightarrow \tilde{\mathbf{M}}(3.11)$, $\tilde{\mathbf{A}}_{\mathrm{d}}(3.16)$
  if flexible shaft: $\rightarrow \tilde{\mathbf{M}}(3.11)$, $\tilde{\mathbf{A}}_{\mathrm{fs},i}(3.17)$
  if propulsion torque: $\rightarrow \tilde{\mathbf{B}}$ (section 3.4.1)
  if clutch: $\rightarrow \tilde{\mathbf{B}}$ (section 3.4.1),
          if engaged $\rightarrow \mathbf{J}_{\mathrm{f}}(3.67)$
  if connector: $\rightarrow \mathbf{J}_{\mathrm{f}}$: **if** ground (3.21)
                          if spur gear set (3.22)
                          if plan. gear set (3.30)

Nullspace computation
(3.38)

Matrix transformation
1) (3.42)
2) check if $\bar{\mathbf{M}}$ is regular

Output file (*.xls*)
- state vector $\mathbf{q}$, input vector $\mathbf{u}$, output vector $\mathbf{y}$
- symbolic matrices $\bar{\mathbf{M}}_i, \bar{\mathbf{A}}_i, \bar{\mathbf{B}}_i$ and state-space matrices $\mathbf{A}_i, \mathbf{B}_i$
- parameter list
- numeric matrices $\bar{\mathbf{M}}_i, \bar{\mathbf{A}}_i, \bar{\mathbf{B}}_i$ and state-space matrices $\mathbf{A}_i, \mathbf{B}_i$
- coordinate mapping $\mathbf{J}_{\mathrm{x},\mathrm{q}_i}$

***Figure 3.13:** Work flow of the modeling algorithm in the DT modeling software*

3.6.2 Implementation of the modeling algorithm

Due to the well-structured and modular modeling algorithm presented in Section 3.4, the algorithm has been implemented straight forward into the modeling software. Figure 3.13 summarizes the work flow of the algorithm. It produces an output in *.xls*-format.

3.6.3 Masked subsystems

The consideration of torque sensors in Section 3.5.2 suggest customizing the combination of arbitrary basic modeling components to encapsulated subsystems. To do
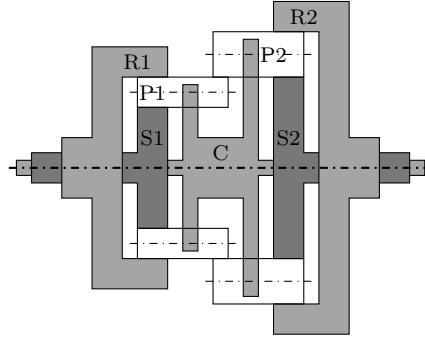
Figure 3.14: *Scheme of an exemplary Ravigneaux planetary gear set composition of a Ravigneaux gear set, featuring two PGSs with a common carrier and meshing planets.*
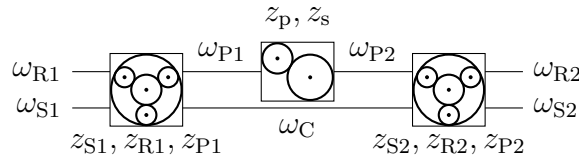
Figure 3.15: *Abstraction of a Ravigneaux gear set (cf. Figure 3.14) with basic modeling components*

so two adaptions in the software tool are necessary: First a new port component is introduced, which functions as interface to the subsystem. The second adaption enables masking of the component parameters used inside the subsystem. An example for the application of a subsystem is the modeling of a driving wheel, which converts the rotation of the driveshaft into translation of the vehicle. The driving wheel, with radius r_W, can be modeled by a spur gear set with the following parameter setting:

$$z_\mathrm{p} = r_\mathrm{W}, \tag{3.88}$$
$$z_\mathrm{s} = -1 \tag{3.89}$$

Another application of such a parameter masking can be used for simplified modeling of some combined PGSs, for example the extended Ravigneaux gear set. A Ravigneaux gear set features two PGSs with each one set of planets mounted on a common carrier. Additionally, the planets of the first and the second gear set are meshing. Figure 3.14 shows scheme of an exemplary Ravigneaux gear set composition. Figure 3.15 illustrates the abstraction of a Ravigneaux gear set using the basic modeling components: The gears wheels of the spur gear set are actually the planet gears of the PGSs:

$$z_\mathrm{P1} = z_\mathrm{p}, \tag{3.90}$$
$$z_\mathrm{P2} = z_\mathrm{s}.$$

The relations in (3.90) can be stated in the mask of the subsystem.
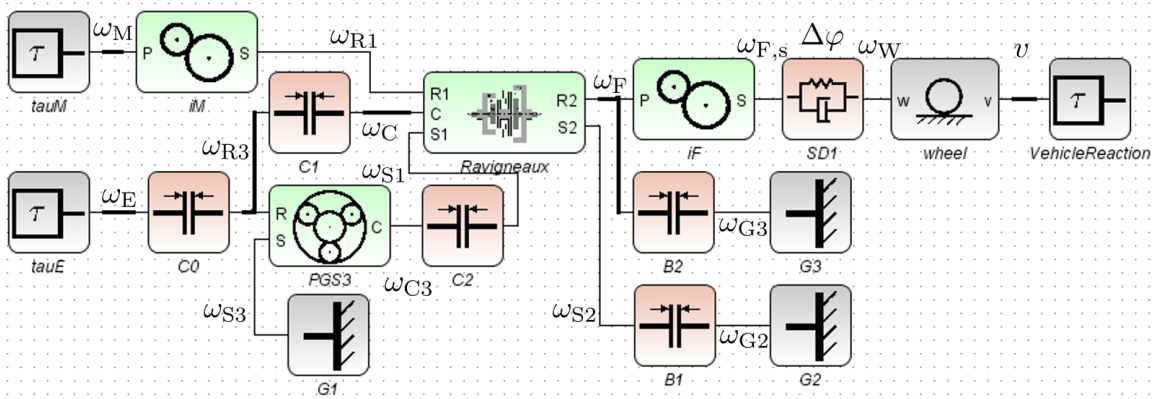
Figure 3.16: *Abstraction of the single-EM dedicated hybrid DT*

3.6.4 Example

The functionality of the modeling software is now demonstrated for exemplary dedicated hybrid DT. The considered topology (see [15]) is the single-EM dedicated hybrid DT, which is the actual object of research of this thesis. The modeling example restricts to the symbolic computations, since the numeric results feature less physical insight. Table 3.6 lists the modeling components which are needed to model this DT.

Table 3.6: *Modeling components and parameters for the exemplary single-EM dedicated hybrid DT*

components	number	parameters
flexible shaft	1	k, d
propulsion torque	3	
clutch	5	
ground	3	
spur gear set	2	$z_{M,p}, z_{M,s}, z_{F,p}, z_{F,s}$
planetary gear set	1	z_{S3}, z_{R3}, z_{P3}
wheel	1	r_W
Ravigneaux gear set	1	$z_{S1}, z_{R1}, z_{P1}, z_{S2}, z_{R2}, z_{P2}$

Two clutches are actually breaks, which are modeled by clutches with grounded secondary plate. One propulsion torque component is used to model the impact of an resistive force F_v acting on the vehicle due to for example rolling resistance, air drag, or road gradient. The implementation of the subsystems *Ravigneaux gear set* and *wheel* have been discussed in the last section. Figure 3.16 shows the arrangement of the components listed in Table 3.6. 15 rigid shafts are connecting the components. 6 of them are inert and damped. Table 3.7 lists the corresponding parameters.

Table 3.7: *Inert and damped, rigid shafts and corresponding parameters for the exemplary single-EM dedicated hybrid DT*

shaft	parameters
ω_{E}	$J_{\mathrm{E}}, d_{\mathrm{E}}$
ω_{R3}	$J_{\mathrm{R3}}, d_{\mathrm{R3}}$
ω_{M}	$J_{\mathrm{M}}, d_{\mathrm{M}}$
ω_{F}	$J_{\mathrm{F}}, d_{\mathrm{F}}$
v	m, d_{V}
ω_{C}	$J_{\mathrm{C}}, d_{\mathrm{C}}$

In combination with the flexible shaft a state vector with 16 elements is needed:

$$\mathbf{x} = \begin{bmatrix} \omega_{\mathrm{E}} & \omega_{\mathrm{R3}} & \omega_{\mathrm{M}} & \omega_{\mathrm{F}} & \Delta\varphi & v & \omega_{\mathrm{S1}} & \omega_{\mathrm{R1}} \dots \end{bmatrix} \tag{3.91}$$

$$\begin{bmatrix} \omega_{\mathrm{S2}} & \omega_{\mathrm{F,s}} & \omega_{\mathrm{C}} & \omega_{\mathrm{S3}} & \omega_{\mathrm{C3}} & \omega_{\mathrm{G2}} & \omega_{\mathrm{G3}} & \omega_{\mathrm{W}} \end{bmatrix}^{T}. \tag{3.92}$$

According to the 3 propulsion torque and 5 clutch components the input vector $\mathbf{u}$ is:

$$\mathbf{u} = \begin{bmatrix} \tau_{\mathrm{E}} & \tau_{\mathrm{M}} & F_{\mathrm{v}} & \tau_{\mathrm{C0}} & \tau_{\mathrm{C1}} & \tau_{\mathrm{C2}} & \tau_{\mathrm{B1}} & \tau_{\mathrm{B2}} \end{bmatrix}^{T} \tag{3.93}$$

$$\tag{3.94}$$

The rotational speeds of the ICE and the EM as well as the velocity of the vehicle are selected as output quantities:

$$\mathbf{y} = \begin{bmatrix} \omega_{\mathrm{E}} & \omega_{\mathrm{M}} & v \end{bmatrix}^{T}. \tag{3.95}$$

The required priorities of the elements in the vectors $\mathbf{x}$, $\mathbf{u}$ and $\mathbf{y}$ has already been considered in their definition.

The output of the DT modeling software is:

$$\mathbf{q} = \begin{bmatrix} \omega_{\mathrm{E}} & \omega_{\mathrm{R3}} & \omega_{\mathrm{M}} & \omega_{\mathrm{F}} & \Delta\varphi & v \end{bmatrix}^{T}. \tag{3.96}$$

$$\bar{\mathbf{M}} = \begin{bmatrix} J_{\mathrm{E}} & 0 & 0 & 0 & 0 & 0 \\ 0 & J_{\mathrm{R3}} & 0 & 0 & 0 & 0 \\ 0 & 0 & J_{\mathrm{C}}\frac{z_{\mathrm{M,p}}^{2}z_{\mathrm{R1}}^{2}}{z_{\mathrm{M,s}}^{2}(z_{\mathrm{R1}}+z_{\mathrm{R2}})^{2}} + J_{\mathrm{M}} & -J_{\mathrm{C}}\frac{z_{\mathrm{M,p}}z_{\mathrm{R1}}z_{\mathrm{R2}}}{z_{\mathrm{M,s}}^{2}(z_{\mathrm{R1}}+z_{\mathrm{R2}})^{2}} & 0 & 0 \\ 0 & 0 & -J_{\mathrm{C}}\frac{z_{\mathrm{M,p}}z_{\mathrm{R1}}z_{\mathrm{R2}}}{z_{\mathrm{M,s}}(z_{\mathrm{R1}}+z_{\mathrm{R2}})^{2}} & J_{\mathrm{C}}\frac{z_{\mathrm{R2}}^{2}}{(z_{\mathrm{R1}}+z_{\mathrm{R2}})^{2}} + J_{\mathrm{F}} & 0 & 0 \\ 0 & 0 & 0 & 0 & k & 0 \\ 0 & 0 & 0 & 0 & 0 & m \end{bmatrix} \tag{3.97}$$

$$\bar{\mathbf{A}} = \begin{bmatrix} -d_{\mathrm{E}} & 0 & 0 & 0 & 0 & 0 \\ 0 & -d_{\mathrm{R3}} & 0 & 0 & 0 & 0 \\ 0 & 0 & \frac{-d_{\mathrm{C}}z_{\mathrm{M,p}}^2 z_{\mathrm{R1}}^2}{z_{\mathrm{M,s}}^2 (z_{\mathrm{R1}}+z_{\mathrm{R2}})^2} + d_{\mathrm{M}} & \frac{d_{\mathrm{C}}z_{\mathrm{M,p}}z_{\mathrm{R1}}z_{\mathrm{R2}}}{z_{\mathrm{M,s}}(z_{\mathrm{R1}}+z_{\mathrm{R2}})^2} & 0 & 0 \\ 0 & 0 & \frac{d_{\mathrm{C}}z_{\mathrm{M,p}}z_{\mathrm{R1}}z_{\mathrm{R2}}}{z_{\mathrm{M,s}}(z_{\mathrm{R1}}+z_{\mathrm{R2}})^2} & \frac{-d_{\mathrm{C}}z_{\mathrm{R2}}^2}{(z_{\mathrm{R1}}+z_{\mathrm{R2}})^2} - d_{\mathrm{F}} - \frac{dz_{\mathrm{F,p}}^2}{z_{\mathrm{F,s}}^2} & k\frac{z_{\mathrm{F,p}}}{z_{\mathrm{F,s}}} & -d\frac{z_{\mathrm{F,p}}}{r_{\mathrm{W}}z_{\mathrm{F,s}}} \\ 0 & 0 & 0 & -k\frac{z_{\mathrm{F,p}}}{z_{\mathrm{F,s}}} & 0 & -\frac{k}{r_{\mathrm{W}}} \\ 0 & 0 & 0 & -d\frac{z_{\mathrm{F,p}}}{r_{\mathrm{W}}z_{\mathrm{F,s}}} & \frac{k}{r_{\mathrm{W}}} & -\frac{d}{r_{\mathrm{W}}^2} - d_{\mathrm{V}} \end{bmatrix}$$

$$(3.98)$$

$$\bar{\mathbf{B}} = \begin{bmatrix} 1 & 0 & 0 & -1 & 0 & 0 & 0 & 0 \\ 0 & 0 & 0 & 1 & -1 & \frac{-z_{\mathrm{R3}}}{z_{\mathrm{R3}}+z_{\mathrm{S3}}} & 0 & 0 \\ 0 & 1 & 0 & 0 & \frac{-z_{\mathrm{M,p}}z_{\mathrm{R1}}}{z_{\mathrm{M,s}}(z_{\mathrm{R1}}+z_{\mathrm{R2}})} & \frac{z_{\mathrm{M,p}}z_{\mathrm{R1}}(z_{\mathrm{R2}}-z_{\mathrm{S1}})}{z_{\mathrm{M,s}}z_{\mathrm{S1}}(z_{\mathrm{R1}}+z_{\mathrm{R2}})} & \frac{z_{\mathrm{M,p}}z_{\mathrm{R1}}(z_{\mathrm{R2}}+z_{\mathrm{S2}})}{z_{\mathrm{M,s}}z_{\mathrm{S2}}(z_{\mathrm{R1}}+z_{\mathrm{R2}})} & 0 \\ 0 & 0 & 0 & 0 & \frac{z_{\mathrm{R2}}}{z_{\mathrm{R2}}+z_{\mathrm{S2}}} & \frac{z_{\mathrm{R2}}(z_{\mathrm{R1}}+z_{\mathrm{S1}})}{z_{\mathrm{S1}}(z_{\mathrm{R1}}+z_{\mathrm{R2}})} & \frac{z_{\mathrm{R2}}(z_{\mathrm{R1}}-z_{\mathrm{S2}})}{z_{\mathrm{S2}}(z_{\mathrm{R1}}+z_{\mathrm{R2}})} & 1 \\ 0 & 0 & 0 & 0 & 0 & 0 & 0 & 0 \\ 0 & 0 & 1 & 0 & 0 & 0 & 0 & 0 \end{bmatrix}$$

$$(3.99)$$

The illustration of the final state-space matrices $\mathbf{A}$ and $\mathbf{B}$ is omitted due to the size of the symbolic expressions in the matrix elements.

3.7 Plant model for mode operation

At the end of this chapter the linear DT models computed by the introduced modeling software tool shall be extended by control output equation to state plant models for later control purpose. While this section covers the plant models for mode operation, the next section will consider the mode transition and hence a plant model for gear shifting.

The impact of a set of engaged clutches on the DT's dynamics has already been discussed in Section 3.5.1. To simplify the notation, the symbols Σ and $\Sigma_{\boldsymbol{\kappa}_i}$ are introduced, as proposed in [34]. They denote the dynamical system with disengaged clutches,

$$\Sigma : \bar{\mathbf{M}}\dot{\mathbf{q}} = \bar{\mathbf{A}}\mathbf{q} + \bar{\mathbf{B}}\mathbf{u}, \tag{3.100}$$

respectively, the dynamical system, which considers a set of engaged clutches as defined by the binary clutch state vector $\boldsymbol{\kappa}_i$,

$$\Sigma_{\boldsymbol{\kappa}_i} : \bar{\mathbf{M}}_i\dot{\mathbf{q}}_i = \bar{\mathbf{A}}_i\mathbf{q}_i + \bar{\mathbf{B}}_i\mathbf{u}. \tag{3.101}$$

According to Section 2.5 there are two quantities of interest for control of mode operation: the torque at the driving wheel τ_{W}, in order to ensure the DT's drivability, and the mode specific hybrid DoF λ in order to ensure fuel efficiency. These two quantities shall be now stated as control output equations.

As discussed in Section 3.5.2, the torque at a shaft can be modeled considering the locking torque of a fictitious, engaged clutch. Hence, the wheel torque τ_{W} can be

computed with (3.85). If the rotational speed of the driving wheels is an element of the state vector $\mathbf{q}_i$, which can always be ensured by assigning high priority to his state, equivalently this torque can be calculated with:

$$y_{i,\mathrm{P}} = \tau_{\mathrm{W}} = \underbrace{\mathbf{e}_{\mathrm{W}}^T \mathbf{J}_{\mathrm{q},\mathrm{q}_i} \bar{\mathbf{A}}_i}_{\mathbf{c}_{i,\mathrm{P}}^T} \mathbf{q}_i + \underbrace{\mathbf{e}_{\mathrm{W}}^T \mathbf{J}_{\mathrm{q},\mathrm{q}_i} \bar{\mathbf{B}}_i}_{\mathbf{d}_{i,\mathrm{P}}^T} \mathbf{u}, \tag{3.102}$$

which delivers the first control output. Vector $\mathbf{e}_{\mathrm{W}}$ selects the rotational speed of the driving wheels from state vector $\mathbf{q}$:

$$\mathbf{e}_{\mathrm{W}}^T \mathbf{q} = \omega_{\mathrm{W}}. \tag{3.103}$$

The second control output $y_{i,\lambda,\mathrm{mode}}$ concerns the mode-specific hybrid DoF λ:

$$y_{i,\lambda,\mathrm{mode}} = \lambda = \mathbf{c}_{i,\lambda,\mathrm{mode}}^T \mathbf{q}_i + \mathbf{d}_{i,\lambda,\mathrm{mode}}^T \mathbf{u}. \tag{3.104}$$

Table 3.8 lists the mode specific output equations, with respect to the hybrid DoFs. For electric, conventional and hybrid CVT mode, these equations are simply the selection of the rotational speeds of ICE or EM from state the vector $\mathbf{q}$, denoted by the selection vectors $\mathbf{e}_{\mathrm{E}}$ and $\mathbf{e}_{\mathrm{M}}$:

$$\mathbf{e}_{\mathrm{E}}^T \mathbf{q} = \omega_{\mathrm{E}}, \quad \mathbf{e}_{\mathrm{M}}^T \mathbf{q} = \omega_{\mathrm{M}}. \tag{3.105}$$

The output equation for hybrid parallel mode, concerning the torque split factor follows from (2.2):

$$\mu = \frac{P_{\mathrm{E}}}{P_{\mathrm{E}} + P_{\mathrm{M}}} = \frac{\omega_{\mathrm{E}} \tau_{\mathrm{E}}}{\omega_{\mathrm{E}} \tau_{\mathrm{E}} + \omega_{\mathrm{M}} \tau_{\mathrm{M}}} = \frac{\omega_{\mathrm{E}} \tau_{\mathrm{E}}}{\omega_{\mathrm{E}} \tau_{\mathrm{E}} + \omega_{\mathrm{E}} \frac{i_{\mathrm{M}}}{i_{\mathrm{E}}} \tau_{\mathrm{M}}} = \frac{\tau_{\mathrm{E}}}{\tau_{\mathrm{E}} + \frac{i_{\mathrm{M}}}{i_{\mathrm{E}}} \tau_{\mathrm{M}}} \tag{3.106}$$

It is actually a non-linear output equation with respect to the input vector $\mathbf{u}$.

Table 3.8: Mode specific output equations with respect to the hybrid DoFs

Mode	abbr.	λ	$\mathbf{c}_{i,\lambda,\mathrm{mode}}^T$	$\mathbf{d}_{i,\lambda,\mathrm{mode}}^T \mathbf{u}$
electric	El	ω_{E}	$\mathbf{e}_{\mathrm{E}}^T \mathbf{J}_{\mathrm{q},\mathrm{q}_i}$	$\mathbf{0}$
conventional	Co	ω_{M}	$\mathbf{e}_{\mathrm{M}}^T \mathbf{J}_{\mathrm{q},\mathrm{q}_i}$	$\mathbf{0}$
hybrid CVT	CV	ω_{E}	$\mathbf{e}_{\mathrm{E}}^T \mathbf{J}_{\mathrm{q},\mathrm{q}_i}$	$\mathbf{0}$
hybrid parallel	Pa	μ	$\mathbf{0}$	$\frac{\tau_{\mathrm{E}}}{\tau_{\mathrm{E}} + \frac{i_{\mathrm{M}}}{i_{\mathrm{E}}} \tau_{\mathrm{M}}}$

With (3.101), consequently, the plant model for control of the mode operation phase can be written in a general from:

Plant models for mode operation control:

$$\Sigma_{\boldsymbol{\kappa}_i}^{\mathrm{mode}} : \quad \bar{\mathbf{M}}_i \dot{\mathbf{q}}_i = \bar{\mathbf{A}}_i \mathbf{q}_i + \bar{\mathbf{B}}_i \mathbf{u}$$

$$\mathbf{y}_{i,\mathrm{mode}} = \begin{bmatrix} y_{i,\mathrm{P}} \\ y_{i,\lambda,\mathrm{mode}} \end{bmatrix} = \begin{bmatrix} \mathbf{c}_{i,\mathrm{P}}^T \\ \mathbf{c}_{i,\lambda,\mathrm{mode}}^T \end{bmatrix} \mathbf{q}_i + \begin{bmatrix} \mathbf{d}_{i,\mathrm{P}}^T \\ \mathbf{d}_{i,\lambda,\mathrm{mode}}^T \end{bmatrix} \mathbf{u} \tag{3.107}$$

For sake of completeness also a plant model for control of the charge mode shall be given:

$$\Sigma_{\boldsymbol{\kappa}_i}^{\mathrm{Ch}} \quad \bar{\mathbf{M}}_i \dot{\mathbf{q}}_i = \bar{\mathbf{A}}_i \mathbf{q}_i + \bar{\mathbf{B}}_i \mathbf{u} \tag{3.108}$$

$$\mathbf{y}_{i,\mathrm{Ch}} = \begin{bmatrix} y_{i,\mathrm{Ch},\omega} \\ y_{i,\mathrm{Ch},\tau} \end{bmatrix} = \begin{bmatrix} \mathbf{e}_{\mathrm{E}}^T \mathbf{J}_{\mathrm{q},\mathrm{q}_i} \\ \mathbf{0} \end{bmatrix} \mathbf{q}_i + \begin{bmatrix} \mathbf{0} \\ \mathbf{e}_{\mathbf{u},\mathrm{E}}^T \end{bmatrix} \mathbf{u}, \tag{3.109}$$

where the vector $\mathbf{e}_{\mathbf{u},\mathrm{E}}$ selects the ICE torque in input vector $\mathbf{u}$:

$$\mathbf{e}_{\mathbf{u},\mathrm{E}}^T \mathbf{u} = \tau_{\mathrm{E}}. \tag{3.110}$$

In charge mode there is no control output concerning the wheel torque, since it can not be controlled in this mode. The two control outputs $y_{i,\mathrm{Ch},\omega}$ and $y_{i,\mathrm{Ch},\tau}$ are used to control the charging power and efficiency of ICE, while charging.

3.8 Plant model for mode transition

Gear shifting is the general process of engaging or disengaging one or several clutches. According to (3.101) a general gear shift from a clutch state $\boldsymbol{\kappa}_i$ to another clutch state $\boldsymbol{\kappa}_j$ ($\boldsymbol{\kappa}_i \to \boldsymbol{\kappa}_j$), hence, can be modeled by the following switching LTI system:

$$\Sigma_{\boldsymbol{\kappa}_i \to \boldsymbol{\kappa}_j} = \begin{cases} \Sigma_{\boldsymbol{\kappa}_i} & \text{for} \quad \boldsymbol{\kappa} = \boldsymbol{\kappa}_i, \\ \Sigma_{\boldsymbol{\kappa}_j} & \text{for} \quad \boldsymbol{\kappa} = \boldsymbol{\kappa}_j. \end{cases} \tag{3.111}$$

Figure 3.17 illustrates the relations to the system Σ according to (3.67) and (3.68).
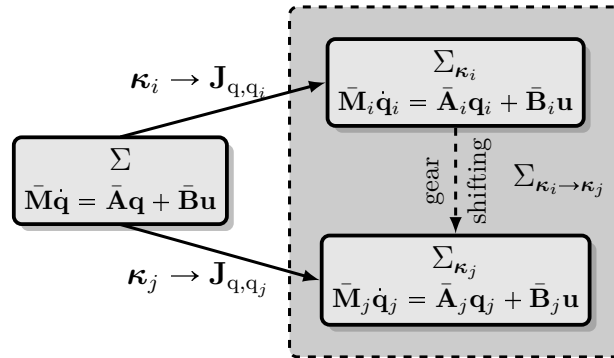
Figure 3.17: *Switched LTI model for a general gear shift $\boldsymbol{\kappa}_i \to \boldsymbol{\kappa}_j$*

The Σ-notation is based on the general notation of hybrid dynamical systems, which has been applied to hybrid drivetrains in [58].

The clutches, which change their state during the shift, are determined by the binary vector $\Delta\boldsymbol{\kappa}_{ij}$:

$$\Delta\boldsymbol{\kappa}_{ij} := \boldsymbol{\kappa}_i \veebar \boldsymbol{\kappa}_j. \tag{3.112}$$

A special gear shift occurs if,

$$\Delta\boldsymbol{\kappa}_{ij}^T \Delta\boldsymbol{\kappa}_{ij} = 1. \tag{3.113}$$

In this case only one single clutch state is changed. This kind of gear shift is of special interest, since an arbitrary gear shift can always be split into a series of these shifts. Therefore, they are referred to as elementary gear shifts. The concept of smooth and lossless gear shifting in single-EM dedicated hybrid DTs exclusively applies to elementary gear shifts. This is due to the fact that it is in general not possible to avoid dissipation in more than one clutch, while simultaneously maintain drivability, with two propulsion torques.

3.8.1 Smooth and lossless clutch transitions

In order to further investigate the concept of smooth and lossless gear shifting, at this point the transitions between the locked and released clutch states (clutch engagement and disengagement) and their impact on drivability and efficiency are considered in detail:

Clutch engagement: When engaging a clutch, the current in the coil (i_{C}) of the valve is increased until the clutch transitions into locked state. According to [15] the condition for this transition is:

$$\Delta\omega_{\mathrm{C}} = 0 \quad \wedge \quad \tau_{\mathrm{C,lk}} < \tau_{\mathrm{C,sl}}. \tag{3.114}$$

$\tau_{\mathrm{C,lk}}$ is the locking torque that would be transmitted, if the clutch was in locked state. It is a function of the states $\mathbf{q}$ and inputs $\mathbf{u}$:

$$\tau_{\mathrm{C,lk}} = f(\mathbf{q}, \mathbf{u}). \tag{3.115}$$

$\tau_{\mathrm{C,sl}}$ is the slipping torque according to the clutch slip and the pressure on the clutch plates:

$$\tau_{\mathrm{C,sl}} = \mathrm{sign}(\Delta\omega_{\mathrm{C}})\mu_{\mathrm{kin}}f(i_{\mathrm{C}}). \tag{3.116}$$

For clutch engagement $f(i_{\mathrm{C}}(t))$ can be assumed to be a monotonically increasing function. μ_{kin} is the kinetic friction coefficient of the clutch plate surface.

Since the power $P_{\mathrm{C,diss}}$, which is dissipated in the slipping clutch, is

$$P_{\mathrm{C,diss}} = \Delta\omega_{\mathrm{C}}\tau_{\mathrm{C,sl}}, \tag{3.117}$$

the only possibility to avoid dissipation is to reach $\Delta\omega_{\mathrm{C}} = 0$, before engaging the clutch.

> **Lossless clutch engagement:**
>
> The clutch has to be fully synchronized ($\Delta\omega_{\mathrm{C}} = 0$), before the engagement is initiated ($i_{\mathrm{C}} \uparrow$).

Clutch disengagement: The upper limit for the torque transmitted in a locked clutch $\bar{\tau}_{\mathrm{C,lk}}$ is given by

$$\bar{\tau}_{\mathrm{C,lk}} = \mu_{\mathrm{stat}} f(i_{\mathrm{C}}), \tag{3.118}$$

where μ_{stat} is the static friction coefficient of the clutch plate surface. If $\tau_{\mathrm{C,lk}}$ exceeds this limit,

$$\tau_{\mathrm{C,lk}} > \bar{\tau}_{\mathrm{C,lk}}, \tag{3.119}$$

the clutch transitions to slipping state, with slipping torque:

$$\tau_{\mathrm{C,sl}} = \mu_{\mathrm{kin}} f(i_{\mathrm{C}}). \tag{3.120}$$

This always causes a torque step, since $\mu_{\mathrm{kin}} < \mu_{\mathrm{stat}}$. Due to the assumption that $f(i_{\mathrm{C}})$ is a monotonically increasing function, the avoidance of this step is only possible for $\tau_{\mathrm{C,lk}} = 0$, before the clutch is fully disengaged $i_{\mathrm{C}} \to 0$. Furthermore, this avoids slipping of the clutch after the transition and, consequently, dissipation according to (3.117).

> **Smooth clutch disengagement:**
>
> The clutch has to be fully unloaded $(\tau_{\mathrm{C,lk}} = 0)$, before the disengagement is initiated $(i_{\mathrm{C}} \downarrow)$.

Figure 3.18 summarizes the conditions for smooth and lossless clutch engagement.
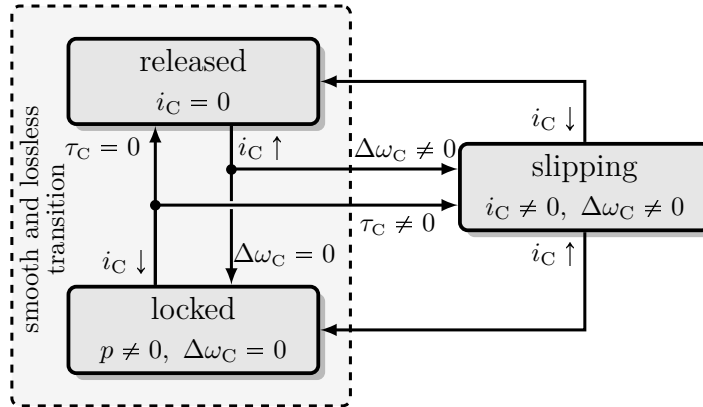

Figure 3.18: *Smooth and lossless clutch transitions*

3.8.2 Output equations for the control of smooth and lossless gear shifts

With the above consideration the control variables for controlling a smooth and lossless clutch engagement $(\Delta\omega_{\mathrm{C}})$ respectively disengagement $(\tau_{\mathrm{C,lk}})$ are fixed. They are equivalent to the clutch sensor outputs, which have been discussed in Section 3.5.2. Hence, equation (3.86) can be used to provide a full plant model for control of elementary, smooth and lossless gear shifts. The corresponding output equations are now stated for clutch engagement and disengagement:

Clutch engagement:

$$\Delta \boldsymbol{\kappa}_{ij}^T \Delta \boldsymbol{\kappa}_{ij} = 1 \quad \text{and} \quad \boldsymbol{\kappa}_i^T \boldsymbol{\kappa}_i < \boldsymbol{\kappa}_j^T \boldsymbol{\kappa}_j. \tag{3.121}$$

From (3.62) follows:

Output equation for lossless clutch engagement:

$$y_{ij,\mathrm{C,lk}} := \Delta \omega_{\mathrm{C},ij} = \Delta \boldsymbol{\kappa}_{ij}^T \Delta \boldsymbol{\omega}_{\mathrm{C}} = \Delta \boldsymbol{\kappa}_{ij}^T \bar{\mathbf{B}}_{i,\mathrm{C}}^T \mathbf{q}_i = \mathbf{c}_{ij,\mathrm{lk}}^T \mathbf{q}_i. \tag{3.122}$$

Clutch disengagement:

$$\Delta \boldsymbol{\kappa}_{ij}^T \Delta \boldsymbol{\kappa}_{ij} = 1 \quad \text{and} \quad \boldsymbol{\kappa}_i^T \boldsymbol{\kappa}_i > \boldsymbol{\kappa}_j^T \boldsymbol{\kappa}_j. \tag{3.123}$$

From (3.85) follows:

Output equation for smooth clutch disengagement:

$$y_{ij,\mathrm{C,rl}} := \tau_{\mathrm{C,lk},ij} = - \left[\Delta \boldsymbol{\kappa}_{ij}^T \bar{\mathbf{B}}_{j,\mathrm{C}}^T \bar{\mathbf{M}}_j^{-1} \bar{\mathbf{B}}_{j,\mathrm{C}} \Delta \boldsymbol{\kappa}_{ij} \right]^{-1} \Delta \boldsymbol{\kappa}_{ij}^T \bar{\mathbf{B}}_{j,\mathrm{C}}^T \bar{\mathbf{M}}_j^{-1} \dots$$
$$\left[\bar{\mathbf{A}}_j \mathbf{J}_{\mathrm{q}_j,\mathrm{q}_i} \mathbf{q}_i + \bar{\mathbf{B}}_{j,\mathrm{P}} \boldsymbol{\tau}_{\mathrm{P}} + \bar{\mathbf{B}}_{j,\mathrm{C}}(\bar{\boldsymbol{\kappa}}_i) \boldsymbol{\tau}_{\mathrm{C,sl}} \right] = \mathbf{c}_{ij,\mathrm{rl}}^T \mathbf{q}_i + \mathbf{d}_{ij,\mathrm{rl}}^T \mathbf{u}. \tag{3.124}$$

The output definitions in (3.122), (3.124) and (3.102) complete the plant models for controlling the preparation of a smooth and lossless gear shift for both cases (releasing and locking a clutch), notated by the symbols $\Sigma_{\boldsymbol{\kappa}_i}^{\boldsymbol{\kappa}_{j,\mathrm{lk}}}$ and $\Sigma_{\boldsymbol{\kappa}_i}^{\boldsymbol{\kappa}_{j,\mathrm{rl}}}$:

Plant models for mode transition control:

$$\Sigma_{\boldsymbol{\kappa}_i}^{\boldsymbol{\kappa}_{j,\mathrm{lk}}} : \quad \bar{\mathbf{M}}_i \dot{\mathbf{q}}_i = \bar{\mathbf{A}}_i \mathbf{q}_i + \bar{\mathbf{B}}_i \mathbf{u}$$
$$\mathbf{y}_{ij} = \begin{bmatrix} y_{i,\mathrm{P}} \\ y_{ij,\mathrm{C,lk}} \end{bmatrix} = \begin{bmatrix} \mathbf{c}_{i,\mathrm{P}}^T \\ \mathbf{c}_{ij,\mathrm{lk}}^T \end{bmatrix} + \begin{bmatrix} \mathbf{d}_{i,\mathrm{P}}^T \\ \mathbf{d}_{ij,\mathrm{lk}}^T \end{bmatrix} \tag{3.125}$$

$$\Sigma_{\boldsymbol{\kappa}_i}^{\boldsymbol{\kappa}_{j,\mathrm{rl}}} : \quad \bar{\mathbf{M}}_i \dot{\mathbf{q}}_i = \bar{\mathbf{A}}_i \mathbf{q}_i + \bar{\mathbf{B}}_i \mathbf{u}$$
$$\mathbf{y}_{ij} = \begin{bmatrix} y_{i,\mathrm{P}} \\ y_{ij,\mathrm{C,rl}} \end{bmatrix} = \begin{bmatrix} \mathbf{c}_{i,\mathrm{P}}^T \\ \mathbf{c}_{ij,\mathrm{rl}}^T \end{bmatrix} + \begin{bmatrix} \mathbf{d}_{i,\mathrm{P}}^T \\ \mathbf{d}_{ij,\mathrm{rl}}^T \end{bmatrix} \tag{3.126}$$

3.9 Model extensions and application

In [15] a generic, real-time DT model is proposed. It extends an LTI kernel by a non-linear system, which detects the clutch transitions. It furthermore contributes an real-time DT observer. This observer can be applied in order to track the transitions of the switched LTI model in (3.111). The generic-real-time model in [15] also includes peripheral models, which model the possibly non-linear and dynamic behavior of several PT components (cf. Section 2.1), which are not considered in this chapter:

- ICE model
- EM model
- Hydraulic clutch model
- Hydrodynamic torque converter model
- Longitudinal vehicle model

Furthermore, it proposes a model generalization to include non-linear effects like:

- Non-linear spring behavior
- Gear wheel clearance
- Tire-road-interaction

The generic, real-time DT model in [15] is also one major application of the modeling approach proposed in this chapter, since it relies on an LTI kernel, modeling the DT mechanics. The real-time model can be applied in various MiL, SiL an HiL simulation and validation environments. Furthermore, it is the basis for a generic real-time DT observer, which has to be parametrized. Although in [15] a model parametrization tool is proposed, this tool suffers from some drawbacks, which already have been discussed in Section 3.1. The DT modeling approach and in consequence the modeling software tool presented in this chapter overcomes these drawbacks and hence raises the contributions of [15].

3.10 Summary and contribution

This chapter presents a generic and modular modeling approach for automotive DTs. The approach is based on a compact set of comprehensible modeling components and follows Lagrange formalism. It uses a coordinate partitioning method to determine a set of generalized coordinates.

The presented modeling approach overcomes some limitations of state-of-the-art approaches and frameworks, namely:

- It provides a model in comprehensible state-space representation.
- It is applicable to all common geared automotive DTs, and hence to all modes of a single-EM dedicated hybrid DT.
- It tackles complex kinematics of arbitrary combined PGSs.

The modeling approach features high potential for automation and hence it is implemented in a DT modeling software tool with a GUI. This tool enables DT modeling for non-experts in the field of mechanical engineering. The state-space models computed by the software tool can be used directly for various validation scenarios, like MiL, SiL or HiL simulations. Furthermore, it simplifies the parametrization of extended models and model-based software components like DT control systems and real-time observers (e.g. in [15]). In summary, the modeling approach contributes the support of the DT development process in general.

The modeling approach lays the basis for the model-based analysis and control approaches in the next chapters of this thesis. A switching LTI model for gear shifting

is proposed. Furthermore, control variables for the control of smooth and lossless gear shifting have been stated.

Model-based drivetrain analysis

Chapter 3 provides the computation of a comprehensible model to each clutch state of a given DT. This chapter presents a model-based method, which automates the analysis of these DT models. The method starts with the assignment of operation modes to all possible clutch state vectors. Based on this assignment, gear ratios are computed. In combination with a given ICE and EM and vehicle data this enables the computation of possible traction forces in the single gears. Subsequently, the shiftability of the DT is investigated, including the potential for smooth and lossless gear shifting.

4.1 Motivation and problem statement

To motivate the content of this chapter, it is necessary to recall the central objective of this thesis, stated at the end of Chapter 2: *Development of model-based approaches to improve drivability and efficiency of DT control systems, with a special focus on control of gear shifting.*

To this general objective the last chapter contributes a mathematical model Σ in (3.100), which models the dynamics of a given DT topology. Furthermore, the impact of a set of engaged clutches to this model, $\Sigma_{\boldsymbol{\kappa}_i}$ (3.101), has been investigated. Finally, a model for gear shifting, $\Sigma_{\boldsymbol{\kappa}_i \to \boldsymbol{\kappa}_j}$ in (3.111), has been proposed. Based on these contributions, several questions arise, which define the problem statement of this chapter:

Problem statement:

A model-based analysis method shall be applied to answer the following questions, based on a given DT model Σ and ICE, EM and vehicle data:

- Which clutch state vectors $\boldsymbol{\kappa}_i$ are of interest for the operation of the DT?
- How does each of these clutch states vectors $\boldsymbol{\kappa}_i$ contribute to the drivability of the DT, considering specific ICE, EM and vehicle data?
- Which gear shifts $\boldsymbol{\kappa}_i \rightarrow \boldsymbol{\kappa}_j$ are possible and hence of interest to improve drivability and efficiency?
- Which gear shifts $\boldsymbol{\kappa}_i \rightarrow \boldsymbol{\kappa}_j$ feature a potential for smooth and lossless gear shifting?

The problem statement is furthermore illustrated in Figure 4.1. In order to tackle the

input **method** **output**

- Σ
- ICE, EM & vehicle data

Model-based DT analysis

- Gears
- Drivability
- Shifts
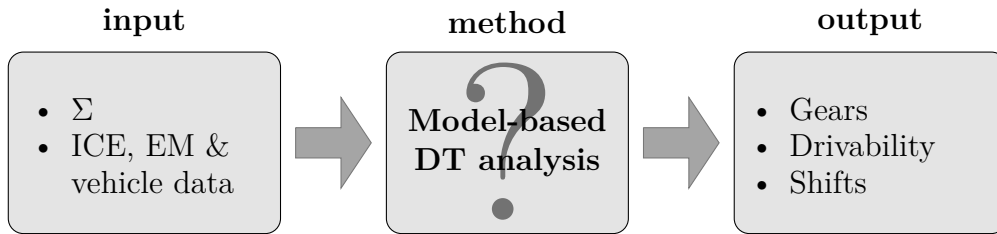
***Figure 4.1:** Problem statement: Model-based DT analysis*

problem statement the chapter is structured as follows.

- **Gear analysis:** In a first step the relation of specific clutch state vector $\boldsymbol{\kappa}_i$ to the mode characteristic according to Table 2.1 is investigated.
- **Traction force analysis:** Based on step one and specific ICE, EM and vehicle data, the drivability of single gears as well as the DT's overall drivability is considered.
- **Shift analysis:** Finally, the shifting opportunities between the gears, including the potential for smooth and lossless gear shifts, are represented graphically and possible shift sequences are determined.

The exemplary single-EM dedicated hybrid DT introduced in Chapter 3, will be used to illustrate the single analysis steps.

The answers to the above questions are essential for the design of a model-based control system, but also of interest for DT control and in DT topology development. The computations, which are covered by the model-based DT analysis method, are usually done by mechanical engineers based on the DT construction sheets. This work requires expertise and experience in order to keep both time effort and error rate in acceptable ranges. The proposed automated method does not target on replacing, but on optimally supporting this state-of-the-art development process. Furthermore, the results of the analysis method are essential for EMS development, see Chapter 2.5. Hence, also the second stage of the single-EM dedicated hybrid DTs development process is supported.

4.2 Gear analysis

The gear analysis targets on the assignment of a specific operation mode characteristic to a specific dynamic system $\Sigma_{\boldsymbol{\kappa}_i}$. To do so, in a first step the kinematics of all possible modes of a single-EM dedicated hybrid DT listed in Table 2.1 will be investigated.

4.2.1 Theoretical basis

The information of interest is the kinematic relation between the rotational speeds of input and output shafts, namely ICE shaft (ω_E), EM shaft (ω_M) and the final transmission output shaft (w_F). For this investigation a simplified DT, which features exclusively these three shafts, is considered (see Figure 4.2). The conclusions made on this simplified consideration will be generalized afterwards.

$$\tau_E, \omega_E, J_E \underbrace{\qquad} \quad \tau_M, \omega_M, J_M \quad \boxed{\bar{\mathbf{B}}_C(\boldsymbol{\kappa}_i)^T \mathbf{q} = \mathbf{0}} \quad \tau_F, w_F, J_F$$
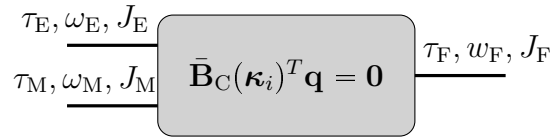
Figure 4.2: *Simplified DT model for gear analysis*

The dynamic model of the simplified DT can be stated easily, according to Chapter 3:

$$\underbrace{\begin{bmatrix} J_F & 0 & 0 \\ 0 & J_E & 0 \\ 0 & 0 & J_M \end{bmatrix}}_{\bar{\mathbf{M}}} \underbrace{\begin{bmatrix} \dot{\omega}_F \\ \dot{\omega}_E \\ \dot{\omega}_M \end{bmatrix}}_{\dot{\mathbf{q}}} = \underbrace{\begin{bmatrix} \tau_F \\ \tau_E \\ \tau_M \end{bmatrix}}_{\mathbf{u}} \tag{4.1}$$

As illustrated in Figure 4.2, the motion of the three shafts is now constrained according to a set of engaged clutches. Different constraints,

$$\bar{\mathbf{B}}_C(\boldsymbol{\kappa}_i)^T \mathbf{q} = \mathbf{0}, \tag{4.2}$$

yield different coordinate mappings $\mathbf{J}_{q,q_i}$,

$$\mathbf{q} = \mathbf{J}_{q,q_i} \mathbf{q}_i \quad \text{with:} \quad \mathbf{J}_{q,q_i} := \left(\mathbf{E}_{\mathcal{N}\left(\bar{\mathbf{B}}_C(\boldsymbol{\kappa}_i)^T \right)^T} \right)^T . \tag{4.3}$$

The mappings can be uniquely assigned to the operation modes in Table 2.1. Table 4.1 summarizes this assignment, listening the constraints and the resulting mappings. The constraints are given in normalized form. A constant multiplier for the rows in $\bar{\mathbf{B}}_C(\boldsymbol{\kappa}_i)^T$ does not influence the mapping $\mathbf{J}_{q,q_i}$. These basic kinematic relations between the rotational speeds of the input and output shafts also occur in the general case of an arbitrary single-EM dedicated hybrid DT.

Table 4.1: *Mode specific kinematics*

	mode	$\bar{\mathbf{B}}_{\mathrm{C}}(\boldsymbol{\kappa}_i)^T$	$\mathbf{J}_{\mathrm{q},\mathrm{q}_i}$	$\mathbf{q}_i$	w_{F}
0	neutral	$\begin{bmatrix} & \end{bmatrix}$	$\begin{bmatrix} 1 & 0 & 0 \\ 0 & 1 & 0 \\ 0 & 0 & 1 \end{bmatrix}$	$\begin{bmatrix} w_{\mathrm{F}} \\ \omega_{\mathrm{E}} \\ \omega_{\mathrm{M}} \end{bmatrix}$	w_{F}
1.1	charge neutral	$\begin{bmatrix} 0 & 1 & -\frac{1}{i_{\mathrm{M}}} \end{bmatrix}$	$\begin{bmatrix} 1 & 0 \\ 0 & 1 \\ 0 & i_{\mathrm{M}} \end{bmatrix}$	$\begin{bmatrix} w_{\mathrm{F}} \\ \omega_{\mathrm{E}} \end{bmatrix}$	w_{F}
1.2	charge blocked	$\begin{bmatrix} 1 & 0 & 0 \\ 0 & 1 & -\frac{1}{i_{\mathrm{M}}} \end{bmatrix}$	$\begin{bmatrix} 0 \\ 1 \\ i_{\mathrm{M}} \end{bmatrix}$	ω_{E}	0
2	electric	$\begin{bmatrix} 1 & 0 & -\frac{1}{i_{\mathrm{M}}} \end{bmatrix}$	$\begin{bmatrix} 1 & 0 \\ 0 & 1 \\ i_{\mathrm{M}} & 0 \end{bmatrix}$	$\begin{bmatrix} w_{\mathrm{F}} \\ \omega_{\mathrm{E}} \end{bmatrix}$	$\frac{1}{i_{\mathrm{M}}}\omega_{\mathrm{M}}$
3	conv	$\begin{bmatrix} 1 & -\frac{1}{i_{\mathrm{E}}} & 0 \end{bmatrix}$	$\begin{bmatrix} 1 & 0 \\ i_{\mathrm{E}} & 0 \\ 0 & 1 \end{bmatrix}$	$\begin{bmatrix} w_{\mathrm{F}} \\ \omega_{\mathrm{M}} \end{bmatrix}$	$\frac{1}{i_{\mathrm{E}}}\omega_{\mathrm{E}}$
4	hyb. par	$\begin{bmatrix} 1 & -\frac{1}{i_{\mathrm{E}}} & 0 \\ 1 & 0 & -\frac{1}{i_{\mathrm{M}}} \end{bmatrix}$	$\begin{bmatrix} 1 \\ i_{\mathrm{E}} \\ i_{\mathrm{M}} \end{bmatrix}$	w_{F}	$\frac{1}{i_{\mathrm{E}}}\omega_{\mathrm{E}} = \frac{1}{i_{\mathrm{M}}}\omega_{\mathrm{M}}$
5	hyb. CVT	$\begin{bmatrix} 1 & -\frac{1}{i_{\mathrm{E}}} & -\frac{1}{i_{\mathrm{M}}} \end{bmatrix}$	$\begin{bmatrix} 1 & 0 \\ 0 & 1 \\ i_{\mathrm{M}} & -\frac{i_{\mathrm{M}}}{i_{\mathrm{E}}} \end{bmatrix}$	$\begin{bmatrix} w_{\mathrm{F}} \\ \omega_{\mathrm{E}} \end{bmatrix}$	$\frac{1}{i_{\mathrm{E}}}\omega_{\mathrm{E}} + \frac{1}{i_{\mathrm{M}}}\omega_{\mathrm{M}}$

4.2.2 Analysis method

In order to assign operation modes and clutch states, two information from the DT model Σ in (3.100) are necessary:

- clutch input matrix $\bar{\mathbf{B}}_{\mathrm{C}}$
- position $k_{\mathrm{F}}, k_{\mathrm{E}}, k_{\mathrm{M}}$ of the rotational speeds $w_{\mathrm{F}}, \omega_{\mathrm{E}}, \omega_{\mathrm{M}}$ in the state vector $\mathbf{q}$.

First the coordinate mappings $\mathbf{J}_{\mathrm{q},\mathrm{q}_i}$ due to all possible clutch states $\boldsymbol{\kappa}_i$ have to be computed. In a second step a matrix $\bar{\mathbf{J}}_{\mathrm{q},\mathrm{q}_i}$ selecting the rows and columns of $\mathbf{J}_{\mathrm{q},\mathrm{q}_i}$ corresponding to the input and output shafts with,

$$\begin{aligned} q_{k_{\mathrm{F}}} &= w_{\mathrm{F}}, & q_{k_{\mathrm{E}}} &= \omega_{\mathrm{E}}, & q_{k_{\mathrm{M}}} &= \omega_{\mathrm{M}}, \\ q_{i,k_{\mathrm{F}}} &= w_{\mathrm{F}}, & q_{i,k_{\mathrm{E}}} &= \omega_{\mathrm{E}}, & q_{i,k_{\mathrm{M}}} &= \omega_{\mathrm{M}}, \end{aligned} \tag{4.4}$$

is defined:

$$\begin{bmatrix} \cdots & q_{i,k_{\mathrm{F}}} & \cdots & q_{i,k_{\mathrm{E}}} & \cdots & q_{i,k_{\mathrm{M}}} & \cdots \end{bmatrix}$$

$$\begin{bmatrix} \vdots \\ q_{k_{\mathrm{F}}} \\ \vdots \\ q_{k_{\mathrm{E}}} \\ \vdots \\ q_{k_{\mathrm{M}}} \\ \vdots \end{bmatrix} \begin{matrix} \\ \rightarrow \\ \\ \rightarrow \\ \\ \rightarrow \\ \end{matrix} \begin{bmatrix} \vdots & \vdots & \vdots \\ \cdots & k_1 & \cdots & k_4 & \cdots & k_7 & \cdots \\ \vdots & \vdots & \vdots \\ \cdots & k_2 & \cdots & k_5 & \cdots & k_8 & \cdots \\ \vdots & \vdots & \vdots \\ \cdots & k_3 & \cdots & k_6 & \cdots & k_9 & \cdots \\ \vdots & \vdots & \vdots \end{bmatrix}, \tag{4.5}$$

$$\bar{\mathbf{J}}_{\mathrm{q,q}_i} := \begin{bmatrix} k_1 & k_4 & k_7 \\ k_2 & k_5 & k_8 \\ k_3 & k_6 & k_9 \end{bmatrix}. \tag{4.6}$$

Note that while $q_{k_{\mathrm{E}}}, q_{k_{\mathrm{M}}}$ can be assumed to exist, they possibly vanish when the system is transformed into generalized coordinates. Hence, $q_{i,k_{\mathrm{E}}}$ or $q_{i,k_{\mathrm{M}}}$, or both, may not exist. In this case the selection of columns in (4.5) is skipped. Therefore, the matrix elements $k_4, \ldots, k_9$ may be empty, which consequently yields matrices $\bar{\mathbf{J}}_{\mathrm{q,q}_i}$ of different matrix dimensions.

The assignment of an operation mode to a matrix $\bar{\mathbf{J}}_{\mathrm{q,q}_i}$, finally is done by comparing its non-zero elements to the matrices $\mathbf{J}_{\mathrm{q,q}_i}$ in Table 4.1. This comparison, simultaneously determines the corresponding gear ratios $(i_{\mathrm{E}}, i_{\mathrm{M}})$. A clutch state vector $\boldsymbol{\kappa}_i$, for which $\bar{\mathbf{J}}_{\mathrm{q,q}_i}$ can not be matched to any $\bar{\mathbf{J}}_{\mathrm{q,q}_i}$, does not feature any operational functionality, since Table 4.1 is complete for single-EM dedicated hybrid DTs.

Once this assignment has been done for all clutch states, it is common to introduce a unique gear naming with respect to the operation mode and decreasing gear ratios. The results of the gear analysis method can be represented in a so-called gear table. In summary such a gear table includes the following information:

Gear table

Information for each gear:
- clutch state vector $\boldsymbol{\kappa}_i$
- operation mode
- gear ratios
- unique identifier

Figure 4.3 gives an overview of the presented gear analysis method.

4.2.3 Example

The gear analysis method is now applied to the exemplary single-EM dedicated hybrid DT. The assignment of operation modes is done exemplarily for two different clutch
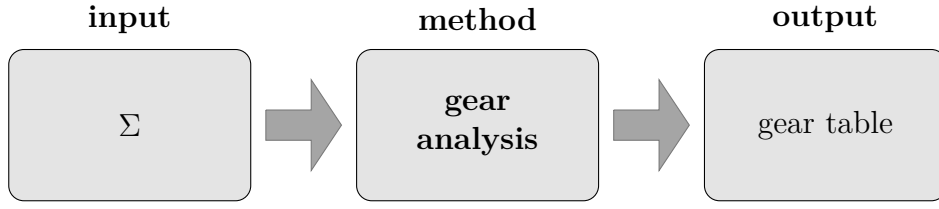
Figure 4.3: Overview – gear analysis

state vectors. The clutch input matrix from (3.99) is:

$$\bar{\mathbf{B}}_{\mathrm{C}} = \begin{bmatrix} -1 & 0 & 0 & 0 & 0 \\ 1 & -1 & \frac{-z_{\mathrm{R3}}}{z_{\mathrm{R3}}+z_{\mathrm{S3}}} & 0 & 0 \\ 0 & \frac{z_{\mathrm{M,p}}z_{\mathrm{R1}}}{z_{\mathrm{M,s}}(z_{\mathrm{R1}}+z_{\mathrm{R2}})} & \frac{z_{\mathrm{M,p}}z_{\mathrm{R1}}(z_{\mathrm{S1}}-z_{\mathrm{R2}})}{z_{\mathrm{S1}}z_{\mathrm{M,s}}(z_{\mathrm{R1}}+z_{\mathrm{R2}})} & \frac{-z_{\mathrm{M,p}}z_{\mathrm{R1}}(z_{\mathrm{R2}}+z_{\mathrm{S2}})}{z_{\mathrm{S2}}z_{\mathrm{M,s}}(z_{\mathrm{R1}}+z_{\mathrm{R2}})} & 0 \\ 0 & \frac{z_{\mathrm{R2}}}{z_{\mathrm{R2}}+z_{\mathrm{S2}}} & \frac{z_{\mathrm{R2}}(z_{\mathrm{R1}}+z_{\mathrm{S1}})}{z_{\mathrm{S1}}(z_{\mathrm{R1}}+z_{\mathrm{R2}})} & \frac{z_{\mathrm{R2}}(z_{\mathrm{R1}}-z_{\mathrm{S2}})}{z_{\mathrm{S2}}(z_{\mathrm{R1}}+z_{\mathrm{R2}})} & 1 \\ 0 & 0 & 0 & 0 & 0 \\ 0 & 0 & 0 & 0 & 0 \end{bmatrix}. \tag{4.7}$$

The corresponding state vector $\mathbf{q}$ is:

$$\mathbf{q} = \begin{bmatrix} \omega_{\mathrm{E}} & \omega_{\mathrm{R3}} & \omega_{\mathrm{M}} & w_{\mathrm{F}} & \Delta\varphi & v \end{bmatrix}^{T}. \tag{4.8}$$

At first $\bar{\mathbf{B}}_{\mathrm{C}}$ is rearranged according to

$$\bar{\mathbf{q}} = \begin{bmatrix} w_{\mathrm{F}} & \omega_{\mathrm{E}} & \omega_{\mathrm{M}} & \omega_{\mathrm{R3}} & \Delta\varphi & v \end{bmatrix}^{T}: \tag{4.9}$$

$$\bar{\mathbf{B}}_{\mathrm{C}} = \begin{bmatrix} 0 & \frac{z_{\mathrm{R2}}}{z_{\mathrm{R2}}+z_{\mathrm{S2}}} & \frac{z_{\mathrm{R2}}(z_{\mathrm{R1}}+z_{\mathrm{S1}})}{z_{\mathrm{S1}}(z_{\mathrm{R1}}+z_{\mathrm{R2}})} & \frac{z_{\mathrm{R2}}(z_{\mathrm{R1}}-z_{\mathrm{S2}})}{z_{\mathrm{S2}}(z_{\mathrm{R1}}+z_{\mathrm{R2}})} & 1 \\ -1 & 0 & 0 & 0 & 0 \\ 0 & \frac{z_{\mathrm{M,p}}z_{\mathrm{R1}}}{z_{\mathrm{M,s}}(z_{\mathrm{R1}}+z_{\mathrm{R2}})} & \frac{z_{\mathrm{M,p}}z_{\mathrm{R1}}(z_{\mathrm{S1}}-z_{\mathrm{R2}})}{z_{\mathrm{S1}}z_{\mathrm{M,s}}(z_{\mathrm{R1}}+z_{\mathrm{R2}})} & \frac{-z_{\mathrm{M,p}}z_{\mathrm{R1}}(z_{\mathrm{R2}}+z_{\mathrm{S2}})}{z_{\mathrm{S2}}z_{\mathrm{M,s}}(z_{\mathrm{R1}}+z_{\mathrm{R2}})} & 0 \\ 1 & -1 & \frac{-z_{\mathrm{R3}}}{z_{\mathrm{R3}}+z_{\mathrm{S3}}} & 0 & 0 \\ 0 & 0 & 0 & 0 & 0 \\ 0 & 0 & 0 & 0 & 0 \end{bmatrix}. \tag{4.10}$$

Hence, the corresponding shaft indices are:

$$k_{\mathrm{F}} = 1, \quad k_{\mathrm{E}} = 2, \quad k_{\mathrm{M}} = 3. \tag{4.11}$$

This rearrangement is necessary in order to assign priorities to the shafts similar to the simplified DT above ($k_{\mathrm{F}} < k_{\mathrm{E}} < k_{\mathrm{M}}$). The first considered clutch state is:

$$\boldsymbol{\kappa}_1 = \begin{bmatrix} 1 & 1 & 0 & 0 & 0 \end{bmatrix}. \tag{4.12}$$

The corresponding coordinate mapping,

$$\mathbf{J}_{\mathrm{q},\mathrm{q}_1} = \begin{bmatrix} 1 & 0 & 0 & 0 \\ 0 & 1 & 0 & 0 \\ \frac{z_{\mathrm{M,s}}z_{\mathrm{R2}}}{z_{\mathrm{M,p}}z_{\mathrm{R1}}} & \frac{-z_{\mathrm{M,s}}(z_{\mathrm{R1}}+z_{\mathrm{R2}})}{z_{\mathrm{M,p}}z_{\mathrm{R1}}} & 0 & 0 \\ 0 & 1 & 0 & 0 \\ 0 & 0 & 1 & 0 \\ 0 & 0 & 0 & 1 \end{bmatrix}, \tag{4.13}$$

defines a vector of generalized coordinates $\mathbf{q}_1$:

$$\mathbf{q}_1 = \begin{bmatrix} w_\mathrm{F} & \omega_\mathrm{E} & \Delta\varphi & v \end{bmatrix}^T, \tag{4.14}$$

with,

$$q_{1,k_\mathrm{F}} = q_{1,1}, \quad q_{1,k_\mathrm{E}} = q_{1,2}, \quad q_{1,k_\mathrm{M}} = [\ ]. \tag{4.15}$$

According to (4.11) and (4.15) the first three rows of the first two columns of $\mathbf{J}_{\mathrm{q},\mathrm{q}_i}$ compose $\bar{\mathbf{J}}_{\mathrm{q},\mathrm{q}_1}$:

$$\bar{J}_{\mathrm{q},\mathrm{q}_1} = \begin{bmatrix} 1 & 0 \\ 0 & 1 \\ \dfrac{z_\mathrm{M,s} z_\mathrm{R2}}{z_\mathrm{M,p} z_\mathrm{R1}} & \dfrac{-z_\mathrm{M,s}(z_\mathrm{R1}+z_\mathrm{R2})}{z_\mathrm{M,p} z_\mathrm{R1}} \end{bmatrix}. \tag{4.16}$$

The comparison with Table 4.1 shows that with clutch state $\boldsymbol{\kappa}_1$ the DT operates in a hybrid CVT mode. The corresponding ratios are:

$$i_\mathrm{E} = \frac{z_\mathrm{R2}}{z_\mathrm{R1} + z_\mathrm{R2}}, \quad i_\mathrm{M} = \frac{z_\mathrm{M,s} z_\mathrm{R2}}{z_\mathrm{M,p} z_\mathrm{R1}}. \tag{4.17}$$

The second exemplary clutch state is:

$$\boldsymbol{\kappa}_2 = \begin{bmatrix} 1 & 1 & 0 & 1 & 0 \end{bmatrix}. \tag{4.18}$$

The corresponding coordinate mapping,

$$\mathbf{J}_{\mathrm{q},\mathrm{q}_2} = \begin{bmatrix} 1 & 0 & 0 \\ \dfrac{z_\mathrm{R2}}{z_\mathrm{R2}+z_\mathrm{S2}} & 0 & 0 \\ \dfrac{z_\mathrm{M,s} z_\mathrm{R2}(z_\mathrm{S2}-z_\mathrm{R1})}{z_\mathrm{M,p} z_\mathrm{R1}(z_\mathrm{R2}+z_\mathrm{S2})} & 0 & 0 \\ \dfrac{z_\mathrm{R2}}{z_\mathrm{R2}+z_\mathrm{S2}} & 0 & 0 \\ 0 & 1 & 0 \\ 0 & 0 & 1 \end{bmatrix}, \tag{4.19}$$

defines a state vector $\mathbf{q}_2$:

$$\mathbf{q}_2 = \begin{bmatrix} w_\mathrm{F} & \Delta\varphi & v \end{bmatrix}^T, \tag{4.20}$$

with,

$$q_{2,k_\mathrm{F}} = q_{1,1}, \quad q_{2,k_\mathrm{E}} = [\ ], \quad q_{2,k_\mathrm{M}} = [\ ]. \tag{4.21}$$

According to (4.11) and 4.21 the mapping $\bar{J}_{\mathrm{q},\mathrm{q}_2}$ consist of the first three rows and of the first columns of $J_{\mathrm{q},\mathrm{q}_2}$:

$$\bar{\mathbf{J}}_{\mathrm{q},\mathrm{q}_2} = \begin{bmatrix} 1 \\ \dfrac{z_\mathrm{R2}}{z_\mathrm{R2}+z_\mathrm{S2}} \\ \dfrac{z_\mathrm{M,s} z_\mathrm{R2}(z_\mathrm{S2}-z_\mathrm{R1})}{z_\mathrm{M,p} z_\mathrm{R1}(z_\mathrm{R2}+z_\mathrm{S2})} \end{bmatrix} \tag{4.22}$$

Table 4.2: *Symbolic gear table for the exemplary single-EM dedicated hybrid DT*

$\boldsymbol{\kappa}$	mode	i_{E}	i_{M}
$\begin{bmatrix}0 & 0 & 0 & 0 & 0\end{bmatrix}$	neutral	0	0
$\begin{bmatrix}0 & 0 & 0 & 1 & 0\end{bmatrix}$	electric	0	$-\frac{z_{\mathrm{M,s}}z_{\mathrm{R2}}(z_{\mathrm{R1}}-z_{\mathrm{S2}})}{z_{\mathrm{M,p}}z_{\mathrm{R1}}(z_{\mathrm{R2}}+z_{\mathrm{S2}})}$
$\begin{bmatrix}0 & 0 & 1 & 0 & 0\end{bmatrix}$	neutral	0	0
$\begin{bmatrix}0 & 0 & 1 & 1 & 0\end{bmatrix}$	electric	0	$-\frac{z_{\mathrm{M,s}}z_{\mathrm{R2}}(z_{\mathrm{R1}}-z_{\mathrm{S2}})}{z_{\mathrm{M,p}}z_{\mathrm{R1}}(z_{\mathrm{R2}}+z_{\mathrm{S2}})}$
$\begin{bmatrix}0 & 1 & 0 & 0 & 0\end{bmatrix}$	neutral	0	0
$\begin{bmatrix}0 & 1 & 0 & 1 & 0\end{bmatrix}$	electric	0	$-\frac{z_{\mathrm{M,s}}z_{\mathrm{R2}}(z_{\mathrm{R1}}-z_{\mathrm{S2}})}{z_{\mathrm{M,p}}z_{\mathrm{R1}}(z_{\mathrm{R2}}+z_{\mathrm{S2}})}$
$\begin{bmatrix}0 & 1 & 1 & 0 & 0\end{bmatrix}$	electric	0	$-\frac{z_{\mathrm{M,s}}z_{\mathrm{R2}}(z_{\mathrm{R1}}z_{\mathrm{R3}}+z_{\mathrm{R1}}z_{\mathrm{S3}}+z_{\mathrm{S1}}z_{\mathrm{S3}})}{z_{\mathrm{M,p}}z_{\mathrm{R1}}(z_{\mathrm{R2}}z_{\mathrm{R3}}+z_{\mathrm{R2}}z_{\mathrm{S3}}-z_{\mathrm{S1}}z_{\mathrm{S3}})}$
$\begin{bmatrix}1 & 0 & 0 & 0 & 0\end{bmatrix}$	neutral	0	0
$\begin{bmatrix}1 & 0 & 0 & 1 & 0\end{bmatrix}$	electric	0	$-\frac{z_{\mathrm{M,s}}z_{\mathrm{R2}}(z_{\mathrm{R1}}-z_{\mathrm{S2}})}{z_{\mathrm{M,p}}z_{\mathrm{R1}}(z_{\mathrm{R2}}+z_{\mathrm{S2}})}$
$\begin{bmatrix}1 & 0 & 1 & 0 & 0\end{bmatrix}$	CVT	$\frac{z_{\mathrm{R2}}(z_{\mathrm{R1}}+z_{\mathrm{S1}})(z_{\mathrm{R3}}+z_{\mathrm{S3}})}{z_{\mathrm{R3}}z_{\mathrm{S1}}(z_{\mathrm{R1}}+z_{\mathrm{R2}})}$	$-\frac{z_{\mathrm{M,s}}z_{\mathrm{R2}}(z_{\mathrm{R1}}+z_{\mathrm{S1}})}{z_{\mathrm{M,p}}z_{\mathrm{R1}}(z_{\mathrm{R2}}-z_{\mathrm{S1}})}$
$\begin{bmatrix}1 & 0 & 1 & 0 & 1\end{bmatrix}$	charge	1	$\frac{z_{\mathrm{R3}}z_{\mathrm{S1}}z_{\mathrm{M,s}}(z_{\mathrm{R1}}+z_{\mathrm{R2}})}{z_{\mathrm{M,p}}z_{\mathrm{R1}}(z_{\mathrm{R3}}+z_{\mathrm{S3}})(z_{\mathrm{R2}}-z_{\mathrm{S1}})}$
$\begin{bmatrix}1 & 0 & 1 & 1 & 0\end{bmatrix}$	Parallel	$\frac{z_{\mathrm{R2}}(z_{\mathrm{R3}}+z_{\mathrm{S3}})(z_{\mathrm{S1}}+z_{\mathrm{S2}})}{z_{\mathrm{R3}}z_{\mathrm{S1}}(z_{\mathrm{R2}}+z_{\mathrm{S2}})}$	$-\frac{z_{\mathrm{M,s}}z_{\mathrm{R2}}(z_{\mathrm{R1}}-z_{\mathrm{S2}})}{z_{\mathrm{M,p}}z_{\mathrm{R1}}(z_{\mathrm{R2}}+z_{\mathrm{S2}})}$
$\begin{bmatrix}1 & 1 & 0 & 0 & 0\end{bmatrix}$	CVT	$\frac{z_{\mathrm{R2}}}{z_{\mathrm{R1}}+z_{\mathrm{R2}}}$	$\frac{z_{\mathrm{M,s}}z_{\mathrm{R2}}}{z_{\mathrm{M,p}}z_{\mathrm{R1}}}$
$\begin{bmatrix}1 & 1 & 0 & 0 & 1\end{bmatrix}$	charge	1	$-\frac{z_{\mathrm{M,s}}(z_{\mathrm{R1}}+z_{\mathrm{R2}})}{z_{\mathrm{M,p}}z_{\mathrm{R1}}}$
$\begin{bmatrix}1 & 1 & 0 & 1 & 0\end{bmatrix}$	Parallel	$\frac{z_{\mathrm{R2}}}{z_{\mathrm{R2}}+z_{\mathrm{S2}}}$	$\frac{z_{\mathrm{M,s}}z_{\mathrm{R2}}(z_{\mathrm{S2}}-z_{\mathrm{R1}})}{z_{\mathrm{M,p}}z_{\mathrm{R1}}(z_{\mathrm{R2}}+z_{\mathrm{S2}})}$
$\begin{bmatrix}1 & 1 & 1 & 0 & 0\end{bmatrix}$	Parallel	$\frac{z_{\mathrm{R2}}(z_{\mathrm{R3}}+z_{\mathrm{S3}})}{z_{\mathrm{R2}}z_{\mathrm{R3}}+z_{\mathrm{R2}}z_{\mathrm{S3}}-z_{\mathrm{S1}}z_{\mathrm{S3}}}$	$-\frac{z_{\mathrm{M,s}}z_{\mathrm{R2}}(z_{\mathrm{R1}}z_{\mathrm{R3}}+z_{\mathrm{R1}}z_{\mathrm{S3}}+z_{\mathrm{S1}}z_{\mathrm{S3}})}{z_{\mathrm{M,p}}z_{\mathrm{R1}}(z_{\mathrm{R2}}z_{\mathrm{R3}}+z_{\mathrm{R2}}z_{\mathrm{S3}}-z_{\mathrm{S1}}z_{\mathrm{S3}})}$

The comparison with Table 4.1 reveals that the DT operates in a hybrid parallel mode, if $\boldsymbol{\kappa}_2$ is engaged, with:

$$i_{\mathrm{E}} = \frac{z_{\mathrm{R2}}}{z_{\mathrm{R2}} + z_{\mathrm{S2}}}, \quad i_{\mathrm{M}} = \frac{z_{\mathrm{M,s}}z_{\mathrm{R2}}\left(z_{\mathrm{S2}} - z_{\mathrm{R1}}\right)}{z_{\mathrm{M,p}}z_{\mathrm{R1}}\left(z_{\mathrm{R2}} + z_{\mathrm{S2}}\right)}. \tag{4.23}$$

The gear analysis is now applied to all $2^{n_{\mathrm{c}}} = 2^5 = 32$ clutch states of the DT. The gear table 4.2 lists symbolic results. A closer look at Table 4.2 shows that the electric modes according to the clutch states, $\begin{bmatrix}0 & 0 & 0 & 1 & 0\end{bmatrix}$, $\begin{bmatrix}0 & 0 & 1 & 1 & 0\end{bmatrix}$, $\begin{bmatrix}0 & 1 & 0 & 1 & 0\end{bmatrix}$ and $\begin{bmatrix}1 & 0 & 0 & 1 & 0\end{bmatrix}$ feature the same ratio i_{M}. The missing 16 clutch states lead to blocked DT kinematics without any functionality. Table 4.3 summarizes the operation modes of the exemplary single-EM dedicated hybrid DT. Evaluating the symbolic ratios in Table 4.3, with the parameter values listed in Table 4.5, a unique identifier can be assigned to every gear of the exemplary single-EM dedicated hybrid DT (see

Table 4.3: *Overview on the amount of different operation modes of the exemplary single-EM dedicated hybrid DT*

mode	number
neutral	4
charge	2
electric	2 (5)
conventional	0
hybrid parallel	3
hybrid CVT	2
blocked	16

Table 4.4). To distinguish different gears with an identical operation mode parameters, the identifier is extended by lower case letters in alphabetic order.

Table 4.4: *Numeric gear table for the exemplary single-EM dedicated hybrid DT*

κ	mode	identifier	i_E	i_M
$\begin{bmatrix} 0 & 0 & 0 & 0 & 0 \end{bmatrix}$	neutral	Na	0	0
$\begin{bmatrix} 0 & 0 & 1 & 0 & 0 \end{bmatrix}$	neutral	Nb	0	0
$\begin{bmatrix} 0 & 1 & 0 & 0 & 0 \end{bmatrix}$	neutral	Nc	0	0
$\begin{bmatrix} 1 & 0 & 0 & 0 & 0 \end{bmatrix}$	neutral	Nd	0	0
$\begin{bmatrix} 1 & 0 & 1 & 0 & 1 \end{bmatrix}$	charge	Ch1	1	-2.131
$\begin{bmatrix} 1 & 1 & 0 & 0 & 1 \end{bmatrix}$	charge	Ch2	1	3.843
$\begin{bmatrix} 0 & 1 & 1 & 0 & 0 \end{bmatrix}$	electric	E1	0	2.661
$\begin{bmatrix} 0 & 0 & 0 & 1 & 0 \end{bmatrix}$	electric	E2a	0	0.658
$\begin{bmatrix} 0 & 0 & 1 & 1 & 0 \end{bmatrix}$	electric	E2b	0	0.658
$\begin{bmatrix} 0 & 1 & 0 & 1 & 0 \end{bmatrix}$	electric	E2c	0	0.658
$\begin{bmatrix} 1 & 0 & 0 & 1 & 0 \end{bmatrix}$	electric	E2d	0	0.658
$\begin{bmatrix} 1 & 0 & 1 & 1 & 0 \end{bmatrix}$	parallel	Pa1	2.112	0.658
$\begin{bmatrix} 1 & 1 & 1 & 0 & 0 \end{bmatrix}$	parallel	Pa2	1.172	2.661
$\begin{bmatrix} 1 & 1 & 0 & 1 & 0 \end{bmatrix}$	parallel	Pa3	0.651	0.658
$\begin{bmatrix} 1 & 0 & 1 & 0 & 0 \end{bmatrix}$	CVT	CV1	2.421	5.160
$\begin{bmatrix} 1 & 1 & 0 & 0 & 0 \end{bmatrix}$	CVT	CV2	0.480	-1.842

Table 4.5: *Number of teeth of the exemplary single-EM dedicated hybrid DT*

parameter	value
$z_{M,p}$	-29^{1}
$z_{M,s}$	58
$z_{F,p}$	$-17 \cdot 51^{2}$
$z_{F,s}$	$69 \cdot 58$
z_{S1}	37
z_{P1}	26
z_{R1}	89
z_{S2}	44
z_{P2}	19
z_{R2}	82
z_{S3}	41
z_{P3}	22
z_{R3}	85

4.3 Traction force analysis

The stationary traction force is a common characteristic to evaluate the drivability in automotive DTs. It states in stationary case the maximum traction force available at the driving wheels in specific gears for given ICE, EM and vehicle data. The graphical representation of the stationary traction force in dependency of the vehicle speed is called Traction Force Diagram (TFD) – see for example [18, pp. 10]. A trained look at a TFD gives a fast overview on for example maximum vehicle speeds and road gradients in specific gears. In summary, it enables a simple and intuitive evaluation of the vehicle's overall drivability. Hence, it is an important and common tool for the design of DTs ([18, pp. 39]). Figure 2.2 in Chapter 2 schematically shows a TFD.

4.3.1 Theoretical basis

In order to assemble a complete TFD, in this section the mode specific determination of stationary traction forces is investigated in detail for a general single-EM dedicated hybrid DT. To do so, first the general static torque relations in a simplified DT, see Figure 4.4, are considered similar to the determination of mode kinematics in the Section 4.2. The impact of a set of engaged clutches $\boldsymbol{\kappa}_i$ on the dynamical system in (4.1) is already well investigated:

$$\mathbf{J}_{q,q_i}^{T} \bar{\mathbf{M}} \mathbf{J}_{q,q_i} \dot{\mathbf{q}}_i = \mathbf{J}_{q,q_i}^{T} \mathbf{u}. \tag{4.24}$$

---

[1]The sign of $z_{M,p}$ is negative, due to an intermediate gear wheel in the corresponding spur gear set implementation.

[2]The sign of $z_{F,p}$ is negative, since the corresponding spur gear set features a two stage implementation.
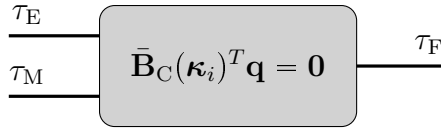
Figure 4.4: *Simplified DT model for the static torque consideration*

Requiring a static case in the sense of,

$$\dot{\mathbf{q}} \overset{!}{=} \mathbf{0}, \tag{4.25}$$

yields a set of algebraic equations on the input torques τ_E, τ_M, τ_F:

$$\mathbf{J}_{q,q_i}^T \mathbf{u} = \mathbf{0}. \tag{4.26}$$

Similar to the consideration of constraints with respect to the rotational speeds, a transformation to generalized torques $\mathbf{u}_i$ can be introduced:

$$\mathbf{u} = \mathbf{J}_{u,u_i}\mathbf{u}_i, \tag{4.27}$$

with:

$$\mathbf{J}_{u,u_i} := \left(\mathbf{E}_{\mathcal{N}\left(\mathbf{J}_{q,q_i}^T\right)^T} \right)^T. \tag{4.28}$$

In analogy to the mappings $\mathbf{J}_{q,q_i}$ in the last section, $\mathbf{J}_{u,u_i}$ states the torque on the final transmission output shaft τ_F, due to the input torques in static case, for a specific operation mode. Table 4.6 lists the mappings $\mathbf{J}_{u,u_i}$ and the resulting ratios for all operation modes in Table 4.1. As the mappings in (4.28) are in direct relation to the mappings $\mathbf{J}_{q,q_i}$, the computation of the resulting final transmission output torque, for a general single-EM dedicated hybrid DT, is straight forward, if the operation modes and the corresponding parameter once are determined according to Section 4.2. For the computation of traction forces the simplified DT model in Figure 4.4 is extended by a final gear ratio and a driving wheel with tire radius r (see Figure 4.5). The
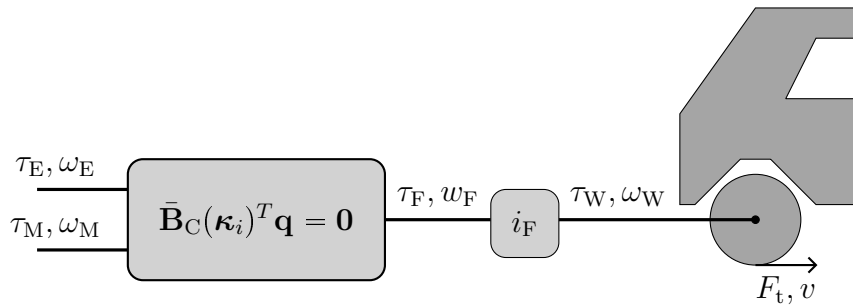
Figure 4.5: *Simplified DT model including a final ratio and a driving wheel for traction force analysis*

relation between vehicle speed v and the rotational speed of the final transmission output shaft w_F is:

$$v = \omega_F \frac{r_W}{i_F}. \tag{4.29}$$

Table 4.6: *Mode specific static torque relations*

	mode	$\bar{\mathbf{B}}_C(\boldsymbol{\kappa}_i)^T$	$\mathbf{J}_{u,u_i}$	$\mathbf{u}_i$	τ_F
0	neutral	$\begin{bmatrix} & \end{bmatrix}$	$\begin{bmatrix} \\ \end{bmatrix}$	$[\,]$	0
1.1	charge neutral	$\begin{bmatrix} 0 & 1 & -\frac{1}{i_M} \end{bmatrix}$	$\begin{bmatrix} 0 \\ 1 \\ -\frac{1}{i_M} \end{bmatrix}$	τ_E	0
1.2	charge blocked	$\begin{bmatrix} 1 & 0 & 0 \\ 0 & 1 & -\frac{1}{i_M} \end{bmatrix}$	$\begin{bmatrix} 1 & 0 \\ 0 & 1 \\ 0 & -\frac{1}{i_M} \end{bmatrix}$	$\begin{bmatrix} \tau_F \\ \tau_E \end{bmatrix}$	τ_F
2	electric	$\begin{bmatrix} 1 & 0 & -\frac{1}{i_M} \end{bmatrix}$	$\begin{bmatrix} 1 \\ 0 \\ -\frac{1}{i_M} \end{bmatrix}$	τ_F	$i_M \tau_M$
3	conv	$\begin{bmatrix} 1 & -\frac{1}{i_E} & 0 \end{bmatrix}$	$\begin{bmatrix} 1 \\ -\frac{1}{i_E} \\ 0 \end{bmatrix}$	τ_F	$i_E \tau_E$
4	hyb. par	$\begin{bmatrix} 1 & -\frac{1}{i_E} & 0 \\ 1 & 0 & -\frac{1}{i_M} \end{bmatrix}$	$\begin{bmatrix} 1 & 0 \\ 0 & 1 \\ -\frac{1}{i_M} & -\frac{i_E}{i_M} \end{bmatrix}$	$\begin{bmatrix} \tau_F \\ \tau_E \end{bmatrix}$	$i_E \tau_E + i_M \tau_M$
5	hyb. CVT	$\begin{bmatrix} 1 & -\frac{1}{i_E} & -\frac{1}{i_M} \end{bmatrix}$	$\begin{bmatrix} 1 \\ -\frac{1}{i_E} \\ -\frac{1}{i_M} \end{bmatrix}$	τ_F	$i_E \tau_E = i_M \tau_M$

The wheel radius r_W is considered to be constant for a simplified consideration. Due to (4.29) the resulting traction force F_t is:

$$F_t = \tau_F \frac{i_F}{r_W}. \tag{4.30}$$

In order to determine the maximum traction force in a specific gear the characteristics of ICE and EM have to be known. These vary according to the implementation and sizing. Figure 4.6 illustrates the principle speed-torque-characteristic of ICE and EM.
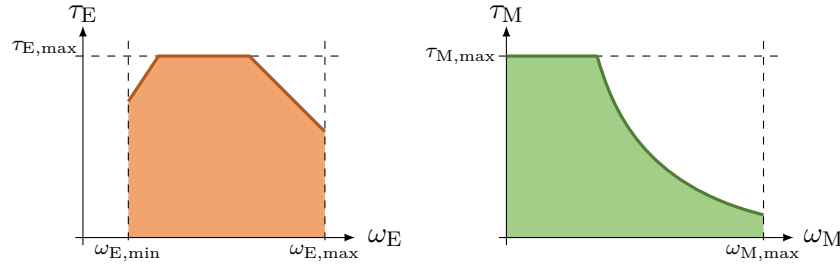
Figure 4.6: *Principle speed-torque-characteristics of an ICE (left) and an EM (right)*

An ICE can provide torque, if operating in a specific speed range:

$$0 < \omega_{E,min} \leqslant \omega_E \leqslant \omega_{E,max}. \tag{4.31}$$

Within this range a torque up to a specific speed dependent limit can be provided:

$$\tau_E \leqslant \tau_{E,max} = f(\omega_E). \tag{4.32}$$

A negative engine torque (motor break) is not considered within this thesis as already noted in Chapter 2. In contrast to the ICE the speed range of an EM is:

$$|\omega_M| \leqslant \omega_{M,max}. \tag{4.33}$$

Within this range an EM may provide positive and negative torques. The absolute value of the torque reaches up to a specific velocity dependent limit:

$$|\tau_M| \leqslant \tau_{M,max} = f(\omega_M) \tag{4.34}$$

Note Figure 4.6 shows the principle speed-toque-characteristic of an EM in one of the four possible quadrants.

4.3.2 Analysis method

According to the last column in Table 4.6 and equations (4.30) it is straight forward to compute the available traction force for given ICE and EM characteristic in gears with the operation modes 1-3, by scaling the available ICE and EM torques according to the gear ratios and to (4.30). The modes 0, 1.1 and 1.2 can not be used to drive the vehicle. Therefore, the only remaining operation mode, which needs some more investigations, is the hybrid CVT mode.

Traction force in hybrid CVT

Tables 4.1 and 4.6 state two equations to the speed and torque relations in hybrid CVT mode:

$$w_F = \frac{1}{i_E}\omega_E + \frac{1}{i_M}\omega_M, \tag{4.35}$$

$$\tau_F = i_E\tau_E = i_M\tau_M. \tag{4.36}$$

As stated in Chapter 2 the ICE speed ω_E is a hybrid DoF in this mode. Hence, it can be controlled to arbitrary values with respect to (4.31), independent of the current vehicle velocity. Therefore, the maximum available traction force at a given vehicle velocity v is the solution of an optimization problem:

$$
\begin{aligned}
\max_{F_\mathrm{t}} \quad & F_\mathrm{t} = \tau_\mathrm{E} \frac{i_\mathrm{E} i_\mathrm{F}}{r_\mathrm{W}} \\
\text{s.t.:} \quad & \tau_\mathrm{M} = \frac{i_\mathrm{E}}{i_\mathrm{M}} \tau_\mathrm{E} \\
& \omega_\mathrm{M} = i_\mathrm{M} \left(v \frac{i_\mathrm{F}}{r_\mathrm{W}} - \frac{1}{i_\mathrm{E}} \omega_\mathrm{E} \right) \\
& 0 \leqslant \omega_\mathrm{E} \leqslant \omega_\mathrm{E,max} \\
& |\omega_\mathrm{M}| \leqslant \omega_\mathrm{M,max} \\
& \tau_\mathrm{E} \leqslant f(\omega_\mathrm{E}) \\
& |\tau_\mathrm{M}| \leqslant f(\omega_\mathrm{M})
\end{aligned}
\tag{4.37}
$$

At this point one exemplary result of the optimization for a hybrid CVT mode is presented and discussed. In the example the following assumption shall be valid:

$$
\begin{aligned}
& i_\mathrm{E}, i_\mathrm{M} > 0, \\
& \tau_\mathrm{E,max} > \tau_\mathrm{M,max}, \\
& \omega_\mathrm{M,max} > \omega_\mathrm{E,max}.
\end{aligned}
\tag{4.38}
$$

Figure 4.7 shows the maximized traction force F_t, obtained by sampling, as well as the considered simplified ICE and EM characteristics. The result is structured into four phases with increasing vehicle velocity:

Phase 1: The first phase covers vehicle launching. ω_E is maintained at a constant level, which enables maximum τ_E. Due to (4.38) this is the maximum available launching torque. A constant ω_E requires increasing ω_M for increasing v. With increasing v the EM switches from generator to motor operation. Taking a lower F_t would enable generator operation of EM also for higher v.

Phase 2: At some v a further increase of ω_M would cause a reduction of F_t. However, F_t can be maintained at its maximum value, if ω_E compensates the increasing v, while ω_M is kept constant. It is obvious that the optimization result is not unique, since a switching of the first two phases would have led to the equivalent F_t.

Phase 3: In phase 3 a decreasing F_t is inevitable for increasing v. The maximum F_t is reached when increasing both ω_E and ω_M.

Phase 4: Due to (4.38) at one point ω_E reaches its limit. F_t decreases further. At the end of this phase also ω_M reaches its limit and the maximum v in this hybrid CVT operation mode is reached.

In order to determine maximum vehicle speeds and road gradients in specific gears, it is necessary to model the resistive force acting on the vehicle. The main effects, which affect this force are: rolling resistance, road gradient and air drag. The following equation can be used to approximate the resistive force for a given road gradient α
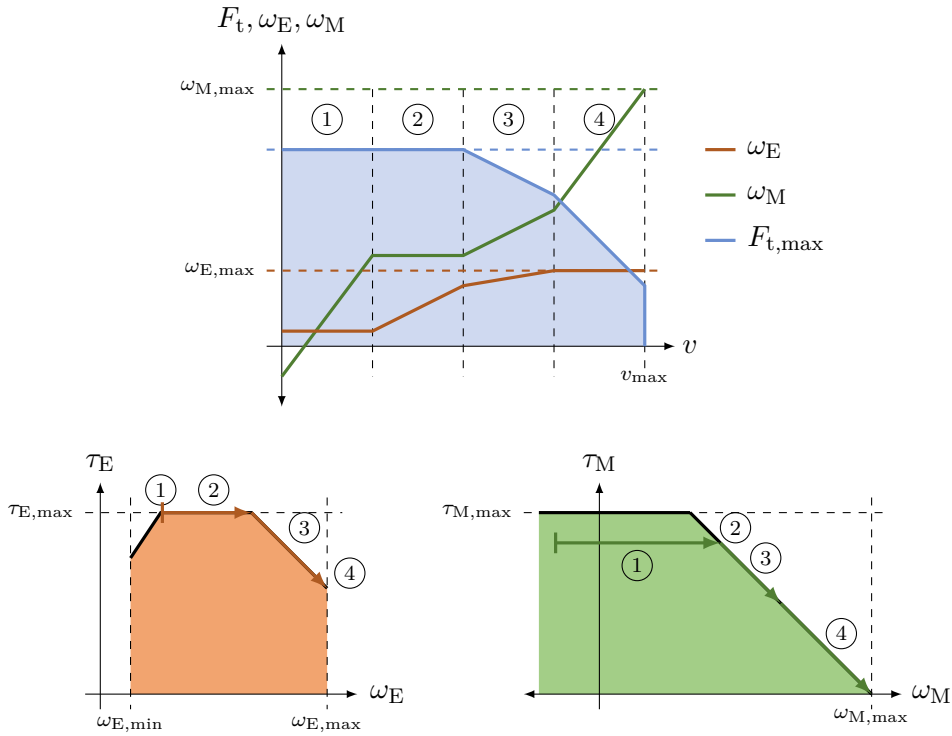
Figure 4.7: *Traction force optimization for an exemplary hybrid CVT operation mode (top center) and the corresponding torque levels of ICE (bottom, left) and EM (bottom, right)*

(cf. [15]):

$$F_{\mathrm{v}}(v, \alpha) = f_0 + \sin(\alpha)\, mg + \frac{1}{2} A\, c_{\mathrm{w}}\, \rho\, v^2 \tag{4.39}$$

This quadratic function with respect to the vehicle velocity v can be added to the TFD for different road gradients α. The intersection of these lines with the maximum traction forces determines the maximal vehicle speed with respect to α.

Figure 4.8 summarizes the presented traction force analysis method.
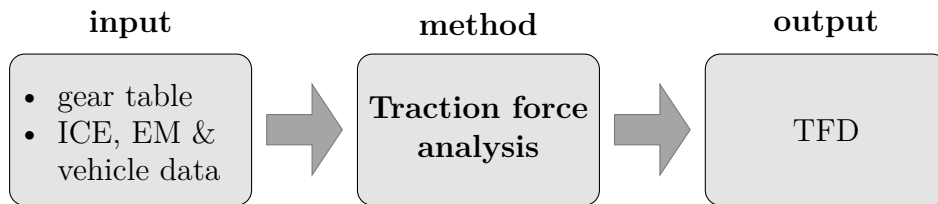
Figure 4.8: *Overview – traction force analysis*

4.3.3 Limitations

Although, the consideration of static traction forces is a good and common measure to evaluate the principle drivability of a DT, it omits dynamic effects. For example the

kinetic energy of shafts affects the actual traction force. Furthermore, losses, which occur in each gear meshing, have been omitted. While these losses do not affect the kinematic relations in the DT, they reduce the resulting output torques and, hence, traction forces. For details to the modeling of theses losses see for example [59].

4.3.4 Example

The above traction force analysis method, is now applied to the exemplary single-EM dedicated hybrid DT. Table 4.7 lists the parameters used in (4.39). Figure 4.9 shows the considered ICE and EM characteristic. The complete TFD of this exemplary DT is illustrated in Figure 4.10. Some remark can be made considering this exemplary TFD:

Table 4.7: Exemplary vehicle data

variable	parameter	value
m	vehicle mass	1350 kg
c_w	drag coefficient	0.32
A	maximum vehicle cross section	2 m^2
ρ	air density	1.275 $\frac{\mathrm{kg}}{\mathrm{m}^3}$
g	standard acceleration due to gravity	9.81 $\frac{\mathrm{m}}{\mathrm{s}^2}$
f_0	constant	107
r_W	wheel radius	0.317 m
i_F	final ratio	4.616

- For each **parallel hybrid gear**, two traction forces are depicted: the solid lines consider exclusively the ICE torque, while the dashed lines correspond to the maximum available torque in total, including the EM torque.
- **Vehicle launching** is not possible without EM. In case of sufficient battery SoC the electric gears E1 and E2 can be used for vehicle launching. In case of a low battery SoC, the hybrid CVT gears can be applied since the offer maximum traction at low vehicle speeds force operating EM in generator mode. Another possibility to launch the vehicle with low SoC is to first charge the battery applying a charge gear (Ch1 or Ch2) for subsequent electric launching.
- The **overall maximum traction force** is available in gear Pa2 (with electrical boost) at $v = 30$km/h.
- The **maximum vehicle speed** (without road gradient) can be reached in gear Pa3: 190 km/h applying the ICE and 230 km/h if applying additionally the EM
- Due to the absence of a negative gear ratio for the ICE, reverse driving is only possible with the EM.
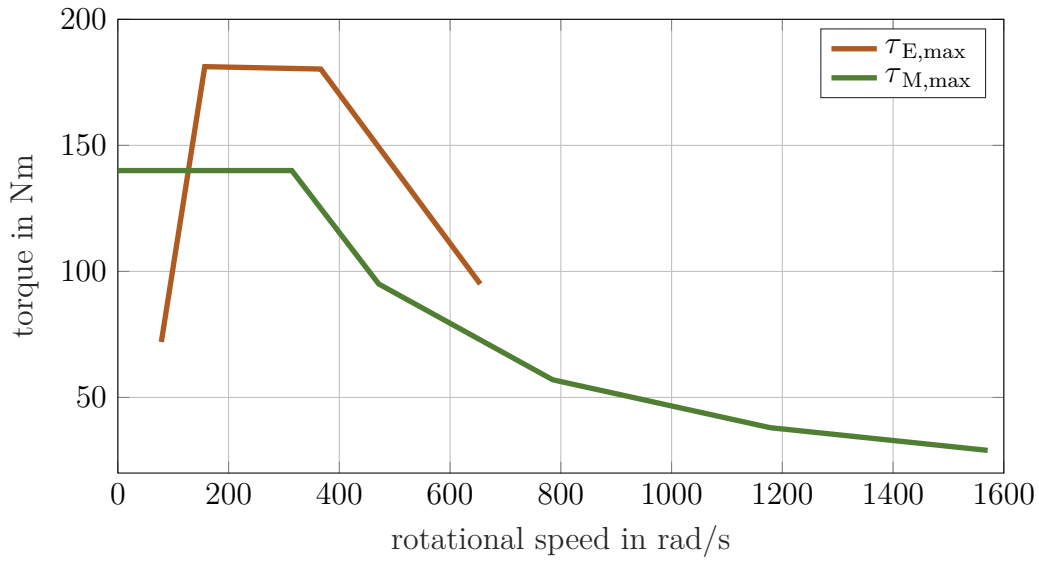
Figure 4.9: *Torque-speed characteristic of an exemplary ICE and EM*
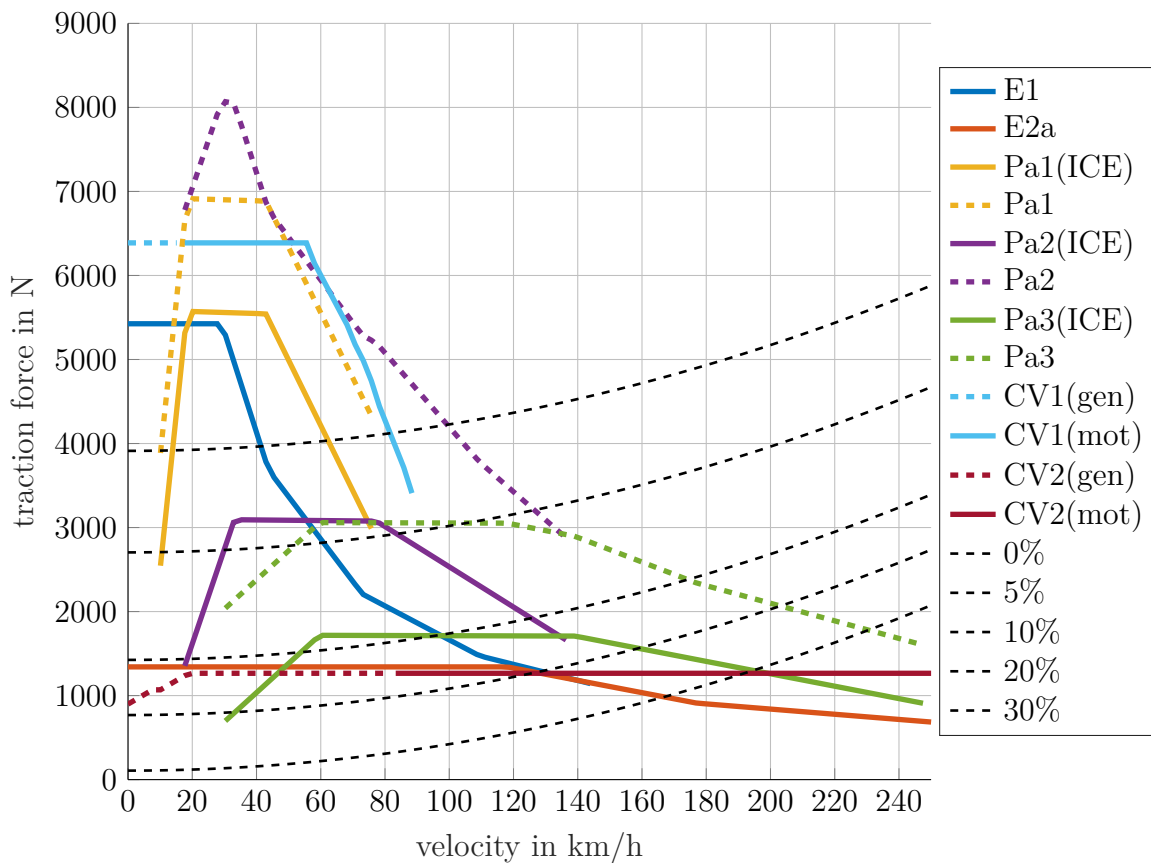
Figure 4.10: *TFD of the exemplary single-EM dedicated hybrid DT*

4.4 Shift analysis

The importance of gear shifting to provide a high level of drivability and efficiency has already been addressed in Chapter 2. Chapter 3 proposed a switching LTI model for gear shifting. The term shiftability, see for example [18, pp. 127], is used to rate the ability to perform the gear shifting in an acceptable manner with respect to drivability and efficiency. The following issues, which concern shiftability of a DT, will be considered in this section:

- Determination of shift sequences
- Traction force intersections
- Potential for smooth and lossless gear shifting

The first two issues are common methods and they are usually considered in the EMS design (see Chapter 2). The automation of these investigations as part of the model-based DT analysis method, hence, supports the state-of-the-art EMS development in general. The third issue is actually the next episode of the concept smooth and lossless gear shifting, which is contributed in this thesis.

4.4.1 Shift sequence

The term shift sequence defines, which clutches have to be actuated (engaged/disengaged), and in which order, to perform a required gear shift $\boldsymbol{\kappa}_i \to \boldsymbol{\kappa}_j$. The introduction of binary clutch state vectors (see Section 2.3), enables the application of combinatorics to this topic.

While the determination of a shift sequence is simple and unique for an elementary gear shifts – engagement or disengagement of a single clutch– the range of possible shift sequences increases with the number of necessary clutch actions $\Delta\boldsymbol{\kappa}_{ij}^T\Delta\boldsymbol{\kappa}_{ij}$. In the general case there are $(\Delta\boldsymbol{\kappa}_{ij}^T\Delta\boldsymbol{\kappa}_{ij})!$ different shift sequences of minimal length. Since it is, from practical point of view, not possible to fully synchronize several clutch transitions, a number of $(\Delta\boldsymbol{\kappa}_{ij}^T\Delta\boldsymbol{\kappa}_{ij} - 1)$ intermediate gears are active temporarily during the shift. Whereas the number of necessary intermediate gears is fixed, the shift sequence defines, which intermediate gears are involved. The overall set of possible intermediate gears consists of $2^{\Delta\boldsymbol{\kappa}_{ij}^T\Delta\boldsymbol{\kappa}_{ij}} - 2$ gears. Table 4.8 summarizes these combinatorial quantities.

Table 4.8: *Shift sequence parameters for a general gear shift* $\boldsymbol{\kappa}_i \to \boldsymbol{\kappa}_j$

number of	calculation
clutch actions	$\Delta\boldsymbol{\kappa}_{ij}^T\Delta\boldsymbol{\kappa}_{ij}$
necessary intermediate gears	$\Delta\boldsymbol{\kappa}_{ij}^T\Delta\boldsymbol{\kappa}_{ij} - 1$
possible shift sequences	$(\Delta\boldsymbol{\kappa}_{ij}^T\Delta\boldsymbol{\kappa}_{ij})!$
possible intermediate gears	$2^{(\Delta\boldsymbol{\kappa}_{ij}^T\Delta\boldsymbol{\kappa}_{ij})} - 2$

From drivability point of view it is obvious that a specific shift sequence is only feasible, if no intermediate gear features a blocked transmission output shaft. If the gear shift is performed as a series of elementary gear shifts – a so-called split shift – furthermore all intermediate gears with a neutral mode have to be excluded.

This restriction can be relaxed by performing so-called cross-over or power shifts (see for example [18, pp. 49]). In cross-over shifts several clutch actions are performed simultaneously and the propulsion torque is maintained by the support of slipping torques in clutches. For $\Delta\boldsymbol{\kappa}_{ij}^{T}\Delta\boldsymbol{\kappa}_{ij} = 2$ these shifts are well investigated and optimized (see for example [60]). The shifting in DTs with AMTs or DCTs exclusively relies on this shifting concept. Cross-over shifts with three or more simultaneously actuated clutches ($\Delta\boldsymbol{\kappa}_{ij}^{T}\Delta\boldsymbol{\kappa}_{ij} > 2$), which may be performed in ATs and DHTs, are not yet state of the art and hence a current research topic (see for example [61]). Consequently, it is common to split these shifts into a series of elementary and/or cross-over shifts. Cross-over shifts may also be performed for drivable intermediate gears. However, the dissipation resulting from slipping clutches, which could be avoided, decreases the shifting efficiency.

The automated determination of shift sequences shall now be discussed shortly using the exemplary single-EM dedicated hybrid DT:

Based on the gear table, which has been determined in Section 4.2, it is straight forward to generate a graph, which assembles all unblocked gears and all possible elementary shifts between them – the so-called shift map. Figure 4.11 shows the shift map of the exemplary single-EM dedicated hybrid DT, according to the modes listed in Table 4.4. The arrow labels state the clutch, which has to be engaged/disengaged in the corresponding gear shift.
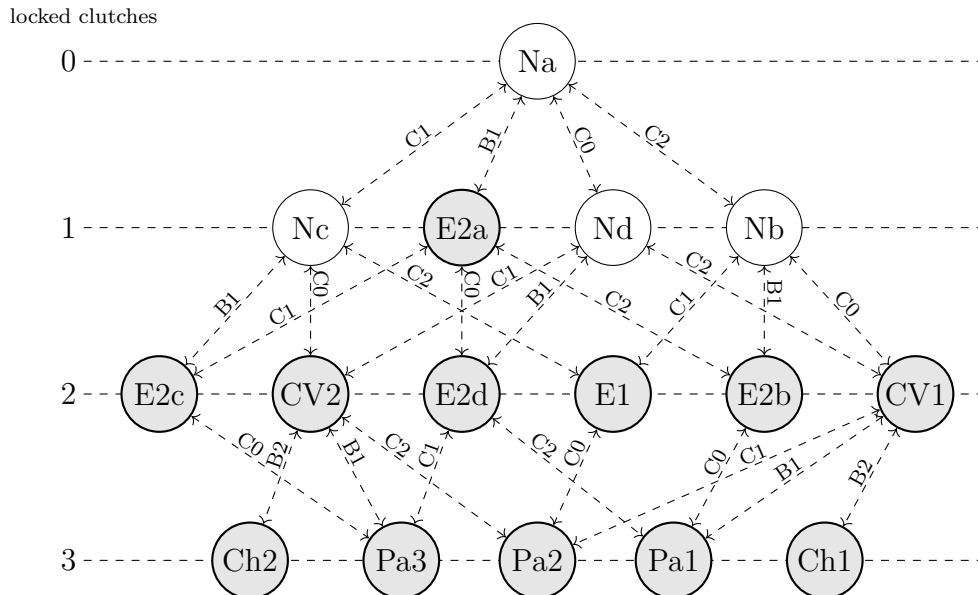
Figure 4.11: *Transitions between gears of the exemplary single-EM dedicated hybrid DT*

The minimal number of necessary clutch actions according to Table 4.8 are listed in

Table 4.8 for all possible gear shifts. This table excludes neutral and charge gears as initial or final gear in a shift, since such a shift would obviously not possible without propulsion torque interruption. The table furthermore is obviously symmetric. Due to

Table 4.9: *Necessary clutch actions for all gear shifts in the exemplary single-EM dedicated hybrid DT*

	E1	E2a	E2b	E2c	E2d	Pa1	Pa2	Pa3	CV1	CV2
E1	x	3	2	2	4	3	1	3	2	2
E2a	3	x	1	1	1	2	4	2	3	3
E2b	2	1	x	2	2	1	3	3	2	4
E2c	2	1	2	x	2	3	3	1	4	2
E2d	4	1	2	2	x	1	3	1	2	2
Pa1	3	2	1	3	1	x	2	2	1	3
Pa2	1	4	3	3	3	2	x	2	1	1
Pa3	3	2	3	1	1	2	2	x	3	1
CV1	2	3	2	4	2	1	1	3	x	2
CV2	2	3	4	2	2	3	1	1	2	x

this symmetry it is sufficient to all shifts beyond or above the diagonal to determine all possible shift sequences. For the exemplary single-EM dedicated hybrid DT this are 214 shift sequences according to Table 4.8 and Table 4.9. The listing of all these shift sequences is abandoned, but the possible shift sequences for two exemplary gear shifts are considered:

The first gear shift (Pa1 → Pa2) features a single possible shift sequence,

$$\text{Pa1} \rightarrow \text{Pa2}: \quad \text{Pa1} \rightarrow \text{CV1} \rightarrow \text{Pa2}, \tag{4.40}$$

which does not involve a blocked gear. As discussed above, this shift with $\Delta\boldsymbol{\kappa}_{ij}^T\Delta\boldsymbol{\kappa}_{ij} = 2$ can be performed in both approaches, a series of two elementary shifts and a cross-over shift.

The second considered gear shift shall be CV1 → Pa3 with $\Delta\boldsymbol{\kappa}_{ij}^T\Delta\boldsymbol{\kappa}_{ij} = 3$. The automated determination of shift sequences reveals 4 sequences:

$$\text{CV1} \rightarrow \text{Pa3}: \quad \begin{cases} \text{CV1} & \rightarrow & \text{Pa2} & \rightarrow & \text{CV2} & \rightarrow & \text{Pa3} \\ \text{CV1} & \rightarrow & \text{Pa1} & \rightarrow & \text{E2d} & \rightarrow & \text{Pa3} \\ \text{CV1} & \rightarrow & \text{Nd} & \rightarrow & \text{CV2} & \rightarrow & \text{Pa3} \\ \text{CV1} & \rightarrow & \text{Nd} & \rightarrow & \text{E2d} & \rightarrow & \text{Pa3} \end{cases}. \tag{4.41}$$

The intermediate gear Nd can only be bridged with a cross-over shift. Therefore, a series of elementary shifts is only possible in the last two shift sequence.

Whereas the results of this section rely exclusively on combinatorial investigations and principle mode characteristics (blocked, neutral, drivable) within the next two sections model knowledge is applied to evaluate the shiftability of the sequences, which have been determined in this section.

4.4.2 Traction force intersection

First, the mode specific stationary traction forces (see Section 4.3) are used to evaluate the shiftability of shift sequences. In order to ensure drivability, it is necessary to maintain the requested propulsion torque during and after the gear shift. The limits to this requirement can be approximated considering the corresponding maximum traction forces in the TFD (see Section 4.3). The intersection of the areas beyond the curves of the maximum traction force in the initial and final gear define the driving situation (propulsion torque request and vehicle speed) in which a gear shift between these two gears may not affect drivability. Figure 4.12 shows this intersection area for two exemplary gears. The computation of traction force intersections is straight
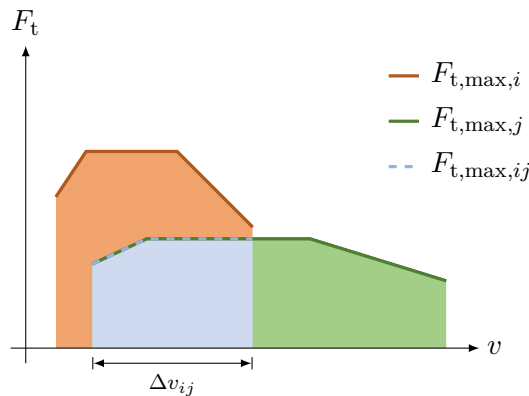
Figure 4.12: *Illustration of traction force intersection (light blue area) between two exemplary gears $\boldsymbol{\kappa}_i$ and $\boldsymbol{\kappa}_j$*

forward, if ones the gear specific traction forces are determined (see Section 4.3). Due to a positive propulsion torque the vehicle is accelerated during the shift. Therefore, it is necessary that the requested propulsion torque can not only be provided for the current vehicle speed, but also for a specific speed range Δv_{ij}, which further restricts the shifting opportunities.

Since in cross-over shifts the propulsion torque is supported by slipping clutch in the intermediate gear, it is sufficient to evaluate the traction force intersection of the initial and final gear. Whereas in split shifts it is necessary to consider the intersection between the initial gear the final gear and all intermediate gears.

Figure 4.13 and 4.14, show exemplary evaluations of the traction force intersections according to the exemplary shift sequences from the last section. In summary the

Traction Force Diagram
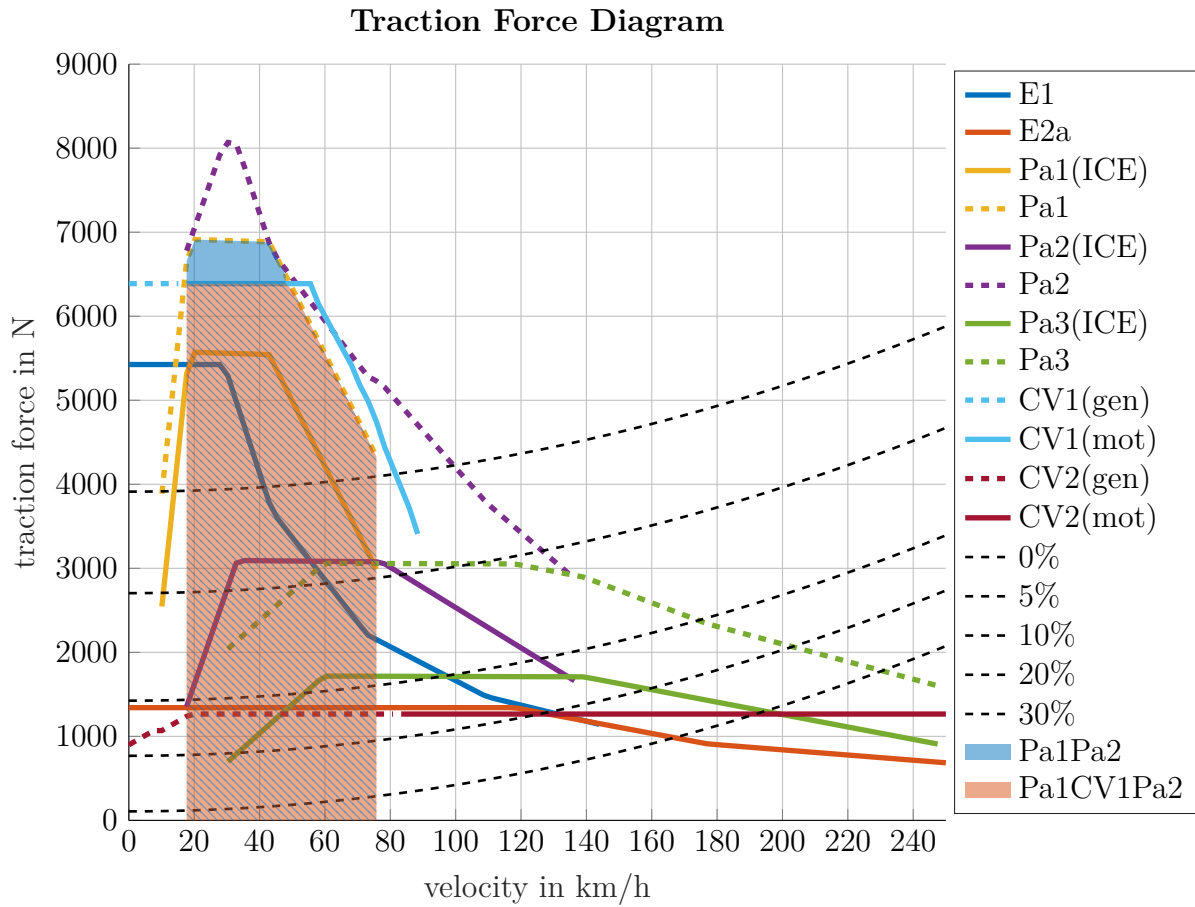
Figure 4.13: *Traction force intersection for the shift Pa1 → Pa2, for elementary shifting (red area) and cross-over shifting (blue area)*

consideration of traction force intersections reduces the possible shift sequences determined in Section 4.4.1. Furthermore, it restricts the shiftability of shift sequences to specific driving situations. Since the traction force diagram is based in static torque considerations, see Section 4.3, it is important to address that traction force intersections are not sufficient to guaranty an acceptable shiftability of certain gear shifts.
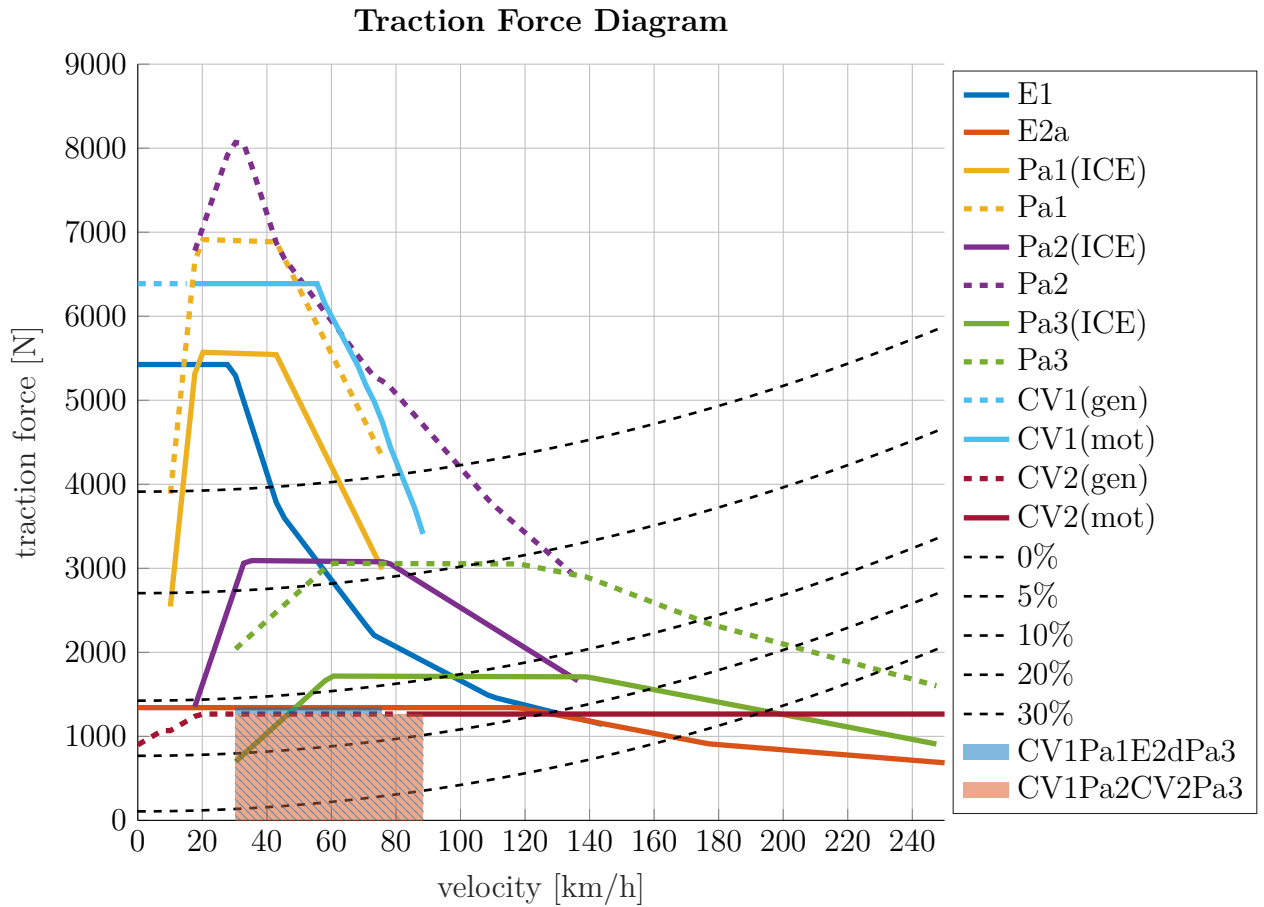
Figure 4.14: *Traction force intersection for the shift CV1 → Pa3, for the two elementary shift sequences CV1 → Pa1 → E2d → Pa3 (blue area) and CV1 → Pa2 → CV2 → Pa3 (red area)*

4.4.3 Potential for smooth and lossless gear shifting

The concept of smooth and lossless shifting is now considered as a second measure to evaluate shiftability of elementary gear shifts. In Section 3.8 plant models $\Sigma_{\kappa_i}^{\kappa_{j,\mathrm{lk}}}$ and $\Sigma_{\kappa_i}^{\kappa_{j,\mathrm{rl}}}$ to control the preparation of a smooth and lossless gear shift have been stated in (3.125) and (3.125). This section targets on the investigation of a mathematical condition based on these plant models, if this preparation can be successful at all. The following results have already been published in [35].

Control problem of smooth and lossless gear shifting

Considering the dynamical systems $\Sigma_{\kappa_i}^{\kappa_{j,\mathrm{lk}}}$(3.125), $\Sigma_{\kappa_i}^{\kappa_{j,\mathrm{rl}}}$(3.126): Is it possible to control y_2 to zero, while applying a tracking control to y_1?

This question can be reformulated in a more general way: Is it possible to independently control two control outputs with two control inputs? Actually, this is a common question in control theory in the field of *decoupling theory*. Its key contribution, with

respect to the above problem, shall be now summarized concisely:

Static state decoupling of MIMO LTI systems: In decoupling theory a general MIMO LTI system is considered:

$$\dot{\mathbf{x}} = \mathbf{A}\mathbf{x} + \mathbf{B}\mathbf{u},$$

$$\mathbf{y} = \mathbf{C}\mathbf{x} + \mathbf{D}\mathbf{u} = \begin{bmatrix} \mathbf{c}_1^T \\ \vdots \\ \mathbf{c}_m^T \end{bmatrix} \mathbf{x} + \begin{bmatrix} \mathbf{d}_1^T \\ \vdots \\ \mathbf{d}_m^T \end{bmatrix} \mathbf{u}. \tag{4.42}$$

It features n states $\mathbf{x}$, m inputs $\mathbf{u}$ and m outputs $\mathbf{y}$. The constant matrices $\mathbf{A}$, $\mathbf{B}$, $\mathbf{C}$ and $\mathbf{D}$ are of appropriate dimensions. The question of decoupling theory is, if there exists a state feedback,

$$\mathbf{u} = \mathbf{V}\mathbf{x} + \mathbf{K}\mathbf{w}, \tag{4.43}$$

which decouples the input-output behavior into Single-Input Single-Output (SISO) channels from the artificial inputs $\mathbf{w}$ to the original outputs $\mathbf{y}$. This question was first answered in a general way by Morgan in [62], who proposed a necessary condition for the existence of the matrices $\mathbf{V}$ and $\mathbf{K}$. Falb and Wolovich later on proposed a necessary and sufficient condition to this problem in [63]:

Theorem - Existence of a decoupling static state feedback

A decoupling static state feedback law (4.43) exists, if and only if the decoupling matrix,

$$\hat{\mathbf{D}} = \begin{bmatrix} \hat{\mathbf{d}}_1^T \\ \vdots \\ \hat{\mathbf{d}}_m^T \end{bmatrix}, \qquad \hat{\mathbf{d}}_i^T := \begin{cases} \mathbf{d}_i^T, & \text{for } \delta_i = 0 \\ \mathbf{c}_i^T \mathbf{A}^{\delta_i - 1} \mathbf{B}, & \text{for } \delta_i > 0, \end{cases} \tag{4.44}$$

is nonsingular. δ_i is the relative degree of output y_i with respect to $\mathbf{u}$:

$$\delta_i := \begin{cases} 0 & \text{for } \mathbf{d}_i \neq \mathbf{0} \\ \min\left\{ j : \mathbf{c}_i^T \mathbf{A}^{j-1} \mathbf{B} \neq \mathbf{0}, \quad j = 1, 2, \ldots, n-1 \right\} & \text{for } \mathbf{d}_i = \mathbf{0} \end{cases}. \tag{4.45}$$

This necessary and sufficient condition of Falb and Wolovich can be applied to the problem of smooth and lossless gear shifting:

Condition on smooth and lossless gear shifting

If, and only if, the matrix $\hat{\mathbf{D}}$ (4.44) of the system $\Sigma_{\boldsymbol{\kappa}_i}^{\boldsymbol{\kappa}_{j,\text{lk}}}$ resp. $\Sigma_{\boldsymbol{\kappa}_i}^{\boldsymbol{\kappa}_{j,\text{rl}}}$ is nonsingular, the system outputs $\mathbf{y}$ can be controlled independently. If so, there are control inputs $\mathbf{u}$, which control the clutch slip of the clutch to be engaged, respectively the locking torque of the clutch to be disengaged, to zero, while simultaneously controlling a requested vehicle propulsion.

Theoretically, it would be sufficient to reach a zero-crossing of $y_{C,lk}/y_{C,rl}$ for shifting to avoid dissipation. In this case the above condition is just sufficient but not necessary. However, the sufficient condition based on decoupling is of major interest from the practical point of view, since robustness is an important issue.

A positive result of the evaluation of this condition is referred to as *potential for smooth and lossless gear shifting*. The term potential is used to indicate that the above condition does not include actuation limitations. The combination with the concept traction force intersections, discussed in Section 4.4.2, as well the reasonable planning of control trajectories, which will be addressed in Chapter 5, enable a more comprehensive evaluation.

On the other side the reverse conclusion to the above condition is much stronger: If the condition is not met, for sure either dissipation in clutches or propulsion torque interruption has to by accepted in the considered gear shift.

The condition based on decoupling theory can be applied to all gear shifts of a given single-EM dedicated hybrid DT following a straight forward procedure:

Evaluation procedure for the potential of smooth and lossless gear shifting

For all $\boldsymbol{\kappa}_i \to \boldsymbol{\kappa}_j$, with $\Delta\boldsymbol{\kappa}_{ij}^T\Delta\boldsymbol{\kappa}_{ij} = 1$:

1. Compute plant models $\Sigma_{\boldsymbol{\kappa}_i}^{\boldsymbol{\kappa}_{j,lk}}$ (3.125) resp. $\Sigma_{\boldsymbol{\kappa}_i}^{\boldsymbol{\kappa}_{j,rl}}$ (3.126).
2. Compute relative degrees δ_i (4.45) and vectors $\hat{\mathbf{d}}_i$ (4.44) by differentiation of the output equations.
3. Assembly decoupling matrix $\hat{\mathbf{D}}$ and check its regularity: $\det\left(\hat{\mathbf{D}}\right) \overset{?}{\neq} 0$.

Figure 4.15 shows the results of this procedure to the exemplary single-EM dedicated hybrid DT (see Section 3.6.4). Solid arrows denote the potential for smooth and lossless gearshifts.

Taking a closer look at Figure 4.15 reveals two noticeable remarks, which have not been investigated in [35]:

- All shifts between drivable modes offer the potential for smooth and lossless gear shifting.
- The evaluation results are bidirectional: If the evaluation is positive for the shift $\boldsymbol{\kappa}_i \to \boldsymbol{\kappa}_j$, it is also positive for the shift $\boldsymbol{\kappa}_j \to \boldsymbol{\kappa}_i$.

It is a reasonable question, if these two observations can be generalized. To answer this question some analytic investigations will be made on elementary gear shifts between drivable gears on a simplified DT model in Figure 4.16:

$$\underbrace{\begin{bmatrix} J_F & 0 & 0 \\ 0 & J_E & 0 \\ 0 & 0 & J_M \end{bmatrix}}_{\bar{\mathbf{M}}} \underbrace{\begin{bmatrix} \dot{\omega}_F \\ \dot{\omega}_E \\ \dot{\omega}_M \end{bmatrix}}_{\dot{\mathbf{q}}} = \underbrace{\begin{bmatrix} -d_F & 0 & 0 \\ 0 & -d_E & 0 \\ 0 & 0 & -d_M \end{bmatrix}}_{\bar{\mathbf{A}}} + \underbrace{\begin{bmatrix} 0 & 0 \\ 1 & 0 \\ 0 & 1 \end{bmatrix}}_{\bar{\mathbf{B}}} \underbrace{\begin{bmatrix} \tau_E \\ \tau_M \end{bmatrix}}_{\mathbf{u}}. \tag{4.46}$$

locked clutches
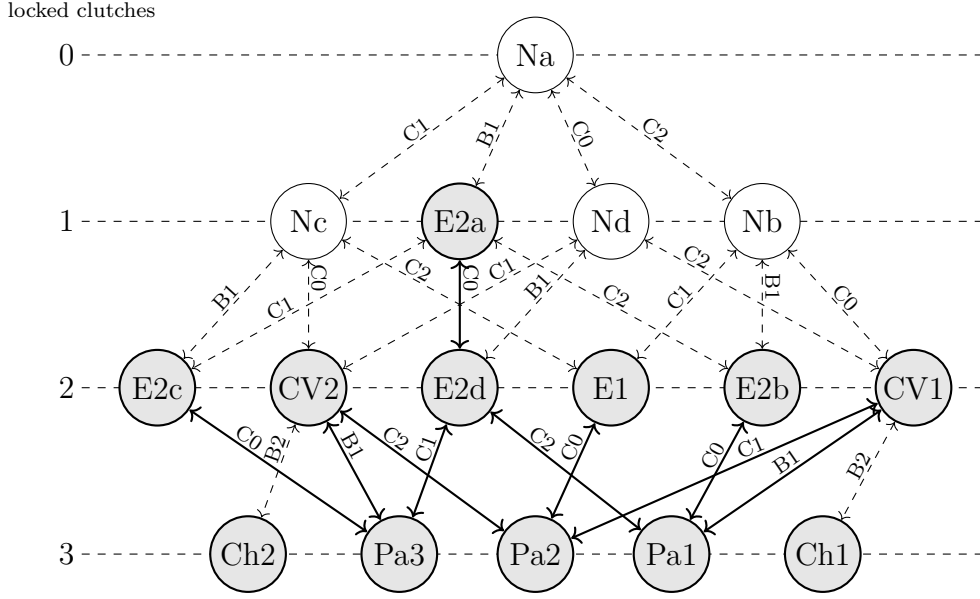
Figure 4.15: *Potential for smooth and lossless gear shifting (solid arrows) in the exemplary single-EM dedicated hybrid DT*
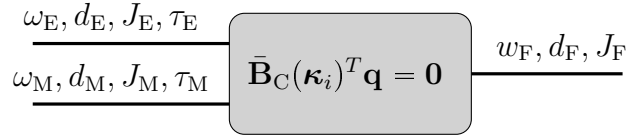
Figure 4.16: *Simplified DT model for decoupling analysis*

The restriction to drivable gears is obvious, since the wheel torque can exclusively be controlled in drivable modes. After applying one constraint according to the drivable modes in Table 4.1 the corresponding model is:

$$\underbrace{\mathbf{J}_{\mathrm{q,q}_i}^T \bar{\mathbf{M}} \mathbf{J}_{\mathrm{q,q}_i}}_{\bar{\mathbf{M}}_i} \dot{\mathbf{q}}_i = \underbrace{\mathbf{J}_{\mathrm{q,q}_i}^T \bar{\mathbf{A}} \mathbf{J}_{\mathrm{q,q}_i}}_{\bar{\mathbf{A}}_i} \mathbf{q}_i + \underbrace{\mathbf{J}_{\mathrm{q,q}_i}^T \bar{\mathbf{B}}_{\mathrm{P}}}_{\bar{\mathbf{B}}_{i,\mathrm{P}}} \boldsymbol{\tau}_{\mathrm{P}}, \tag{4.47}$$

with:

$$\mathbf{q}_i^T = \begin{bmatrix} w_{\mathrm{F}} & \omega_{\mathrm{E}} \end{bmatrix}, \quad \text{or} \quad \mathbf{q}_i^T = \begin{bmatrix} w_{\mathrm{F}} & \omega_{\mathrm{M}} \end{bmatrix}. \tag{4.48}$$

According to (4.46) the input matrix $\bar{\mathbf{B}}_{i,\mathrm{P}}$ is the selection of the second and third row of the matrices $\mathbf{J}_{\mathrm{q,q}_i}$ in Table 4.1. This reveals:

$$\det(\bar{\mathbf{B}}_{i,\mathrm{P}}) \neq 0, \tag{4.49}$$

which will be important in the following investigations. Another important fact is that the matrix $\bar{\mathbf{M}}_i$ is positive definite,

$$\bar{\mathbf{M}}_i > 0, \tag{4.50}$$

Table 4.10: *Drivable modes in the simplified DT (Figure 4.2)*

mode	DoF		ratio	abbreviation
electric	2	ω_F, ω_E	i_M	E_2
conventional	2	ω_F, ω_M	i_E	C_2
hybrid CVT	2	ω_F, ω_E	i_E, i_M	CV
electric	1	ω_F	i_M	E_1
conventional	1	ω_F	i_E	C_1
hybrid parallel	1	ω_F	i_E, i_M	Pa

which has been proofed in Section 3.5.1.

Table. 4.10 lists all drivable modes according to Table 2.1, and the corresponding mechanical DoFs, which can occur in the simplified DT. The indices 1 and 2 indicate the mechanical DoFs, which are not fixed in electric and conventional mode.

Figure 4.17 illustrates all possible elementary gear shifts, from drivable modes with two DoFs into drivable modes with one DoF according to Table. 4.10. Additionally, the coefficients of a general constraint,

$$\bar{\mathbf{b}}_{i,\mathrm{C,lk}}^T \mathbf{q}_i = \begin{bmatrix} a & b \end{bmatrix} \mathbf{q}_i = 0, \tag{4.51}$$

which yields the corresponding shift,

$$\boldsymbol{\kappa}_i \overset{\bar{\mathbf{b}}_{i,\mathrm{C,lk}}}{\rightarrow} \boldsymbol{\kappa}_j, \tag{4.52}$$

are stated. These coefficients are also listed in Table 4.11. In order to investigate the
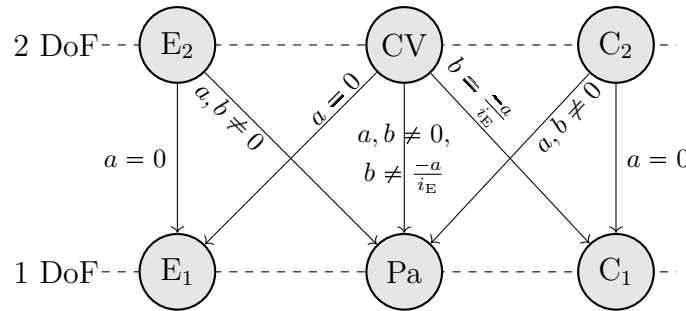
Figure 4.17: *Shifting between drivable modes with 2 DoFs into drivable modes with one DoF and corresponding constraint coefficients according to (4.51)*

potential for smooth and lossless gear shifting, in a first step the decoupling matrix $\mathbf{D}_{ij,\mathrm{lk}}$ shall now be stated in a general form, which is feasible for all of the 7 shifts (from 2-DoF drivable modes into 1-DoF drivable modes) in Figure 4.17 following the

Table 4.11: *Constraint coefficients according to (4.51) for shifts between drivable modes*

shift	a	b
$E_2 \rightarrow E_1$	0	b
$E_2 \rightarrow Pa$	$\neq 0$	$\neq 0$
$CV \rightarrow E_1$	0	$\neq 0$
$CV \rightarrow Pa$	$\neq 0$	$\neq 0, \neq \frac{-a}{i_E}$
$CV \rightarrow C_1$	$\neq 0$	$\frac{-a}{i_E}$
$C_2 \rightarrow Pa$	$\neq 0$	$\neq 0$
$C_2 \rightarrow C_1$	0	$\neq 0$

above procedure. The first considered output equation concerns the torque at the final shaft, according to (3.102):

$$y_{i,P} = \mathbf{e}_i^T \bar{\mathbf{M}}_i \dot{\mathbf{q}}_i = \mathbf{e}_i^T \bar{\mathbf{A}}_i \mathbf{q}_i + \mathbf{e}_i^T \bar{\mathbf{B}}_{i,P} \boldsymbol{\tau}_P, \tag{4.53}$$

with,

$$\mathbf{e}_i^T = \begin{bmatrix} 1 & 0 \end{bmatrix}. \tag{4.54}$$

Due to (4.49) the relative degree of this output equation is zero (direct feed-through). The corresponding row in the decoupling matrix hence is:

$$\hat{\mathbf{d}}_{i,P} = \mathbf{e}_i^T \bar{\mathbf{B}}_{i,P} \neq \mathbf{0}. \tag{4.55}$$

The second output equation, see (3.122), concerns the slip of the clutch, which will be engaged:

$$y_{C,lk} = \bar{\mathbf{b}}_{i,C,lk} \mathbf{q}_i. \tag{4.56}$$

Since there is no direct feed-through in this output equation, it is differentiated with respect to time:

$$\dot{y}_{C,lk} = \bar{\mathbf{b}}_{i,C,lk}^T \dot{\mathbf{q}}_i = \bar{\mathbf{b}}_{i,C,lk}^T \bar{\mathbf{M}}_i^{-1} \bar{\mathbf{A}}_i \mathbf{q}_i + \bar{\mathbf{b}}_{i,C,lk}^T \bar{\mathbf{M}}_i^{-1} \bar{\mathbf{B}}_{i,P}. \tag{4.57}$$

Due to (4.49) and (4.50) this reveals a relative degree $\delta = 1$ and hence:

$$\hat{\mathbf{d}}_{i,C,lk} = \bar{\mathbf{b}}_{i,C,lk}^T \bar{\mathbf{M}}_i^{-1} \bar{\mathbf{B}}_{i,P} \neq \mathbf{0}. \tag{4.58}$$

Equations (4.55) and (4.58) assemble the decoupling matrix:

$$\mathbf{D}_{ij,lk} = \begin{bmatrix} \hat{\mathbf{d}}_{i,P} \\ \hat{\mathbf{d}}_{i,C,lk} \end{bmatrix} = \begin{bmatrix} \mathbf{e}_i^T \bar{\mathbf{B}}_{i,P} \\ \bar{\mathbf{b}}_{i,C,lk}^T \bar{\mathbf{M}}_i^{-1} \bar{\mathbf{B}}_{i,P} \end{bmatrix} = \begin{bmatrix} \mathbf{e}_i^T \\ \bar{\mathbf{b}}_{i,C,lk}^T \bar{\mathbf{M}}_i^{-1} \end{bmatrix} \bar{\mathbf{B}}_{i,P}. \tag{4.59}$$

The determinant of $\mathbf{D}_{ij,\mathrm{lk}}$ can be computed as a product of two determinants:

$$\det\left(\mathbf{D}_{ij,\mathrm{lk}}\right) = \det\left(\begin{bmatrix} \mathbf{e}_i^T \\ \bar{\mathbf{b}}_{i,\mathrm{C,lk}}^T \bar{\mathbf{M}}_i^{-1} \end{bmatrix}\right) \cdot \det\left(\bar{\mathbf{B}}_{i,\mathrm{P}}\right). \tag{4.60}$$

From (4.55), (4.58) and (4.49) follows:

$$\det\left(\mathbf{D}_{ij,\mathrm{lk}}\right) \neq 0 \quad \Leftrightarrow \quad \mathbf{e}_i^T \neq c \cdot \bar{\mathbf{b}}_{i,\mathrm{C,lk}}^T \bar{\mathbf{M}}_i^{-1}, \quad \forall c \neq 0. \tag{4.61}$$

This actually requires that vectors $\mathbf{e}_i^T$ and $\bar{\mathbf{b}}_{i,\mathrm{C,lk}}^T \bar{\mathbf{M}}_i^{-1}$ are linearly independent.
Let $\bar{\mathbf{M}}_i^{-1}$ be

$$\bar{\mathbf{M}}_i^{-1} = \begin{bmatrix} m_{11} & m_{12} \\ m_{12} & m_{22} \end{bmatrix}. \tag{4.62}$$

From (4.51) and (4.54) follows:

$$\begin{bmatrix} 1 & 0 \end{bmatrix} \neq c \begin{bmatrix} a \cdot m_{11} + b \cdot m_{12} & a \cdot m_{12} + b \cdot m_{22} \end{bmatrix} \quad \Rightarrow \quad b \neq -a\frac{m_{12}}{m_{22}}. \tag{4.63}$$

If this inequality holds the shifts feature the potential for smooth and lossless gear shifting. Two important remarks to this inequality with respect to the relations of the constraint coefficients a and b (see Table 4.11) can be made:

- The inequality (4.63), always holds for $m_{12} = 0$. According to Table 4.1, $m_{12} \neq 0$ exclusively occurs in hybrid CVT mode.
- The inequality (4.63), relates gear ratios and inertia. Hence, it is a mathematical special case and not of practical relevance. Therefore, in practice the inequality can be considered to be valid.

In a second step the decoupling matrix $\mathbf{D}_{ji,\mathrm{rl}}$ of the reverse shifts (from 1-DoF drivable modes into 2-DoF drivable modes) shall be considered in a general form similar to $\mathbf{D}_{ij,\mathrm{lk}}$:
The first output equation $y_{j,\mathrm{P}}$ is:

$$y_{j,\mathrm{P}} = \mathbf{e}_j^T \mathbf{J}_{\mathrm{q}_i,\mathrm{q}_j}^T \bar{\mathbf{M}}_i \mathbf{J}_{\mathrm{q}_i,\mathrm{q}_j} \dot{\mathbf{q}}_j = \mathbf{e}_j^T \mathbf{J}_{\mathrm{q}_i,\mathrm{q}_j}^T \bar{\mathbf{A}}_i \mathbf{J}_{\mathrm{q}_i,\mathrm{q}_j} \mathbf{q}_j + \mathbf{e}_j^T \mathbf{J}_{\mathrm{q}_i,\mathrm{q}_j}^T \bar{\mathbf{B}}_{i,\mathrm{P}} \boldsymbol{\tau}_\mathrm{P}, \tag{4.64}$$

with:

$$\mathbf{e}_j^T = 1. \tag{4.65}$$

Matrix $\mathbf{J}_{\mathrm{q}_i,\mathrm{q}_j}$ is the coordinate mapping according to (3.41), due to the general constraint in (4.51):

$$\mathbf{J}_{\mathrm{q}_i,\mathrm{q}_j} = \left(\mathbf{E}_{\mathcal{N}\left(\bar{\mathbf{b}}_{i,\mathrm{C,lk}}^T\right)^T}\right)^T. \tag{4.66}$$

This reveals a relative degree $\delta = 0$, due to (4.65), (4.64) and (4.49), and hence:

$$\hat{\mathbf{d}}_{j,\mathrm{P}} = \mathbf{e}_j^T \mathbf{J}_{\mathrm{q}_i,\mathrm{q}_j}^T \bar{\mathbf{B}}_{i,\mathrm{P}} \neq \mathbf{0}. \tag{4.67}$$

The second output equation concerns the locking torque at the clutch, which will be disengaged, which is:

$$y_{\mathrm{C,rl}} = -\left[\bar{\mathbf{b}}_{i,\mathrm{C,lk}}^T \bar{\mathbf{M}}_i^{-1} \bar{\mathbf{b}}_{i,\mathrm{C,lk}}\right]^{-1} \bar{\mathbf{b}}_{i,\mathrm{C,lk}}^T \bar{\mathbf{M}}_i^{-1} \left(\bar{\mathbf{A}}_i \mathbf{J}_{\mathrm{q}_i,\mathrm{q}_j} \mathbf{q}_j + \bar{\mathbf{B}}_{i,\mathrm{P}} \boldsymbol{\tau}_{\mathrm{P}}\right),\tag{4.68}$$

according to (3.124). The scalar $-\left[\bar{\mathbf{b}}_{i,\mathrm{C,lk}}^T \bar{\mathbf{M}}_i^{-1} \bar{\mathbf{b}}_{i,\mathrm{C,lk}}\right]^{-1}$ is non-zero due to (4.50). With (4.50) and (4.49), this reveals once again a relative degree $\delta = 0$ and hence:

$$\hat{\mathbf{d}}_{j,\mathrm{C,rl}} = -\left[\bar{\mathbf{b}}_{i,\mathrm{C,lk}}^T \bar{\mathbf{M}}_i^{-1} \bar{\mathbf{b}}_{i,\mathrm{C,lk}}\right]^{-1} \bar{\mathbf{b}}_{i,\mathrm{C,lk}}^T \bar{\mathbf{M}}_i^{-1} \bar{\mathbf{B}}_{i,\mathrm{P}} \neq \mathbf{0}.\tag{4.69}$$

Consequently, the corresponding decoupling matrix is:

$$\mathbf{D}_{ji,\mathrm{rl}} = \begin{bmatrix} \hat{\mathbf{d}}_{j,\mathrm{P}} \\ \hat{\mathbf{d}}_{j,\mathrm{C,rl}} \end{bmatrix} = \begin{bmatrix} \mathbf{e}_j^T \mathbf{J}_{\mathrm{q}_i,\mathrm{q}_j}^T \bar{\mathbf{B}}_{i,\mathrm{P}} \\ -\left[\bar{\mathbf{b}}_{i,\mathrm{C,lk}}^T \bar{\mathbf{M}}_i^{-1} \bar{\mathbf{b}}_{i,\mathrm{C,lk}}\right]^{-1} \bar{\mathbf{b}}_{i,\mathrm{C,lk}}^T \bar{\mathbf{M}}_i^{-1} \bar{\mathbf{B}}_{i,\mathrm{P}} \end{bmatrix}.\tag{4.70}$$

The determinant of $\mathbf{D}_{ji,\mathrm{rl}}$ can be computed as a product of three determinants:

$$\det\left(\mathbf{D}_{ji,\mathrm{rl}}\right) = \dots$$
$$\det\left(\begin{bmatrix} \mathbf{e}_j^T & 0 \\ 0 & -\left[\bar{\mathbf{b}}_{i,\mathrm{C,lk}}^T \bar{\mathbf{M}}_i^{-1} \bar{\mathbf{b}}_{i,\mathrm{C,lk}}\right]^{-1} \end{bmatrix}\right) \cdot \det\left(\begin{bmatrix} \mathbf{J}_{\mathrm{q}_i,\mathrm{q}_j}^T \\ \bar{\mathbf{b}}_{i,\mathrm{C,lk}}^T \bar{\mathbf{M}}_i^{-1} \end{bmatrix}\right) \cdot \det\left(\bar{\mathbf{B}}_{i,\mathrm{P}}\right).\tag{4.71}$$

Due to (4.65), (4.50) and (4.49) only the second determinant might be zero:

$$\det\left(\mathbf{D}_{ji,\mathrm{rl}}\right) \neq 0 \quad \Leftrightarrow \quad \mathbf{J}_{\mathrm{q}_i,\mathrm{q}_j}^T \neq c \cdot \bar{\mathbf{b}}_{i,\mathrm{C,lk}}^T \bar{\mathbf{M}}_i^{-1}, \quad \forall c \neq 0\tag{4.72}$$

In contrast to (4.61) this condition is always valid, also from mathematical point of view, since:

$$\mathbf{J}_{\mathrm{q}_i,\mathrm{q}_j}^T = k \cdot \bar{\mathbf{b}}_{i,\mathrm{C,lk}}^T \bar{\mathbf{M}}_i^{-1} \quad \Rightarrow \quad \bar{\mathbf{b}}_{i,\mathrm{C,lk}}^T \mathbf{J}_{\mathrm{q}_i,\mathrm{q}_j} = 0 = c \cdot \bar{\mathbf{b}}_{i,\mathrm{C,lk}}^T \bar{\mathbf{M}}_i^{-1} \bar{\mathbf{b}}_{i,\mathrm{C,lk}},\tag{4.73}$$

which is in conflict to $\bar{\mathbf{M}}_i > 0$. Consequently, $\mathbf{D}_{ji,\mathrm{rl}}$ is for sure regular.

Summarized, in the simplified DT topology (Figure 4.2) all the elementary gear shifts between drivable modes with different number of mechanical DoFs feature the potential for smooth and lossless gear shifting. In order to formulate a more general statement first the restriction to the simplified DT topology shall be relaxed.

As already mentioned in the Section 4.2 in a general DT topology the mode specific kinematics is equivalent to the kinematics considered in the simplified case. The mechanical DoFs, however, increase according to an arbitrary number of additional shafts. Therefore, the state vector $\mathbf{q}$ in (4.48) is extended to n elements. This yields a new state vector $\tilde{\mathbf{q}}_i$:

$$\tilde{\mathbf{q}}_i = \begin{bmatrix} \mathbf{q}_i \\ \bar{\mathbf{q}}_i \end{bmatrix}.\tag{4.74}$$

According to $\tilde{\mathbf{q}}_i$ all matrices of the above investigations are extended:

$$\tilde{\mathbf{B}}_{i,\mathrm{P}} = \begin{bmatrix} \bar{\mathbf{B}}_{i,\mathrm{P}} \\ \mathbf{0} \end{bmatrix}, \quad \tilde{\mathbf{b}}_{i,\mathrm{C,lk}} = \begin{bmatrix} \bar{\mathbf{b}}_{i,\mathrm{C,lk}} \\ \mathbf{0} \end{bmatrix}, \quad \tilde{\mathbf{J}}_{\mathrm{q}_i,\mathrm{q}_j} = \begin{bmatrix} \mathbf{J}_{\mathrm{q}_i,\mathrm{q}_j} \\ \mathbf{I} \end{bmatrix},\tag{4.75}$$

$$\tilde{\mathbf{e}}_i = \begin{bmatrix} \mathbf{e}_i \\ \mathbf{0} \end{bmatrix}, \quad \tilde{\mathbf{e}}_j = \begin{bmatrix} \mathbf{e}_j \\ \mathbf{0} \end{bmatrix}.\tag{4.76}$$

Using this extension, it is straight forward to show that the above considerations are still valid, for a general elementary gear shift between drivable modes with different number of mechanical DoFs.

A further generalization can be made on the propulsion output y_P: If decoupling is possible considering the torque at transmission output shaft, it is also possible for torques, which are dynamically related exclusively to this torque, although the relative degree is increased. Consequently, for example the consideration of a flexible driveshaft, which connects the transmission output shaft and the driving wheels (see Figure 4.18), does not affect the potential for smooth and lossless gear shifting.
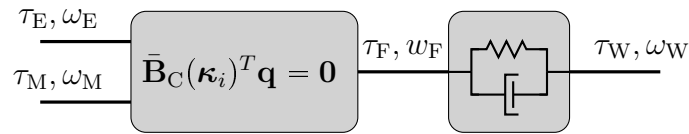
Figure 4.18: *Simplified DT topology with flexible driveshaft*

Therefore, finally, a generalization of the observations with respect to the exemplary single-EM dedicated hybrid DT is feasible:

> **Elementary gear shifts between drivable modes**
>
> Every elementary gear shift in a single-EM dedicated hybrid DT from one drivable mode (see Tables 4.10 and 4.11) into another, features the potential for smooth and lossless shifting. For all other shifts the procedure presented at the beginning of this section can be applied.

In analogy to the shift preparation also mode specific decoupling matrices according to (3.107) in Section 3.7 could be considered to proof the possibility to control the system output independently. Obviously, these matrices are regular, since otherwise the definition of the hybrid DoFs would be infeasible.

If the potential for smooth and lossless gear shifting once has been evaluated for all elementary gear shifts, this information can be used to evaluate all shift sequences, which might be performed as split shifts.

In summary, the shift analysis method presented in this section contributes a shift map, including the potential for smooth and lossless gear shifting, and evaluated shift sequences, considering additionally traction force intersections. Figure 4.19 gives an overview of this shift analysis method.
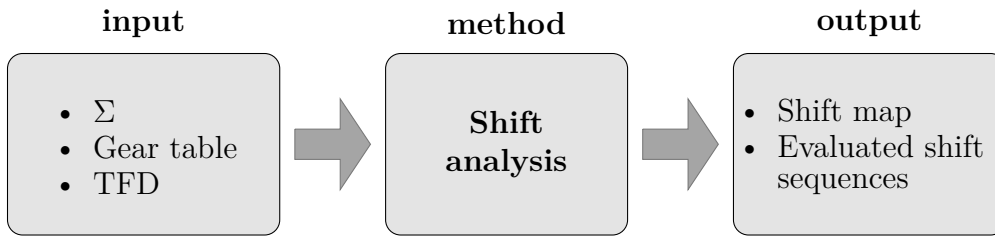
Figure 4.19: *Overview: shift analysis*

4.5 Summary and contribution

In this chapter an automated model-based DT analysis method based on the DT model proposed in Chapter 3 is presented. The method consists of three parts:

- The **gear analysis** outputs a gear table, which assigns an operation mode to each clutch state vector $\boldsymbol{\kappa}_i$ and lists the corresponding gear ratios and a unique gear naming.
- In combination with given ICE, EM and vehicle data, the **traction force analysis** states stationary traction forces for each gear, summarized graphically in a TFD, which can be used for evaluation of the DT drivability.
- The **shift analysis**, finally, considers the transition between gears, illustrated in a shift map. Possible shift sequences are determined and evaluated, with respect to traction force intersections and the potential for smooth and lossless shifting.

Figure 4.20 gives a summarizing overview of the presented model-based DT analysis method. The results of this analysis method are essential for the design of a DT
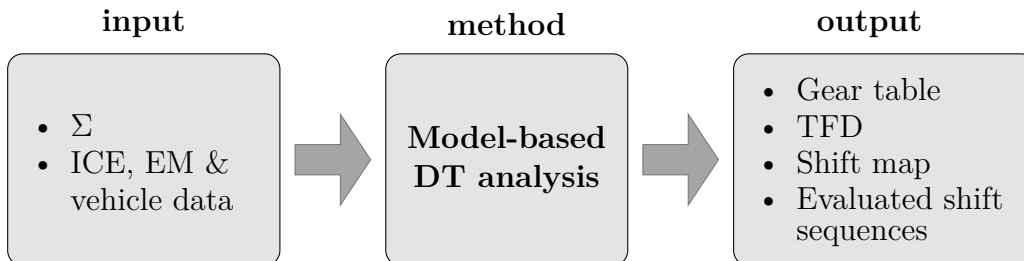
Figure 4.20: *Model-based DT analysis*

control system. In combination with the DT modeling software tool, presented in Chapter 3, the method supports the DT topology and EMS development process in general. It enables fast evaluation, validation and optimization of DT concepts in an early development phase.

5

Model-based drivetrain control system design

The preliminary investigations and contributions of the Chapters 2, 3 and 4 shall now be combined in order to implement a model-based control system to perform smooth and lossless gear shifts in a given dedicated hybrid DT. Based on a sequence of shift phases, with respect to switching control plants and control tasks, an IMC system will be proposed. The testing and evaluation of the control system will be done in Chapter 6.

5.1 Problem statement and outline

At the beginning of this chapter a short recap of the contributions of Chapters 2, 3 and 4 according to the problem statement in Section 2.6 shall be made. These contributions are:

- the concept of active smooth and lossless gear shifting to increase efficiency and drivability (Chapter 2),
- a generic computation of plant models for smooth and lossless gear shifting (Chapter 3),
- and a model-based shift analysis method including the potential for smooth and lossless gear shifting (Chapter 4).

The upcoming parts of the thesis try to bring together these contributions and to apply them in a model-based DT control system for gear shifting. The design of this control system is presented in this chapter. The testing and evaluation of the control system will be covered in Chapter 6.

Chapter 2 states the two general tasks of a DT control system:

- **Mode operation:** driving in a specific gear (control of wheel torque and hybrid DoFs, as discussed in Section 3.7)
- **Mode transition:** gear shifting (control of wheel torque, clutch slip / locking torque and clutch torques, as discussed in Section 3.8)

In order to combine both tasks for an exemplary implementation of a general DT
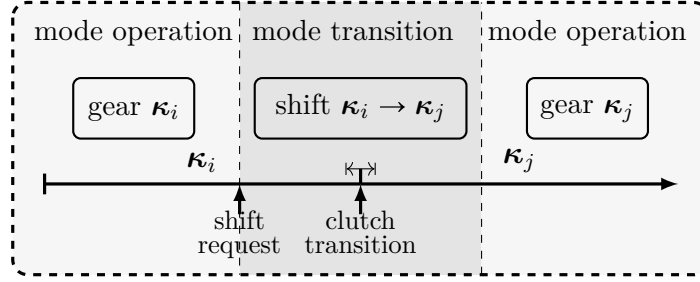
Figure 5.1: *Embedded gear shift*

control system, a gear shift can be embedded in between the operation of two gears: the initial gear ($\boldsymbol{\kappa}_i$) and the final gear ($\boldsymbol{\kappa}_j$). These so-called embedded gear shifts, see Figure 5.1, will be considered in this chapter. A DT control system shall be provided, which applies the concept of smooth and lossless gear shifting. According to Section 4.4.3 there are seven different, bidirectional shifts in single-EM dedicated hybrid DTs, listed in Table 4.11, which feature potential for smooth and lossless shifting. The presented DT control system focuses on the shifts between hybrid CVT and hybrid parallel modes (CV $\leftrightarrow$ Pa). However, opportunities for generalization will be pointed at the end of this chapter.

> **Problem statement:**
>
> Development and implementation of an exemplary DT control system for embedded gear shifts between a hybrid CVT and hybrid parallel mode based on the concept of smooth and lossless shifting

Section 2.5.2 states the input and output signals of a DT control system within a torque-based PT control structure. Figure 5.2 summarizes the input and output interface of the required DT control system. Two matched input signals – the gear request
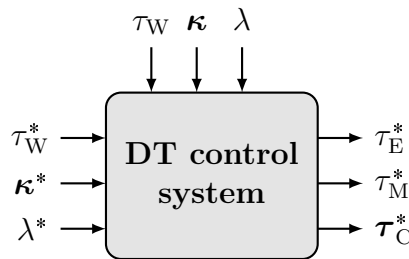
Figure 5.2: *Input and output signals of the DT control system implemented into a torque-based PT control system*

$\boldsymbol{\kappa}^*$ and the mode-specific hybrid DoF request λ^* – are provided by the EMS. It is necessary to use the mode information $\boldsymbol{\kappa}^*$ to interpret a request λ^*. For the considered embedded shifts applies:

$$\boldsymbol{\kappa}^* \in \{\boldsymbol{\kappa}_i, \boldsymbol{\kappa}_j\}. \tag{5.1}$$

The wheel torque request τ_{W}^* is computed by the driver interpretation system based on the accelerator pedal position. The actual values of the control variables $\tau_{\mathrm{W}}, \boldsymbol{\kappa}, \lambda$ are considered to be provided by an DT observer (see for example [15]). The output signals of the DT control system are ICE, EM and clutch torque requests $(\tau_{\mathrm{E}}^*, \tau_{\mathrm{M}}^*, \boldsymbol{\tau}_{\mathrm{C}}^*)$.

This chapter is structured as follows:

- Definition of a general sequence of consecutive shift phases and determination of corresponding plant models and control tasks
- Proposal of a switching IMC concept
- Exemplary implementation for a given single-EM dedicated hybrid DT

Before going into detail, a short statement on the state of the art is necessary.

5.1.1 State of the art

The concept of active smooth and lossless gear shifting in single-EM dedicated hybrid DTs is quite novel. The actual state of the art is hard to determine, since this research topic is mainly investigated in confidence by OEMs and Tier-1 suppliers. Partial aspects of smooth and lossless gear shifting, however, have been considered since many years. This section shall provide a concise selection on some publication to this topic.

Publication [64] considers a dedicated hybrid DT with two EMs. It proposes an optimal clutch slip control, with respect to vehicle jerk and dissipative clutch power, for a gear shift from a hybrid CVT to a hybrid parallel mode. Several other publications consider series-parallel hybrid DTs with one electric mode and one parallel mode, with the focus on smooth and quick clutch engagement, which is crucial for fuel efficiency and drivability within such DTs: In [65] a model reference control, in [66] a robust H_∞, and in [67] a Model Predictive Control (MPC) approach is applied to this control problem.

The control of conventional DTs is investigated in detail in [16, pp. 193] and [17, pp. 413] including transmission speed and torque control and active damping of DT oscillations. The transition to single-EM dedicated hybrid DTs can be considered as a generalization of these investigations.

In its principle form the control concept proposed in this chapter is similar to the one presented in [68] for the control of DT oscillation.

5.2 Sequence of shift phases

According to the above problem statement the embedded gear shift consists of three consecutive phases (see Figure 5.1) with different control tasks: mode operation of initial gear, shift between initial and final gear and mode operation of final gear. The application of the concept of smooth and lossless gear shifting requires a further splitting of the mode transition phase into shift preparation, clutch actuation and shift completion. Therefore, the control system in total has to handle five consecutive control phases, which are illustrated in Figure 5.3. The single phases of the shift
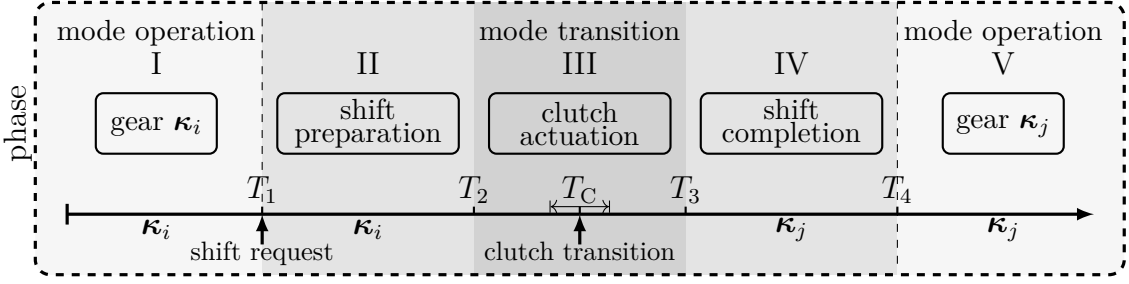
Figure 5.3: *Sequence of shift phases for control of an embedded smooth and lossless gear shift*

schedule in Figure 5.3, are now discussed in detail with respect to the control tasks and the corresponding plant models.

5.2.1 Mode operation

In the first phase the operation of the initial gear is controlled. A gear shift request has not been received yet. Therefore, the gear request corresponds with the actual gear:

$$\boldsymbol{\kappa}^* = \boldsymbol{\kappa} = \boldsymbol{\kappa}_i. \tag{5.2}$$

The DT control system has to handle three control tasks:

- tracking of the wheel torque τ_W, according to a request τ_W^*,
- tracking of the mode-specific hybrid DoF λ, according to a request λ^*,
- and maintaining the current gear $\boldsymbol{\kappa}_i$ engaged according to a requested gear $\boldsymbol{\kappa}^*$.

The third control task is related exclusively to the clutch torque requests. In order to maintain all engaged clutches engaged the following clutch torque request is sent to the clutch control system, which is responsible for the electro-hydraulic actuation of the clutch valve (see Figure 2.6):

$$\boldsymbol{\tau}_C^* = \boldsymbol{\kappa}_i \tau_{C,max}^*. \tag{5.3}$$

The parameter $\tau_{C,max}^*$ is specified in the clutch control system. This request corresponds to the maximum available hydraulic pressure at the clutch. For sake of simplicity $\tau_{C,max}^*$ is considered to be equal for all clutches. Actually, this parameter differs for each clutch according to its mechanical and hydraulic implementation, as well as the operation strategy of the DT. A relaxation of this simplification would simply require the consideration of a parameter vector $\boldsymbol{\tau}_{C,max}^*$. The clutch torque request (5.3) might be not optimal from efficiency perspective, since, the maximum torque, which can be transmitted according to this request, might be far higher than the actually transmitted torques. For steady mode operation, therefore, it is reasonable to constantly adapt this clutch torque requests to the actually transmitted torque, which can be estimated using a virtual clutch sensor as presented in Section 3.5.2 or using a state observer.

The remaining two control tasks have to be controlled by providing suitable torque requests for the ICE (τ_E^*) and the EM (τ_M^*). Section 3.7 provides plant models to this tasks, which state the dynamic relation between τ_W, λ and τ_E, τ_M (see Figure 5.4). The
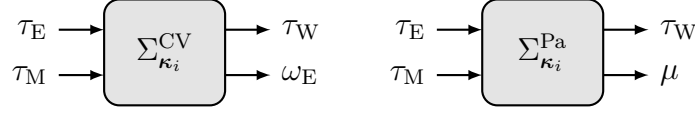
Figure 5.4: *Plant models for mode operation in hybrid CVT (left) respectively hybrid parallel (right) gear $\boldsymbol{\kappa}_i$*

mode operation phase of the final gear (fifth phase) is equivalent to this phase with $\boldsymbol{\kappa} = \boldsymbol{\kappa}_j$.

5.2.2 Mode transition

The mode operation phase ends, when a gear shift is requested by the EMS. This is the case, if the actual engaged gear $\boldsymbol{\kappa}$ differs from the gear request $\boldsymbol{\kappa}^*$:

$$\boldsymbol{\kappa}^* = \boldsymbol{\kappa}_j \neq \boldsymbol{\kappa} = \boldsymbol{\kappa}_i. \tag{5.4}$$

The occurrence of this event initiates the mode transition phase, which is split into three phases, according to the shift schedule in Figure 5.3:

- shift preparation,
- clutch actuation,
- and shift completion.

Shift preparation As already discussed in Sections 2.5.1, 3.8.1 and 4.4.3 the enabler of smooth and lossless gear shifts is the full synchronization respectively unloading of the actuated clutch. Whereas the tracking task of the wheel torque persists, in the shift preparation phase, therefore, the hybrid DoF request λ^* is temporarily ignored in the shift preparation phase. This task is replaced by the task to control clutch synchronization respectively unloading. Section 3.8 provides the control plants for this task for both cases clutch engagement and disengagement. According to their number of mechanical DoFs (see Tables 2.1 and 4.10) the first case applies for the shift CV $\rightarrow$ Pa and the second case for the shift Pa $\rightarrow$ CV. Figure 5.5 shows the corresponding plant models. In contrast to the tracking control tasks for mode operation control, the active
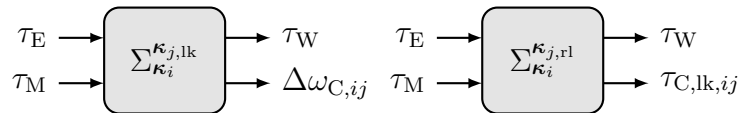
Figure 5.5: *Plant models for shift preparation ($\boldsymbol{\kappa}_i \rightarrow \boldsymbol{\kappa}_j$) in hybrid CVT (left) respectively hybrid parallel (right) gear $\boldsymbol{\kappa}_i$*

control of clutch synchronization respectively unloading requires also planning of an

appropriate reference trajectory. A polynomial approach will be discussed in section 5.3.2 to provide a reference trajectory $\Delta\omega_{\mathrm{C},ij}^*(t)/\tau_{\mathrm{C},\mathrm{lk},ij}^*(t)$. While the final value of this trajectory is fixed to zero, its initial value has to be coordinated to the mode operation phase (see Section 5.2.3). At the end of the shift preparation phase the clutch is ready for smooth and lossless engagement respectively disengagement.

During the shift preparation phase the current gear is still maintained engaged. In the case of a planned clutch engagement a predefined torque request $\tau_{\mathrm{C},\mathrm{KP}}^*$ is requested to the clutch ($\Delta\boldsymbol{\kappa}_{ij} \wedge \boldsymbol{\kappa}_j$). According to this request the clutch control system, controls the clutch to the so-called kiss-point (see for example [18, pp. 133]). After this so-called clutch filling at this kiss-point the clutch is ready for a fast engagement within the next control phase. Hence, the clutch torque request in the shift preparation phase computes as:

$$\boldsymbol{\tau}_{\mathrm{C},\mathrm{SP}}^* = \boldsymbol{\kappa}_i \tau_{\mathrm{C},\mathrm{max}}^* + (\Delta\boldsymbol{\kappa}_{ij} \wedge \boldsymbol{\kappa}_j)\tau_{\mathrm{C},\mathrm{KP}}^*. \tag{5.5}$$

Clutch actuation The clutch actuation phase is a prolongation of the shift preparation phase, with a fixed reference value:

$$\Delta\omega_{\mathrm{C},ij}^*/\tau_{\mathrm{C},\mathrm{lk},ij}^* = 0. \tag{5.6}$$

Therefore, the hybrid DoF request λ^* is still ignored. The new task in the clutch actuation control is to enforce the clutch transition from released into locked state (CV $\rightarrow$ Pa), respectively from locked into released state (Pa $\rightarrow$ CV). Therefore, in the first case (clutch engagement) the clutch torque request is ramped up from $\tau_{\mathrm{C},\mathrm{KP}}^*$ to $\tau_{\mathrm{C},\mathrm{max}}^*$. In the second case (clutch disengagement) it is ramped down from $\tau_{\mathrm{C},\mathrm{max}}^*$ to zero:

$$\boldsymbol{\tau}_{\mathrm{C},\mathrm{CA}}^*(t_{\mathrm{CA}}) = \boldsymbol{\kappa}_i \tau_{\mathrm{C},\mathrm{max}}^* + \Delta\boldsymbol{\kappa}_{ij}\Delta\tau_{\mathrm{C}}^*(t_{\mathrm{CA}}), \quad \forall t_{\mathrm{CA}} \in [0, T_{\mathrm{CA}}], \tag{5.7}$$

with:

$$\Delta\tau_{\mathrm{C}}^*(t_{\mathrm{CA}}) = \begin{cases} \frac{(\tau_{\mathrm{C},\mathrm{max}}^* - \tau_{\mathrm{C},\mathrm{KP}}^*)}{T_{\mathrm{CA}}} \cdot t_{\mathrm{CA}} & \text{for:} \quad \boldsymbol{\kappa}_i^T \boldsymbol{\kappa}_i < \boldsymbol{\kappa}_j^T \boldsymbol{\kappa}_j \\ -\frac{\tau_{\mathrm{C},\mathrm{max}}^*}{T_{\mathrm{CA}}} \cdot t_{\mathrm{CA}} & \text{for:} \quad \boldsymbol{\kappa}_i^T \boldsymbol{\kappa}_i > \boldsymbol{\kappa}_j^T \boldsymbol{\kappa}_j \end{cases}, \quad \forall t_{\mathrm{CA}} \in [0, T_{\mathrm{CA}}]. \tag{5.8}$$

The conditions for clutch transitions have been discussed in Section 3.8.1. According to (3.114) a minimal non-zero pressure on the clutch plates ($\tau_{\mathrm{C}}^* > \tau_{\mathrm{C},\mathrm{KP}}^*$), will lock the clutch, if it is fully synchronized ($\Delta\omega_{\mathrm{C},ij} = 0$). Consequently, in nominal case (perfect model matching and no disturbances) the transition will occur at the beginning of clutch transition phase. In practice the control system will always face model uncertainties and disturbances. The ramped clutch torque request in (5.8) ensures that residual clutch slip ($\Delta\omega_{\mathrm{C},ij,\mathrm{res}} \neq 0$) is handled with low dissipation. However, the clutch transition in this case will occur later within the clutch actuation phase.

On the other side a fully unloaded clutch ($\tau_{\mathrm{C},\mathrm{lk},ij} = 0$) releases for zero pressure on the clutch plates, according to (3.119). Considering the ramped clutch torque request in (5.8), hence, in nominal case the transition is expected at the end of clutch actuation

phase. Due to a unavoidable residual clutch torque ($\tau_{\mathrm{C,lk},ij,\mathrm{res}} \neq 0$) this transition may occur earlier.

In summary, the clutch actuation strategy in (5.8) is robust with respect to model uncertainties and disturbances. Since it is not possible to give guaranties about the maximal residual clutch slip $\Delta\omega_{\mathrm{C},ij,\mathrm{res}}$, respectively clutch torque $\tau_{\mathrm{C,lk},ij,\mathrm{res}}$, it is advisable for safety reasons to limit these values, when implementing a prototype control software. This keeps the possible clutch dissipation and hence temperature in a limited range in order to avoid clutch damage. If these residual limits are not met, the control system has to provide a safe failure mode, like for example the return to mode operation of the initial gear.

Shift completion   After the clutch actuation phase the DT has to be brought back into a stationary driving situation (mode operation). Therefore, the requested value for the hybrid DoF λ^*, which has been ignored in the last two phases, has to be recovered. In order to enable a smooth transition, a reference trajectory from the actual value λ to the request value λ^* is planned and tracked. Since this increases the locking torque respectively clutch slip at the clutch, which has been actuated in the clutch actuation phase, this phase can be considered as reversal of the shift preparation phase. Figure 5.6 illustrates the plant models for this control phase, which are equivalent to the plant models in the first shift phase for the final gear $\boldsymbol{\kappa}_j$.
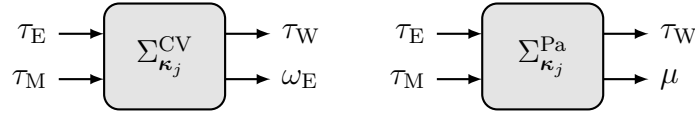
Figure 5.6: *Plant models for mode operation in hybrid CVT(left) respectively hybrid parallel (right) gear* $\boldsymbol{\kappa}_j$

The clutch torque request is equal to the request in mode operation of gear $\boldsymbol{\kappa}_j$:

$$\boldsymbol{\tau}^*_{\mathrm{C,SC}} = \boldsymbol{\kappa}_j \tau^*_{\mathrm{C,max}}. \tag{5.9}$$

Summary   In summary the clutch torque request according to the single control phases in (5.5), (5.7) and (5.9), is:

$$\tau^*_{\mathrm{C}}(t) = \begin{cases} \boldsymbol{\tau}^*_{\mathrm{C,SP}} & \text{for} \quad t \in [0, T_{\mathrm{SP}}], \\ \boldsymbol{\tau}^*_{\mathrm{C,CA}}(t) & \text{for} \quad t \in [T_{\mathrm{SP}}, T_{\mathrm{SP}} + T_{\mathrm{CA}}], \quad t = t_{\mathrm{CA}} - T_{\mathrm{CA}}, \\ \boldsymbol{\tau}^*_{\mathrm{C,SC}} & \text{for} \quad t \in [T_{\mathrm{SP}} + T_{\mathrm{CA}}, T_{\mathrm{SP}} + T_{\mathrm{CA}} + T_{\mathrm{SC}}]. \end{cases} \tag{5.10}$$

Figure 5.7 illustrates this clutch torque request for the clutch $\Delta\boldsymbol{\kappa}_{ij}$.

Figure 5.8 extends Figure 5.3 by the corresponding plant models and control tasks, which have been discussed in this section. Considering the entire shift schedule, the plant model shows a switching behavior: At $t = T_1$ and $t = T_3$ the control output is switched and at $t = T_{\mathrm{C}}$ the system dynamics switches according o the clutch transition. A detailed consideration of these plant model transitions is crucial in order to propose a continuous control of the entire embedded gear shift.
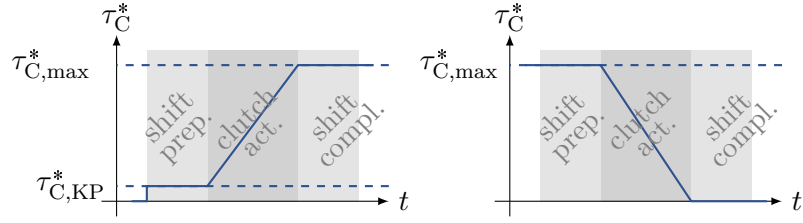
Figure 5.7: *Clutch torque request τ_C^* for clutch $\Delta\boldsymbol{\kappa}_{ij}$ in different shift phases according to (5.10) for clutch engagement (left) and disengagement (right)*
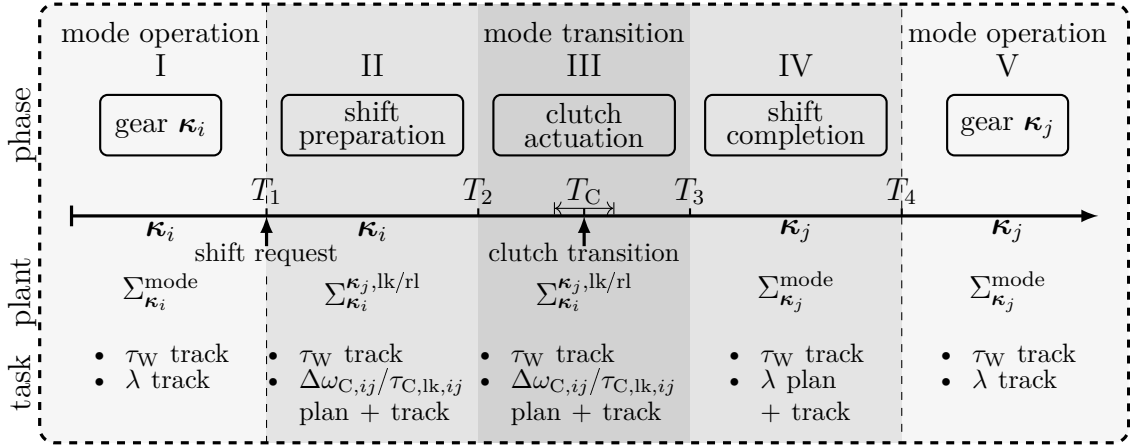
Figure 5.8: *Shift schedule, with corresponding control plants and tasks for the control of an embedded smooth and lossless gear shift*

5.2.3 Plant model transitions

The aforementioned three plant model transitions are now discussed in detail.

At $t = T_1$ one control output equation is switched from the hybrid DoF to the clutch slip resp. locking torque. In order to investigate this transition, the relation between the engine speed ω_E and the clutch slip of the clutch $\Delta\omega_{C,ij}$ which has to be engaged, respectively the relation between the torque split factor μ and the locking torque $\tau_{C,lk,ij}$ of the clutch which has to be disengaged, have to be considered.

According to Section 4.4.3 the relation between ω_E and $\Delta\omega_{C,ij}$ is determined by the constraint of the clutch $\Delta\boldsymbol{\kappa}_{ij}$:

$$\Delta\omega_{C,ij} = \Delta\boldsymbol{\kappa}_{ij}^T \bar{\mathbf{B}}_{i,C}^T \mathbf{q}_i = b_E\omega_E + b_F w_F. \tag{5.11}$$

Therefore, an equivalence condition for the plant models $\Sigma_{\boldsymbol{\kappa}_i}^{CV}$ and $\Sigma_{\boldsymbol{\kappa}_i}^{\boldsymbol{\kappa}_{j,lk}}$ for given w_F can be stated:

$$\Sigma_{\boldsymbol{\kappa}_i}^{CV} \triangleq \Sigma_{\boldsymbol{\kappa}_i}^{\boldsymbol{\kappa}_{j,lk}}\Big|_{(5.11)}. \tag{5.12}$$

For a parallel hybrid mode the investigations according to the mode specific kinematics and torques in Sections 4.2 and 4.3 show that the propulsion torques τ_E and τ_M sum to a propulsion torque acting at the final transmission shaft:

$$\tau_{F,P} = \mathbf{e}_F^T \mathbf{J}_{q,q_i} \bar{\mathbf{B}}_{i,P} = i_E\tau_E + i_M\tau_M, \tag{5.13}$$
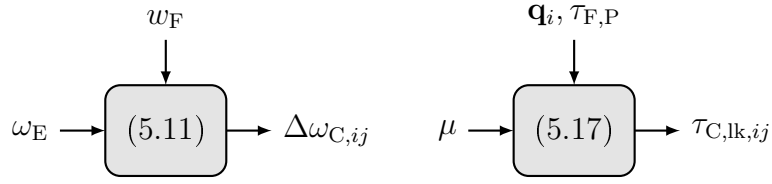
Figure 5.9: *Relations for plant model transitions between shift phases I and II ($t = T_1$)*

as stated in (3.85), with:

$$\mathbf{e}_{\mathrm{F}}^T \mathbf{q} = w_{\mathrm{F}}. \tag{5.14}$$

In combination with the torque split definition (mode specific hybrid DoF) in (3.106),

$$\mu = \frac{\tau_{\mathrm{E}}}{\tau_{\mathrm{E}} + \frac{i_{\mathrm{M}}}{i_{\mathrm{E}}} \tau_{\mathrm{M}}}, \tag{5.15}$$

hence, the input torque requests $\tau_{\mathrm{E}}^*, \tau_{\mathrm{M}}^*$ to achieve a specific torque $\tau_{\mathrm{F,P}}$ and a required torque split factor μ^* are uniquely defined:

$$\boldsymbol{\tau}_{\mathrm{P}} = \begin{bmatrix} \tau_{\mathrm{E}}^* \\ \tau_{\mathrm{M}}^* \end{bmatrix} = \begin{bmatrix} \frac{\mu^*}{i_{\mathrm{E}}} \\ \frac{(1-\mu^*)}{i_{\mathrm{M}}} \end{bmatrix} \tau_{\mathrm{F,P}}. \tag{5.16}$$

Using (3.85) delivers a relation to the torque transmitted at the clutch $\Delta\boldsymbol{\kappa}_{ij}$:

$$\tau_{\mathrm{C,lk},ij} = \mathbf{c}_{ij,\mathrm{rl}}^T \mathbf{q}_i + \mathbf{d}_{ij,\mathrm{rl}}^T \boldsymbol{\tau}_{\mathrm{P}} = \mathbf{c}_{ij,\mathrm{rl}}^T \mathbf{q}_i + \begin{bmatrix} k_{\mathrm{E}} & k_{\mathrm{M}} \end{bmatrix} \begin{bmatrix} \frac{\mu^*}{i_{\mathrm{E}}} \\ \frac{(1-\mu^*)}{i_{\mathrm{M}}} \end{bmatrix} \tau_{\mathrm{F,P}}^*$$

$$= \left[\mathbf{c}_{ij,\mathrm{rl}}^T \mathbf{q}_i + \frac{k_{\mathrm{M}}}{im} \tau_{\mathrm{F,P}}^* \right] + \left[\frac{k_{\mathrm{E}}}{i_{\mathrm{E}}} - \frac{k_{\mathrm{M}}}{i_{\mathrm{M}}} \right] \tau_{\mathrm{F,P}}^* \cdot \mu^*. \tag{5.17}$$

This reveals that $\tau_{\mathrm{C,lk},ij}$ is uniquely defined for a given request μ^* and driving situation (states $\mathbf{q}_i$ and $\tau_{\mathrm{F,P}}$):

$$\Sigma_{\boldsymbol{\kappa}_i}^{\mathrm{Pa}} \triangleq \Sigma_{\boldsymbol{\kappa}_i}^{\boldsymbol{\kappa}_{j,\mathrm{rl}}} \Big|_{(5.17)}. \tag{5.18}$$

Figure 5.9 illustrates the relations for plant model transition at $t = T_1$.

The next considered plant model transition is the actual clutch transition at $t = T_{\mathrm{C}}$, which is planned to occur in shift phase III. In a first step the clutch $\Delta\boldsymbol{\kappa}_{ij}$ in system $\Sigma_{\boldsymbol{\kappa}_i}^{\boldsymbol{\kappa}_{j,\mathrm{lk}}}$ is assumed to be fully synchronized:

$$\Delta\omega_{\mathrm{C},ij} = \Delta\boldsymbol{\kappa}_{ij}^T \bar{\mathbf{B}}_{i,\mathrm{C}}^T \mathbf{q}_i = 0 \quad \Rightarrow \quad \mathbf{q}_i = \mathbf{J}_{\mathrm{q}_i,\mathrm{q}_j} \mathbf{q}_j. \tag{5.19}$$

In order to maintain the clutch synchronized also the derivative of the clutch slip has to be zero:

$$\Delta\dot{\omega}_{\mathrm{C},ij} = \Delta\boldsymbol{\kappa}_{ij}^T \bar{\mathbf{B}}_{i,\mathrm{C}}^T \dot{\mathbf{q}}_i = \Delta\boldsymbol{\kappa}_{ij}^T \bar{\mathbf{B}}_{i,\mathrm{C}}^T \bar{\mathbf{M}}_i^{-1} \left[\bar{\mathbf{A}}_i \mathbf{q}_i + \bar{\mathbf{B}}_{i,\mathrm{P}} \boldsymbol{\tau}_{\mathrm{P}} \right] = 0. \tag{5.20}$$

On the other side the assumption of a fully unloaded clutch $\Delta \boldsymbol{\kappa}_{ij}$ in system $\Sigma_{\boldsymbol{\kappa}_j}^{\boldsymbol{\kappa}_{i,\mathrm{rl}}}$ in a second step reveals:

$$\tau_{\mathrm{C,lk},ij} = -\left[\Delta \boldsymbol{\kappa}_{ij}^T \bar{\mathbf{B}}_{\mathrm{C},i}^T \bar{\mathbf{M}}_i^{-1} \bar{\mathbf{B}}_{\mathrm{C},i} \Delta \boldsymbol{\kappa}_{ij}\right]^{-1} \Delta \boldsymbol{\kappa}_{ij}^T \bar{\mathbf{B}}_{\mathrm{C},i}^T \bar{\mathbf{M}}_i^{-1} \left[\bar{\mathbf{A}}_i \mathbf{J}_{\mathbf{q}_i,\mathbf{q}_j} \mathbf{q}_i + \bar{\mathbf{B}}_{i,\mathrm{P}} \boldsymbol{\tau}_{\mathrm{P}}\right] = 0, \tag{5.21}$$

with:

$$\det\left(\left[\Delta \boldsymbol{\kappa}_{ij}^T \bar{\mathbf{B}}_{\mathrm{C},i}^T \bar{\mathbf{M}}_i^{-1} \bar{\mathbf{B}}_{\mathrm{C},i} \Delta \boldsymbol{\kappa}_{ij}\right]\right) \neq 0. \tag{5.22}$$

The comparison between (5.19) and (5.20) with (5.21) reveals that input torques $\boldsymbol{\tau}_{\mathrm{P}}$ applied to the system $\Sigma_{\boldsymbol{\kappa}_i}^{\boldsymbol{\kappa}_{j,\mathrm{lk}}}$, which maintain the clutch synchronized, maintain the clutch unloaded when they are applied to the system $\Sigma_{\boldsymbol{\kappa}_j}^{\boldsymbol{\kappa}_{i,\mathrm{rl}}}$:

$$\Sigma_{\boldsymbol{\kappa}_i}^{\boldsymbol{\kappa}_{j,\mathrm{lk}}}\bigg|_{\Delta \omega_{\mathrm{C},ij}, \Delta \dot{\omega}_{\mathrm{C},ij}=0} \stackrel{\triangle}{=} \Sigma_{\boldsymbol{\kappa}_j}^{\boldsymbol{\kappa}_{i,\mathrm{rl}}}\bigg|_{\tau_{\mathrm{C,lk},ij}=0}. \tag{5.23}$$

Equivalently applies:

$$\Sigma_{\boldsymbol{\kappa}_i}^{\boldsymbol{\kappa}_{j,\mathrm{rl}}}\bigg|_{\tau_{\mathrm{C,lk},ij}=0} \stackrel{\triangle}{=} \Sigma_{\boldsymbol{\kappa}_j}^{\boldsymbol{\kappa}_{i,\mathrm{lk}}}\bigg|_{\Delta \omega_{\mathrm{C},ij}, \Delta \dot{\omega}_{\mathrm{C},ij}=0}. \tag{5.24}$$

This fact proofs that it is feasible to use one controller for the entire shift phase III although the plant model dynamics switches within this phase.

Finally, (5.12) and (5.18) can be reused to investigate the remaining plant model transition between shift phases III and IV at $t = T_2$:

$$\Sigma_{\boldsymbol{\kappa}_i}^{\boldsymbol{\kappa}_{j,\mathrm{lk}}} \stackrel{\triangle}{=} \Sigma_{\boldsymbol{\kappa}_j}^{\mathrm{Pa}}\bigg|_{(5.11)}, \tag{5.25}$$

$$\Sigma_{\boldsymbol{\kappa}_i}^{\boldsymbol{\kappa}_{j,\mathrm{rl}}} \stackrel{\triangle}{=} \Sigma_{\boldsymbol{\kappa}_j}^{\mathrm{CV}}\bigg|_{(5.17)}. \tag{5.26}$$

The investigations about the plant model transitions substantiates that it is possible to apply a switching controller, which produces continuous control requests τ_{E}^* and τ_{M}^*. Furthermore, these investigations enable an interesting opportunity to transform control tasks according to (5.12) and (5.18) at $t = T_1$, respectively (5.25) and (5.26) at $t = T_3$: For given w_{F} there is a unique engine speed,

$$\omega_{\mathrm{E}} = \omega_{\mathrm{E,sync}}(w_{\mathrm{F}}), \tag{5.27}$$

for which the clutch is synchronized. Hence, the original control task of clutch synchronization can be transformed to an ICE speed control:

$$\Delta \omega_{\mathrm{C},ij} \to 0 \quad \mapsto \quad \omega_{\mathrm{E}} \to \omega_{\mathrm{E,sync}}(w_{\mathrm{F}}). \tag{5.28}$$

Equivalently, for given $\mathbf{q}_i$ and $\tau_{\mathrm{F,P}}$ there is a unique torque split factor,

$$\mu = \mu_{\mathrm{unload}}(\mathbf{q}_i, \tau_{\mathrm{F,P}}), \tag{5.29}$$

for which the clutch is unloaded. Hence, the original control task of clutch unloading can be transformed to a torque split factor control:

$$\tau_{\mathrm{C,lk},ij} \to 0 \quad \mapsto \quad \mu \to \mu_{\mathrm{unload}}(\mathbf{q}_i, \tau_{\mathrm{F,P}}). \tag{5.30}$$

Due to the implicit character of a control approach following these transformations, the terms implicit clutch synchronization respectively. implicit clutch unloading (cf. [35]) are suitable. Equivalently, the control tasks of shift completion phase (IV) can be transformed. The decision, if a transformation of control tasks is beneficial, is related to the availability of physical and virtual sensors. For example, if a clutch slip sensor is implemented at the corresponding clutch, it is reasonable to directly control the clutch slip, in order to prevent inaccuracy according to a control task transformation. In contrast, if a clutch slip sensor is absent, whereas a precise engine speed sensor is available it might be beneficial to transform the control task to engine speed control. Since (5.23) respectively (5.24) are static relations, a transformation of control tasks is not applicable for $\Delta\omega_{\mathrm{C},ij} \leftrightarrow \tau_{\mathrm{C,lk},ij}$.

Table 5.1 lists special sequences of plant models for a general shift between a hybrid CVT and a hybrid parallel gear with respect to the proposed control task transformations. The sequences target on a minimum number of different plant models in order to reduced control implementation effort. The set of in total three different plant models $(\Sigma_{\boldsymbol{\kappa}_i}^{\mathrm{CV}}, \Sigma_{\boldsymbol{\kappa}_j}^{\mathrm{Pa}}, \Sigma_{\boldsymbol{\kappa}_i}^{\boldsymbol{\kappa}_j,\mathrm{lk}})$, will be used for the exemplary control implementation in Section 5.4. These sequences of plant models and corresponding control tasks are the

Table 5.1: *Sequences of plant models for the shifts* $\mathrm{CV}(\boldsymbol{\kappa}_i) \leftrightarrow \mathrm{Pa}(\boldsymbol{\kappa}_j)$ *with a minimal number of models in total*

gears		phase plant models				
initial	final	I	II	III	IV	V
$\mathrm{CV}(\boldsymbol{\kappa}_i)$	$\mathrm{Pa}(\boldsymbol{\kappa}_j)$	$\Sigma_{\boldsymbol{\kappa}_i}^{\mathrm{CV}}$	$\Sigma_{\boldsymbol{\kappa}_i}^{\boldsymbol{\kappa}_j,\mathrm{lk}}$	$\Sigma_{\boldsymbol{\kappa}_i}^{\boldsymbol{\kappa}_j,\mathrm{lk}}$	$\Sigma_{\boldsymbol{\kappa}_j}^{\mathrm{Pa}}$	$\Sigma_{\boldsymbol{\kappa}_j}^{\mathrm{Pa}}$
$\mathrm{Pa}(\boldsymbol{\kappa}_j)$	$\mathrm{CV}(\boldsymbol{\kappa}_i)$	$\Sigma_{\boldsymbol{\kappa}_j}^{\mathrm{Pa}}$	$\Sigma_{\boldsymbol{\kappa}_j}^{\mathrm{Pa}}$	$\Sigma_{\boldsymbol{\kappa}_i}^{\boldsymbol{\kappa}_j,\mathrm{lk}}$	$\Sigma_{\boldsymbol{\kappa}_i}^{\mathrm{CV}}$	$\Sigma_{\boldsymbol{\kappa}_i}^{\mathrm{CV}}$

basis for the design of a switching control system.

5.3 Model-based control concept

This section proposes a concept for the control of an embedded, smooth and lossless gear shift with respect to the shift phases and plant models in Figure 5.8 and Table 5.1. The proposed concept relies on a classical inversion-based feedforward control design, which is extended to an IMC system. Low-pass filtering and polynomial trajectory planning are applied to generate appropriate reference signals. Finally, the implementation of the concept in discrete time is considered, which is mandatory for the application in an automotive control unit.

5.3.1 Inversion-based feedforward control

The basic idea of inversion-based feedforward control is to design a controller, which inverts the system dynamics of the control plant in order to achieve perfect reference tracking in the nominal case. As any feedforward control design this concept is only applicable for stable plant dynamics. However, also in case of stable plant dynamics in practical application an extension by a feedback loop is mandatory in order to ensure robustness with respect to model uncertainties and disturbances. Such a feedback loop extension will be discussed in Section 5.3.3. The concept of inversion-based feedforward control shall now be considered in more detail for linear SISO plant models, before it is generalized for the planned application to linear MIMO plant models, for the control of gear shifts.

The input-output characteristic of a general SISO system,

$$\Sigma: \quad \dot{\mathbf{x}} = \mathbf{A}\mathbf{x} + \mathbf{b}u, \tag{5.31}$$

$$y = \mathbf{c}^T\mathbf{x} + du, \tag{5.32}$$

can be described in the frequency domain by its transfer function:

$$G(s) = \frac{y(s)}{u(s)} = \mathbf{c}^T\left(s\mathbf{I} - \mathbf{A}\right)^{-1}\mathbf{b} + d = \frac{b(s)}{a(s)} = \frac{b_p s^p + \cdots + b_1 s + b_0}{s^n + a_{n-1}s^{n-1} + \cdots + a_1 s + a_0}. \tag{5.33}$$

In order to apply a control signal $u(t)$ (see Figure 5.10), which achieves a perfect tracking of the system output $y(t)$, with respect to a reference trajectory $w(t)$,

$$y(t) = w(t) \quad \forall t \geqslant 0, \tag{5.34}$$

the controller transfer function $C(s)$ has to be the inverse of the transfer function $G(s)$:

$$y(s) = G(s)\tilde{C}(s)w(s) \stackrel{!}{=} w(s) \quad \Rightarrow \quad \tilde{C}(s) = \frac{u(s)}{w(s)} \stackrel{!}{=} G(s)^{-1}. \tag{5.35}$$
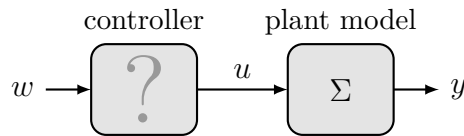
Figure 5.10: *Feedforward control structure with reference trajectory w, controller, system input u, plant model Σ and system output y.*

According to (5.33) the transfer function of the controller is:

$$G^{-1}(s) = \frac{a(s)}{b(s)} = \frac{s^n + a_{n-1}s^{n-1} + \cdots + a_1 s + a_0}{b_p s^p + \cdots + b_1 s + b_0}. \tag{5.36}$$

The difference of the degrees of the polynomials $a(s)$ and $b(s)$ is called relative degree δ of the system in (5.31):

$$\delta = n - p. \tag{5.37}$$

This system parameter has already been discussed in detail in Section 4.4.3. For $\delta > 0$, $G^{-1}(s)$ is an improper transfer function, which can not be implemented as a dynamical system. In literature, for example in [69], the term non-realizability is used to describe this property. A splitting of the polynomial $a(s)$ into two polynomials of degree δ and p,

$$a(s) = \bar{a}(s) \cdot \tilde{a}(s), \tag{5.38}$$

with,

$$\bar{a}(s) = s^\delta + \bar{a}_{\delta-1}s^{\delta-1} + \cdots + \bar{a}_1 s + \bar{a}_0, \tag{5.39}$$

$$\tilde{a}(s) = s^p + \tilde{a}_{p-1}s^{p-1} + \cdots + \tilde{a}_1 s + \tilde{a}_0, \tag{5.40}$$

yields a two-stage controller (see Figure 5.11):

$$G^{-1}(s) = \underbrace{\bar{a}(s)}_{\bar{C}(s)} \cdot \underbrace{\frac{\tilde{a}(s)}{b(s)}}_{C(s)}, \tag{5.41}$$

where $\bar{C}(s)$ is a improper and $C(s)$ a proper transfer function. A consideration of the
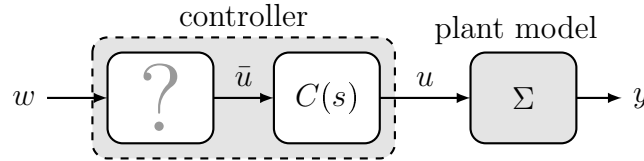
Figure 5.11: *Two-stage controller, with improper transfer function $\bar{C}(s)$ and proper transfer function $C(s)$*

improper controller $\bar{C}(s)$ in time domain delivers:

$$\bar{u}(s) = \bar{C}(s)w(s)$$

$$\bar{u}(t) = w^{(\delta)} + \bar{a}_{\delta-1}w^{(\delta-1)} + \cdots + \bar{a}_1\dot{w}(t) + \bar{a}_0 w(t) = \bar{\mathbf{c}}^T\mathbf{w}_\delta(t), \tag{5.42}$$

with:

$$\bar{\mathbf{c}}^T := \begin{bmatrix} \bar{a}_0 & \bar{a}_1 & \ldots & \bar{a}_{\delta-1} & 1 \end{bmatrix}, \tag{5.43}$$

$$\mathbf{w}_\delta(t) := \begin{bmatrix} w(t) & \dot{w}(t) & \ldots & w^{(\delta)}(t) \end{bmatrix}. \tag{5.44}$$

Consequently, the computation of the control signal $\bar{u}(t)$ turns into an algebraic equation, if the reference trajectory $w(t)$ and its δ derivatives are known in advance. Therefore, all trackable reference trajectories, have to be δ-times differentiable functions. Two possibilities for the generation of such trajectories and their derivatives will be considered in Section 5.3.2.
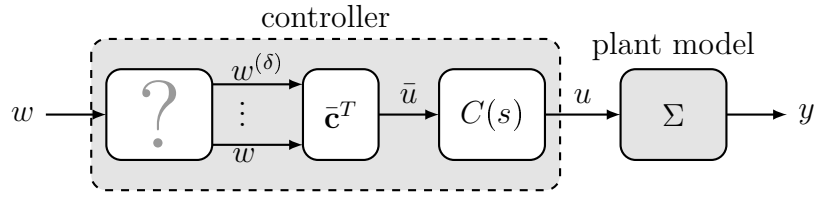
Figure 5.12: *Inversion-based feedforward control structure for a SISO plant model, consisting of the algebraic equation (5.42) and the proper transfer function $C(s)$ in (5.41)*

The resulting inversion-based feedforward controller, see Figure 5.12, hence is the combination of an algebraic equation (5.42) and the linear filter $C(s)$ in (5.41). Although $C(s)$ is for sure a proper transfer function, it might be unstable, if the plant transfer function $G(s)$ includes unstable zeros,

$$b(s_i) = 0, \quad \text{with} \quad \text{Re}\{s_i\} \geqslant 0. \tag{5.45}$$

The feedforward control and later IMC of such so-called non-minimum phase systems is covered for example in [69]. As this behavior does not occur in the control of gear shifts, it will not be considered within this thesis.

Before considering the generation of trajectories $w(t), \ldots, w^{(\delta)}(t)$, the basic structure of this inversion-based feedforward control design is generalized to MIMO systems:

$$\Sigma: \quad \dot{\mathbf{x}} = \mathbf{A}\mathbf{x} + \mathbf{B}\mathbf{u}, \tag{5.46}$$

$$\mathbf{y} = \mathbf{C}\mathbf{x} + \mathbf{D}\mathbf{u}. \tag{5.47}$$

The input-output characteristic of this system in frequency domain is defined by a transfer matrix:

$$\mathbf{G}(s) = \frac{\mathbf{y}(s)}{\mathbf{u}(s)} = \mathbf{C}\left(s\mathbf{I} - \mathbf{A}\right)^{-1}\mathbf{B} + \mathbf{D} = \begin{bmatrix} G_{11}(s) & \ldots & G_{1p}(s) \\ \vdots & & \vdots \\ G_{m1}(s) & \ldots & G_{mp}(s) \end{bmatrix}, \tag{5.48}$$

where each element of the transfer matrix is a transfer function:

$$G_{ij}(s) = \frac{b_{ij}(s)}{a_{ij}(s)}, \quad i = 1, \ldots, m, \quad j = 1, \ldots, p. \tag{5.49}$$

The number of rows in $\mathbf{G}(s)$ corresponds to the number of system outputs (m) and the number of columns to the number of system inputs (p). An inverse transfer matrix $\mathbf{G}^{-1}(s)$,

$$\mathbf{G}(s)^{-1}\mathbf{G}(s) = \mathbf{I}, \tag{5.50}$$

exists and is unique for an equal number ($p = m$) of linearly independent inputs and outputs (see for example [70, p. 10]):

$$\mathbf{G}(s)^{-1} = \begin{bmatrix} \hat{G}_{11}(s) & \ldots & \hat{G}_{1m}(s) \\ \vdots & & \vdots \\ \hat{G}_{m1}(s) & \ldots & \hat{G}_{mm}(s) \end{bmatrix}, \tag{5.51}$$

with:

$$\hat{G}_{ij}(s) = \frac{\hat{a}_{ij}(s)}{\hat{b}_{ij}(s)} = \frac{s^{n_{ij}} + \hat{a}_{ij,n_{ij}-1}s^{n_{ij}-1} + \cdots + \hat{a}_{ij,1}s + \hat{a}_{ij,0}}{\hat{b}_{ij,m_{ij}}s^{m_{ij}} + \cdots + \hat{b}_{ij,1}s + \hat{b}_{ij,0}}, \quad i,j = 1,\ldots,m. \tag{5.52}$$

Accept for the special case that $\mathbf{G}(s)$ is a diagonal matrix, the transfer functions $\hat{G}_{ij}(s)$ can not be computed by the inversion of the transfer functions $G_{ij}(s)$:

$$\hat{G}_{ij}(s) \neq G_{ij}^{-1}(s), \quad i,j = 1,\ldots,m. \tag{5.53}$$

Like in the SISO case, a splitting of the polynomials $\hat{a}_{i,j}(s)$,

$$\hat{a}_{ij}(s) = \bar{a}_{ij}(s) \cdot \tilde{a}_{ij}(s), \quad i,j = 1,\ldots,m, \tag{5.54}$$

can be applied, where $\bar{a}_{ij}(s)$ is a polynomial of degree δ_{ij}, with

$$\delta_{ij} = n_{ij} - p_{ij}, \tag{5.55}$$

which is the relative degree of the transfer function $\hat{G}_{ij}^{-1}(s)$, and $\tilde{a}_{ij}(s)$ is a polynomial of degree p_{ij}. This splits the transfer functions $\hat{G}_{ij}(s)$ into a proper part,

$$C_{ij}(s) = \frac{\tilde{a}_{ij}(s)}{\hat{b}_{ij}(s)}, \quad i,j = 1,\ldots,m, \tag{5.56}$$

and an improper part:

$$\bar{C}_{ij}(s) = \bar{a}_{ij}(s), \quad i,j = 1,\ldots,m, \tag{5.57}$$

As every row of the matrix $\mathbf{G}^{-1}(s)$ concerns the same reference input, it is reasonable to determine the maximum $\bar{\delta}_i$ of all relative degrees δ_{ij} of the transfer functions $\hat{G}_{ij}^{-1}(s)$, in each row of the matrix $\mathbf{G}^{-1}(s)$:

$$\bar{\delta}_i := \max\left(\delta_{ij}\right), \quad j = 1,\ldots,m. \tag{5.58}$$

The parameters $\bar{\delta}_i$, consequently, define the number derivatives of the reference trajectories $w_1(t),\ldots,w_m(t)$, which are necessary to implement the improper part of the controller $\bar{C}_{ij}(s)$ in algebraic equations:

$$\bar{u}_{ij}(t) = \bar{\mathbf{a}}_{ij}^T \mathbf{w}_{i,\delta_i}, \quad i,j = 1,\ldots,m. \tag{5.59}$$

with:

$$\bar{\mathbf{c}}_{ij}^T := \begin{bmatrix} \bar{a}_{ij,0} & \ldots & \bar{a}_{ij,\delta_{ij}-1} & 1 & \mathbf{0}_{1\times(\delta_i-\delta_{ij})} \end{bmatrix}, \quad i,j = 1,\ldots,m, \tag{5.60}$$

$$\mathbf{w}_{i,\delta_i}(t) := \begin{bmatrix} w_i(t) & \dot{w}_i(t) & \ldots & w_i^{(\bar{\delta}_i)}(t) \end{bmatrix}, \quad i = 1,\ldots,m. \tag{5.61}$$

Note that the parameters $\bar{\delta}_i$ differ from the relative degrees δ_i of the output y_i with respect to $\mathbf{u}$ as defined in (4.45) in Section 4.4.3.
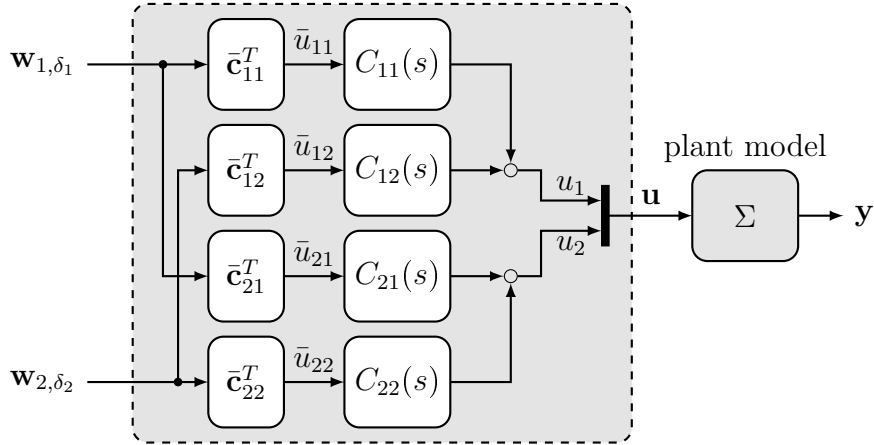
Figure 5.13: *Implementation of an inversion-based feedforward control structure for a MIMO plant model with two control inputs and two control outputs, consisting of the algebraic equations (5.59) and the proper transfer functions $C_{ij}(s)$ in (5.56) with respect to two reference trajectory vectors $\mathbf{w}_{1,\delta_1}$ and $\mathbf{w}_{2,\delta_2}$*

Figure 5.13 shows the final structure of the inversion-based MIMO feedforward controller with $m = 2$.

To conclude the inversion-based feedforward control of MIMO LTI systems some remarks are necessary: As already discussed in SISO case unstable zeros of a transfer function (non-minimum phase behavior) have to be considered in the feedforward control design in order to avoid an unstable controller. The zeros of MIMO systems (see for example [71, pp. 37] and [72, pp. 47]) do not correspond to the zeros of the transfer functions $G_{ij}(s)$ in general. They can be determined for example by transformation of the transfer matrix into Smith-McMillan form. A comprehensive survey on the poles and zeros of MIMO LTI systems can be found in [73]. The stability of an inversion-based feedforward controller, which might be influenced by these zeros, can be evaluated considering the poles of the transfer functions $\hat{G}_{ij}(s)$. In addition to the requirement of a stable controller, it is necessary for MIMO systems to check whether the control outputs can be controlled independently. This so-called decoupling problem has already been discussed in Section 4.4.3.

5.3.2 Generation of reference trajectories

The inversion-based feedforward control design presented in the last section requires the knowledge of a reference trajectory $w(t)$ and its r derivatives $\dot{w}(t), \ldots, w^{(r)}(t)$ (see Figure 5.12):

$$\mathbf{w}(t) = \begin{bmatrix} w(t) \\ \dot{w}(t) \\ \vdots \\ w^{(r)}(t) \end{bmatrix}. \tag{5.62}$$

In this section two possibilities to generate such trajectory vectors **w** are discussed. The fist one, a low-pass filter approach, is applicable, if the generated trajectory has to replicate the course of a given reference signal. The second one, a polynomial planning approach, is applicable, if the trajectory shall provide a smooth transition in finite time with respect to a set-point reference signal. While the first approach will be applied for the tracking control of the wheel torque and the hybrid DoF, the second approach will be applied in the shift preparation and completion phase for smooth clutch synchronization and unloading.

Trajectory generation by a low-pass filtering

A general, given reference signal $w(t)$ can not be considered to be continuously differentiable. Therefore, it has to be modified, in order to provide a trajectory vector **w**. A simple approach is to apply a linear filter (see Figure 5.14).

filter

$$w \longrightarrow \boxed{\Sigma_{\mathrm{F}}} \begin{array}{c} \longrightarrow w_{\mathrm{F}}^{(r)} \\ \vdots \\ \longrightarrow w_{\mathrm{F}} \end{array}$$
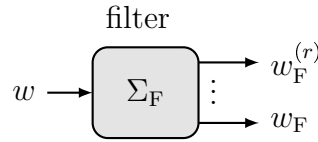
Figure 5.14: *Linear filter with transfer matrix* **F**(s) *in (5.67) to generate a trajectory* $w_{\mathrm{F}}(t)$ *and (r) derivatives*

A possible transfer function for such a filter is,

$$F(s) = \frac{w_{\mathrm{F}}(s)}{w(s)} = \frac{1}{(sT_{\mathrm{F}} + 1)^r}, \tag{5.63}$$

which is a general low-pass filter of order r, with filter time constant τ_{F}. According to τ_{F}, high frequency components of $w(t)$ are damped. For sufficiently slow changes in $w(t)$ holds:

$$w_{\mathrm{F}}(t) \approx w(t). \tag{5.64}$$

A transformation of the corresponding derivatives into frequency domain,

$$w_{\mathrm{F}}^{(i)}(t) \circ\!\!\!-\!\!\!\bullet\, s^i w_{\mathrm{F}}(s) = s^i F(s) w_{\mathrm{F}}(s), \quad i = 1, \ldots, r. \tag{5.65}$$

shows that a trajectory vector $\mathbf{w}_{\mathrm{F}}$, can be obtained by

$$\mathbf{w}_{\mathrm{F}} = \begin{bmatrix} w_{\mathrm{F}} & \dot{w}_{\mathrm{F}} & \ldots & w_{\mathrm{F}}^{(r)} \end{bmatrix}^T = \mathbf{F}(s) w(s), \tag{5.66}$$

with:

$$\mathbf{F}(s) = \begin{bmatrix} F(s) \\ sF(s) \\ \vdots \\ s^r F(s) \end{bmatrix}. \tag{5.67}$$
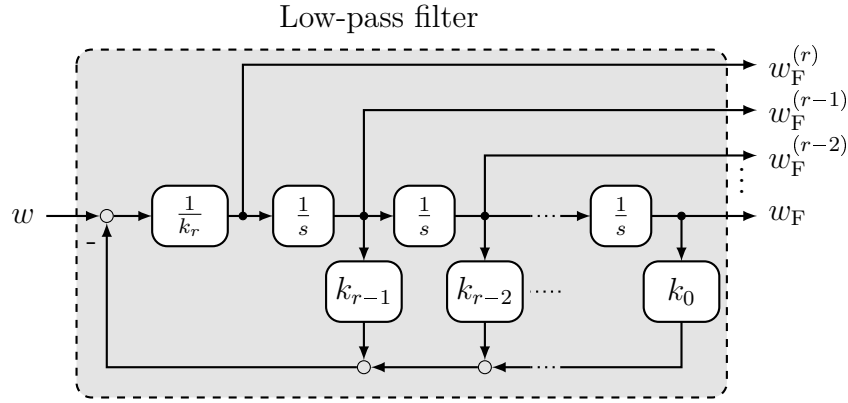
Low-pass filter

Figure 5.15: *Exemplary implementation of a low-pass filter to compute a smooth reference trajectory and its derivatives*

Figure 5.15 shows an exemplary implementation of the filter as proposed in [69, p. 61].

The constants $k_0, \ldots, k_r$ refer to the expansion of (5.63):

$$F(s) = \frac{1}{(sT_{\mathrm{F}} + 1)^r} = \frac{1}{k_r s^r + k_{r-1} s^{r-1} + k_1 s + k_0}. \tag{5.68}$$

As presented in [57] the coefficients $k_0, \ldots, k_r$ can be computed with:

$$k_i = \binom{r}{i} T_{\mathrm{F}}^i, \quad i = 0, \ldots, r. \tag{5.69}$$

Trajectory generation by planning of polynomials

A different approach to generate a reference trajectory vector $\mathbf{w}$ is motivated by the common task to control a system with respect to a piece-wise constant reference signal – a so-called set-point reference signal. In such applications a trajectory for a smooth transition to the new set-point value within a given finite transition time has to be planned. Hence, from mathematical point of view the task is to plan a r-times differentiable trajectory $w_{\mathrm{P}}(t)$ within the interval $t \in [T_{\mathrm{i}}, T_{\mathrm{f}}]$ according to given boundary conditions (see Figure 5.16). These boundary conditions separate into initial boundary conditions (at $t = T_{\mathrm{i}}$):

$$\mathbf{w}_{\mathrm{P}}(T_{\mathrm{i}}) \overset{!}{=} \mathbf{w}_{\mathrm{i}}, \tag{5.70}$$

with:

$$\mathbf{w}_{\mathrm{P}}(T_{\mathrm{i}}) := \begin{bmatrix} w_{\mathrm{P}}(T_{\mathrm{i}}) & \dot{w}_{\mathrm{P}}(T_{\mathrm{i}}) & \ldots & w_{\mathrm{P}}^{(r)}(T_{\mathrm{i}}) \end{bmatrix}^T, \tag{5.71}$$

$$\mathbf{w}_{\mathrm{i}} := \begin{bmatrix} w_{\mathrm{i}} & \dot{w}_{\mathrm{i}} & \ldots & w_{\mathrm{i}}^{(r)} \end{bmatrix}^T, \tag{5.72}$$

and final boundary conditions (at $t = T_{\mathrm{f}}$):

$$\mathbf{w}_{\mathrm{P}}(T_{\mathrm{f}}) \overset{!}{=} \mathbf{w}_{\mathrm{f}}, \tag{5.73}$$

with:

$$\mathbf{w}_{\mathrm{P}}(T_{\mathrm{f}}) := \begin{bmatrix} w_{\mathrm{P}}(T_{\mathrm{f}}) & \dot{w}_{\mathrm{P}}(T_{\mathrm{f}}) & \ldots & w_{\mathrm{P}}^{(r)}(T_{\mathrm{f}}) \end{bmatrix}^T, \tag{5.74}$$

$$\mathbf{w}_{\mathrm{f}} := \begin{bmatrix} w_{\mathrm{f}} & \dot{w}_{\mathrm{f}} & \ldots & w_{\mathrm{f}}^{(r)} \end{bmatrix}^T. \tag{5.75}$$

Consequently, the total number of boundary conditions is $(2r + 2)$. According to this number of boundary conditions the lowest order of a polynomial function, which meets all boundary conditions, is $(2r + 1)$:

$$w_{\mathrm{P}}(t) = \sum_{i=0}^{2r+1} a_i t^i, \quad \forall t \in [T_{\mathrm{i}}, T_{\mathrm{f}}]. \tag{5.76}$$

With respect to the boundary conditions in (5.70) and (5.73) the coefficients
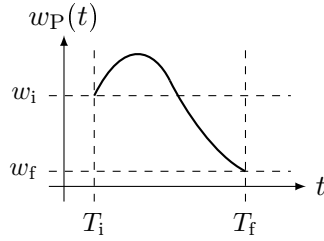
Figure 5.16: *Polynomial trajectory $w_{\mathrm{P}}(t)$ with boundary conditions*

$a_0, \ldots, a_{2r+1}$ are uniquely defined for $T_{\mathrm{i}} \neq T_{\mathrm{f}}$ by the following linear equation system:

$$\underbrace{\begin{bmatrix} b_{\mathrm{i},(0,0)} & \cdots & b_{\mathrm{i},(0,2r+1)} \\ \vdots & & \vdots \\ b_{\mathrm{i},(r,0)} & \cdots & b_{\mathrm{i},(r,2r+2)} \\ b_{\mathrm{f},(0,0)} & \cdots & b_{\mathrm{f},(1,2r+1)} \\ \vdots & & \vdots \\ b_{\mathrm{f},(r,1)} & \cdots & b_{\mathrm{f},(r,2r+2)} \end{bmatrix}}_{\mathbf{A}_{\mathrm{P}}} \underbrace{\begin{bmatrix} a_0 \\ \vdots \\ a_r \\ a_{r+1} \\ \vdots \\ a_{2r+1} \end{bmatrix}}_{\mathbf{a}} = \underbrace{\begin{bmatrix} w_{\mathrm{i}} \\ \vdots \\ w_{\mathrm{i}}^{(r)} \\ w_{\mathrm{f}} \\ \vdots \\ w_{\mathrm{f}}^{(r)} \end{bmatrix}}_{\mathbf{b}_{\mathrm{P}}}, \tag{5.77}$$

with:

$$b_{\mathrm{i/f},(j,i)} = \begin{cases} \frac{i!}{(i-j)!} T_{\mathrm{i/f}}^{i-j} & \text{for} \quad i \geqslant j, \\ 0 & \text{for} \quad i < j, \end{cases} \quad i = 0, \ldots, (2r+1), \quad j = 0, \ldots, r. \tag{5.78}$$

The definition of coefficients a_i^j enables a closed formula for $w_{\mathrm{P}}(t)$ and its derivatives:

$$w_{\mathrm{P}}^{(j)}(t) = \sum_{i=0}^{2r+1} a_i^j t^{(i-j)}, \quad j \geqslant 0, \quad \forall t \in [T_{\mathrm{i}}, T_{\mathrm{f}}], \tag{5.79}$$

with:

$$a_i^j = \begin{cases} a_i \frac{i!}{(i-j)!} & \text{for} \quad i \geqslant j, \\ 0 & \text{for} \quad i < j \end{cases}, \quad i = 0, \dots, (2r+1), \quad j \geqslant 0. \tag{5.80}$$

Therefore, all derivatives above $2r + 1$ are zero:

$$w_{\mathrm{P}}^{(j)}(t) = 0, \quad j > 2r + 1. \tag{5.81}$$

Figure 5.17 illustrates a block scheme for the polynomial trajectory planning as documented in this section, with the vectors:

$$\mathbf{a}^j := \begin{bmatrix} a_0^j & \dots & a_{2r+1}^j \end{bmatrix}^T, \quad j = 0, \dots, r, \tag{5.82}$$

and

$$\mathbf{w}_{\mathrm{P}}(t) = \begin{bmatrix} w_{\mathrm{P}}(t) \\ \vdots \\ w_{\mathrm{P}}^{(r)}(t) \end{bmatrix} = \begin{bmatrix} \sum_{i=0}^{2r+1} a_i^0 t^i \\ \vdots \\ \sum_{i=0}^{2r+1} a_i^r t^{(i-r)} \end{bmatrix}. \tag{5.83}$$
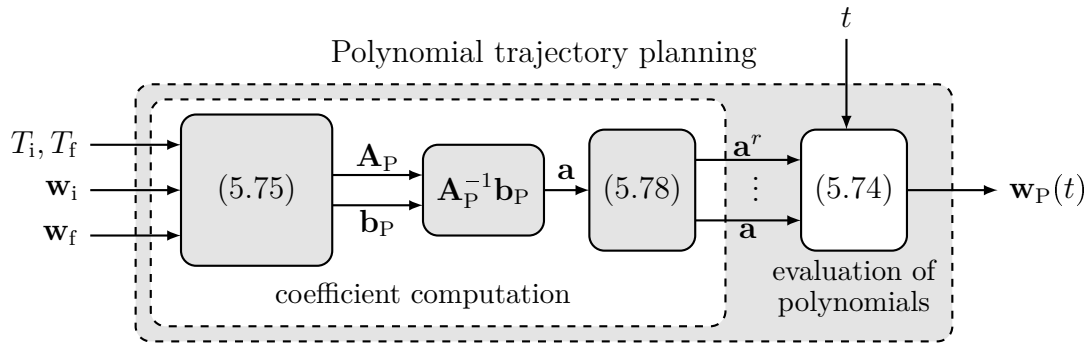
Figure 5.17: *Implementation of polynomial trajectory planning*

A simplifying special case occurs for homogeneous boundary conditions in the derivatives (see Figure 5.18):

$$\dot{w}_{\mathrm{i}}, \dots, w_{\mathrm{i}}^{(r)}, \dot{w}_{\mathrm{f}}, \dots, w_{\mathrm{f}}^{(r)} = 0. \tag{5.84}$$

In this case, the polynomial coefficients can be computed considering a normalized polynomial, with:

$$T_{\mathrm{i}} = w_{\mathrm{i}} = 0, \quad T_{\mathrm{f}} = w_{\mathrm{f}} = 1. \tag{5.85}$$

Subsequently, arbitrary boundary conditions,

$$w_{\mathrm{P}}(T_{\mathrm{i}}) \stackrel{!}{=} w_{\mathrm{i}}, \tag{5.86}$$

$$w_{\mathrm{P}}(T_{\mathrm{f}}) \stackrel{!}{=} w_{\mathrm{f}},$$
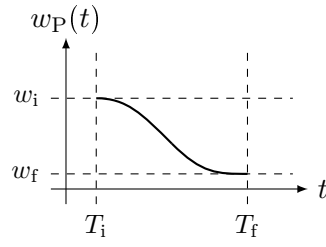
Figure 5.18: *Polynomial trajectory $w_{\mathrm{P}}(t)$ with homogeneous boundary conditions in the derivatives*

can be met by scaling of the normalized polynomial:

$$w_{\mathrm{P}}(t) = w_{\mathrm{i}} + (w_{\mathrm{f}} - w_{\mathrm{i}}) \sum_{i=0}^{2r+1} a_i \left(\frac{t - T_{\mathrm{i}}}{T_{\mathrm{f}} - T_{\mathrm{i}}} \right)^i . \tag{5.87}$$

While the coefficients $a_0, \ldots, a_r$ are zero, the coefficients $a_{r+1}, \ldots, a_{2r+1}$ are the unique solution of the linear equation system:

$$\begin{bmatrix} b_{(0,0)} & \vdots & b_{(0,r)} \\ b_{(1,0)} & \vdots & b_{(1,r)} \\ \ldots & & \ldots \\ b_{(r,0)} & \ldots & b_{(r,r)} \end{bmatrix} \begin{bmatrix} a_{r+1} \\ a_{r+2} \\ \vdots \\ a_{2r+1} \end{bmatrix} = \begin{bmatrix} 1 \\ 0 \\ \vdots \\ 0 \end{bmatrix}, \tag{5.88}$$

with,

$$b_{(j,i)} = \frac{(r + i + 1)!}{(r + i - j + 1)!}, \quad i, j = 0, \ldots, r. \tag{5.89}$$

Equation (5.88) shows that the coefficients $a_{r+1}, \ldots a_{2r+1}$, depend exclusively on the parameter r. Hence, the investigation of an analytic expression to compute these coefficients with respect to a given parameter r is self-evident. Without proof, such an analytic expression for the unique solution is:

$$a_i = \frac{(-1)^{i-r-1} \cdot (2r + 1)!}{(2r + 1 - i)! \cdot (i - r - 1)! \cdot r! \cdot i}, \quad i = r + 1, \ldots 2r + 1. \tag{5.90}$$

From (5.87) follows the computation of derivatives of $w_{\mathrm{P}}(t)$:

$$w_{\mathrm{P}}^{(j)}(t) = \frac{(w_{\mathrm{f}} - w_{\mathrm{i}})}{(T_{\mathrm{f}} - T_{\mathrm{i}})^j} \sum_{i=0}^{2r+1} a_i^j \left(\frac{t - T_{\mathrm{i}}}{T_{\mathrm{f}} - T_{\mathrm{i}}} \right)^{(i-j)}, \quad j \geqslant 1, \tag{5.91}$$

with coefficients a_i^j from (5.80).

Of course, also the low-pass filter approach presented in the last section may be applied to set-point reference signals. The drawback of this application shall be discussed considering an example. Figure 5.19 shows two different trajectories and their first derivative generated with respect to a step in the reference signal $w(t)$. The first

trajectory is obtained by application of a second order low-pass filter as discussed in Section 5.3.2 with a filter time constant $\tau_F = 0.2$ s:

$$F(s) = \frac{1}{(0.2s + 1)^2}. \tag{5.92}$$

The second trajectory is obtained be applying the polynomial planning approach presented in this chapter with $r = 2$ and:

$$T_i = 0, \quad T_f = 1, \quad w_i = \dot{w}_i = \dot{w}_f = 0, \quad w_f = 1. \tag{5.93}$$

The resulting polynomial is:

$$w_P(t) = \begin{cases} 0, & t < 0, \\ -2t^3 + 3t^2, & t \in [0, 1], \\ 1, & t > 1. \end{cases} \tag{5.94}$$
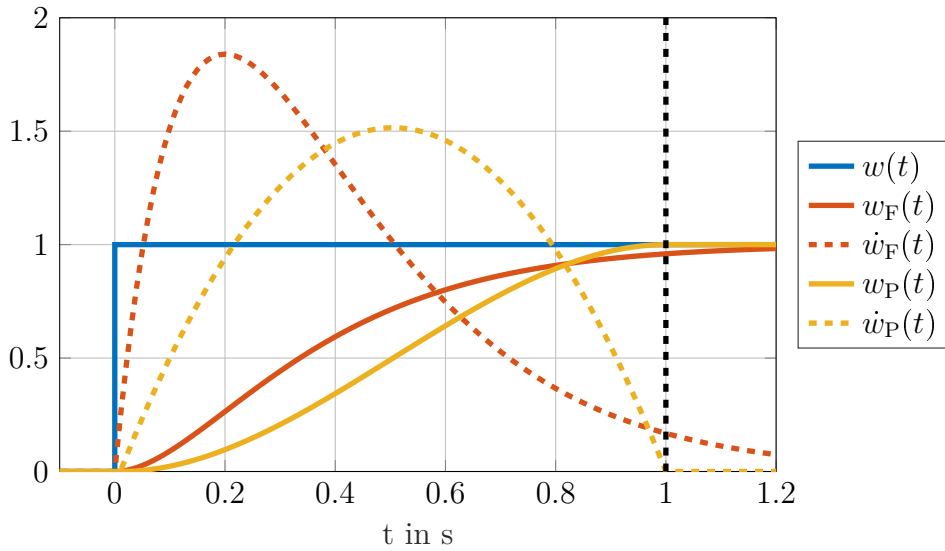
Figure 5.19: *Comparison between low-pass filter (w_F) and polynomial planning (w_P) approach for the generation of trajectories*

Figure 5.19 shows that while w_P reaches the final value of the reference signal in the planned time ($t = 1$ s), w_F has not yet reached these value, although the maximum value of its derivative $\dot{\omega}_F(t)$ is higher than the maximum value of $\dot{w}_P(t)$. A reduction of the residual to the reference value at $t = 1$ s by decreasing the filter time constant would further increase the maximum of $\dot{\omega}_F$. As in the application of an inversion-based feedforward controller also the derivatives of the trajectory contribute to the resulting control input (see Section 5.3.1), the advantage of the polynomial planning approach, according to the control target (change of set-point) and with respect to a low actuation effort, is obvious.

5.3.3 Internal model control

An inversion-based feedforward control, as presented in the last section yields perfect reference tracking in the nominal case (perfect matching $\Sigma = \tilde{\Sigma}$ of physical process Σ and model $\tilde{\Sigma}$) and in absence of disturbances. In practical applications, however, this case is out of reach: A control system is always faced with model uncertainties ($\Sigma \neq \tilde{\Sigma}$) and disturbances on both the system input (actuation disturbance) and output (measurement disturbance). Therefore, it is necessary to extend the feedforward control by a feedback loop. The extension of the inversion-based feedforward control by a simple feedback loop has been introduced as IMC in 1982 in [74] for linear systems. In [75] this approach was extended to nonlinear systems. The book [76] summarizes the fundamentals of IMC and in [69] IMC is applied to automotive systems. This section provides a concise overview of the principle in IMC for SISO systems and its combination with a polynomial trajectory planning approach. The generalization for MIMO system is straight forward.

The central idea of IMC is to use the difference between the measured outputs y and the expected outputs $\tilde{y}$, with respect to the plant model $\tilde{\Sigma}$, for an adaption of the reference trajectory. Figure 5.20 shows the simple IMC structure as presented in [69, p. 57]. If the controller is a perfect inversion of the plant model $\tilde{\Sigma}^{-1}$ holds:
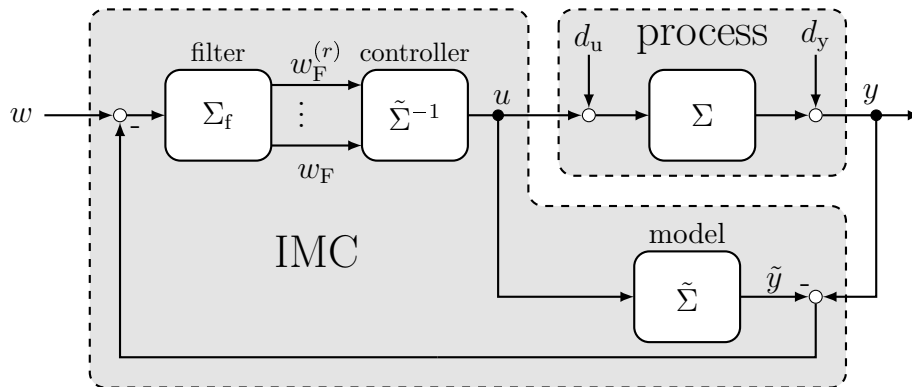
Figure 5.20: *Classical IMC structure using a filtered reference signal*

$$w_{\mathrm{F}}(t) = \tilde{y}(t). \tag{5.95}$$

Therefore, it is actually not necessary to compute $\tilde{y}$. This consideration results in a simplified IMC structure (see Figure 5.21) without model implementation, which has been proposed in [69, p. 63].

The IMC structure in [69] relies on the filter approach for the trajectory generation. The next section proposes the application of the polynomial trajectory planning approach according to Section in an IMC structure.

Polynomial trajectory planning in an IMC structure

In IMC structure the reference value w is constantly adapted according to the difference of the expected output in nominal case and the measured output (see Figure 5.21).
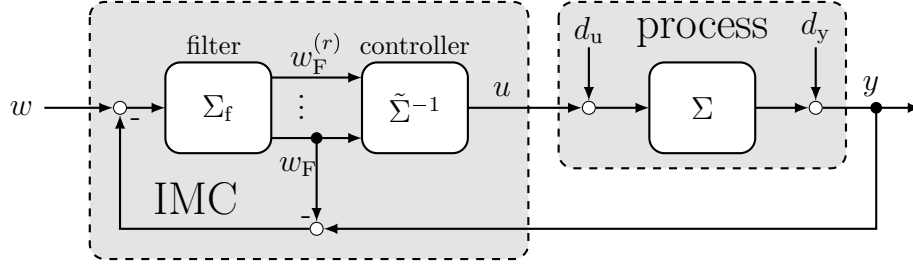
Figure 5.21: *Simplified IMC structure using a filtered reference signal*

This concept can be transferred to the polynomial planning approach considering an adapted final value of the trajectory w_f. This adaption implies a consecutive replanning of the polynomial, with respect to adapted boundary conditions. A recursive algorithm for this consecutive replanning is now specified considering discrete computational steps:

$$t \to t_k \in [T_\mathrm{i}, T_\mathrm{f}], \quad \text{with:} \quad t_{k+1} = t_k + \Delta t_k. \tag{5.96}$$

The trajectory planning starts at $t = t_0 = T_\mathrm{i}$. A new notation is introduced to consider updated boundary conditions:

$$\mathbf{w}_\mathrm{i} \to \mathbf{w}_{\mathrm{i},k}, \quad \text{with} \quad \mathbf{w}_{\mathrm{i},0} = \mathbf{w}_\mathrm{i}, \tag{5.97}$$

$$\mathbf{w}_\mathrm{f} \to \mathbf{w}_{\mathrm{f},k}, \quad \text{with} \quad \mathbf{w}_{\mathrm{f},0} = \mathbf{w}_\mathrm{f}. \tag{5.98}$$

Based on the boundary conditions $\mathbf{w}_{\mathrm{i},0}$ and $\mathbf{w}_{\mathrm{f},0}$ the coefficients $\mathbf{a}_0^j$ can be computed according to (5.77), (5.80) and (5.82):

$$\mathbf{a}_0^j = \begin{bmatrix} a_{0,0}^j \\ \vdots \\ a_{2r+1,0}^j \end{bmatrix} = \mathbf{f}(\mathbf{w}_\mathrm{i}, \mathbf{w}_\mathrm{f}, T_\mathrm{i}, T_\mathrm{f}), \quad j = 0, \dots, r. \tag{5.99}$$

This yields a trajectory $w_{\mathrm{P},0}(t)$ and its derivatives:

$$\mathbf{w}_{\mathrm{P},0}(t) = \begin{bmatrix} w_{\mathrm{P},0}(t) \\ \vdots \\ w_{\mathrm{P},0}^{(r)}(t) \end{bmatrix} = \begin{bmatrix} \sum_{i=0}^{2r+1} a_{i,0}^0 t^i \\ \vdots \\ \sum_{i=0}^{2r+1} a_{i,0}^r t^{i-r} \end{bmatrix}. \tag{5.100}$$

These polynomials are used to compute updated initial condition for the next time step $t_1 = t_0 + \Delta t_0$, in order to ensure a continuous trajectory:

$$\mathbf{w}_{\mathrm{i},1} := \mathbf{w}_{\mathrm{P},0}(t_1). \tag{5.101}$$

with:

$$T_{\mathrm{i},1} = t_1. \tag{5.102}$$

The final boundary conditions are considered to be persistent except for the final value of the trajectory w_F, which is adapted according to the difference between the predicted model output and actual output signal, equivalently to the filter approach:

$$\mathbf{w}_{\mathrm{f},1} := \begin{bmatrix} w_{\mathrm{f},0} - (y(t_1) - w_{\mathrm{P},0}(t_1)) \\ \dot{w}_{\mathrm{f},0} \\ \vdots \\ w_{\mathrm{f},0}^{(r)} \end{bmatrix}. \tag{5.103}$$

Based on these updated boundary conditions the polynomial coefficients $\mathbf{a}_1^j$ can be computed, which leads us back to (5.99) in the next time step. The iterative application of these computations yields a recursive algorithm, which can be summarized by the following equations:

$$T_{\mathrm{i},k} = \begin{cases} T_\mathrm{i}, & k = 0 \\ t_k, & k > 0 \end{cases}, \tag{5.104}$$

$$\mathbf{w}_{\mathrm{i},k} := \begin{cases} \mathbf{w}_{\mathrm{i},0} & k = 0 \\ \mathbf{w}_{\mathrm{P},k-1}(t_k) & k > 0 \end{cases}, \tag{5.105}$$

$$w_{\mathrm{f},k} := \begin{cases} w_{\mathrm{f},0} & k = 0 \\ w_{\mathrm{f},0} - (y(t_k) - w_{\mathrm{P},k-1}(t_k)) & k > 0 \end{cases}, \tag{5.106}$$

$$\mathbf{a}_k^j = \begin{bmatrix} a_{0,k}^j \\ \vdots \\ a_{2r+1,k}^j \end{bmatrix} = \mathbf{f}(T_{\mathrm{i},k}, \mathbf{w}_{\mathrm{i},k}, T_\mathrm{f}, \mathbf{w}_{\mathrm{f},k}), \quad j = 0, \dots, r, \tag{5.107}$$

$$\mathbf{w}_{\mathrm{P},k}(t) = \begin{bmatrix} w_{\mathrm{P},k}(t) \\ \vdots \\ w_{\mathrm{P},k}^{(r)}(t) \end{bmatrix} = \begin{bmatrix} \sum_{i=0}^{2r+1} a_{i,k}^0 t^i \\ \vdots \\ \sum_{i=0}^{2r+1} a_{i,k}^r t^{i-r} \end{bmatrix}. \tag{5.108}$$

The resulting trajectory vector is a continuous series of polynomials (see Figure 5.22):

$$w_\mathrm{P}(t) = w_{\mathrm{P},k}(t), \quad t_k \in (t_k, t_{k+1}], \quad k \geqslant 0, \tag{5.109}$$

with:

$$w_\mathrm{P}(t_0) = w_\mathrm{i}. \tag{5.110}$$

Figure 5.23 illustrates the recursive trajectory planning algorithm as part of IMC system. The algorithm is based on discrete computational steps t_k. If entire IMC is implemented in discrete time (cf. Section 5.3.4), several possibilities appear with respect to the choice of the replanning intervals Δt_k. Three approaches shall be shortly discussed:
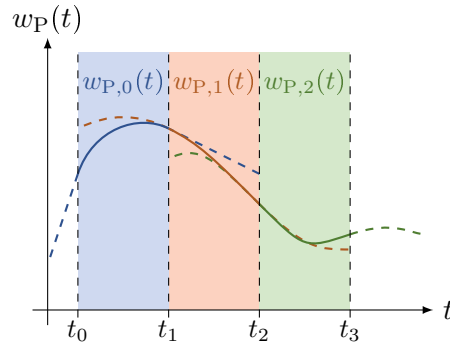
Figure 5.22: *Final trajectory $w_\mathrm{P}(t)$ consisting of a continuous series of polynomial trajectories $w_{\mathrm{p},0}(t), w_{\mathrm{p},1}(t), w_{\mathrm{p},2}(t))$*
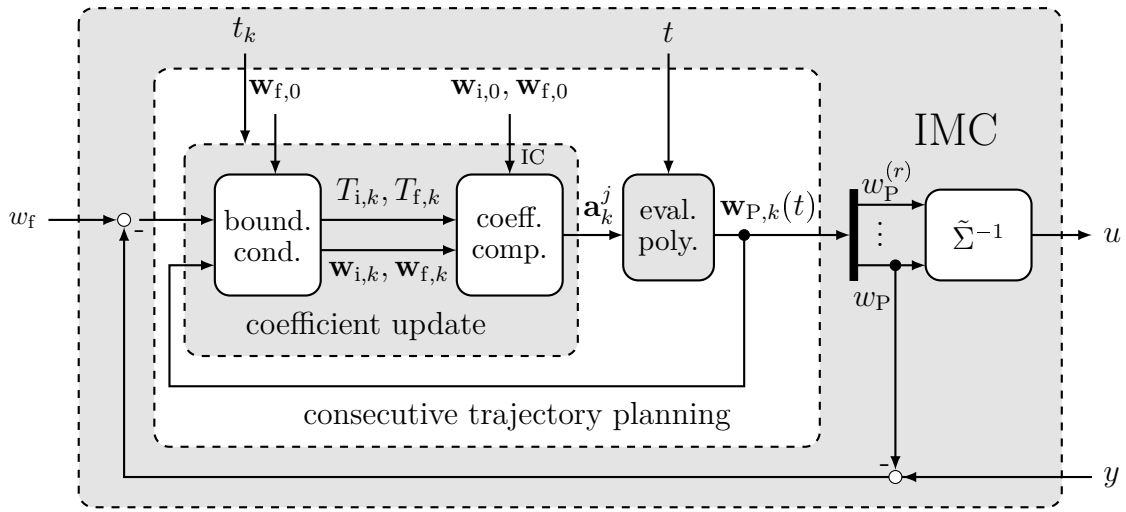
Figure 5.23: *Recursive polynomial trajectory planning algorithm in an IMC structure*

- First, the replanning intervals Δt_k are equivalent to the fundamental sampling time T_d:

$$\Delta t_k = T_\mathrm{d}. \tag{5.111}$$

Hence, the trajectory is replanned in every time step.

- Another possibility is to let Δt_k be a multiple of the fundamental sampling time T_d:

$$\Delta t_k = c T_\mathrm{d}, \quad c \in \mathbb{N}. \tag{5.112}$$

This approach reduces the computational effort, taking a decreased tracking performance.

- The computational effort might be further reduced applying an event-based re-planning approach:

$$t_k = t \quad \text{for} \quad |y(t) - w_\mathrm{P}(t)| > e_\mathrm{max}. \tag{5.113}$$

The replanning is triggered, if the error between expected and real plant behavior exceeds a predefined limit $e_{\max}$.

Independent of the choice of Δt_k, it is advisable to reduce the computational effort of the replanning, which is mainly due to the matrix inversion for the computation of the polynomial coefficients in (5.77):

$$\mathbf{a} = \mathbf{A}_P^{-1}\mathbf{b}_P. \tag{5.114}$$

It is obvious that the computational effort increases with increasing order of the polynomials. The computational effort can be reduced by restructuring of the linear equation system according to persistent boundary conditions.

The final planning time T_f so far has been considered to be constant:

$$T_{f,k} := T_f. \tag{5.115}$$

This implies an approaching planning horizon and, hence, the planning duration T_P of the trajectory decreases to zero:

$$T_P(t) = T_f - T_{i,k} \to 0, \quad \text{for:} \quad t \to T_f. \tag{5.116}$$

In the non-nominal case $(y(t) - w_P(t)) \neq 0$ this yields diverging coefficients $\mathbf{a}_k$. Hence, the replanning algorithm is only valid for $t < T_f$. Two approaches shall now be discussed, which avoid this limitation. The first one is to move the planning horizon in order to keep the planning duration T_P constant. Therefore, T_f has to be increased as T_i increases:

$$T_{f,k} := t_k + (T_f - T_i), \quad k \geqslant 0, \tag{5.117}$$

with:

$$T_P = T_{f,k} - T_{i,k} = T_f - T_i = \text{const.} \quad \forall k > 0. \tag{5.118}$$

Figure 5.24 illustrates the comparison between a receding and approaching horizon
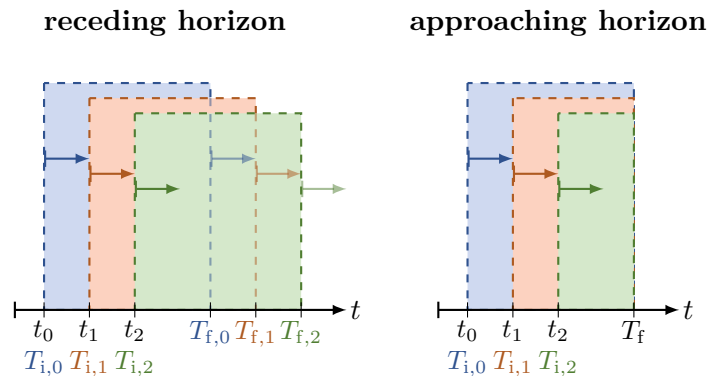
Figure 5.24: *Illustration of receding and approaching planning horizon*

for the polynomial trajectory planning. The obvious drawback of the receding horizon

approach is that it loses the advantage of a finite transition time in non-nominal case in comparison to the simple low-pass filter approach.

An alternative approach is to come back to the original approaching planning horizon, with an bounded minimum planning duration $T_{\mathrm{P,min}}$:

$$T_{\mathrm{f},k} := \begin{cases} T_{\mathrm{f}}, & T_{\mathrm{f}} - t_k \geqslant T_{\mathrm{P,min}} \\ T_{\mathrm{P,min}}, & T_{\mathrm{f}} - t_k < T_{\mathrm{P,min}} \end{cases} . \tag{5.119}$$

This definition combines the approaching and receding planning horizon. For $t < T_{\mathrm{f}} - T_{\mathrm{P,min}}$ the planning duration is decreased. As the limit $t = T_{\mathrm{f}} - T_{\mathrm{P,min}}$ is reached a receding planning horizon is applied in order to ensure bounded coefficients $\mathbf{a}_k^j$ and an application of the approach for $t > T_{\mathrm{f}}$.

Both trajectory planning IMC approaches (receding horizon and limited approaching horizon) shall now be compared to the low-pass filter IMC approach and to the pure feedforward control with trajectory planning considering an educational example:

Example

Let the transfer function of the modeled plant $\tilde{\Sigma}$ be:

$$\tilde{G}(s) = \frac{1}{(s+1)^2}. \tag{5.120}$$

The model-based feedforward controller is designed as presented Section 5.3.1:

$$\tilde{G}(s)^{-1} = (s+1)^2 = s^2 + 2s + 1 = \bar{a}(s) \quad \Rightarrow \quad \bar{\mathbf{c}}^T = \begin{bmatrix} 1 & 2 & 1 \end{bmatrix}, \quad C(s) = 1. \tag{5.121}$$

According to the relative degree $\delta = 2$ and a filter time constant $\tau_{\mathrm{F}} = 0.12$ s the transfer matrix of the low-pass filter is:

$$\mathbf{F}(s) = \begin{bmatrix} 1 \\ s \\ s^2 \end{bmatrix} \cdot \frac{1}{(0.12s + 1)^2}. \tag{5.122}$$

With respect to a unit step reference signal the following boundary conditions for the polynomial trajectory planning are given:

$$T_{\mathrm{i}} = 0, \quad w_{\mathrm{i}} = \dot{w}_{\mathrm{i}} = \ddot{w}_{\mathrm{i}} = 0, \tag{5.123}$$
$$T_{\mathrm{f}} = 1, \quad w_{\mathrm{f}} = 1, \quad \dot{w}_{\mathrm{f}} = \ddot{w}_{\mathrm{f}} = 0. \tag{5.124}$$

Consequently, the trajectory will be a polynomial of order $2\delta + 1 = 5$. For the limited approaching horizon planning a minimum planning duration of $T_{\mathrm{P,min}} = 0.1$ s is chosen. A first set of simulations are made in the nominal case:

$$\Sigma = \tilde{\Sigma}. \tag{5.125}$$
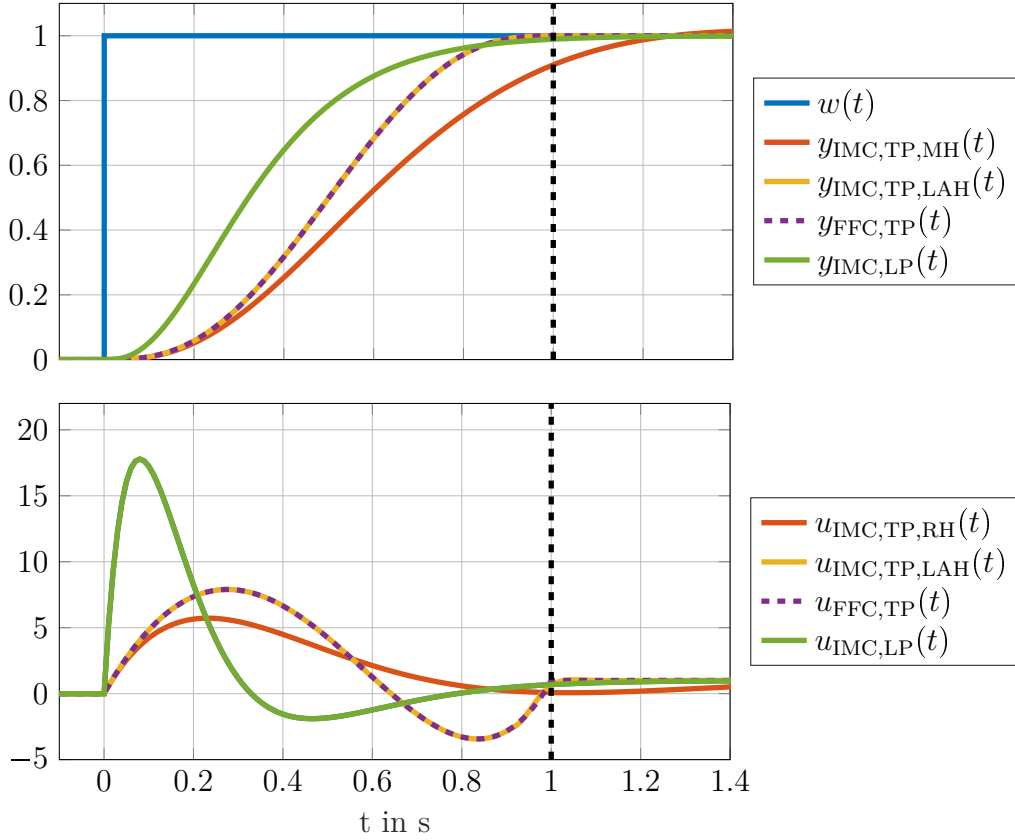
Figure 5.25: *Comparison of feedforward control and different IMC approaches in nominal case*

Figure 5.25 shows the system outputs according to a reference step $w(t)$ and the corresponding control signals $u(t)$ for all four control systems.

The feedback loop is inactive in nominal case, since:

$$w_{\mathrm{F/P}}(t) - y(t) = 0, \quad \forall t \geqslant 0. \tag{5.126}$$

Therefore, the feedforward control achieves perfect results: a smooth finite time transition to the new set-point. The comparison to the IMC with low-pass filter has already been discussed in Section 5.3.2. The receding horizon trajectory planning IMC does not achieve acceptable performance even in the nominal case, since the original transition time is constantly postponed. The limited approaching horizon approach, however, achieves equivalent performance than the pure feedforward control.

A more interesting evaluation of the control systems can be done considering the non-nominal case. To do so the actual plant dynamics shall be:

$$\Sigma : \quad G(s) = \frac{0.8}{(s + 0.8)(s + 1.2)}, \tag{5.127}$$

whereas the controller is still designed based on the plant model transfer function in (5.120). Figure 5.26 shows the system outputs $y(t)$ according to a reference step $w(t)$
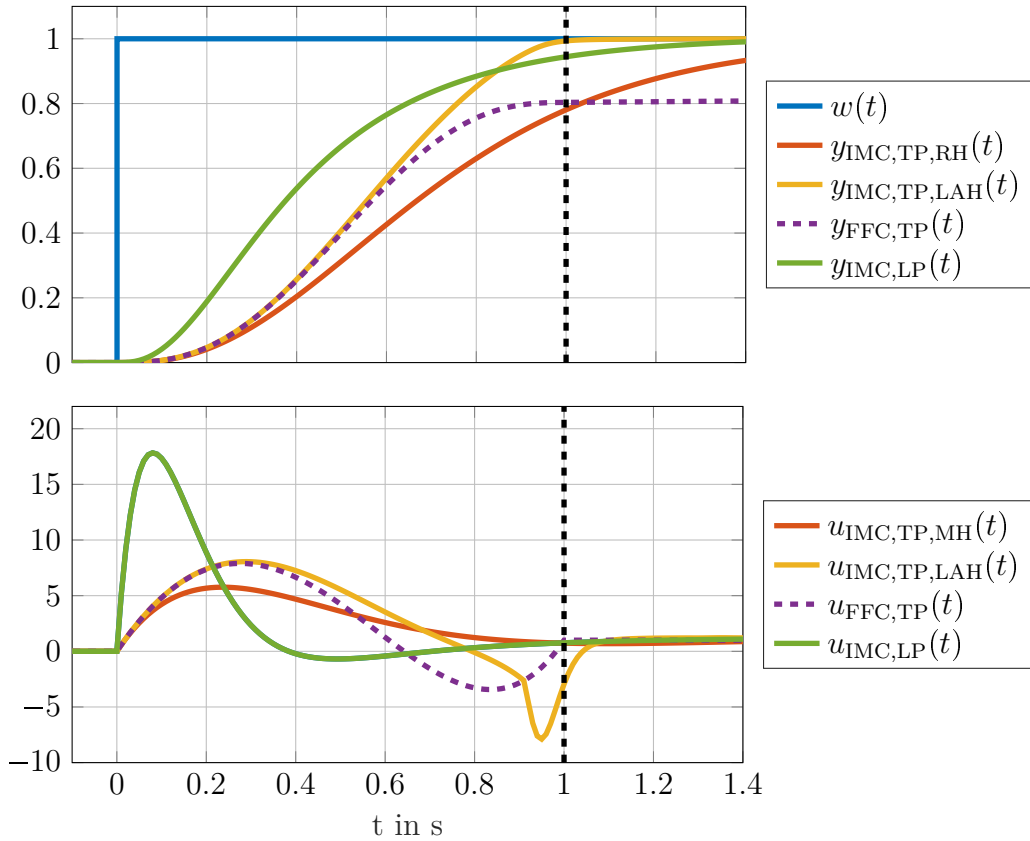
Figure 5.26: *Comparison of feedforward control and different IMC approaches in non-nominal case*

and the corresponding input signals $u(t)$ for all four control systems, similar to the nominal case.

Due to the missing feedback loop the pure feedforward control system can not react on the difference between planned and actual model output. Consequently, a remaining steady state control error occurs. The low-pass filter IMC achieves an acceptable result: the final set point is reached with short latency, the performance with respect to the nominal case, however, decreased. The performance can be increased with a smaller filter time constant with respect to the step height. As already mentioned in Section this yields higher maximum values of the control input $u(t)$.

As the receding horizon trajectory planning IMC produced superior results already in the nominal case, the results for the non-nominal case are even worse, as one might expect. The results of the limited approaching horizon trajectory planning IMC, however, shows promising performance: even for the non-nominal case: a smooth, finite time transition to the new set-point is achieved. For $t \in [0.9, 1]$ the impact of the limited planning duration can be noticed in the input signal $u(t)$. Due to this promising simulation results the limited approaching horizon IMC will be implemented in the shift preparation and shift completion phase for gear shift control.

5.3.4 Discretization of control concept

As finally the DT control system has to run on an automotive control unit, it is advisable to consider an application of the control concept in discrete time with a fixed sample time T_d:

$$t = k \cdot T_d, \quad k \in \mathbb{N}_0. \tag{5.128}$$

Therefore, the derivation of the last sections is revised with respect to a discrete time state-space model,

$$\Sigma_d: \quad \mathbf{x}_{k+1} = \mathbf{A}_d \mathbf{x}_k + \mathbf{B}_d \mathbf{u}_k, \tag{5.129}$$

$$\mathbf{y}_k = \mathbf{C}\mathbf{x}_k + \mathbf{D}\mathbf{u}_k, \tag{5.130}$$

which shall be a discretized version of Σ in (5.46) with (see for example [72, p. 439]):

$$\mathbf{A}_d = \mathbf{e}^{\mathbf{A}T_d}, \tag{5.131}$$

$$\mathbf{B}_d = \int_0^{T_d} \mathbf{e}^{\mathbf{A}\tau} d\tau \, \mathbf{B}.$$

Similar to continuous time systems, the input-output-behavior can be described with a discrete time transfer matrix in frequency domain:

$$\mathbf{G}_d(z) = \mathbf{C} \left(z\mathbf{I} - \mathbf{A}_d \right)^{-1} \mathbf{B}_d + \mathbf{D} \tag{5.132}$$

Also in discrete-time systems the relative degree of transfer function is related to the realizability, equivalently to continuous time. The relative degree of a discrete SISO transfer function,

$$G_d(z) = \frac{b_d(z)}{a_d(z)} = \frac{b_{d,p}z^p + \cdots + b_{d,1}z + b_{d,0}}{z^n + a_{d,n-1}z^{n-1} + \cdots + a_{d,1}z + a_{d,0}}, \tag{5.133}$$

is:

$$\delta_d = n - p. \tag{5.134}$$

The relation between the relative degree δ of the transfer function $G(s)$ of a continuous time system and the relative degree δ_d of the transfer function $G_d(z)$ of the discretized system is (see for example [77, p. 182]):

$$\delta_d = \begin{cases} 0, & \text{for } \delta = 0, \\ 1, & \text{for } \delta \neq 0. \end{cases} \tag{5.135}$$

The relative degree of a discrete transfer function determines the time delay of the system reaction in the discrete output sequence y_k on a discrete input sequence u_k. Therefore, the conservation of a direct feed-through of the continuous time system with respect to time discretization is quite intuitive. Furthermore, this reveals that $\delta_d > 1$ would be related to a dead-time in the continuous time system, which is not covered be the system representation in (5.46).

The fact that the relative degree of a continuous time system may differ from the relative degree of the discretized system, leads to the appearance of additional zeros in $G_\mathrm{d}(z)$, which do not correspond to zeros of $G(s)$. These additional zeros are called sampling zeros. If these zeros are unstable, a classical inversion-based feedforward control design can not be applied, as this would produce an unstable controller. The consideration of these unstable, non-physical (no equivalent in continuous time) zeros is covered in [77], relying on the findings of [78]. This consideration is based on the so-called delta-domain, with

$$\Delta x = \frac{x_{k+1} - x_k}{T_\mathrm{d}}, \tag{5.136}$$

which enables an equivalence between a continuous time and the corresponding discrete-time system for $T_\mathrm{d} \to 0$.

The feedforward control design is equivalent to the continuous time consideration in Section 5.3.1:

1. Computation of inverse transfer matrix:

$$\mathbf{G}_\mathrm{d}(z)^{-1} = \begin{bmatrix} \hat{G}_{\mathrm{d},11}(z) & \dots & \hat{G}_{\mathrm{d},1m}(z) \\ \vdots & & \vdots \\ \hat{G}_{\mathrm{d},m1}(z) & \dots & \hat{G}_{\mathrm{d},mm}(z) \end{bmatrix}, \tag{5.137}$$

with:

$$\hat{G}_{\mathrm{d},ij}(z) = \frac{\hat{a}_{\mathrm{d},ij}(z)}{\hat{b}_{\mathrm{d},ij}(z)} \tag{5.138}$$

$$= \frac{z^{n_{ij}} + \hat{a}_{\mathrm{d},ij,n_{ij}-1} z^{n_{ij}-1} + \cdots + \hat{a}_{\mathrm{d},ij,1} z + \hat{a}_{\mathrm{d},ij,0}}{\hat{b}_{\mathrm{d},ij,p_{ij}} z^{p_{ij}} + \cdots + \hat{b}_{\mathrm{d},ij,1} z + \hat{b}_{\mathrm{d},ij,0}}, \quad i,j = 1, \dots, m.$$

2. Determination of the relative degrees $\delta_{\mathrm{d},ij}$:

$$\delta_{\mathrm{d},ij} = n_{ij} - p_{\mathrm{d},ij}. \tag{5.139}$$

3. Splitting of polynomials $\hat{a}_{\mathrm{d},ij}(z)$ into a polynomial $\bar{a}_{\mathrm{d},ij}(z)$ of degree $\delta_{\mathrm{d},ij}$ and $\tilde{a}_{\mathrm{d},ij}(z)$ of degree $p_{\mathrm{d},ij}$:

$$\hat{a}_{\mathrm{d},ij}(z) = \bar{a}_{\mathrm{d},ij}(z) \cdot \tilde{a}_{\mathrm{d},ij}(z), \quad i,j = 1, \dots, m. \tag{5.140}$$

4. Computation of a controller (transfer functions $C_{\mathrm{d},ij}(z)$ and vectors $\vec{c}_{\mathrm{d},ij}^{\,T}$):

$$C_{\mathrm{d},ij}(z) = \frac{\tilde{a}_{\mathrm{d},ij}(z)}{\hat{b}_{\mathrm{d},ij}(z)}, \quad i,j = 1, \dots, m, \tag{5.141}$$

$$\vec{c}_{\mathrm{d},ij}^{\,T} := \begin{bmatrix} \bar{a}_{\mathrm{d},ij,0} & \dots & \bar{a}_{\mathrm{d},ij,\delta_{\mathrm{d},ij}-1} & 1 & \mathbf{0}_{1 \times (\delta_i - \delta_{\mathrm{d},ij})} \end{bmatrix}, \quad i,j = 1, \dots, m, \tag{5.142}$$

with:

$$\bar{\delta}_{\mathrm{d},i} := \max\left(\delta_{\mathrm{d},ij}\right), \quad j = 1, \dots, m. \tag{5.143}$$

The transformation back to time domain of the following expression,

$$\bar{u}(z) = \bar{a}_{\mathrm{d}}(z)w(z) = \left(z^{\delta_{\mathrm{d}}} + \bar{a}_{\mathrm{d},\delta_{\mathrm{d}}-1}z^{\delta_{\mathrm{d}}-1} + \cdots + \bar{a}_{\mathrm{d},1}z + \bar{a}_{\mathrm{d},0}\right)\bar{u}(z) \qquad (5.144)$$

$$\bar{u}_k = w_{k+\delta_{\mathrm{d}}} + \bar{a}_{\mathrm{d},\delta_{\mathrm{d}}-1}w_{k+\delta_{\mathrm{d}}-1} + \cdots + \bar{a}_{\mathrm{d},1}w_{k+1} + \bar{a}_{\mathrm{d},0}w_k,$$

reveals that the knowledge of derivatives to the trajectory $w(t)$ in continuous time is replaced by the knowledge of future samples of the sequence w_k in discrete time. Consequently, the vectors $\mathbf{w}_{i,\delta_{\mathrm{d},i},k}$ are:

$$\mathbf{w}_{i,\delta_{\mathrm{d},i},k} := \begin{bmatrix} w_{i,k} & w_{i,k+1} & \dots & w_{i,k+\delta_{\mathrm{d,i}}} \end{bmatrix}, \quad i = 1, \dots, m. \qquad (5.145)$$

Figure 5.27 shows a simple delay chain, which can be used to provide future samples of the discrete time reference sequence w_k. The generation of a trajectory vector $\mathbf{w}_{\mathrm{D}}$
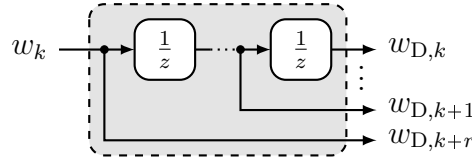
Figure 5.27: *Delay chain for to provide future samples of the discrete time sequence w_k*

for inversion-based feedforward control hence is straight forward. In nominal case the actual value of w_k is reached with at latest one sample delay according to the relative degree $\delta_{\mathrm{D}} \leqslant 1$ of a discrete transfer function without dead-time.

The objective of the time discretization, however, is not to implement the theoretical limits of discrete time control but to approximate the continuous time concept, which has been proposed in this chapter. Therefore, the requirements to the control system are still:

- smooth reference tracking
- and smooth transition for set-point change.

One possibility to compute a discretized version of the low-pass filter in (5.63) is to determine a minimal state-space realization of the filter, for example in controllable canonical from (see [72, p. 153]), and to subsequently apply the time-discretization in (5.131). The application of polynomial trajectory planning in a discrete time control system has already been discussed in Section 5.3.3. In both cases the derivatives of the modified reference trajectories are not used in discrete time. They are replaced by the future samples of the reference sequence obtained by a delay chain (see Figure 5.27).

5.3.5 Torque request limitations

As in most control applications, also in DT control plant input saturations have to be considered in order ensure sufficient performance of the control system. In case

Table 5.2: *Impact of the transition time on the input limitations*

phase	limits			
	CV→Pa		Pa→CV	
	$\tau_{\mathrm{max}}/\tau_{\mathrm{min}}$	$\dot{\tau}_{\mathrm{max}}/\dot{\tau}_{\mathrm{min}}$	$\tau_{\mathrm{max}}/\tau_{\mathrm{min}}$	$\dot{\tau}_{\mathrm{max}}/\dot{\tau}_{\mathrm{min}}$
II	$\sim \frac{1}{T_{\mathrm{f}}-T_{\mathrm{i}}}$	$\sim \frac{1}{(T_{\mathrm{f}}-T_{\mathrm{i}})^2}$	$\not\propto (T_{\mathrm{f}} - T_{\mathrm{i}})$	$\sim \frac{1}{T_{\mathrm{f}}-T_{\mathrm{i}}}$
IV	$\not\propto (T_{\mathrm{f}} - T_{\mathrm{i}})$	$\sim \frac{1}{T_{\mathrm{f}}-T_{\mathrm{i}}}$	$\sim \frac{1}{T_{\mathrm{f}}-T_{\mathrm{i}}}$	$\sim \frac{1}{(T_{\mathrm{f}}-T_{\mathrm{i}})^2}$

of plant input saturations the input signals computed by the controller deviate from the actually acting input signals, due to physical limitations of the actuator. Whereas reactive input saturation strategies, like classical anti-windup, try to limit the effects of such deviations, preventive methods, like MPC, try to completely avoid these deviations. In IMC this problem may be tackled in a preventive way at trajectory generation level. To do so, in [69, p. 86] a low-pass filter structure is proposed, in which the highest derivative $w_{\mathrm{F}}^{(r)}$ is saturated in order to prevent plant input saturation. Also the polynomial planning approach, as presented in Section 5.3.2, is predestined for a preventive consideration of input saturations. Once the polynomial coefficients have been computed they enable the computation of the reference trajectory and its derivatives for the entire planning interval in nominal case. Consequently, also the corresponding plant inputs are known in advance in the nominal case and can be checked according their compliance with the plant input limits, which is a reasonable estimation for the non-nominal case. Since the transition time for the change of a set point (cf. Section) is a control design parameter, its choice might be an opportunity to enforce this compliance. This opportunity shall be shortly discussed considering the transformed control tasks in the shift preparation phase (see Section 5.2.2 and 5.2.3.

The transformed control task,

$$\omega_{\mathrm{E}} \rightarrow \omega_{\mathrm{E,sync}}(w_{\mathrm{F}}), \tag{5.146}$$

can be considered simplified as a required acceleration or deceleration of the ICE. Therefore, in a constant driving situation, the necessary input torques are primary related to the derivative of the trajectory on speed level. According to (5.91), hence, specific maximum and minimum values $\tau_{\mathrm{max}}/\tau_{\mathrm{min}}$ may be met for adapting the transition time $T_{\mathrm{f}} - T_{\mathrm{i}}$. In contrast, the transformed control task,

$$\mu \rightarrow \mu_{\mathrm{unload}}(\mathbf{q}_i, \tau_{\mathrm{F,P}}), \tag{5.147}$$

is on torque level. Therefore, according to (5.16) the maximum respectively minimum value of the input torques are related to the boundary conditions of the trajectory and, hence, they can not be adapted by modifying the transition time $T_{\mathrm{f}}-T_{\mathrm{i}}$. This simplified consideration can be applied to limits in the gradients of the input torques $\dot{\tau}_{\mathrm{max}}/\dot{\tau}_{\mathrm{min}}$. The results are summarized with respect to the shift phases in in Table 5.2. At the end of this short excursus it is necessary to mention that the preventive consideration of input saturations in a constant driving situation is related to the evaluation of the shiftability considering the TFD in Section 4.4.2. Hence, in the control of single-EM dedicated hybrid DTs the consideration of input saturations is partially covered by the EMS, which excludes certain shifts in certain driving situations.

5.4 Implementation of control concept

The control concept presented in the last section shall now be implemented for an exemplary single-EM dedicated hybrid DT. The considered DT has been used for demonstrating the contributions on DT modeling in Chapter 3 and model-based DT analysis in Chapter 4. The mechanical topology has been introduced in Figure 3.16 and in Section 3.6.4 a corresponding state-space model,

$$\mathbf{q} = \bar{\mathbf{M}}^{-1}\bar{\mathbf{A}}\mathbf{q} + \bar{\mathbf{M}}^{-1}\bar{\mathbf{B}}\mathbf{u}, \tag{5.148}$$

with,

$$\mathbf{q} = \begin{bmatrix} \omega_{\mathrm{E}} & \omega_{\mathrm{R3}} & \omega_{\mathrm{M}} & \omega_{\mathrm{F}} & \Delta\varphi & v \end{bmatrix}^{T}, \tag{5.149}$$

$$\mathbf{u} = \begin{bmatrix} \tau_{\mathrm{E}} & \tau_{\mathrm{M}} & F_{\mathrm{v}} & \tau_{\mathrm{C0}} & \tau_{\mathrm{C1}} & \tau_{\mathrm{C2}} & \tau_{\mathrm{B1}} & \tau_{\mathrm{B2}} \end{bmatrix}^{T}. \tag{5.150}$$

has been computed. The parameters in Table 5.3 and Table 4.5 enable the numeric evaluation of the symbolic matrices in (3.96)-(3.99):

$$\bar{\mathbf{M}} = \begin{bmatrix} 64.0 \cdot 10^{-3} & 0 & 0 & 0 & 0 & 0 \\ 0 & 10.0 \cdot 10^{-3} & 0 & 0 & 0 & 0 \\ 0 & 0 & 32.5 \cdot 10^{-3} & 0 & 0 & 0 \\ 0 & 0 & 0 & 333.3 \cdot 10^{-3} & 0 & 0 \\ 0 & 0 & 0 & 0 & 4000 & 0 \\ 0 & 0 & 0 & 0 & 0 & 1350 \end{bmatrix} \tag{5.151}$$

$$\bar{\mathbf{A}} = \begin{bmatrix} 0 & 0 & 0 & 0 & 0 & 0 \\ 0 & 0 & 0 & 0 & 0 & 0 \\ 0 & 0 & 0 & 0 & 0 & 0 \\ 0 & 0 & 0 & -0.94 & -866.57 & 13.67 \\ 0 & 0 & 0 & 0.22 & 0 & -3.15 \\ 0 & 0 & 0 & 13.67 & 12618.30 & -199.03 \end{bmatrix} \tag{5.152}$$

$$\bar{\mathbf{B}} = \begin{bmatrix} 1 & 0 & 0 & -1 & 0 & 0 & 0 & 0 \\ 0 & 1 & 0 & 1 & -1 & -0.676 & 0 & 0 \\ 0 & 0 & 0 & 0 & 0.260 & -0.316 & -0.745 & 0 \\ 0 & 0 & 0 & 0 & 0.480 & 1.633 & 0.491 & 1 \\ 0 & 0 & 0 & 0 & 0 & 0 & 0 & 0 \\ 0 & 0 & -1 & 0 & 0 & 0 & 0 & 0 \end{bmatrix}. \tag{5.153}$$

The matrices $\bar{\mathbf{M}}, \bar{\mathbf{A}}, \bar{\mathbf{B}}$ represent the model information of the DT, which is used to implement a model-based control structure. Due to the fact that the velocity dependent damping of the shafts is hard to determine in practice the corresponding parameters have been set to zero for the inversion-based feedforward control implementation:

$$d_{\mathrm{E}} = d_{\mathrm{R3}} = d_{\mathrm{M}} = d_{\mathrm{C}} = d_{\mathrm{F}} = d_{\mathrm{V}} = d_{\mathrm{J}} = 0. \tag{5.154}$$

***Table 5.3:** Physical parameters of the exemplary single-EM dedicated hybrid DT*

symbol	value	unit
J_{E}	$64.0 \cdot 10^{-3}$	$\mathrm{kg} \cdot \mathrm{m}^2$
J_{R3}	$10.0 \cdot 10^{-3}$	$\mathrm{kg} \cdot \mathrm{m}^2$
J_{M}	$32.5 \cdot 10^{-3}$	$\mathrm{kg} \cdot \mathrm{m}^2$
J_{C}	0	$\mathrm{kg} \cdot \mathrm{m}^2$
J_{F}	$333.3 \cdot 10^{-3}$	$\mathrm{kg} \cdot \mathrm{m}^2$
m	1350	kg
d	20	$\mathrm{N\,m} \cdot \mathrm{s}$
k	4000	$\mathrm{N\,m}$
r_{W}	0.317	m

Consequently, the feedback loop will have to manage the model deviation with respect to non-zero damping parameters.

According to Table 4.4 and Figure 4.15 there are 8 gear shifts in the scope of the problem statement of this chapter (elementary shifts between hybrid CVT and hybrid parallel mode) for the exemplary DT topology. These shifts are listed in Table 5.4. According to Section 4.4.3 all of these shifts feature potential for smooth and lossless

***Table 5.4:** Elementary gear shifts between hybrid CVT and hybrid parallel gears in an exemplary single-EM dedicated hybrid DT*

	1	2	3	4	5	6	7	8
initial	CV1	Pa1	CV1	Pa2	CV2	Pa2	CV2	Pa3
final	Pa1	CV1	Pa2	CV1	Pa2	CV2	Pa3	CV2

gear shifting. The computation of feedforward controllers to the single plant models, see Figure 5.8 and Table 5.1, will be now computed following the design procedure presented in this chapter, which summarizes as:

Summary of control design procedure

1. Computation of mode specific plant models according to Section 3.5.1:

$$\Sigma, \boldsymbol{\kappa}_i, \boldsymbol{\kappa}_j \rightarrow \Sigma^{\mathrm{CV}}_{\boldsymbol{\kappa}_i}, \Sigma^{\boldsymbol{\kappa}_{j,\mathrm{lk}}}_{\boldsymbol{\kappa}_i}, \Sigma^{\mathrm{P}a}_{\boldsymbol{\kappa}_j}. \tag{5.155}$$

2. Discretization of the plant models with respect to a sample time $T_{\mathrm{d}} = 0.01$ s, according to (5.131):

$$\Sigma \rightarrow \Sigma_{\mathrm{d}}. \tag{5.156}$$

3. Inversion of transfer matrices in frequency domain:

$$\Sigma_{\mathrm{d}} \rightarrow \mathbf{G}_{\mathrm{d}}(z) \rightarrow \mathbf{G}^{-1}_{\mathrm{d}}(z). \tag{5.157}$$

4. Computation of inversion-based feedforward controllers $(C_{\mathrm{d},ij}(z), \bar{\mathbf{c}}^T_{\mathrm{d},ij})$, according to Section 5.3.1

The transfer functions $C_{\mathrm{d},ij}(z)$ are implemented in a single MIMO state-space realization:

$$C_{\mathrm{d},ij}(z) \mapsto \Sigma_{\mathrm{d,C}}(z), \quad i,j = 1, 2. \tag{5.158}$$

Instead of the wheel toque τ_{W}, the traction force F_{t} of the driving wheels,

$$F_{\mathrm{t}} = \frac{\tau_{\mathrm{W}}}{r_{\mathrm{W}}}, \tag{5.159}$$

assuming a constant wheel radius r_{W} will be controlled in order to meet the interface specifications for the later application of the DT control system within a given PT control system.

5.4.1 Exemplary controller parametrization

This section lists the parametrization of the model-based controllers, which have been proposed in this chapter, for exemplary, embedded, smooth and lossless gear shifts in the exemplary single-EM hybrid DT.

Hybrid CVT controller

$$\left[\Sigma^{\mathrm{CV}}_{\boldsymbol{\kappa}_i}\right]^{-1} : \quad \begin{bmatrix} \mathbf{w}_{F_{\mathrm{t}}} \\ \mathbf{w}_{\omega_{\mathrm{E}}} \end{bmatrix} \mapsto \begin{bmatrix} \tau_{\mathrm{E},k} \\ \tau_{\mathrm{M},k} \end{bmatrix} \tag{5.160}$$

- CV1:

$$\bar{\mathbf{c}}^T_{11} = \begin{bmatrix} 1 & -1.91292 & 0.97092 \end{bmatrix}, \qquad \bar{\mathbf{c}}^T_{21} = \begin{bmatrix} 1 & -1 \end{bmatrix} \tag{5.161}$$
$$\bar{\mathbf{c}}^T_{12} = \begin{bmatrix} 1 & -1.97219 & 0.99071 \end{bmatrix}, \qquad \bar{\mathbf{c}}^T_{22} = \begin{bmatrix} 1 & -1 \end{bmatrix}$$

$$\mathbf{C}(z): \quad \mathbf{x}_{k+1} = \begin{bmatrix} 7.63125 & 0 \\ 0 & 7.63125 \end{bmatrix} \cdot 10^{-7} \mathbf{x}_k + \begin{bmatrix} 1 & 0 \\ 0 & 1 \end{bmatrix} \begin{bmatrix} \bar{u}_{11,k} \\ \bar{u}_{12,k} \end{bmatrix} \quad (5.162)$$

$$\begin{bmatrix} \tau_{\mathrm{E},k}^* \\ \tau_{\mathrm{M},k}^* \end{bmatrix} = \begin{bmatrix} 0.51477 & 0 \\ 0 & 0.85399 \end{bmatrix} \mathbf{x}_k + \begin{bmatrix} 7.40000 & 0 \\ 0 & -6.92718 \end{bmatrix} \begin{bmatrix} \bar{u}_{21,k} \\ \bar{u}_{22,k} \end{bmatrix}$$

- CV2:

$$\bar{\mathbf{c}}_{11}^T = \begin{bmatrix} 1 & -1.91270 & 0.97081 \end{bmatrix}, \qquad \bar{\mathbf{c}}_{21}^T = \begin{bmatrix} 1 & -1 \end{bmatrix} \qquad (5.163)$$
$$\bar{\mathbf{c}}_{12}^T = \begin{bmatrix} 1 & -1.93295 & 0.97758 \end{bmatrix}, \qquad \bar{\mathbf{c}}_{22}^T = \begin{bmatrix} 1 & -1 \end{bmatrix}$$

$$\mathbf{C}(z): \quad \mathbf{x}_{k+1} = \begin{bmatrix} 2.25349 & 0 \\ 0 & 2.25349 \end{bmatrix} \cdot 10^{-6} \mathbf{x}_k + \begin{bmatrix} 1 & 0 \\ 0 & 1 \end{bmatrix} \begin{bmatrix} \bar{u}_{11,k} \\ \bar{u}_{12,k} \end{bmatrix} \quad (5.164)$$

$$\begin{bmatrix} \tau_{\mathrm{E},k}^* \\ \tau_{\mathrm{M},k}^* \end{bmatrix} = \begin{bmatrix} 2.59371 & 0 \\ 0 & -0.89328 \end{bmatrix} \mathbf{x}_k + \begin{bmatrix} 7.40000 & 0 \\ 0 & 12.48876 \end{bmatrix} \begin{bmatrix} \bar{u}_{21,k} \\ \bar{u}_{22,k} \end{bmatrix}$$

Hybrid Pa controller

$$\left[\Sigma_{\boldsymbol{\kappa}_j}^{\mathrm{Pa}} \right]^{-1}: \quad \mathbf{w}_{F_{\mathrm{t}}} \mapsto \tau_{\mathrm{F,P},k} \qquad (5.165)$$

- Pa1:

$$\bar{\mathbf{c}}^T = \begin{bmatrix} 1 & -1.95444 & 0.98479 \end{bmatrix} \qquad (5.166)$$

$$C(z): \quad x_{k+1} = 6.53804 \cdot 10^{-7} x_k + \bar{u}_k \qquad (5.167)$$
$$\tau_{\mathrm{F,P},k} = 2.50356 x_k$$

- Pa2:

$$\bar{\mathbf{c}}^T = \begin{bmatrix} 1 & -1.95368 & 0.98453 \end{bmatrix} \qquad (5.168)$$

$$C(z): \quad x_{k+1} = 6.75838 \cdot 10^{-7} x_k + \bar{u}_k \qquad (5.169)$$
$$\tau_{\mathrm{F,P},k} = 2.45856 x_k$$

- Pa3:

$$\bar{\mathbf{c}}^T = \begin{bmatrix} 1 & -1.92247 & 0.97408 \end{bmatrix} \qquad (5.170)$$

$$C(z): \quad x_{k+1} = 1.92026 \cdot 10^{-6} x_k + \bar{u}_k \qquad (5.171)$$
$$\tau_{\mathrm{F,P},k} = 1.40982 x_k$$

CVT to Pa synchronization controller

$$\left[\Sigma^{\boldsymbol{\kappa}_{j,\mathrm{lk}}}_{\boldsymbol{\kappa}_i}\right]^{-1}: \quad \begin{bmatrix} \mathbf{w}_{F_\mathrm{t}} \\ \mathbf{w}_{\Delta\omega_\mathrm{C}} \end{bmatrix} \mapsto \begin{bmatrix} \tau_{\mathrm{E},k} \\ \tau_{\mathrm{M},k} \end{bmatrix} \tag{5.172}$$

- CV1 ↔ Pa1:

$$\bar{\mathbf{c}}_{11}^T = \begin{bmatrix} 1 & -1.95638 & 0.98543 \end{bmatrix}, \qquad \bar{\mathbf{c}}_{21}^T = \begin{bmatrix} 1 & -1 \end{bmatrix} \tag{5.173}$$
$$\bar{\mathbf{c}}_{12}^T = \begin{bmatrix} 1 & -1.93312 & 0.97767 \end{bmatrix}, \qquad \bar{\mathbf{c}}_{22}^T = \begin{bmatrix} 1 & -1 \end{bmatrix}$$

$$\mathbf{C}(z): \quad x_{k+1} = \begin{bmatrix} 7.63125 & 0 \\ 0 & 7.63125 \end{bmatrix} \cdot 10^{-7} x_k + \begin{bmatrix} 1 & 0 \\ 0 & 1 \end{bmatrix} \begin{bmatrix} \bar{u}_{11,k} \\ \bar{u}_{12,k} \end{bmatrix} \tag{5.174}$$
$$\begin{bmatrix} \tau_{\mathrm{E},k}^* \\ \tau_{\mathrm{M},k}^* \end{bmatrix} = \begin{bmatrix} 1.08560 & 0 \\ 0 & 0.31964 \end{bmatrix} x_k + \begin{bmatrix} 4.65882 & 0 \\ 0 & -4.36116 \end{bmatrix} \begin{bmatrix} \bar{u}_{21,k} \\ \bar{u}_{22,k} \end{bmatrix}$$

- CV1 ↔ Pa2:

$$\bar{\mathbf{c}}_{11}^T = \begin{bmatrix} 1 & -1.94441 & 0.98144 \end{bmatrix}, \qquad \bar{\mathbf{c}}_{21}^T = \begin{bmatrix} 1 & -1 \end{bmatrix} \tag{5.175}$$
$$\bar{\mathbf{c}}_{12}^T = \begin{bmatrix} 1 & -1.95976 & 0.98656 \end{bmatrix}, \qquad \bar{\mathbf{c}}_{22}^T = \begin{bmatrix} 1 & -1 \end{bmatrix}$$

$$\mathbf{C}(z): \quad x_{k+1} = \begin{bmatrix} 7.63125 & 0 \\ 0 & 7.63125 \end{bmatrix} \cdot 10^{-7} x_k + \begin{bmatrix} 1 & 0 \\ 0 & 1 \end{bmatrix} \begin{bmatrix} \bar{u}_{11,k} \\ \bar{u}_{12,k} \end{bmatrix} \tag{5.176}$$
$$\begin{bmatrix} \tau_{\mathrm{E},k}^* \\ \tau_{\mathrm{M},k}^* \end{bmatrix} = \begin{bmatrix} 0.83158 & 0 \\ 0 & 0.55743 \end{bmatrix} x_k + \begin{bmatrix} -4.75984 & 0 \\ 0 & 4.45572 \end{bmatrix} \begin{bmatrix} \bar{u}_{21,k} \\ \bar{u}_{22,k} \end{bmatrix}$$

- CV2 ↔ Pa2:

$$\bar{\mathbf{c}}_{11}^T = \begin{bmatrix} 1 & -1.92171 & 0.97382 \end{bmatrix}, \qquad \bar{\mathbf{c}}_{21}^T = \begin{bmatrix} 1 & -1 \end{bmatrix} \tag{5.177}$$
$$\bar{\mathbf{c}}_{12}^T = \begin{bmatrix} 1 & -1.84008 & 0.94652 \end{bmatrix}, \qquad \bar{\mathbf{c}}_{22}^T = \begin{bmatrix} 1 & -1 \end{bmatrix}$$

$$\mathbf{C}(z): \quad x_{k+1} = \begin{bmatrix} 2.25349 & 0 \\ 0 & 2.25349 \end{bmatrix} \cdot 10^{-6} x_k + \begin{bmatrix} 1 & 0 \\ 0 & 1 \end{bmatrix} \begin{bmatrix} \bar{u}_{11,k} \\ \bar{u}_{12,k} \end{bmatrix} \tag{5.178}$$
$$\begin{bmatrix} \tau_{\mathrm{E},k}^* \\ \tau_{\mathrm{M},k}^* \end{bmatrix} = \begin{bmatrix} 2.90988 & 0 \\ 0 & -0.35968 \end{bmatrix} x_k + \begin{bmatrix} -3.91365 & 0 \\ 0 & -6.60495 \end{bmatrix} \begin{bmatrix} \bar{u}_{21,k} \\ \bar{u}_{22,k} \end{bmatrix}$$

- CV2 ↔ Pa3:

$$\bar{\mathbf{c}}_{11}^T = \begin{bmatrix} 1 & -1.91796 & 0.97257 \end{bmatrix}, \qquad \bar{\mathbf{c}}_{21}^T = \begin{bmatrix} 1 & -1 \end{bmatrix} \tag{5.179}$$
$$\bar{\mathbf{c}}_{12}^T = \begin{bmatrix} 1 & -1.90188 & 0.96719 \end{bmatrix}, \qquad \bar{\mathbf{c}}_{22}^T = \begin{bmatrix} 1 & -1 \end{bmatrix}$$

$$\mathbf{C}(z): \quad x_{k+1} = \begin{bmatrix} 2.25349 & 0 \\ 0 & 2.25349 \end{bmatrix} \cdot 10^{-6} x_k + \begin{bmatrix} 1 & 0 \\ 0 & 1 \end{bmatrix} \begin{bmatrix} \bar{u}_{11,k} \\ \bar{u}_{12,k} \end{bmatrix} \tag{5.180}$$
$$\begin{bmatrix} \tau_{\mathrm{E},k}^* \\ \tau_{\mathrm{M},k}^* \end{bmatrix} = \begin{bmatrix} 2.76926 & 0 \\ 0 & -0.59701 \end{bmatrix} x_k + \begin{bmatrix} -2.58413 & 0 \\ 0 & -4.36116 \end{bmatrix} \begin{bmatrix} \bar{u}_{21,k} \\ \bar{u}_{22,k} \end{bmatrix}$$

Taking a look at the above controller parametrization one might assume a relative degree of $\delta = 2$ for traction force control and hence a modeled delay, according to Section 5.3.4. However, the relative degree of these transfer functions is actually $\delta = 1$ as expected. Due to the fact that the enumerator polynomials feature complex conjugate roots, a splitting of one single zero would lead to a complex controller. In order to avoid this, the degree of the split polynomials $\bar{a}_{\mathrm{d}}(z)$ is increased. Consequently, there is no direct feedthrough of all signals $\bar{u}_{ij,k}$ to the torque requests $\tau_{\mathrm{E},k}^*, \tau_{\mathrm{M},k}^*$ as it is expected in the presented control design.

5.4.2 Resistive force compensation

As discussed in Section 4.3 a resistive force due to road gradient, air drag and rolling resistance acts on the vehicle. In order to provide a specific propulsion force, the resistive force has to be compensated. One approach for such a compensation is to consider the resistive force as disturbance input, which has to be compensated by the IMC feedback loop. Alternatively, a model of this resistive force, like in (4.39), can be used to consider a compensation in the inversion-based feedforward control design:

$$
\begin{bmatrix} y_1(z) \\ y_2(z) \end{bmatrix} = \begin{bmatrix} G_{11}(z) & G_{12}(z) \\ G_{21}(z) & G_{22}(z) \end{bmatrix} \begin{bmatrix} \tau_{\mathrm{E}}(z) \\ \tau_{\mathrm{M}}(z) \end{bmatrix} + \begin{bmatrix} G_{1,\mathrm{v}}(z) \\ G_{1,\mathrm{v}}(z) \end{bmatrix} F_{\mathrm{v}}(z) \overset{!}{=} \begin{bmatrix} w_1(z) \\ w_2(z) \end{bmatrix}, \qquad (5.181)
$$

$$
\begin{bmatrix} \tau_{\mathrm{E}}(z) \\ \tau_{\mathrm{M}}(z) \end{bmatrix} = \underbrace{\begin{bmatrix} G_{11}(z) & G_{12}(z) \\ G_{21}(z) & G_{22}(z) \end{bmatrix}^{-1} \begin{bmatrix} w_1(z) \\ w_2(z) \end{bmatrix}}_{\text{original feedforward controller}} - \underbrace{\begin{bmatrix} G_{11}(z) & G_{12}(z) \\ G_{21}(z) & G_{22}(z) \end{bmatrix}^{-1} \begin{bmatrix} G_{1,\mathrm{v}}(z) \\ G_{1,\mathrm{v}}(z) \end{bmatrix} F_{\mathrm{v}}(z)}_{\text{compensation}}.
$$

For the implementation of the model-based resistive force compensation the feedforward design procedure in Section 5.3.1 can be followed.

5.4.3 Block diagram

Figure 5.28 shows a possible implementation of the proposed control system for the control of embedded, smooth and lossless gear shifts between a specific hybrid CVT and a specific hybrid parallel, according to the sequence of shift phases in Figure 5.8. The single IMC feedback loops are separated into IMC trajectory generation (low-pass or polynomial planning, see Section 5.3.2) and inversion-based feedforward controller (see Section 5.3.1) as illustrated in Figure 5.29. The input interface assigns the hybrid DoFs signals (λ, λ^*), which are matched to the gear request $\boldsymbol{\kappa}^*$ (cf. Section 5.1).

The control system features three different inversion-based feedforward controllers according to the three plant models in Table 5.1 and six IMC trajectory generation blocks, implementing either with low-pass filter or polynomial trajectory planning approach. These components are triggered by the shift scheduler, which is responsible for the initiation and to monitoring of the single shift phases. Therefore, it is responsible for the switching between control tasks and controllers. Furthermore, it is responsible for the continuous evaluation of the performance of the control system. It decides, if a critical transition (see clutch actuation phase in Section 5.2.2) is performed or if the shifting procedure is aborted in case of any failure. In the upper right corner of
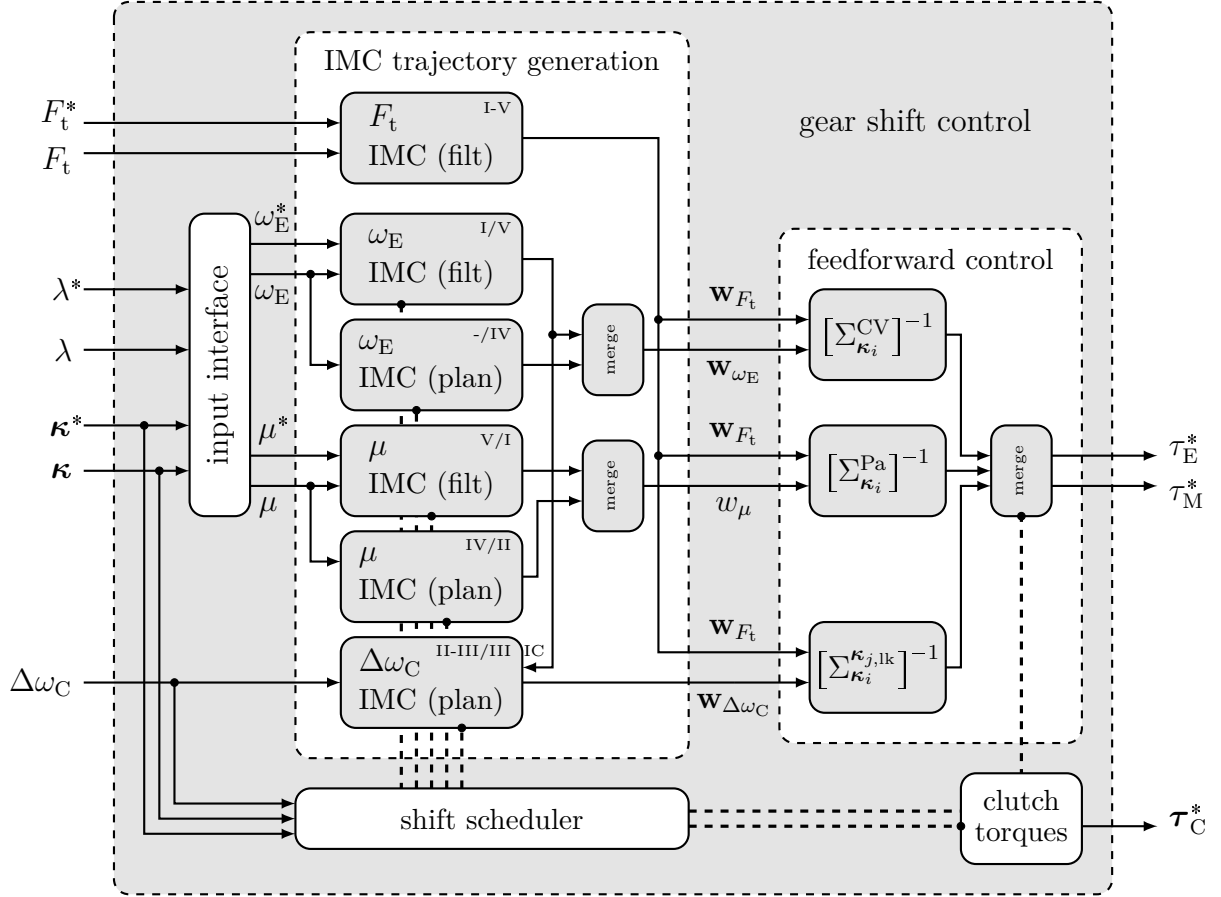
Figure 5.28: *Block scheme of the control system implementation for smooth and loss-less gear shifting*
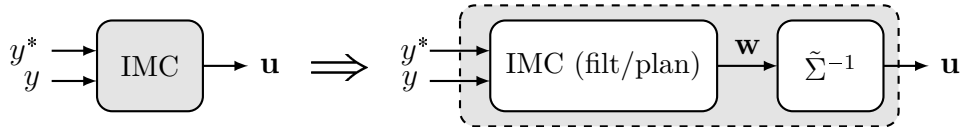
Figure 5.29: *Separation of an IMC structure into IMC trajectory generation and inversion-based feedforward controller*

the single IMC trajectory generation blocks the corresponding shift phases are stated for both shifts (CV $\rightarrow$ Pa/Pa $\rightarrow$ CV). For the clutch torques computation see (5.8). The proposed control system implementation features an easy parametrization, with a low number of comprehensible parameters. Beside the model-based feedforward controllers, the only actual control performance parameters are the durations of the shift phases ($T_{\mathrm{SP}}, T_{\mathrm{CA}}, T_{\mathrm{SC}}$), low-pass filter time constants (T_{F}), the minimum planning duration for the consecutive trajectory planning ($T_{\mathrm{P,min}}$) and the clutch torque request parameters $\tau^*_{\mathrm{C,KP}}$ and $\tau^*_{\mathrm{C,max}}$.
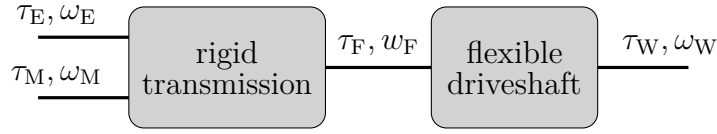
Figure 5.30: *Generalized DT modeling composition: rigid transmission and flexible driveshaft*

5.5 Generalization

Although the proposed control concept and implementation has been applied to exemplary shifts in an exemplary single-EM dedicated hybrid DT, it features a high potential for generalization. This potential shall be addressed in this final section.

The generalization from CV ↔ Pa to arbitrary elementary gear shifts between drivable modes in the exemplary DT, see Figure 4.17, is straightforward. The control phases and tasks, which appear are similar to the discussed ones and, hence, the control concept and implementation can be resumed. A generalization to arbitrary single-EM dedicated hybrid DTs can be made with the definition of a general DT modeling structure (see Figure 5.30), split into a rigid transmission, which combines the propulsion torques τ_E and τ_M to a final transmission torque τ_F and a flexible driveshaft, which transfers τ_F to the driving wheels. The flexible driveshaft is modeled by spring damper configuration and optionally final gear ratios. Figure 3.16 shows that the exemplary DT considered in this chapter features this model structure. The feasibility of this modeling structure has been proven in [15]. Due to this generalized model structure a characteristic set of states consisting of transmission states $\mathbf{q}_\mathrm{t}$ and shaft states $\mathbf{q}_\mathrm{s}$ will always appear in the general state-space vector $\mathbf{q}$:

$$\mathbf{q}_\mathrm{t}, \mathbf{q}_\mathrm{s} \in \mathbf{q}, \tag{5.182}$$

with:

$$\mathbf{q}_\mathrm{t} = \begin{bmatrix} w_\mathrm{F} & \omega_\mathrm{E} & \omega_\mathrm{M} \end{bmatrix}^T \tag{5.183}$$
$$\mathbf{q}_\mathrm{s} = \begin{bmatrix} \Delta\varphi & v \end{bmatrix}^T.$$

Therefore, the consideration mode specific kinematics and static torques can be always directly applied to a general DT with respect to the sates $\mathbf{q}_\mathrm{t}$. In combination with $\mathbf{q}_\mathrm{s}$ the number of mechanical degrees of freedom is fixed for each operation mode. In consequence, the same relative degrees will appear in the controller design and therefore the proposed design procedure in this chapter can be applied without modifications.

The scope of this thesis is on the control of smooth and lossless gear shifts. The fact that the proposed control concept considers embedded gear shifts, however, enables the application of the controllers also for the general mode operation, which is another level of generalization.

5.6 Summary

The contributions of the previous chapters have been utilized in this chapter to proposes a model-based control system of embedded smooth and lossless gear shift between hybrid CVT and hybrid parallel modes in single-EM dedicated hybrid DTs. The proposed switching control system is based on a sequence of shift phases with different control plants and control tasks (Section 5.2) and the input and output signals are matched to a classical torque-based PT control system (cf. Section 2.5). In order compute continuous and smooth control signals (torque requests) the plant model transitions are considered in detail (Section 5.2.3). It features a common IMC structure (Section 5.3.3) with an inversion-based feedforward controller (Section 5.3.1). For the control of set-point reference signals, an alternative to the classical reference trajectory generation with a low-pass filter (see Section) has been proposed: a recursive polynomial trajectory planning algorithm (Section 5.3.3). Since the control system design is required to be applied in real-time in an automotive control unit the discretization with respect to time has been considered (Section 5.3.4). Finally, the chapter gives the controller parametrization for an exemplary single-EM dedicated hybrid DT (see Section 5.4.1) and opportunities for a generalization of the proposed control system (Section 5.5) have been pointed out. The functionality of the proposed control system will be demonstrated in different test scenarios and environments in the next chapter.

6

Validation of drivetrain control system

The DT control concept and the DT control system implementation for active smooth and lossless gear shifting proposed in Chapter 5 shall be finally validated, in terms of evaluating its functionality and performance. To increase the significance of the validation it is performed on three levels based on a state-of-the-art software-to-vehicle process: MiL simulations, SiL simulations and vehicle testing. The results of the different validation levels are illustrated, discussed and evaluated.

6.1 Validation approach

In Section 5.4 an exemplary implementation of the control concept, proposed in Chapter 5 and based on the contributions of Chapters 2, 3 and 4, has been proposed. In order to evaluate the significance of this contribution, it is necessary perform an extensive validation.

Problem statement:

- Evaluation of principle functionality and performance of the control concept and its control software implementation
- Evaluation of the concept's applicability in a real vehicle and identification of potentials for improvement

---

Whereas the first part of the problem statement can be done in simulation, the second part requires testing of the control concept implementation integrated into the PT control system in a demonstrator vehicle. A state-of-the-art software-to-vehicle process is illustrated in Figure 6.1. It shows three major steps: the implementation of the software part, its integration into an existing software framework and finally the code generation for execution on a Vehicle Control Unit (VCU). This process is usually accompanied by an extensive testing procedure (MiL-, SiL- and HiL-simulations as well as vehicle tests) in state-of-the-art automotive software engineering (see for example [79] and [15]).

As the proposed control software is not supposed to be a SOP software (cf. Section 1.5) this testing procedure will be performed in a reduced way on three validation
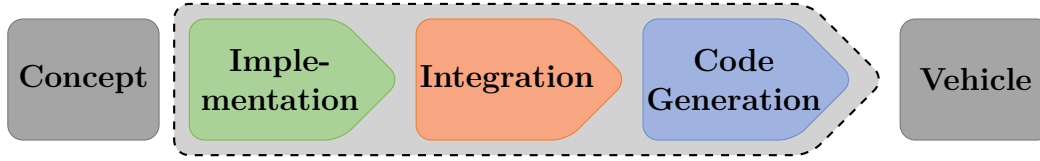
Figure 6.1: *Software-to-vehicle process*

levels:

- **Validation level I:** In a first step the control concept for smooth and lossless gear shifting is implemented in a simulation environment (MATLAB®/Simulink®,[1]). The same simulation environment is used to provide specific reference signals (DT control system inputs) for the control system and to model the control plant using the validated modeling approach proposed in [15]. This model provides the control signals $F_\mathrm{t}, \Delta\kappa_{ij}, \omega_\mathrm{E}, \Delta\omega_\mathrm{C}$ and μ.

- **Validation level II:** On the second validation level the control system, which has been implemented in a simulation environment, is encapsulated into a gear shifting component and integrated into an existing PT control system as software component, ready for automated code generation. Hence, simulation at this validation level can be considered as SiL-simulation, although the simulation is still executed exclusively in one simulation environment (Matlab/Simulink). The driver stimulation is done in terms of defining an accelerator pedal position signal. The required gear shifts are triggered at specific vehicle speeds (v_trig) by specific EMS parameter settings. For the plant model simulation a PT model provided by AVL CRUISE[TM,2] is applied. The vehicle software includes a DT observer, which provides the control signals.

- **Validation level III:** In the third validation level automated C-code generation is applied to the vehicle control software of validation level II. The generated code is transferred to a Rapid Prototyping Control Unit (RPCU)[3] in an AVL demonstrator vehicle featuring a single-EM dedicated hybrid DT. At this validation level the traction force request is provided directly by the driver, who drives the demonstrator at a test track, via the accelerator pedal. Equivalently to level II the required gear shifts are triggered at specific vehicle speeds (v_trig) by the EMS. The real vehicle itself functions as control plant.

At this point it is necessary to mention that the effort to perform validation tests increases for increasing validation level. The increase between level I and level II is on the one hand due to the increased computational effort and on the other hand due to the requirement to provide a software, which is ready for code generation. Additionally, as the same software is subsequently used for vehicle testing, rigorous safety requirements have to be met in order to protect the demonstrator from damage. This safety requirements and their consideration in the implementation of the control system are not in the scope of this thesis. Whereas the first two validation levels can be

---

[1]Matlab®and Simulink® are registered trademarks of The Mathworks Inc.

[2]AVL CRUISE[TM] is a registered trademark of AVL List GmbH (`https://www.avl.com/cruise`).

[3]`https://www.dspace.com/de/gmb/home/products/newprod/microautobox_2.cfm`

performed in the office by a single engineer, the third validation level requires support by a calibration team: a test driver and a software expert for code generation as well as code transfer to the RPCU, parametrization and recording of measurement data in the vehicle during testing. Furthermore, it is obvious that the availability of the demonstrator and the test track is crucial. In order to have at least some test results at all three validation levels, despite the increasing effort, the following restriction with respect to the tested shift scenarios have been made:

- **Validation level I:** CV ↔ Pa,
- **Validation level II:** CV1 → Pa1 → CV1,
- **Validation level III:** CV1 → Pa1.

Consequently, the range of validity decreases for the three validation levels, while the significance of validity increases (see Figure 6.2).
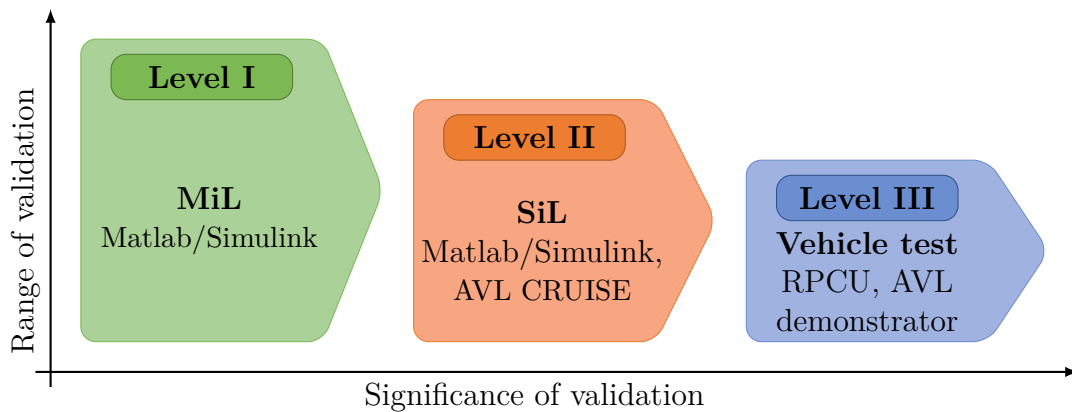
Figure 6.2: *Range and significance of validity of the three validation levels*

Table 6.1 summarizes the test setups (see Figure 6.2) of all three validation levels.

The following sections provide validation results of the different validation levels as well as their discussion. Table 6.2 gives an overview on the structure of the result illustrations. It is split into control variables (subplots 1-5) and control outputs (subplots 6-7). The control variables (for example signal x) are illustrated in terms of four signals:

- the request x^*,
- the planned trajectory x_P^* according to the request, generated by low-pass filtering or polynomial trajectory planning (see Section 5.3.2),
- the actual value x, obtained by a physical or virtual sensor,
- and the IMC request x_{imc}^* according to planned trajectory and the actual value (updated planned trajectory)

Whereas the illustration of the signals x^* and x_{imc}^* shall support the comprehensibility of the control system's functionality, its performance has to evaluated considering the deviation between the signals x_P^* and x, which is the actual control error. Since the clutch state is not controlled directly, but set indirectly by the control system, there is no corresponding feedback loop and hence no IMC request. In the control

system implementation used for validation, furthermore, the feedback loop for controlling the torque split factor μ has been removed. Therefore, the torque split is controlled exclusively in a feedforward structure and, hence, there is no corresponding IMC request. According to the control tasks in the considered single shift phases (see Figure 5.8), some requests, plans and IMC requests are not present and, consequently, not illustrated in some shift phases.

Table 6.3 lists the performance parametrization of the DT control system. The low number of actual control parameters substantiates the easy parametrization of the proposed control system. All other parameters are related to the model-based control design and therefore they can be parametrized using the DT modeling tool presented in Chapter 3.

Table 6.1: *Overview on the setups of the three validation levels*

Validation	Stimulation	Control software	Control plant	Shift scenario
Level I	Matlab/Simulink (DT control system inputs)	Matlab/Simulink (DT control system implementation)	Matlab/Simulink (model in [15])	CV ↔ Pa
Level II	Matlab/Simulink (driver input)	Matlab/Simulink (vehicle control software including shift component with DT control system implementation)	Matlab/Simulink, (AVL CRUISE^{TM})	CV1 → Pa1 → CV1
Level III	Test driver	RPCU (code generation of vehicle control software)	AVL demonstrator	CV1 → Pa1

Table 6.2: Overview on the validation result illustration

subplot	content	signals
1	traction force	$F_\mathrm{t}^*, F_{\mathrm{t,P}}^*, F_\mathrm{t}, F_{\mathrm{t,IMC}}^*$
2	clutch state	$\Delta\kappa_{ij}^*, \Delta\kappa_{ij,\mathrm{P}}^*, \Delta\kappa_{ij}$
3	ICE speed	$\omega_\mathrm{E}^*, \omega_{\mathrm{E,P}}^*, \omega_\mathrm{E}, \omega_{\mathrm{E,IMC}}^*$
4	torque split factor	$\mu^*, \mu_\mathrm{P}^*, \mu$
5	clutch slip/torque	$\Delta\omega_\mathrm{C}^*, \Delta\omega_{\mathrm{C,P}}^*, \Delta\omega_\mathrm{C}, \Delta\omega_{\mathrm{C,IMC}}^* / \tau_{\mathrm{C,lk}}^*, \tau_{\mathrm{C,lk}}$
6	ICE and EM torque request	$\tau_\mathrm{E}^*, \tau_\mathrm{M}^*$
7	clutch torque request	τ_C^*

Table 6.3: Parametrization of DT control system

symbol	value	unit	explanation
T_SP	0.4	s	duration shift preparation phase
T_CA	0.1	s	duration clutch actuation phase
T_SC	0.4	s	duration shift completion phase
$\tau_{\mathrm{C,KP}}^*$	10	Nm	kiss-point clutch torque request
$\tau_{\mathrm{C,max}}^*$	800	Nm	maximum clutch torque request
T_F	0.1	s	low-pass filter time constant
$T_{\mathrm{P,min}}$	0.1	s	minimum planning duration for trajectory planning

6.2 Validation level I (MiL simulation)

6.2.1 Validation level I – Setup

> **Validation level I – Setup**
>
> - **Stimulation:** Matlab/Simulink; DT control system inputs $F_\text{t}^*, \lambda^*, \boldsymbol{\kappa}^*$ (see Figure 5.2)
> - **Control software:** Matlab/Simulink; DT control system implementation (see Figure 5.28)
> - **Control plant:** Matlab/Simulink; validated model from [15]
> - **Shift scenario:** CV ↔ Pa

6.2.2 Validation level I – Test cases

The test cases for validation level I consider acceleration of the vehicle. At specific vehicle speeds a gear shift is triggered and performed. Table 6.4 lists the test cases of the presented results. The set of test cases is defined in order to show the functionality of the proposed DT control system for different gear shifts, traction force requests and hybrid DoF requests.

Table 6.4: Overview of the presented test cases of validation level I

		shift			requests			Figure
		initial	final	$\Delta\kappa_{ij}$	v_trig	F_t^*	ω_E^*	μ^*	
		-	-	-	km/h	kN	rad/s	-	
Level I	1	CV1	Pa1	B1	24.9	1	183	1	(6.3),(6.4)
	2	Pa1	CV1	B1	39.7	1	183	1	(6.5)
	3	CV1	Pa2	C1	30.0	2	300	0.7	(6.6)
	4	Pa3	CV2	B1	35.0	1	200	0	(6.7)
	5	Pa2	CV2	C2	27.1	0.8	250	0.8	(6.8)

6.2.3 Validation level I – Results

Test case 1. Figure 6.3 shows the simulation results of the complete first test case according to Table 6.4. Table 6.5 lists the time schedule of the five shift phases, and the corresponding highlighting in the result illustrations. The beginning of the simulation shows a planned build-up of the traction force F_t according to the request F_t^*. The planned traction force $F_\text{t,P}^*$ is tracked precisely, with an steady error of < 0.1 N. Simultaneously, the ICE ω_E is speeded up from idle speed to the requested speed ω_E^*. The steady state error for the tracking of ω_E is in acceptable the range of 1 rad/s.

Table 6.5: *Simulation times of single control phases for results of test case 1*

phase	I	II	III	IV	V
time in s	0-11	11-11.4	11.4-11.5	11.5-11.9	11.9-15

This initial transient phase is followed by a period of constant vehicle acceleration in CV1 mode with constant traction force and ICE speed requests (cf. Table 6.5). The increasing IMC request $\omega^*_{\mathrm{E,IMC}}$ compensates the neglected damping of the shafts (see Section 5.4). Within the shift phases I and II the torque split factor μ can be calculated, but is not of interest, since the hybrid DoF is assigned to the ICE speed in hybrid CVT mode. According to the clutch slip zero crossing, a passive smooth and lossless gear shift would have been possible at $t \approx 9.5$ s. The gear shift to hybrid parallel mode Pa1 is requested at $t = 11$ s. As the gear shifting is of special interest, Figure 6.4 shows an enlarged illustration of the actual gear shift (phases II-IV). The highlighting of the shift phases follows the color code in Figure 5.8.

Shift preparation. In order to prepare a smooth and lossless clutch transition the non-zero clutch slip has to be controlled to zero, while maintaining the requested traction force. To do so an appropriate smooth clutch slip trajectory $\Delta\omega^*_{\mathrm{C,P}}$ is planned and tracked releasing the ICE speed control according to the hybrid DoF request. The corresponding IMC request $\Delta\omega^*_{\mathrm{C,IMC}}$ takes advantage of the previous shift phases and reuses the offset between the actual ICE speed ω_{E} and the corresponding IMC request $\omega^*_{\mathrm{E,IMC}}$ in order to improve the tracking performance. This approach furthermore ensures smooth torque requests $\tau^*_{\mathrm{E}}, \tau^*_{\mathrm{M}}$ although the control tasks and the corresponding control loop are switched at this transition (see Table 5.1). Within this shift phase, simultaneously, the clutch is actuated to the kiss-point due to the clutch torque request $\tau^*_{\mathrm{C}} = \tau^*_{\mathrm{C,KP}}$ (clutch filling command) according to (5.5). At the end of the shift preparation phase the clutch is fully synchronized and ready for actuation.

Clutch actuation. Due to the fully synchronized clutch, the clutch state transition occurs right at the beginning of the clutch actuation phase as planned, for a clutch torque request $\tau^*_{\mathrm{C}} > \tau^*_{\mathrm{C,KP}}$. The impact of this transition on drivability can be seen in the oscillation of the actual traction force. Due ot the low amplitude of this oscillation (~ 0.4 N) and the fact that the oscillation is damped by the controller, this impact is negligible. The remaining clutch actuation phase is used to increase the clutch torque request to its maximum value $\tau^*_{\mathrm{C,max}}$.

Shift completion. To complete the shift the hybrid DoF request in Pa1 mode has to be recovered. Therefore, a smooth trajectory μ^*_{P} from current value to the request μ^* is planned and tracked. The final request $\mu^* = 1$, cf. (2.2), actually requires shutting off the EM. After the gear shift the vehicle is further accelerated in hybrid parallel mode Pa1.

Test case 2. Figure 6.5 shows test case 2, which considers a gear shift from hybrid parallel mode Pa1 back to hybrid CVT mode CV1. As in all upcoming test case results, exclusively the gear shift, which is embedded into a stationary driving situation similar to test case 1 (see Figure 6.3), is illustrated. When the gear shift from hybrid parallel mode Pa1 to hybrid CVT mode is requested, the torque split factor μ is controlled to μ_{unload} according to (5.30), following a trajectory μ_{P}^*, in order to unload the clutch B1. The course of the locking torque at the clutch $\tau_{\mathrm{C,lk}}$ proofs the feasibility of this implicit approach. During the clutch actuation phase the clutch torque request is decreased from $\tau_{\mathrm{C,max}}^*$ to zero, according to (5.7). Due to the fully unloaded clutch the clutch transition occurs at the end of this phase, as expected. The resulting traction force oscillations are again in a negligible range. In order to recover the hybrid DoF request ω_{E}^* a smooth trajectory $\omega_{\mathrm{E,P}}^*$ for the ICE speed is planned and tracked in the shift completion phase.

Test cases 3-5. The test cases 3-5 (Figures 6.6, 6.7 and 6.8) show equivalent results for different gear shifts (CV1 $\rightarrow$ Pa2, Pa3 $\rightarrow$ CV2 and Pa2 $\rightarrow$ CV2), traction force requests and hybrid DoF requests, according to Table 6.4. Although the magnitude of the traction force oscillation resulting from the clutch transition is higher in test case 5 (Figure 6.8), its magnitude is still in an acceptable range.
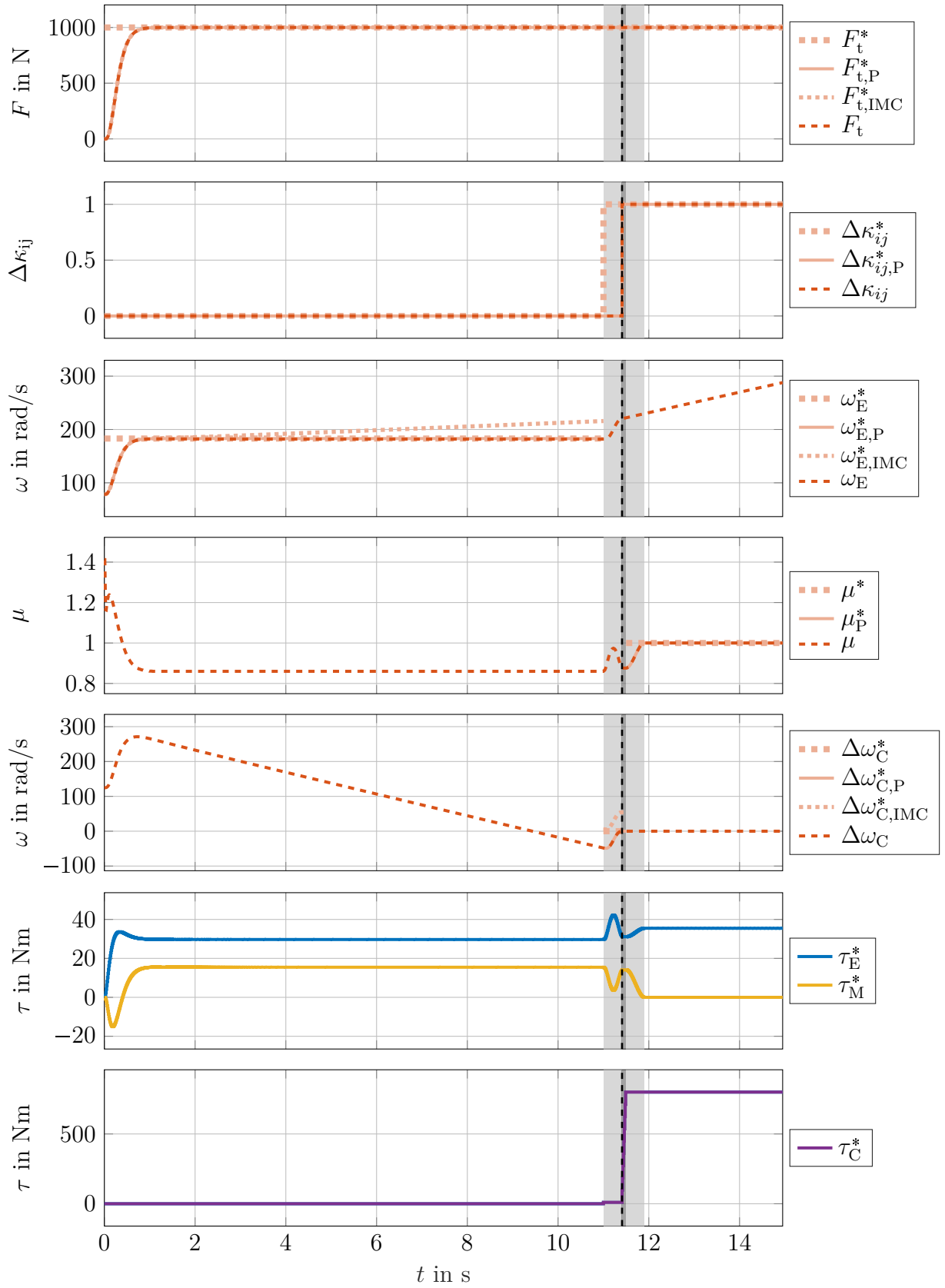
Figure 6.3: *MiL results, test case 1 (*CV1 → Pa1*), total simulation*
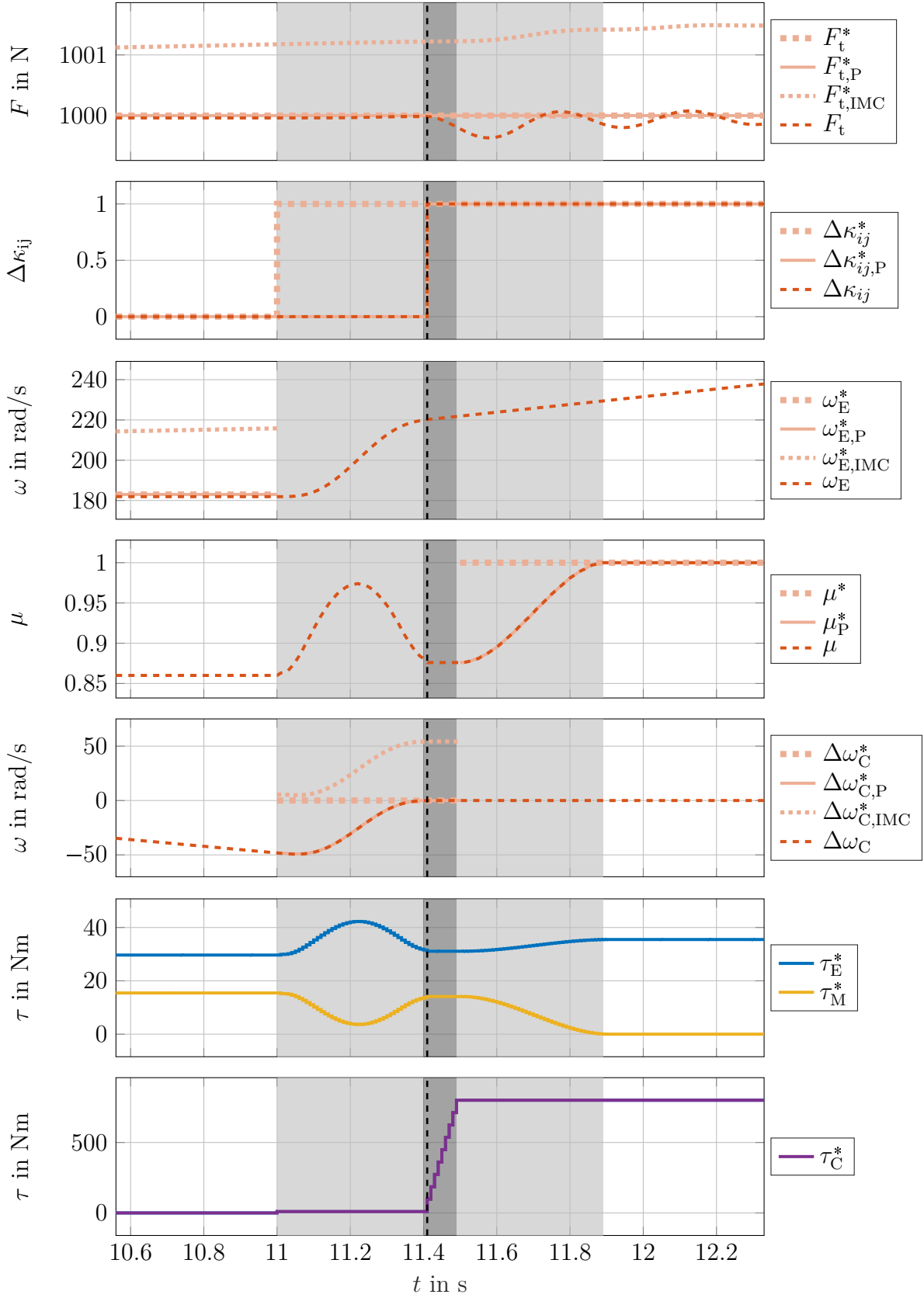
Figure 6.4: *MiL results, test case 1 (*CV1 → Pa1*), gear shift*
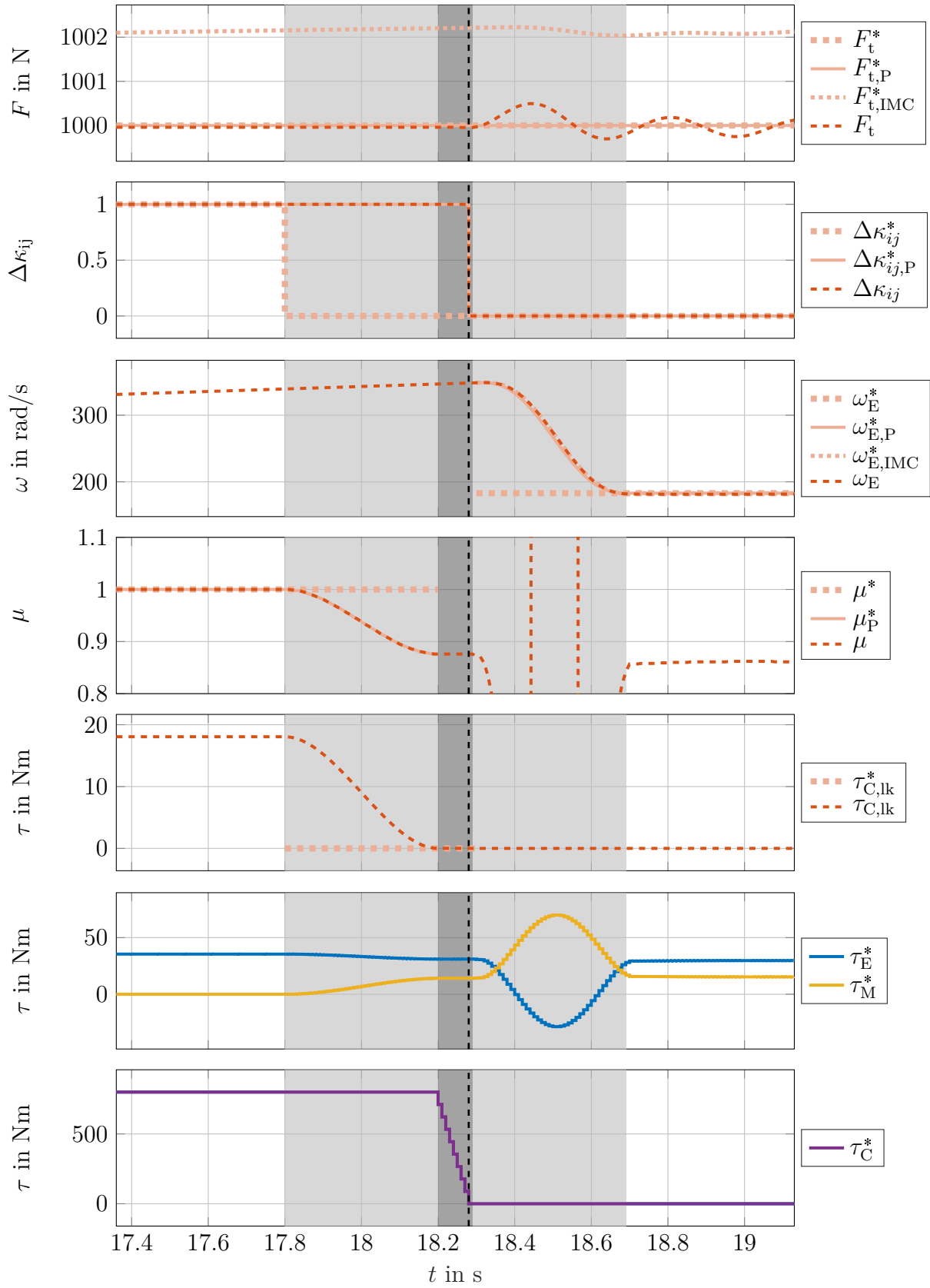
Figure 6.5: *MiL results, test case 2 (*Pa1 → CV1*)*
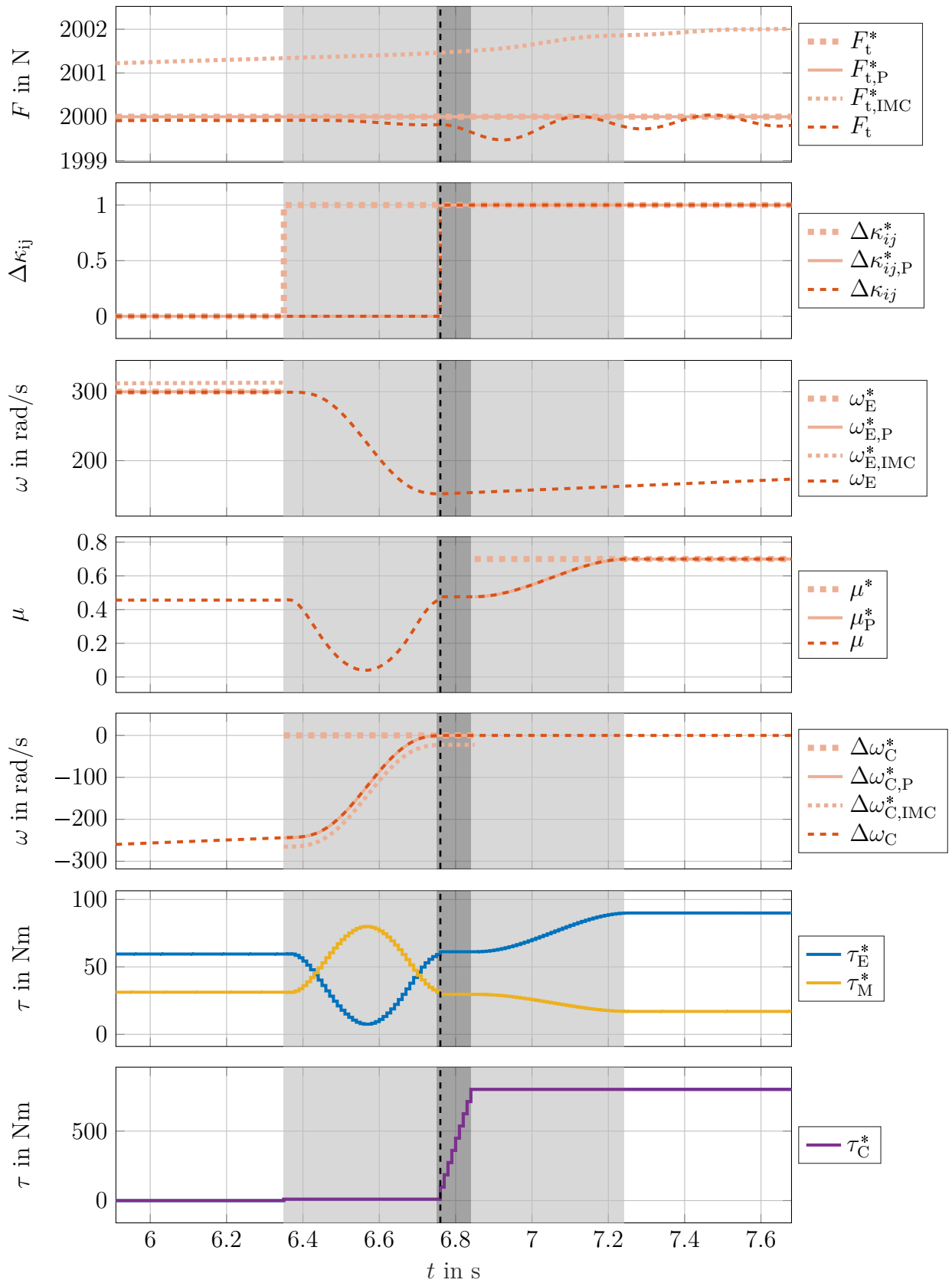
Figure 6.6: *MiL results; test case 3 (CV1 → Pa2)*
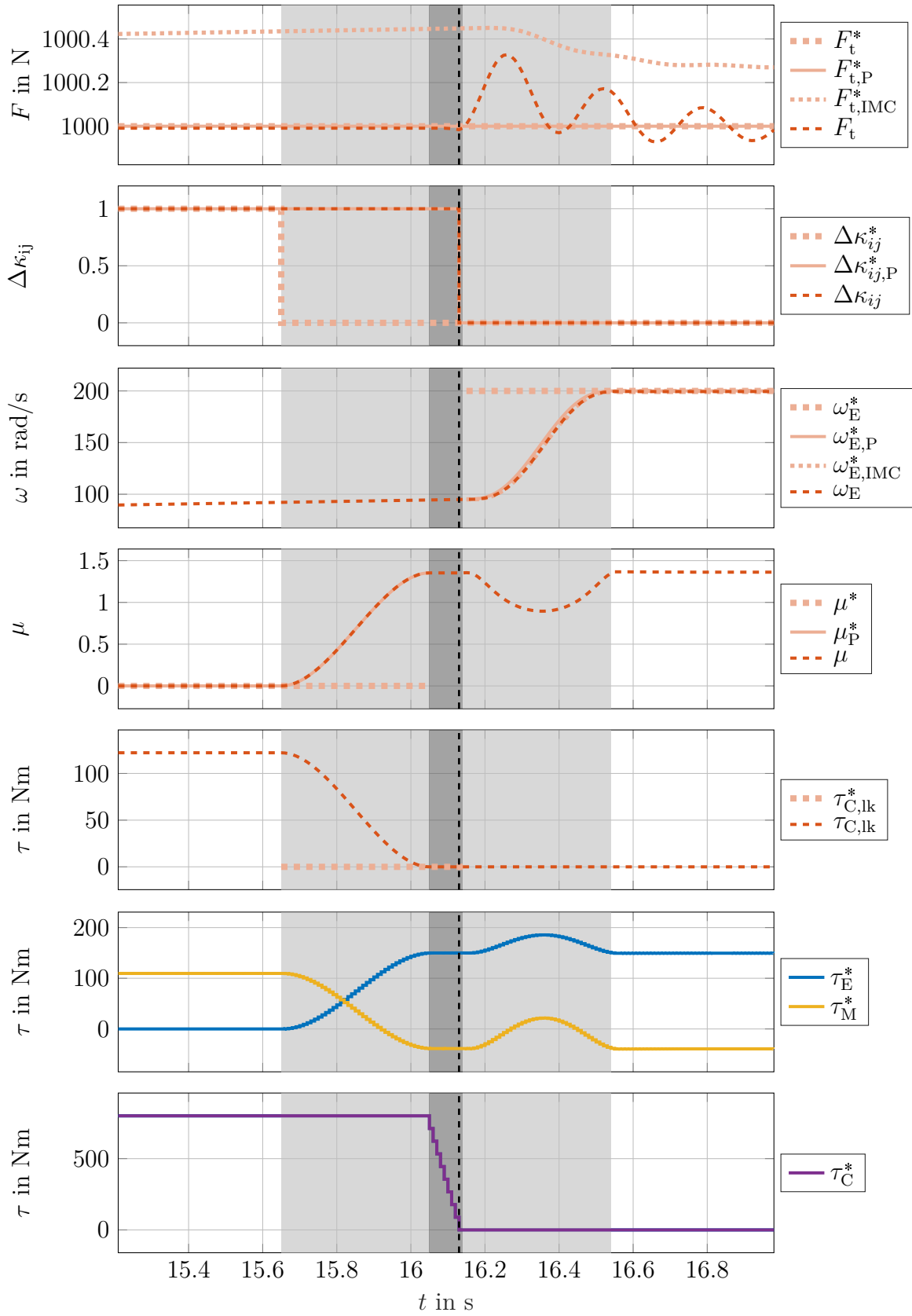
Figure 6.7: *MiL results; test case 4 (*Pa3 → CV2*)*
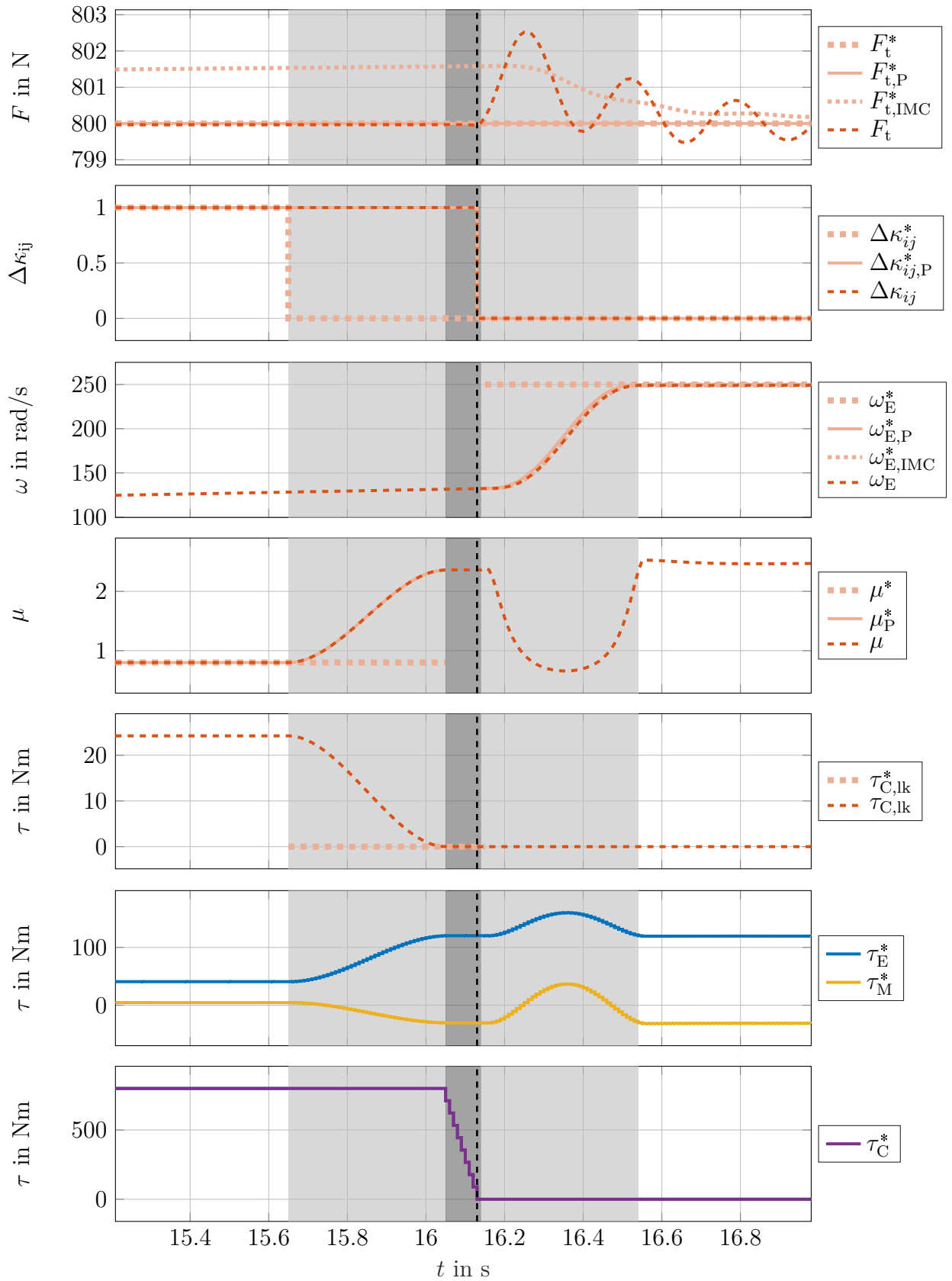
Figure 6.8: *MiL results; test case 5 (Pa2 → CV2)*

6.2.4 Validation level I – Evaluation

The following statements summarize the performance of the gear shifts in the presented MiL simulation results:

- The IMC concept features satisfying tracking performance for the control variables in all control phases. Therefore, the application of the DT control system also for mode operation is feasible.
- The impact of the clutch transition (shifting) on drivability (traction force) is low.
- Clutch slipping and hence dissipation is avoided for both clutch engagement and disengagement.
- The actuation of a synchronized, respectively unloaded, clutch enables a precise prediction of the actual clutch transition.

The promising MiL simulation results proof the applicability of the concept of smooth and lossless gear shifting in general as well as the implementation of the proposed DT control system in particular. Therefore, the results substantiate the encapsulation of the DT control system into shifting components and its integration into an existing vehicle software for further validation. The presented test cases considered reasonable gear shifts, matched to the current driving situation, as such shift requests are expected from the EMS in practical application. This results in feasible ICE and EM torques and speeds within their physical limits. As discussed in Section 5.3.5, however, it is possible the estimated the required torques for a gear shift in advance in order to check feasibility of a received gear request.

6.3 Validation level II (SiL simulation)

6.3.1 Validation level II – Setup

Validation level II – Setup:

- **Stimulation:** Matlab/Simulink; driver input (pedal position in %)
- **Control software:** Matlab/Simulink; entire vehicle control software ready for code generation including shifting components with encapsulated DT control system implementation
- **Control plant:** Matlab/Simulink; AVL CRUISE
- **Shift scenario:** CV1 → Pa1 → CV1

6.3.2 Validation level II – Test cases

In validation level II the control software, encapsulated into a shifting component and integrated into an existing vehicle software, is already prepared for testing in the vehicle. Therefore, also the considered set of test cases (see Table 6.6) are matched to the planned vehicle testing scenarios on the test track. The vehicle is accelerated

in hybrid CVT mode CV1 with different accelerations defined by different accelerator pedal position. Table 6.6 lists the settings of the different test cases. Due to a specific EMS parameter setting a gear shift to hybrid parallel mode Pa1 is requested at a vehicle speed of $v \approx 25$ km/h. Subsequently, the vehicle is further accelerated and finally the shift back to hybrid CVT mode CV1 is requested at $v \approx 40$ km/h. The traction fore

Table 6.6: *Overview of the presented test cases of validation level II*

		shift				requests				Figure
		initial	final	$\Delta\kappa_{ij}$	v_{trig}	pedal	F_t^*	ω_E^*	μ^*	
		-	-	-	km/h	%	kN	rad/s	-	
	1	CV1	Pa1	B1	25.1	20	~1	183	1	(6.9)
	2	Pa1	CV1	B1	40.4	20	~1	183	1	(6.10)
Level II	3	CV1	Pa1	B1	25.2	35	~2	183	1	(6.11)
	4	Pa1	CV1	B1	40.7	35	~2	183	1	(6.12)
	5	CV1	Pa1	B1	25.3	50	~3	183	1	(6.13)
	6	Pa1	CV1	B1	41.5	50	~3	183	1	(6.14)

requests result from given accelerator pedal positions. Except for the clutch torque request for bringing the clutch to the kiss-point, which is set to $\tau_{C,KP}^* = 0.1$ Nm, the parametrization of the DT control system is equivalent to validation level I. As the mode operation of hybrid CVT mode CV1 and hybrid parallel mode Pa1 is controlled by control systems of the existing control software, in addition to these parameters the durations of shift phases I and V (mode operation) of the embedded gear shift according to Figure 5.8 need to be defined:

$$T_{\text{I}} = T_{\text{V}} = 0.5 \text{ s.} \tag{6.1}$$

This implies that mode operation of the current hybrid mode is continued for T_{I} seconds after the gear shift has been requested and for T_{V} seconds after the gear shift has been performed before the gears shift is reported to be finished.

6.3.3 Validation level II – Results

Test case 1. Figure 6.9 illustrates the SiL simulation results for test case 1. Similar to the MiL simulation results, it shows the section of the total simulation, in which the shifting component is active. This section starts with the gear shift request $\Delta\kappa_{ij}^*$, received from the EMS, and ends with a trigger signal, confirming that the shift has been completed.

    Shift preparation. Taking a look at the shift phases I and II it is noticeable that the tracking performance of the traction force control shows potential for improvement, especially in comparison to the MiL simulations. The source of this decreased performance can be found in the actually acting propulsion torques, which are illustrated

in the last subplot in Figure 6.9: In addition to the ICE and EM torque requests, τ_E^* and τ_M^*, which are computed by the DT control system, this subplot shows the actually acting torques τ_E and τ_M. Whereas the actually acting EM torque approximately equals the requested torque, except for a small delay, the actually acting ICE torque shows significant deviations from the corresponding request, especially for dynamic requests as in the shift preparation phase. Hence, the ICE features some dynamical behavior, which has not been considered in the control system design. Therefore, the traction force significantly drops in this phase. The reaction of the control system to this deviation can be noticed in the IMC traction force request $F_{t,IMC}^*$.

In order to reduce the effect of the ICE dynamics, the duration of the shift preparation phase, T_{SP}, could be increased in order to decrease the derivative of the ICE torque request in this phase (see Section 5.3.5 and in particular Table 5.2). Since the validation approach in this chapter focuses on a proof of the general shifting control concept, there is no reason to pursue such a parameter tuning at this point. In section 6.4.5 an outlook on a possibility to handle this problem will be given.

Considering the clutch synchronization reveals the robustness of the implemented IMC concept: In contrast to the traction force tracking, it is not necessary to exactly track the course of the planned clutch slip trajectory, but to reach the required final value at the required time. This is achieved by the IMC concept, regardless of the deviations between requested and actually acting torques. This confirms the robustness of the IMC concept, which has already been supposed in the educational example in Section 5.3.3. The deviation between planned slip trajectory $\Delta\omega_C^*$ and the actual clutch slip $\Delta\omega_C$ substantiates the action of the IMC feedback loop. Nevertheless, the deviations between requested and acting propulsion torques also affect the residual clutch slip and hence the accuracy of the clutch synchronization.

During the shift preparation phase the clutch filling command $\tau_C^* = \tau_{C,KP}^*$ is sent in order to prepare the clutch for its engagement. Due to the small value of $\tau_{C,KP}^*$ this request is not visible in the last subplot.

Clutch actuation. The actual transition to the clutch actuation phase is flexible and initiated, if the following four conditions are met (cf. Section 5.2.2):

- The residual clutch slip has to be below a specific limit:

$$|\Delta\omega_C(T_2)| < \Delta\omega_{C,res} = 3 \text{ rad/s}. \tag{6.2}$$

- Furthermore, the derivative of the clutch slip has to meet a specific limit:

$$|\Delta\dot{\omega}_C(T_2)| < \Delta\dot{\omega}_{C,res} = 1 \text{ rad/s}^2. \tag{6.3}$$

- The clutch filling has to be completed. Hence, the clutch has to be at kiss-point and ready for fast engagement.

- In the control concept a maximum exceeding time of the planned duration of the shift preparation phase is defined. This maximum exceeding time of the shift preparation phase must not by exceeded.

According to the last condition the start of the clutch actuation might occur earlier or later than originally intended. Such an untimely transition is highlighted by a dashed gray line in the upcoming test case results. In this test case (Figure 6.9) the clutch actuation phase is started 10 ms earlier than intended. If the first three conditions would not be met within the planned shift preparation phase (plus maximum exceeding time), the clutch synchronization is considered to be failed. In this case the control system would send an error message to the EMS, recover the hybrid DoF and return to hybrid CVT mode operation of gear CV1.

Within the clutch actuation phase, the clutch torque request is ramped up to its maximum value $\tau_{C,max}^*$, as defined in (5.5), while the clutch slip is still controlled to zero. In contrast to the MiL simulations, the actual clutch transition, highlighted by the black dashed line, does not occur at the beginning of the clutch actuation phase but within this phase. This substantiates the robust design of the clutch actuation. Due to the present residual clutch slip, small dissipation will occur in the clutch. The range of this dissipation, however, is far below the dissipation, which would occur without any clutch synchronization. During this period, furthermore, the drivability is affected by the acting slipping torque in the clutch, noticeable in a drop of the traction force. An extension of the clutch actuation phase would decrease this impact.

Shift completion. In the final shift completion phase the hybrid DoF request for gear Pa1 μ^* is recovered. Within this phase the control system is able to control the traction force F_t back to the requested value F_t^*. Figure 6.9 shows that the effect of the ICE dynamics is higher in hybrid CVT mode than in hybrid parallel mode.

Test case 2. Test case 2 considers the shift from hybrid parallel mode Pa1 back to hybrid CVT mode CV1. The results in figure 6.10 show an unintended increase of the traction force, which is again sourced by the unmodeled ICE dynamics. Within the shift preparation phase the vehicle propulsion torque is partially handed over to the EM in order to unload the clutch, which is requested to be disengaged, according to the computed torque split factor μ_{unload}. Similar to the clutch synchronization, the flexible transition to the clutch actuation phase occurs, if three condition concerning the residual locking torque,

$$|\tau_{C,lk}(T_2)| < \tau_{C,lk,res} = 3 \text{ Nm}, \tag{6.4}$$

its derivative,

$$|\dot{\tau}_{C,lk}(T_2)| < \dot{\tau}_{C,lk,res} = 1 \text{ Nm/s}, \tag{6.5}$$

and a maximum exceeding time of the planned duration of the shift preparation phase are met. As the clutch disengagement does not require a clutch filling, the third condition in the case of clutch engagement is not present in the case of clutch disengagement. As illustrated in Figure 6.10, the start of the clutch actuation phase is postponed for 0.02 s in test case 2, since at this time all three conditions are met at the first time. The actual clutch transition occurs at the end of this phase as expected. Therefore, in contrast to test case 1, the clutch is not operating in slipping state temporarily. This

implies the absence of dissipation as well as a low impact on drivability, which can be seen in the smooth traction force during this phase. Whereas the performance of the DT control system is acceptable until this point, the unmodeled ICE dynamics come back on stage in the shift completion phase. Although the ICE speed recovery (hybrid DoF) is performed in principle, the impact on the traction force control is obvious. This substantiates the observation of test case 1 that the effect of unmodeled ICE dynamics is higher in hybrid CVT mode than in hybrid parallel mode. Except for a small steady state error in the ICE speed the control system, finally, compensates the impact of unmodeled ICE dynamics. The IMC request $\omega_{E,IMC}^*$, furthermore, shows the compensation of the velocity dependent damping of the shafts according to friction, which has been neglected in the DT model.

Test cases 3-6. The test cases 3-6 (Figures 6.11, 6.12, 6.13 and 6.13) repeat the test cases 1-2 with different accelerator the pedal positions (35 and 50 %). The results are almost identical to the discussed test cases 1 and 2, accept for the increased traction force level. In test cases 4 and 5 the control system additionally has to cope with an initial control error concerning the traction force $(F_t - F_t^*)$. This control error is a relic of the performance of the previously active software component of the existing vehicle software, which controlled the hybrid CVT mode operation.
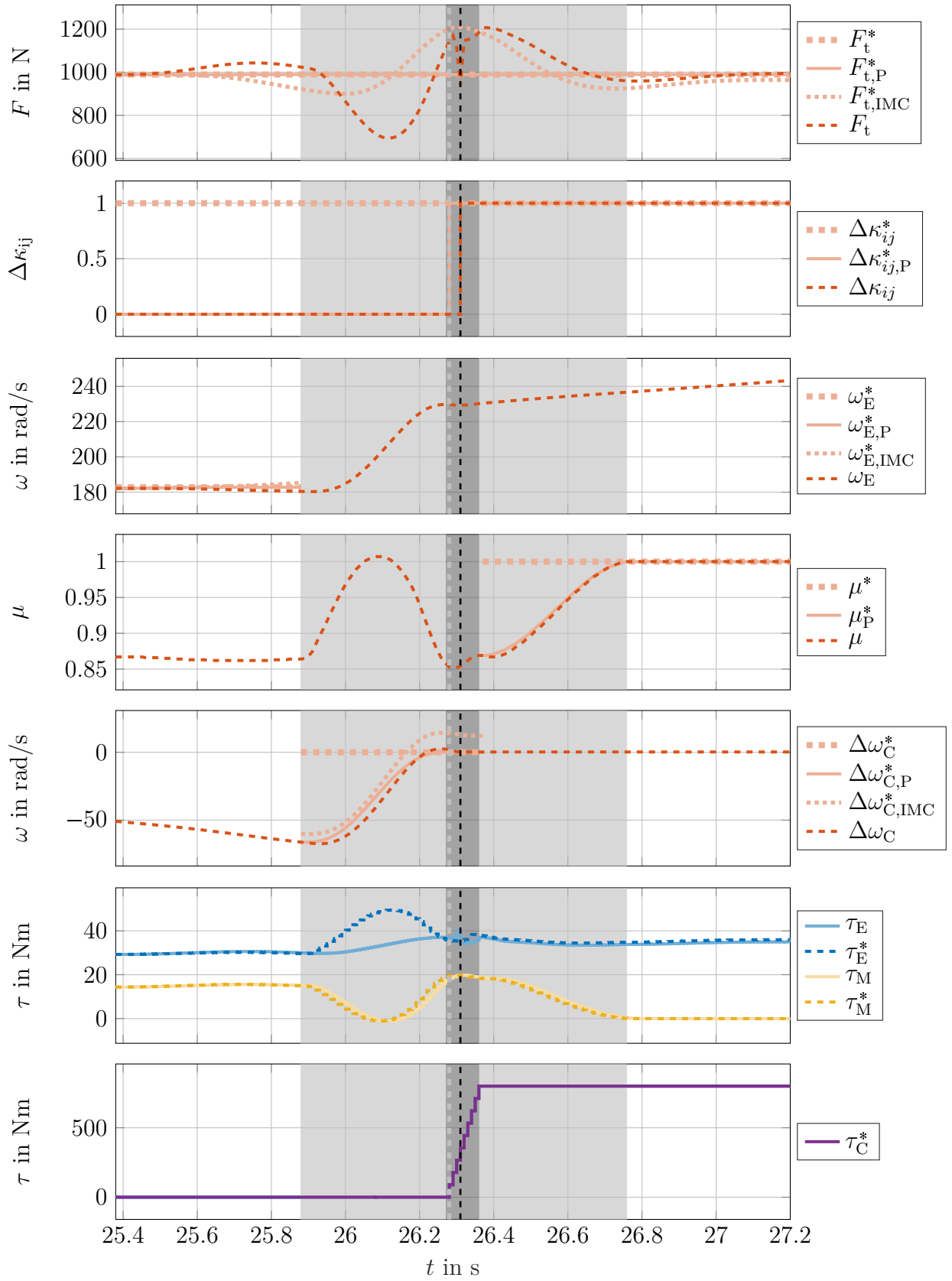
Figure 6.9: *SiL results; test case 1 (*CV1 → Pa1, 20% pedal)
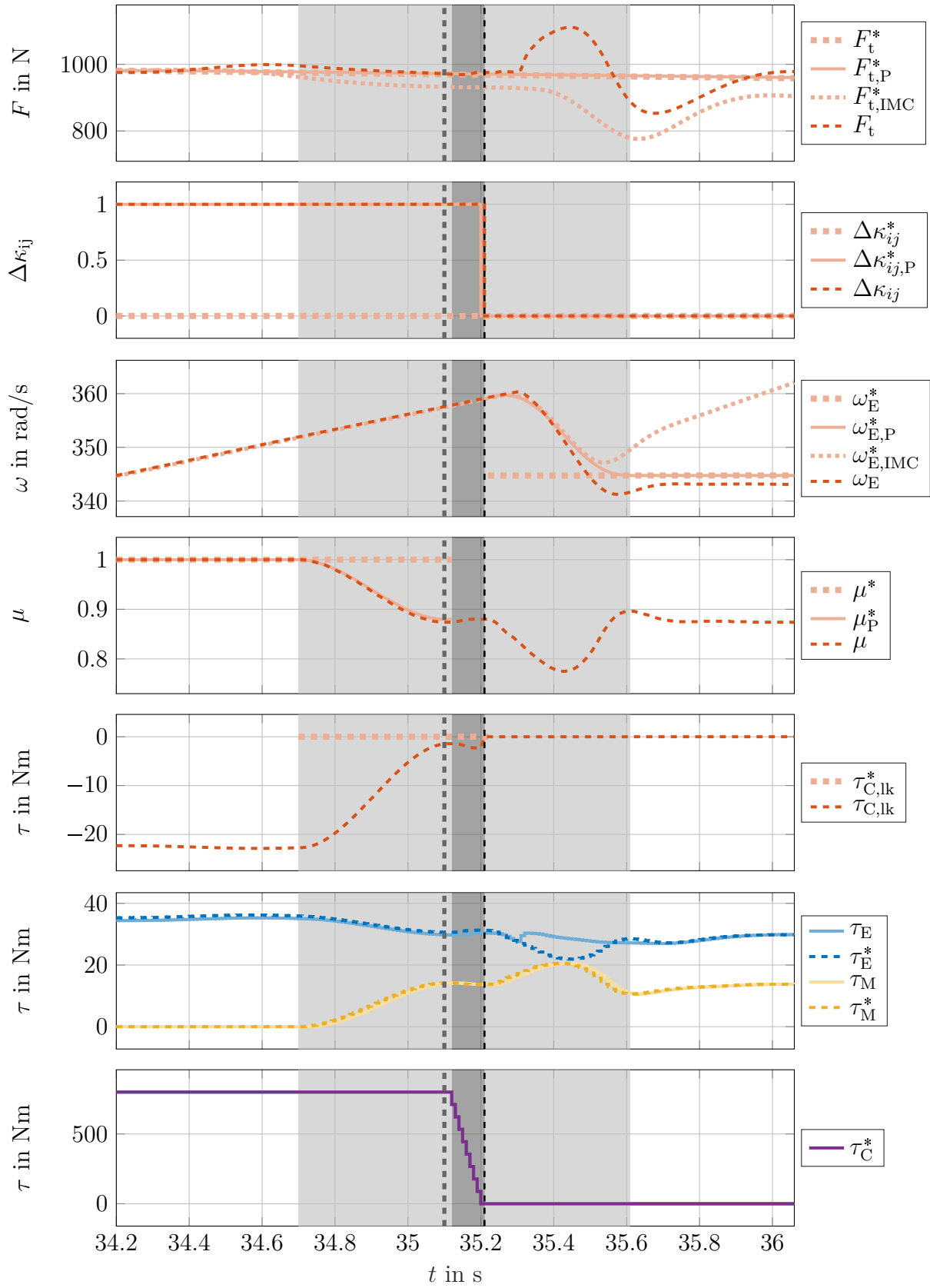
Figure 6.10: *SiL results; test case 2 (*Pa1 → CV1, 20% pedal)*
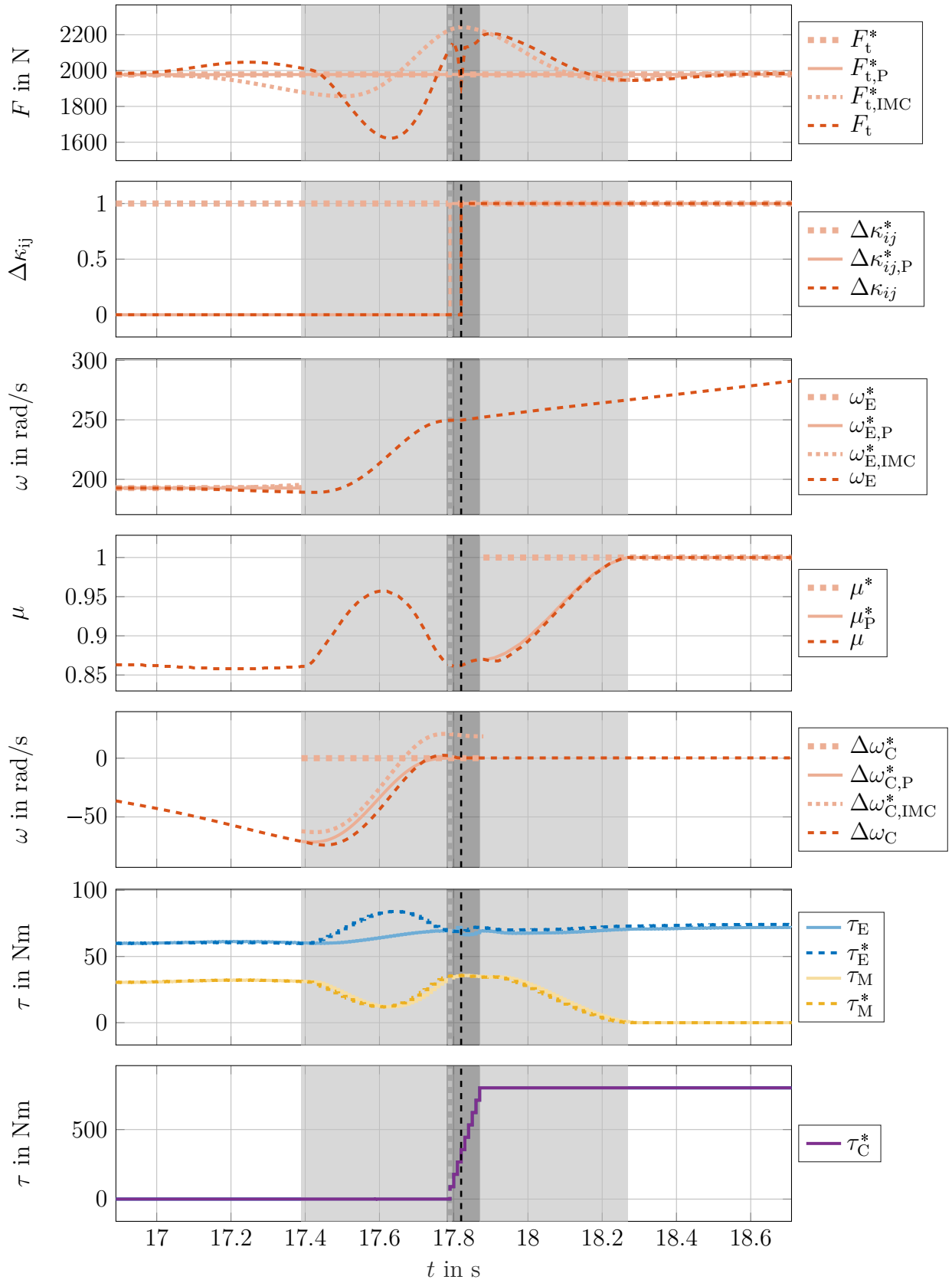
Figure 6.11: *SiL results; test case 3* (CV1 → Pa1, 35% pedal)
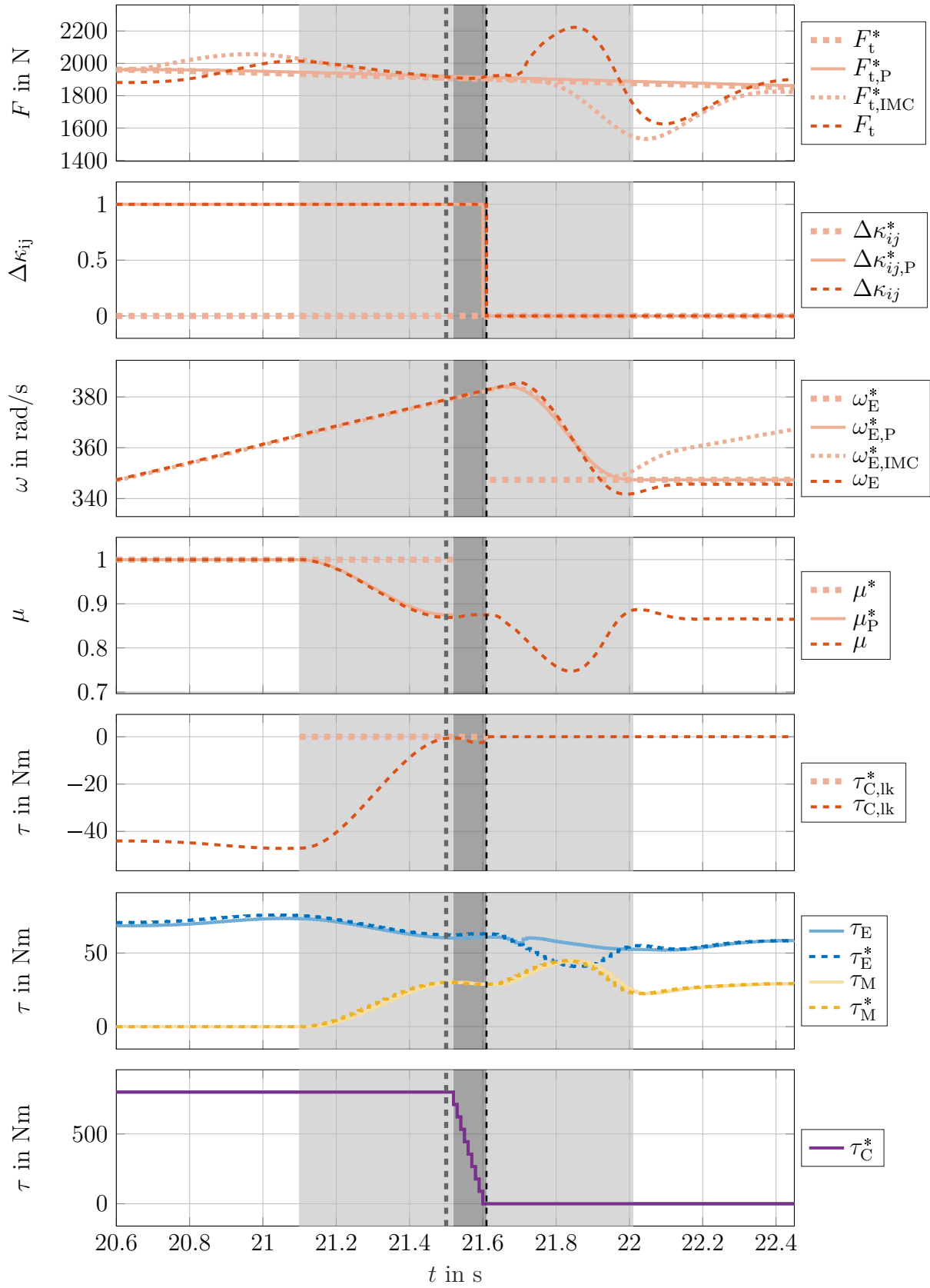
Figure 6.12: *SiL results; test case 4 (*Pa1 → CV1, 35% pedal)*
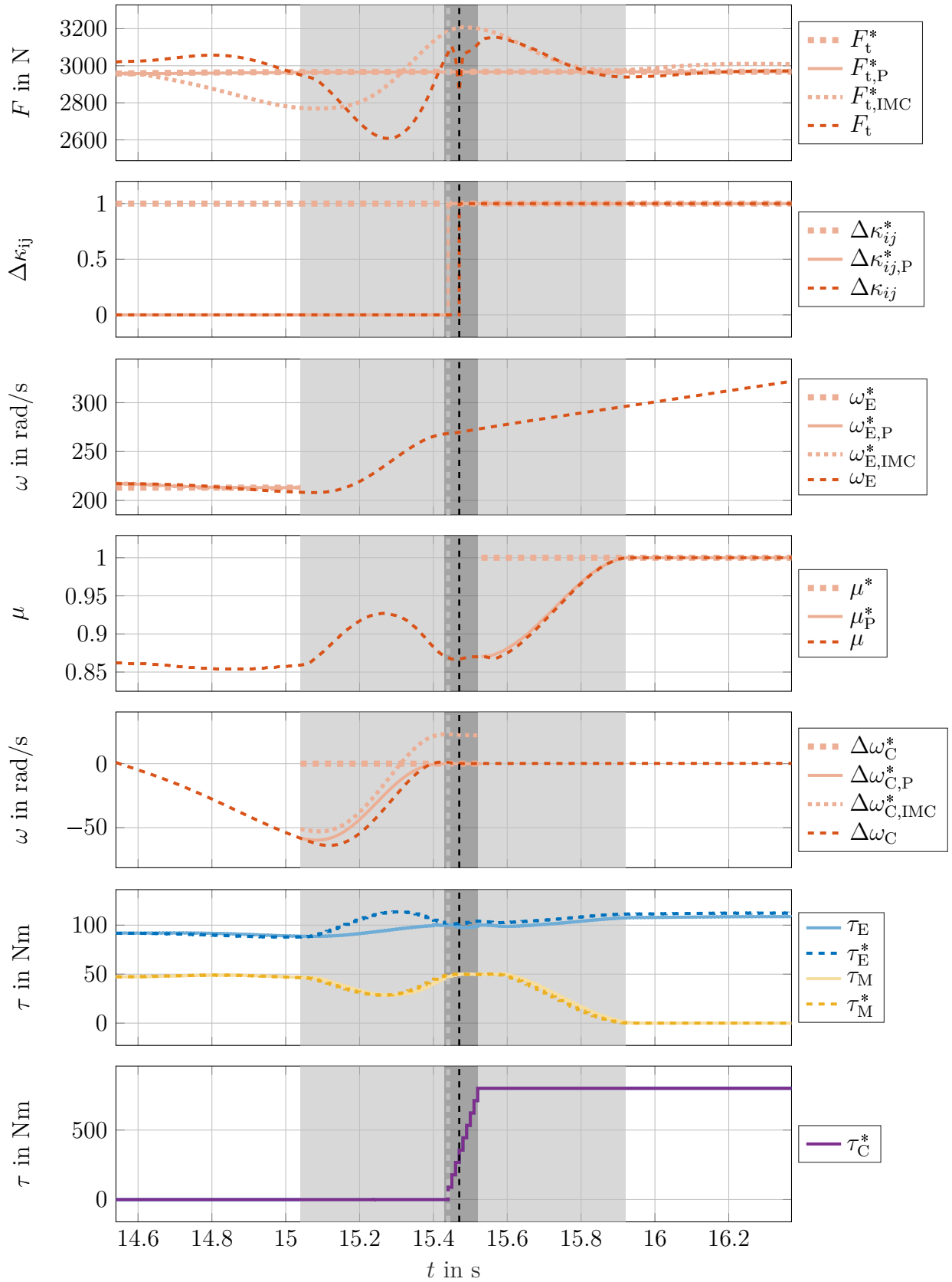
Figure 6.13: *SiL results; test case 5* (CV1 → Pa1, 50% pedal)
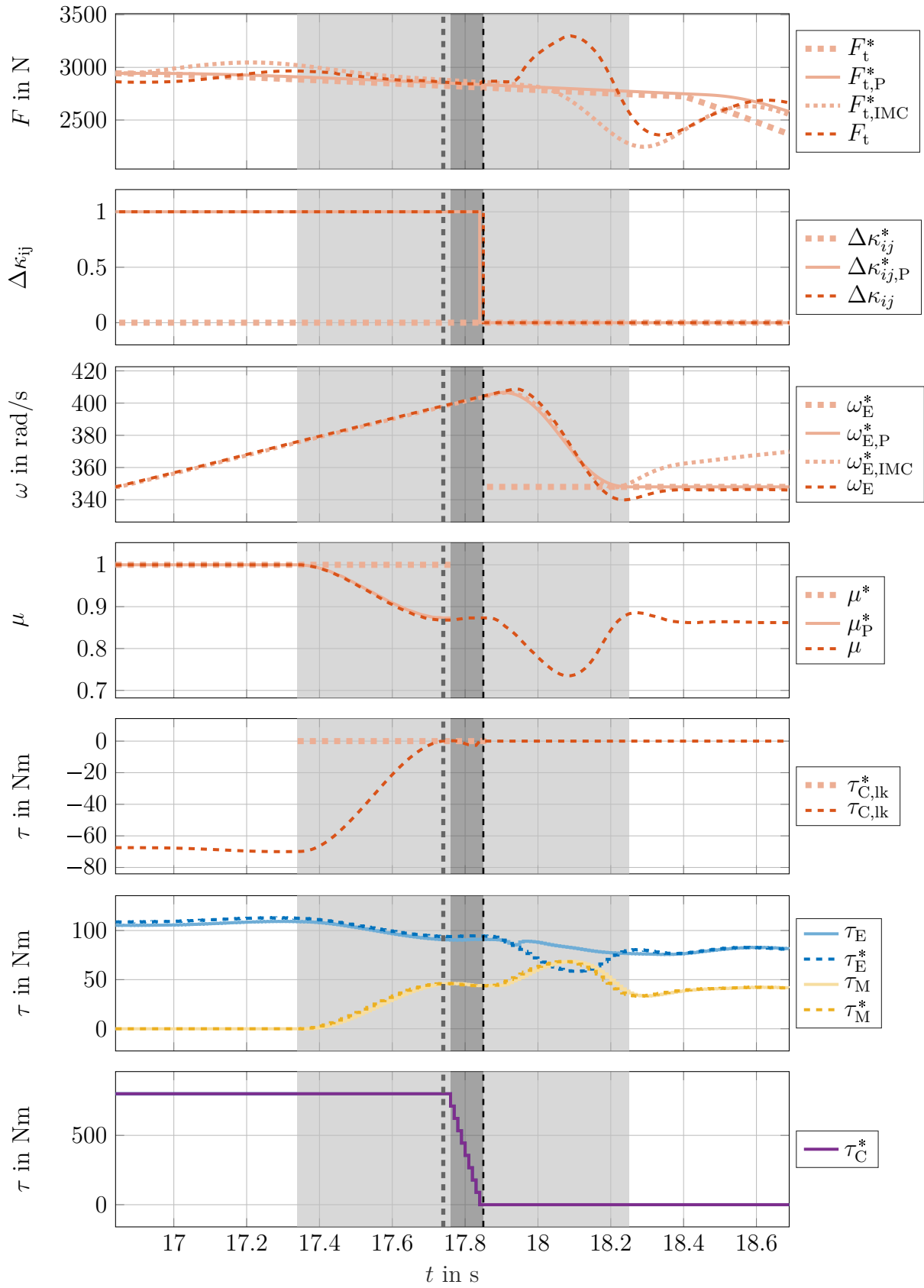
Figure 6.14: *SiL results; test case 6 (*Pa1 → CV1, 50% pedal)*

6.3.4 Validation level II – Evaluation

The following statements summarize the SiL simulation results:

- The traction force control during the proposed shift procedure is highly affected by unmodeled ICE dynamics ($\tau_E^* \neq \tau_E$) in hybrid CVT mode.
- The control concept and the principle functionality of the proposed DT control system is confirmed also on validation level II.

At this point it is necessary to bring back in mind that in general the ECU (cf. Section 2.4) is responsible for the low-level ICE control. This control system is a separated research topic (see for example [17, pp. 145]), which is not in the scope of this thesis. The considered deviations between τ_E and τ_E^*, hence, can actually not be assigned exclusively to the physical ICE dynamics, but to the dynamics of the controlled ICE. An identification of this dynamics, consequently, is possible (see section 6.4.5) but depends on the ECU parametrization. Furthermore, it can be expected that the real ICE dynamics differ from the dynamics in the PT model, which has been used for the SiL simulations in this section. Within the research project, therefore, it was decided to bring the DT control system in this version into the vehicle and perform vehicle tests on the test track without considering this problem in a first step.

6.4 Validation level III (vehicle testing)

6.4.1 Validation level III – Setup

> **Validation level III - Setup:**
>
> - **Stimulation:** test driver (pedal position in %)
> - **Control software:** RPCU; C-code generated from vehicle control software in Matlab/Simulink (Validation level II)
> - **Control plant:** AVL demonstrator with single-EM dedicated hybrid DT
> - **Shift scenario:** CV1 → Pa1

6.4.2 Validation level III – Test cases

For the vehicle tests the functionality of the proposed DT control system is reduced to shift phases II and III (shift preparation and clutch actuation). As a variation of the vehicle speed $v_{\text{trig}} \approx 17$ km/h, at which the gear shift is triggered by the EMS, was not possible according to an EMS software problem, the recorded test cases differ in different planned length of the shift preparation phase. Table 6.7 lists settings for the test cases on validation level III. For vehicle testing the clutch actuation phase has been shortened ($T_{\text{CA}} = 0.05$ s) and instead of ramping up the clutch torque request, a step request is used.

Table 6.7: *Overview of the presented test cases of validation level III*

		shift				requests		Par	Figure
		initial	final	$\Delta\kappa_{ij}$	v_{trig}	pedal	F_{t}^*	T_{SP}	
		-	-	-	km/h	%	kN	s	
Level III	1	CV1	Pa1	B1	17.2	~20	~1	1	(6.15)
	2	CV1	Pa1	B1	17.5	~20	~1	0.6	(6.16)
	3	CV1	Pa1	B1	18.1	~20	~1	0.4	(6.17)
	4	CV1	Pa1	B1	16.9	~20	~1	0.4	(6.18)

6.4.3 Validation level III – Results

Test case 1. Figure 6.15 presents the results of test case 1, extracted from the data, which has been recorded in the vehicle. The control system attempts to compensate a significant initial traction force control error $(F_{\text{t}} - F_{\text{t}}^*)$ by increasing the corresponding IMC request $F_{\text{t,IMC}}^*$. This attempt is hindered again by unmodeled ICE dynamics, which also impacts the clutch synchronization.

Shift preparation. Although the actual clutch slip does not follow the planned synchronization trajectory, the robustness of the IMC structure ensures that the clutch is synchronized at the end of the planned shift preparation time (vertical dashed gray line). The course of the IMC request $\Delta\omega_{\text{C,IMC}}^*$ show the contribution of the feedback loop to the clutch synchronization. As the limit for the derivative of the clutch slip, however, is not met at the intended ending time of the shift preparation phase, the phase is prolonged.

Clutch actuation. The clutch actuation is initiated as all four transition conditions are met at $t = T_2 = 46.53$ s with a delay of 0.26 s. Similar to the SiL simulation results the residual clutch slip is eliminated due to dissipation in the slipping clutch. This slipping torque also impacts the drivability, becoming noticeable in the drop of the traction force. As the clutch transition occurs, the control system confirms the completion of the shift and the control responsibility is handed over to a hybrid mode operation controller for hybrid parallel mode Pa1 of the existing vehicle control software. Figure 6.15, furthermore, shows some initial transient behavior in the torque requests $\tau_{\text{E}}^*, \tau_{\text{M}}^*$. These transients are caused by the attempt of the control system to ensure a smooth transition from the former torque requests, which have been computed by another component of the vehicle software, to the current torque requests.

Test case 2. Figure 6.16 shows the results of test case 2, which is a repetition of test case 1 with an adapted shift preparation time $T_{\text{SP}} = 0.6$ s as defined in Table 6.7. The initial traction force control error is lower than in test case 1. Most likely this is due to the fact that it is hardly impossible for the test driver to exactly reproduce
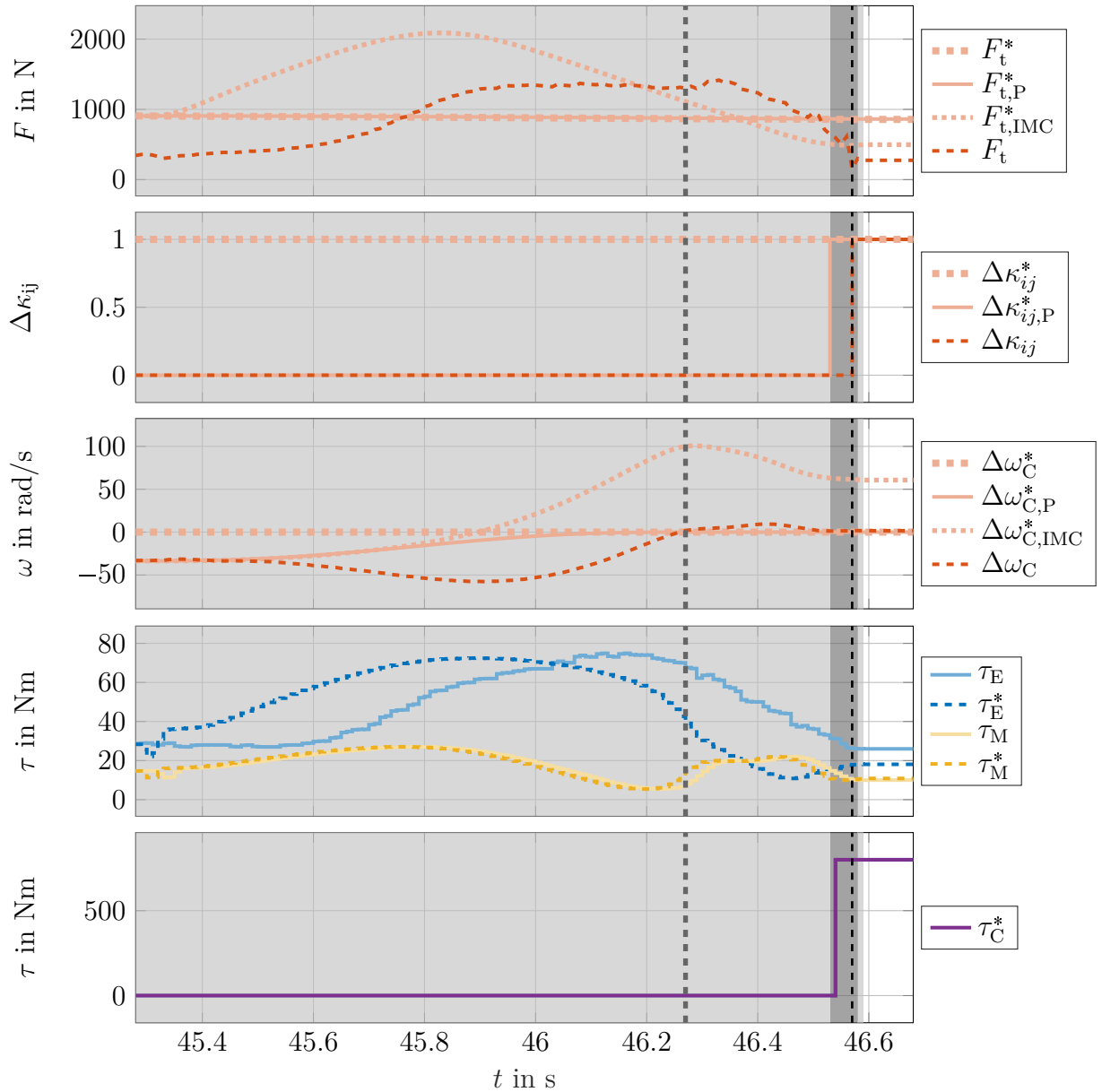
Figure 6.15: *Vehicle testing results; test case 1 (CV1 → Pa1, $T_{\mathrm{SP}} = 1$ s)*

a specific driving situation in the vehicle by the actuation of pedals. This decreased initial control error supports the performance of the control system. The results in general are quite similar to test case 1, except for a decreased exceeding time of the shift preparation phase of 0.07 s.

Test case 3. In test case 3 (Figure 6.16) the shift preparation phase is once again shortened to $T_{\mathrm{SP}} = 0.4$ s. The initial actual traction force in this test case approximately equals the requested traction force. Similar to the already discussed results, the unmodeled ICE dynamics affects the actual traction force, but the IMC system
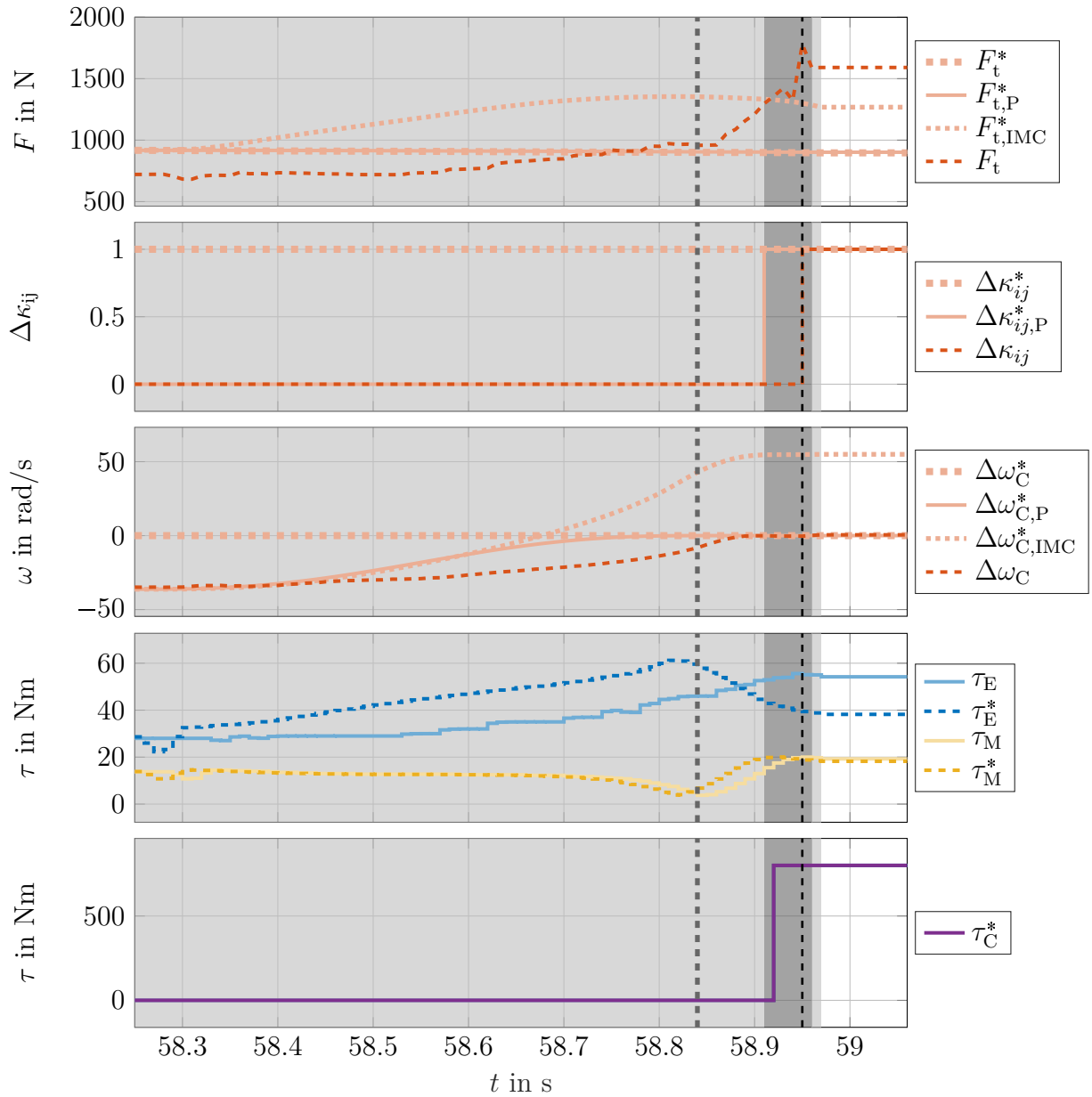
Figure 6.16: *Vehicle testing results; test case 2 (*CV1 → Pa1, $T_{\mathrm{SP}} = 0.6$ s*)*

achieves acceptable clutch synchronization performance. In test case 3 the shift synchronization is completed with a delay of 0.03 s.

Test case 4. As in the test cases 1-3 the reduction of the planned duration of the shift preparation phase always coincided with a reduced initial traction force control error, test case 4 tries to separate these effects by repeating test case 3. Comparing the results of test case 4 to test case 3, it becomes apparent that the different initial traction force control error indeed affects the synchronization performance. Although the impact is low considering the residual clutch slip at the end of the planned shift
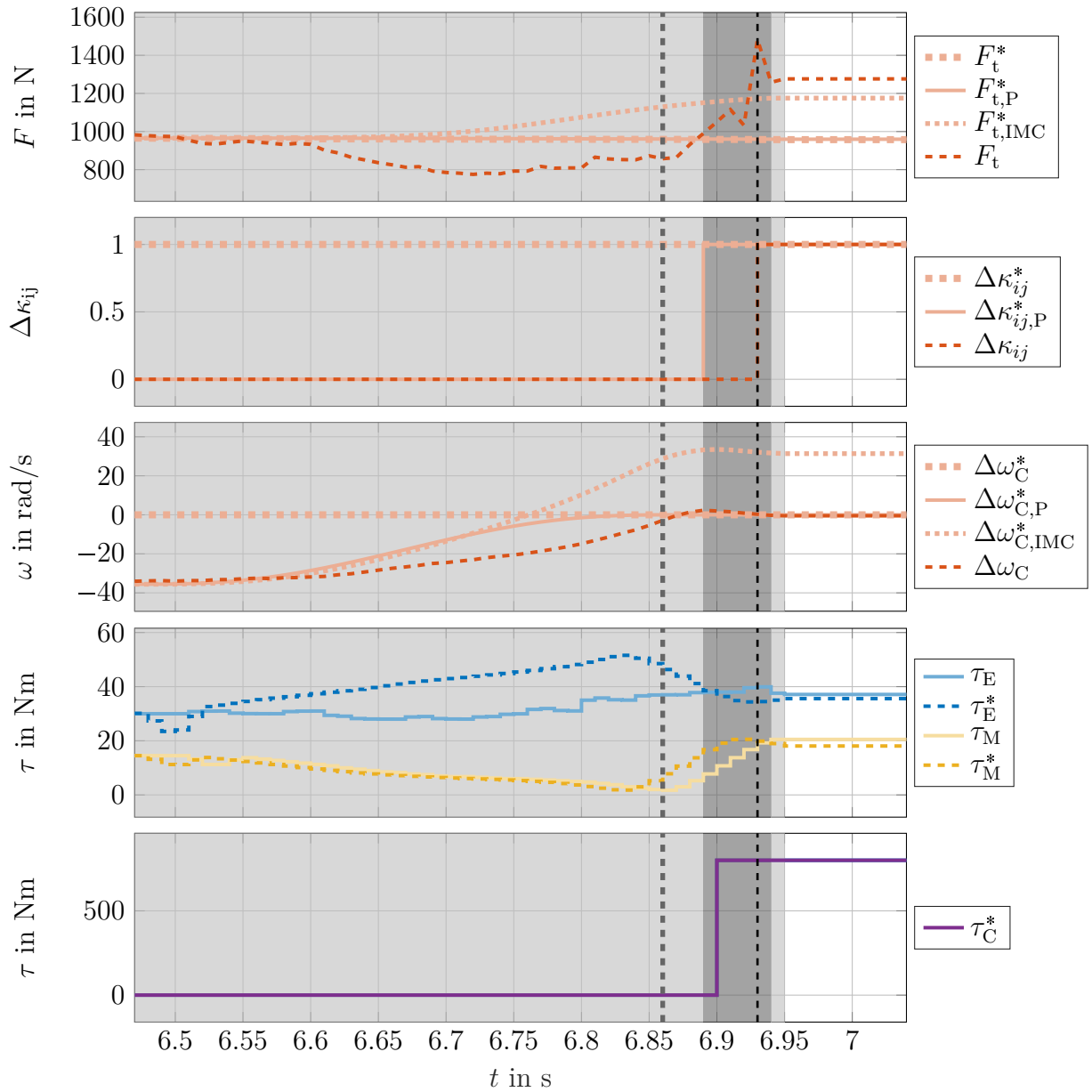
Figure 6.17: *Vehicle testing results; test case 3 (*CV1 → Pa1, $T_{SP} = 0.4$ *s)*

preparation phase, in test case 4 the transition conditions to clutch actuation phase are not met in contrast to test case 3. This subsequently results in a large exceeding of the shift preparation duration (0.26 s).
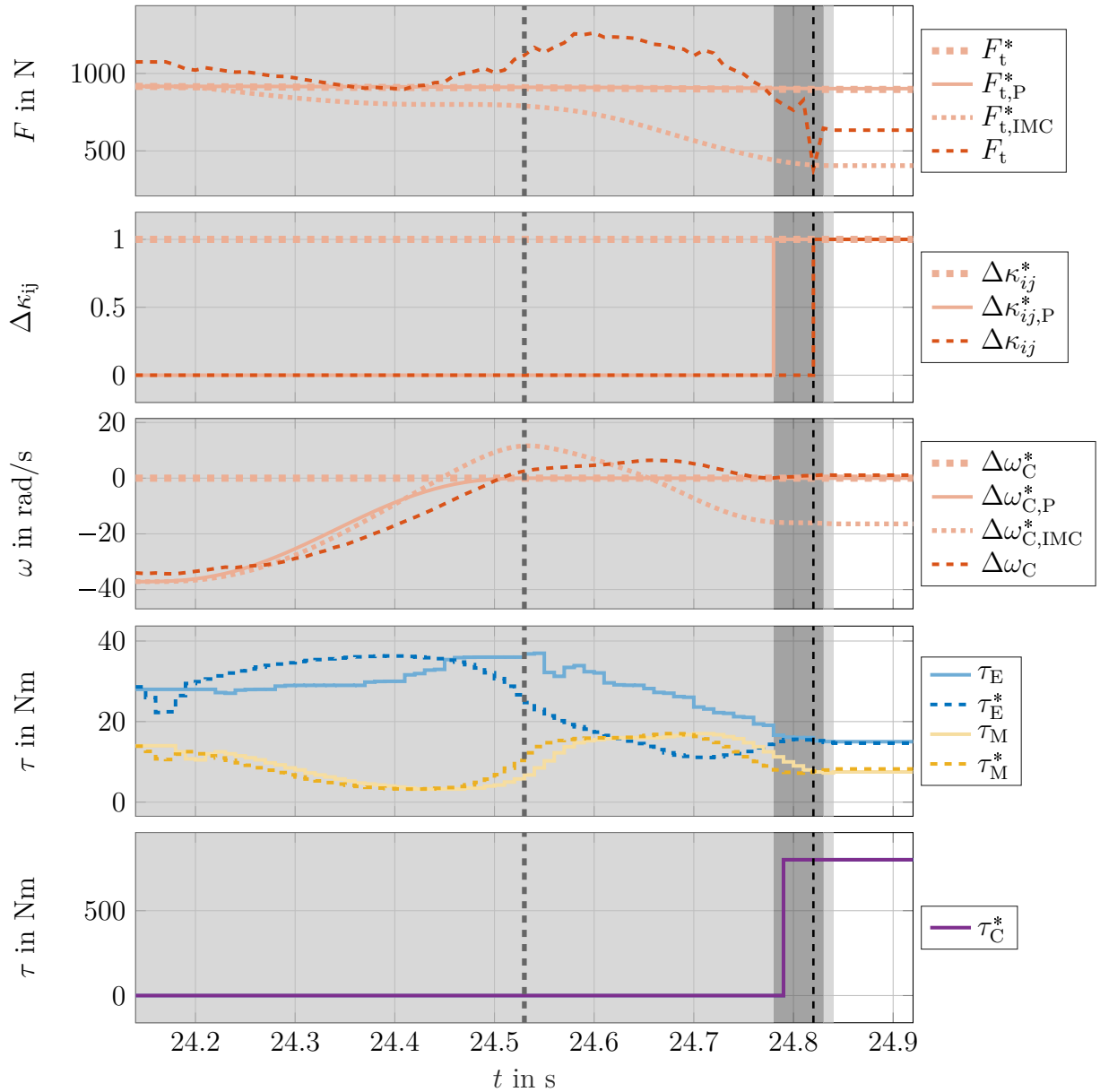
Figure 6.18: *Vehicle testing results; test case 4 (CV1 → Pa1, $T_{\mathrm{SP}} = 0.4$ s)*

6.4.4 Validation level III – Evaluation

Due to the already discussed high effort of arranging vehicle tests, it was not possible to test the full functionality of the propose DT control system implementation within the research project. Nevertheless, the performed tests do not show substantial objections to the gear shifting control concept and the control system implementation proposed, which are proposed in this thesis. In fact, the tests confirmed the validity of the concept and the implementation, although they show huge potential for improvement. Especially, the comparison of test cases 3 and 4 reveals the limitations of the claimed robustness of the control system. Although the control system implementation is

robust with respect to the completion of the gear shift, the robustness of the shift performance is expandable. The most promising potential to improve this robustness obviously is expected by a compensation of the ICE dynamics. The results of some preliminary studies on this topic will be presented in the next section.

6.4.5 Compensation of ICE dynamics
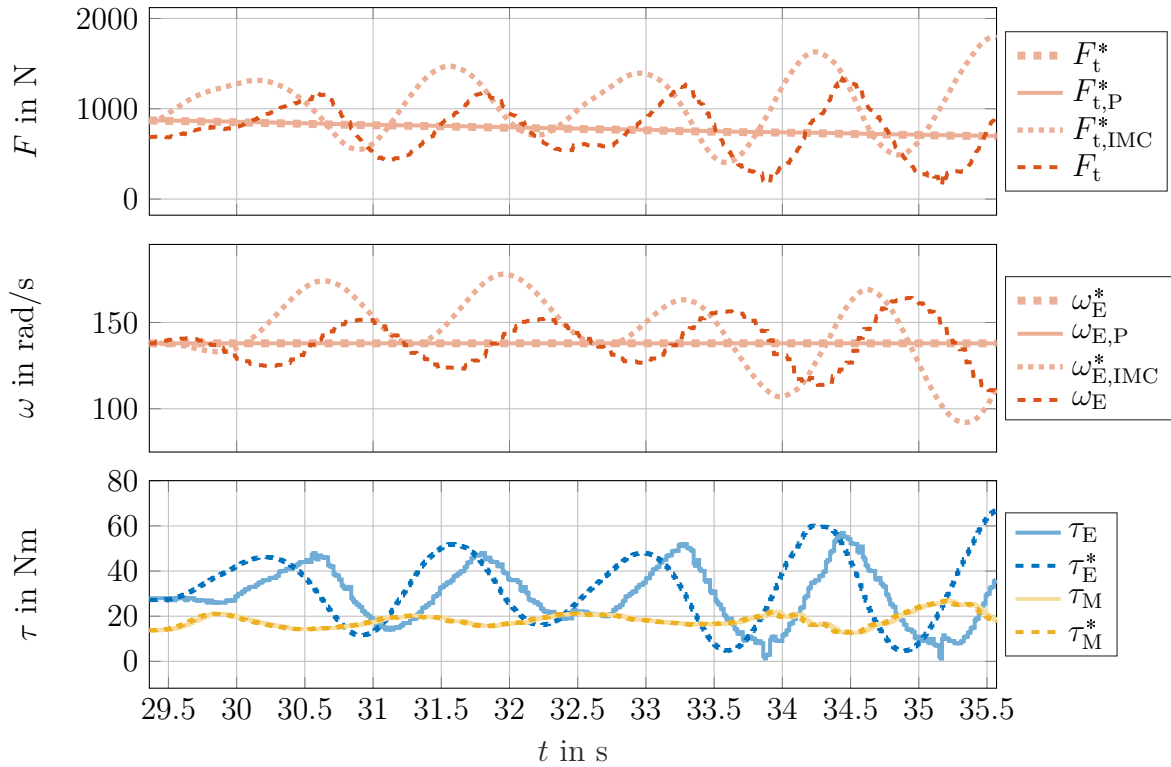
Figure 6.19: *Vehicle testing results;* CV1 *mode operation*

The vehicle tests confirm the observations in the SiL simulations regarding unmodeled ICE dynamics. As the impact of these dynamics especially concerns the hybrid CVT mode, it is obvious to tackle this issue in a first step in CVT mode operation. One possibility for compensating ICE dynamics will be now discussed and first results of corresponding vehicle tests will be shown. Figure 6.19 shows the results of a constant driving test case in gear CV1 operation using the DT control system proposed in this thesis. Initiated by an initial traction force control error it turns out that the unmodeled ICE dynamics beside its impact on the control performance also affect the stability of the control system. In order to compensate these ICE dynamics they have to be modeled in a first step. The vehicle testing results in Section 6.4.3 and further measurements similar to Figure 6.19 provide a data set for an estimation of the ICE dynamics. This data set can be used to give an estimation of these dynamics without physical modeling. A discrete-time second order LTI system with dead-time

is assumed:

$$G_{\text{ICE}}(z) = \frac{\tau_{\text{E}}(z)}{\tau_{\text{E}}^*(z)} = \frac{1}{z^{d_{\text{ICE}}}} \frac{k \cdot z}{(z - z_1)(z - z_2)}. \tag{6.6}$$

The dead-time was estimated with $T_{\text{dead}} = 0.04$ s considering the recorded measurements. With the sample time $T_{\text{d}} = 0.01$ s this reveals:

$$d_{\text{ICE}} = 4. \tag{6.7}$$

The parameters k, z_1, z_2 of (6.6) have been identified applying a least square parameter identification (see for example [80, pp. 176]):

$$G_{\text{ICE}}(z) = \frac{1}{z^4} \cdot \frac{0.0316z}{(z - 0.0789)(z - 0.9634)}. \tag{6.8}$$

The compensation of these ICE dynamics can be done using the inversion-based feed-forward control design presented in Chapter 5. The compensation of the resulting dead-time is straight forward in an IMC structure, as illustrated in Figure 6.20. Such-like a compensation is similar to the classical smith predictor approach (see for example [76, pp. 126] and [81]).
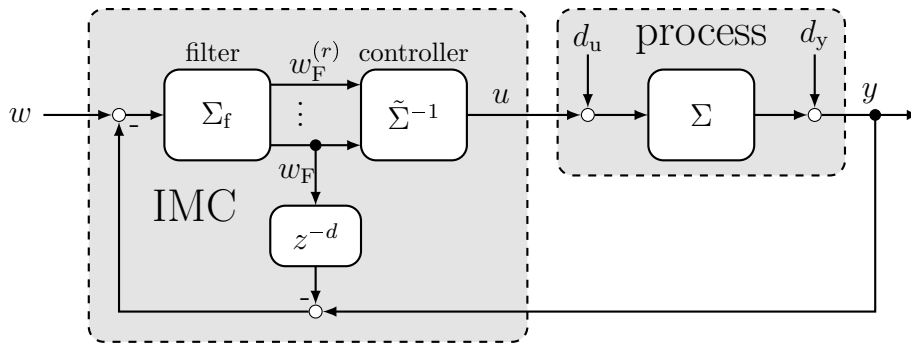
Figure 6.20: *Dead-time compensation in an IMC structure*

Figure 6.21 shows the results of a repetition of the test case in Figure 6.19 using the proposed ICE dynamics compensation. Although the results show still potential for improvement, especially concerning control performance, it reveals that the simple compensation approach produces stable control results. The presentation of this simple ICE dynamics compensation does not intend to provide a solution to this issue, but to give an idea how the problem could be tackled and to show that an adaption of the proposed DT control system is straight forward. A detailed consideration of the ICE dynamics would require dealing also with non-linear (rotational speed) dependent dynamics, as well as the dependency to the ECU parametrization, which has been discussed in Section 6.3.4.
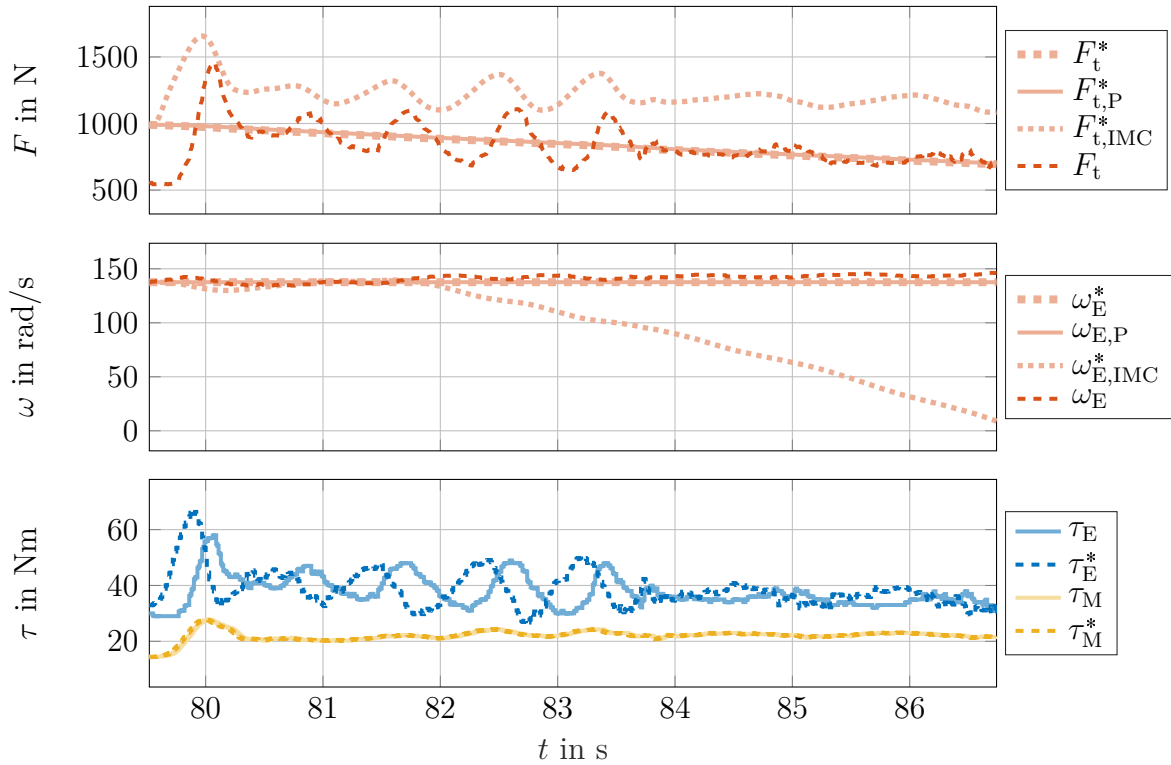
Figure 6.21: *Vehicle testing results;* CV1 *mode operation ICE with ICE dynamics compensation*

6.5 Conclusions of validation

Table 6.8 gives an overview on the presented gear shifting test cases on the three validation levels (MiL simulations , SiL simulations and vehicle testing) which have been presented and discussed in this chapter. In this final section the conclusions of these validation approach shall be stated:

First of all, the validation confirmed the feasibility of the proposed active smooth and lossless gear shifting concept for single-EM dedicated hybrid DTs, including the specific shift phases with switching plant models and control tasks.

Secondly, the presented validation approach evaluates the proposed DT control system implementation, consisting of switching inversion-based feedforward controllers in IMC structure and featuring an easy parametrization with only few actual control parameters. The proposed implementation shows promising results at validation level I. Validation level II proofs its principle robustness considering modeling imperfections (neglected damping of shafts) and also unmodeled significant dynamics (ICE), but also raised some performance limitations according these issues. Validation level III showed that an application of the control system in a real vehicle is possible. This validation level, furthermore, reveals essential potential for improvement, concerning mainly the ICE dynamics and initial control errors. For both issues it is not reasonable to solve them with modifications of the proposed control system implementation, but

Table 6.8: *Overview of the presented test cases on different validation levels*

		shift				requests				Par	Figure
		initial	final	$\Delta\kappa_{ij}$	v_{trig}	pedal	F_{t}^*	ω_{E}^*	μ^*	T_{SP}	
		-	-	-	km/h	%	kN	rad/s	-	s	
Level I	1	CV1	Pa1	B1	24.9	-	1	183	1	0.4	(6.3),(6.4)
	2	Pa1	CV1	B1	39.7	-	1	183	1	0.4	(6.5)
	3	CV1	Pa2	C1	30.0	-	2	300	0.7	0.4	(6.6)
	4	Pa3	CV2	B1	35.0	-	1	200	0	0.4	(6.7)
	5	Pa2	CV2	C2	27.1	-	0.8	250	0.8	0.4	(6.8)
Level II	1	CV1	Pa1	B1	25.1	20	~1	183	1	0.4	(6.9)
	2	Pa1	CV1	B1	40.4	20	~1	183	1	0.4	(6.10)
	3	CV1	Pa1	B1	25.2	35	~2	183	1	0.4	(6.11)
	4	Pa1	CV1	B1	40.7	35	~2	183	1	0.4	(6.12)
	5	CV1	Pa1	B1	25.3	50	~3	183	1	0.4	(6.13)
	6	Pa1	CV1	B1	41.5	50	~3	183	1	0.4	(6.14)
Level III	1	CV1	Pa1	B1	17.2	~20	~1	-	-	1	(6.15)
	2	CV1	Pa1	B1	17.5	~20	~1	-	-	0.6	(6.16)
	3	CV1	Pa1	B1	18.1	~20	~1	-	-	0.4	(6.17)
	4	CV1	Pa1	B1	16.9	~20	~1	-	-	0.4	(6.18)

they have to be considered on the superordinate PT control system level: The first issue has to be tackled in combination with the ECU (some outline on this issue from DT control system point of view has been made in Section 6.4.5). The second issue concerns the coordination between single operative components of the entire vehicle control software.

7

Conclusion

This final chapter provides an executive summary on the research presented within in this thesis. It lists the major contributions and gives an outlook on future research related to the presented results.

7.1 Summary and contribution

Problem statement. The general target of this thesis was to investigate model-based DT control approaches to improve drivability and efficiency of single-EM dedicated hybrid DTs. In particular the focus was on the improvement of opportunities in gear shifting of this class of DTs. Special attention was given to the generalizability of partial results for general DT development, to the compatibility of implemented control system to common PT control structure and to the usability the of presented results.

Chapter 1 deals with general trends in automotive DT development and the special role of dedicated hybrid DTs. Chapter 2 considers the functionality, classification and control of automotive DTs. Based on two classifications of hybrid DTs, the operation modes of single-EM dedicated hybrid DTs are discussed. Finally, the chapter introduces the general concept of active smooth and lossless gear shifting for single-EM dedicated hybrid DTs for enhanced drivability and efficiency, which is the first contribution of this thesis. The investigation of this concept, its application in a model-based control concept, and finally the implementation of this concept for an exemplary DT is the major target of the further chapters of this thesis.

DT modeling. Chapter 3 is dedicated to the modeling of DT mechanics. In order to bridge the gap between common automotive model-based observer and control applications and the increasing mechanical complexity of modern DTs in general and of single-EM dedicated hybrid DTs in particular, a generic and modular modeling approach is proposed. This modeling approach is the second contribution of this thesis. It enables modeling of all common geared DT topologies including combined planetary gear sets. In contrast to existing modeling approaches this approach features a very compact set of elementary modeling components and a high physical comprehensibility

of the computed state-space models. In order to ensure usability of this contribution the approach has been implemented into a DT modeling tool. This tool enables DT modeling by non-experts in mechanical engineering in a graphical user interface using a simple drag-drop-connect method. The automated application of the modeling algorithm subsequently provides symbolic and numeric state-space models in terms of system matrices and state-, input-, and output-lists. Therefore, this tool is able to support various development, simulation and parametrization processes for automotive DTs. The proposed modeling approach is used to state a switching LTI model for gear shifting. The statement of control plants for the control of smooth and lossless gear shifts and mode operation in single-EM dedicated hybrid DTs concludes Chapter 3.

Model-based DT analysis. Chapter 4 contributes a model-based DT analysis method, which automates the computation of operation modes, mode specific gear ratios and traction forces and evaluation of the DT's shiftability in terms shift sequences and traction force intersections. Considering single-EM dedicated hybrid DTs, the method furthermore assesses the potential for smooth and lossless gear shifting, by definition and evaluation of the corresponding decoupling problem. In combination with the modeling tool presented in Chapter 3 this analysis methods enables a fast evaluation of DT topologies in an early development stage.

Model-based DT control. The contributions and investigations of Chapters 2, 3 and 4 are combined in Chapter 5 in order to propose a DT control system, which applies the concept of smooth and lossless gear shifting. The DT control system focuses on shifts between hybrid CVT and hybrid parallel modes of single-EM dedicated hybrid DTs. A sequence of shift phases with corresponding plant models and control tasks is defined. This sequence considers an embedded gear shift and, hence, it also covers the hybrid mode operation with respect to mode specific hybrid DoFs. A classical IMC structure with an inversion-based feedforward controller is applied to the control problem. In order to provide a robust shift preparation (clutch synchronization respectively clutch unloading), a polynomial trajectory planning with consecutive replanning is applied. Finally, Chapter 5 considers the implementation of the DT control system for an exemplary single-EM dedicated hybrid DT. Chapter 5 concludes with a discussion of the control system's potential for generalization.

Validation of DT control system. In Chapter 6 the control concept and its implementation into a DT control system, proposed in Chapter 5, are validated on three validation levels of a state-of-the-art software-to-vehicle process: MiL simulations, SiL simulations and vehicle testing. The validation approach proofed feasibility and applicability of the control concept for active smooth and lossless gear shifting as well as the principle functionality of the proposed DT control system and reveals potential for improvement of robustness and performance, concerning mainly the control of the ICE.

Figure 7.1 illustrates an overview on the content and contributions of the thesis. Since this figure opposes the contributions to the topological restrictions, it simultaneously
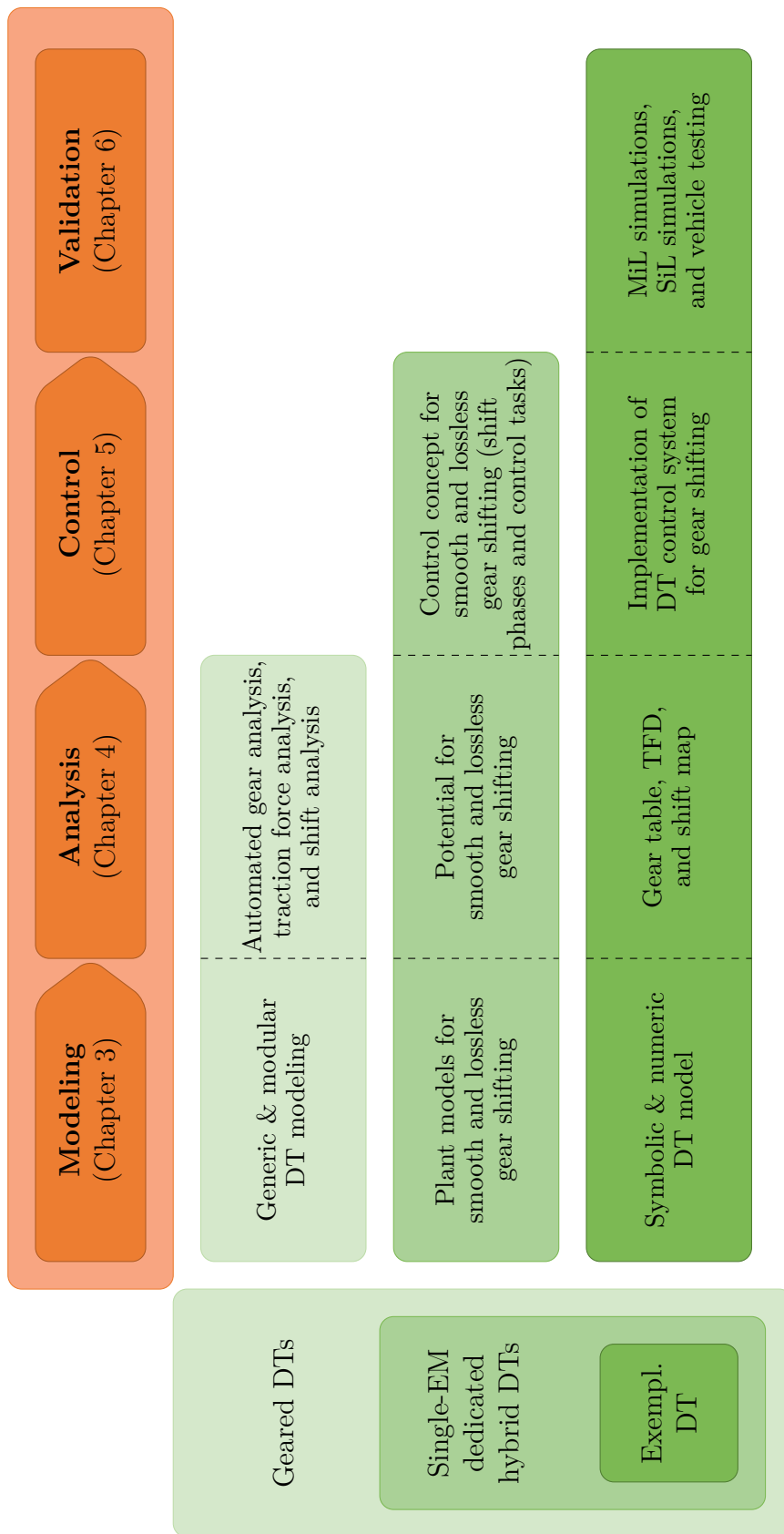
Figure 7.1: *Overview on the technical content and contributions of the thesis*
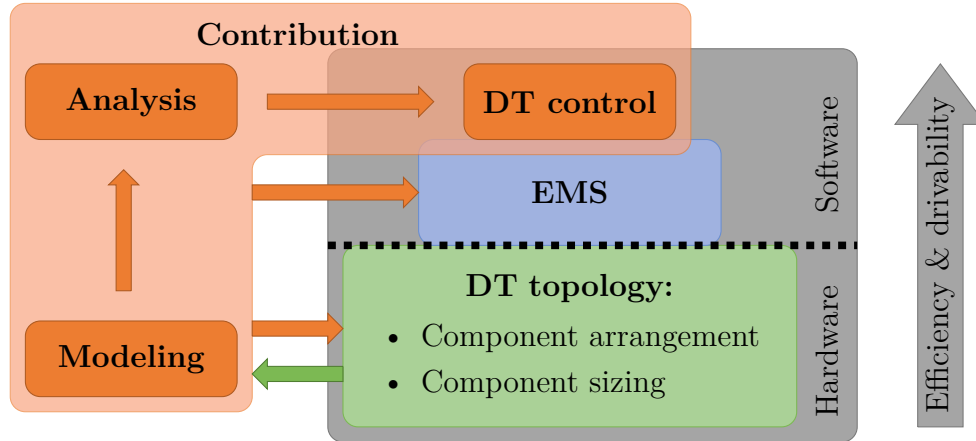
***Figure 7.2:** Thesis contribution to the development process of single-EM dedicated hybrid DTs*

identifies potential for future research on the model-based control of automotive DTs. The summary of the thesis shall be concluded considering Figure 7.2, which has already been illustrated in the introducing chapter of this thesis (Figure 1.2): Although the thesis is focused on the model-based control of single EM dedicated hybrid DTs, the partial results strongly contribute to the general development of these DTs including EMS and hardware development stage. The presented solutions to DT modeling and analysis, furthermore, support the automotive DT development in general (cf. Figure 7.1).

7.2 Outlook

At the very end of this thesis a short outlook on some possible future research steps shall be maid:

- As already discussed in Chapter 6 an obvious next step is to tackle the control of ICE dynamics, including the concept and parametrization of the ECU. A solution of this issue enables further extensive testing of the complete functionality of the DT control system, in order to evaluate its potential for actual application in series-production hybrid vehicles. At this point it will be furthermore necessary to proof the actual improvement of drivability and efficiency.

- In some shifting scenarios, like for specific gear shifts in special driving situations or for gear shifts, which do not feature potential for smooth and lossless gear shifting, dissipation is unavoidable. In this case it is necessary from efficiency point of view to minimize the occurring dissipation, for example by partial clutch synchronization. In such shifting scenarios the application of optimal control strategies like MPC might be beneficial.

- The concept of active control of smooth and lossless gear shifting is an enabler for improved DT hardware design relying on form-fitting shifting elements (dog clutches). In order to apply the presented control concept to such DT topologies,

however, performance guarantees have to be given, since in contrast to friction clutches a too large residual clutch slip might seriously damage the hardware components.

- In order to enlarge their field of application, the presented concepts can be generalized to hybrid multi-mode DTs, considering two or more EMs. Although the principle concept of lossless clutch transitions remains, such a generalization requires in-depth revision of the proposed methods, due to the new possibilities according to an increased number of DoFs in actuation and due to new operation modes, which are not available in single EM dedicated hybrid DTs.

Acronyms

AMT	Automated Manual Transmission
AT	Automatic Transmission
BEV	Battery Electric Vehicle
BMS	Battery Management System
CO_2	Carbon Dioxide
CED	Cumulative Energy Demand
CO	carbon monoxide
CVT	Continuous Variable Transmission
DAE	Differential Algebraic Equation
DCT	Dual Clutch Transmission
DHDT	Dedicated Hybrid Drivetrain
DHT	Dedicated Hybrid Transmission
DoF	degree of freedom
DP	Dynamic Programming
DT	Drivetrain
ECMS	Equivalent Consumption Minimization Strategy
ECU	Engine Control Unit
ECVT	Electric Continuously Variable Transmission
EM	Electrical Machine
EMS	Energy Management Strategy
EU	European Union
EVT	Electric Variable Transmission
FCEV	Fuel Cell Electric Vehicle
GHG	Greenhouse Gas
GUI	Graphical User Interface
HEV	Hybrid Electric Vehicle
HiL	Hardware-in-the-Loop

ICE	Internal Combustion Engine
IMC	Internal Model Control
LTI	linear and time-invariant
MCU	Motor Control Unit
MiL	Model-in-the-Loop
MIMO	Multi-Input Multi-Output
MMT	Hybrid Multi-Mode Transmission
MPC	Model Predictive Control
MT	Manual Transmission
NO_x	Nitrogen Oxides
NEDC	New European Driving Cycle
ODE	Ordinary Differential Equation
OEM	Original Equipment Manufacturer
PGS	Planetary Gear Set
PoET	Powertrain Engineering Tool
PT	powertrain
RDE	Real Driving Emissions
RPCU	Rapid Prototyping Control Unit
SiL	Software-in-the-Loop
SISO	Single-Input Single-Output
SoC	State-of-Charge
SOP	Start of Production
TCU	Transmission Control Unit
TFD	Traction Force Diagram
USP	Unique Selling Proposition
VCU	Vehicle Control Unit
WLTP	Worldwide harmonized Light vehicles Test Procedure
ZEV	Zero Emission Vehicle

Symbols

A	Dynamic matrix
B	Input matrix
C	Output matrix
D	Feed through matrix
x	state vector
u	input vector
y	output vector
T_d	Discretization time (sampling time)
A_d	Discrete-time dynamic matrix
B_d	Discrete-time input matrix
$\hat{\mathbf{D}}$	Decoupling matrix
δ	Relative degree
Σ	Dynamical system
$\bar{\mathbf{M}}$	Inertia matrix
$\bar{\mathbf{A}}$	Scaled dynamic matrix ($\bar{\mathbf{M}}\mathbf{A}$)
$\bar{\mathbf{B}}$	Scaled input matrix ($\bar{\mathbf{M}}\mathbf{B}$)
$\mathbf{J}_\mathrm{f}$	Jacobian matrix of constraints
q	Generalized coordinates
$\mathbf{J}_\mathrm{x,q}$	Coordinate mapping from **q** coordinate to **x** coordinates
e	Unit vector
I	Identity matrix
P	Permutation matrix
v	Velocity
φ	Angular position
ω	Angular velocity (rotational speed)
$\Delta\varphi$	Angular position difference (torsion)
$\Delta\omega$	Angular velocity difference (rotational speed difference)
τ	Torque

J	Inertia
d	Damping constant
k	Stiffness
i	Gear ratio
z	Number of teeth (gear wheel)
F_t	Traction force
r_W	Wheel radius
λ	Hybrid degree of freedom
μ	Torque split factor
$\boldsymbol{\kappa}$	Clutch state vector
$\Delta\boldsymbol{\kappa}$	Differential clutch state vector

List of Figures

List of Tables

Bibliography

[1] "Regulation (EC) No 443/2009 of the European Parliament and of the Council of 23 April 2009 setting emission performance standards for new passenger cars as part of the Community's integrated approach to reduce CO 2 emissions from light-duty vehicles," *Official Journal of the European Communities*, vol. L 171, pp. 1–16, 2007-06-29. (cited on page 2.)

[2] "Regulation (EC) No 715/2007 of the European Parliament and of the Council of 20 June 2007 on type approval of motor vehicles with respect to emissions from light passenger and commercial vehicles (Euro 5 and Euro 6) and on access to vehicle repair and maintenance information," *Official Journal of the European Communities*, vol. L 140, pp. 1–15, 2009-06-05. (cited on page 2.)

[3] J. Y. Yong, V. K. Ramachandaramurthy, K. M. Tan, and N. Mithulananthan, "A review on the state-of-the-art technologies of electric vehicle, its impacts and prospects," *Renewable and Sustainable Energy Reviews*, vol. 49, pp. 365–385, 2015. (cited on pages 3 and 12.)

[4] A. Mahmoudzadeh Andwari, A. Pesiridis, S. Rajoo, R. Martinez-Botas, and V. Esfahanian, "A review of battery electric vehicle technology and readiness levels," *Renewable and Sustainable Energy Reviews*, vol. 78, pp. 414–430, 2017. (cited on pages 3 and 12.)

[5] S. Manzetti and F. Mariasiu, "Electric vehicle battery technologies: From present state to future systems," *Renewable and Sustainable Energy Reviews*, vol. 51, pp. 1004–1012, 2015. (cited on pages 3 and 12.)

[6] Q. Lai, M. Paskevicius, D. a. Sheppard, C. E. Buckley, A. W. Thornton, M. R. Hill, Q. Gu, J. Mao, Z. Huang, H. K. Liu, Z. Guo, A. Banerjee, S. Chakraborty, R. Ahuja, and K. F. Aguey-Zinsou, "Hydrogen storage materials for mobile and stationary applications: Current state of the art," *ChemSusChem*, vol. 8, no. 17, pp. 2789–2825, 2015. (cited on page 3.)

[7] R. Fischer, "Dedicated Hybrid Transmission (DHT) – the new hybrid transmission category," in *Proc. 2015 CTI Symposium Berlin*, Dec. 2015. (cited on page 3.)

[8] "Dedicated hybrid transmission for plug-in vehicles," *automotion 2017 – Issue 01 (IAV Automotive Engineering)*. (cited on page 4.)

[9] J. Liu and H. Peng, "A systematic design approach for two planetary gear split hybrid vehicles," *Vehicle System Dynamics*, vol. 48, no. 11, pp. 1395–1412, 2010. (cited on pages 4, 15 and 28.)

[10] N.-T. Hoang and H.-S. Yan, "Configuration synthesis of novel series-parallel hybrid transmission systems with eight-bar mechanisms," *Energies*, vol. 10, no. 12, p. 1044, 2017. (cited on pages 4, 16 and 19.)

[11] H. Ngo and H. Yan, "Configuration synthesis of series-parallel hybrid transmissions," *Proceedings of the Institution of Mechanical Engineers, Part D: Journal of Automobile Engineering*, vol. 230, no. 5, pp. 664–678, 2016. (cited on pages 4, 16 and 19.)

[12] ——, "Configuration synthesis of parallel hybrid transmissions," *Mechanism and Machine Theory*, vol. 97, pp. 51–71, 2016. (cited on pages 4, 15, 16 and 19.)

[13] F. R. Salmasi, "Control strategies for hybrid electric vehicles: Evolution, classification, comparison, and future trends," *IEEE Transactions on Vehicular Technology*, vol. 56, no. 5, pp. 2393–2404, 2007. (cited on pages 4 and 21.)

[14] A. Sciarretta and L. Guzzella, "Control of hybrid electric vehicles," *IEEE Control Systems*, vol. 27, no. 2, pp. 60–70, 2007. (cited on pages 4 and 21.)

[15] M. Bachinger, "Generic real-time model and embedded observer for automotive step-ratio transmission topologies," Ph.D. dissertation, Graz University of Technology, 2016. (cited on pages 9, 21, 28, 29, 54, 59, 61, 62, 79, 99, 138, 141, 142, 145 and 147.)

[16] U. Kiencke and L. Nielsen, *Automotive Control Systems - For Engine, Driveline, and Vehicle.* Berlin Heidelberg: Springer Science and Business Media, 2005. (cited on pages 9, 28 and 99.)

[17] L. Eriksson and L. Nielsen, *Modeling and Control of Engines and Drivelines.* New York: John Wiley and Sons, 2014. (cited on pages 9, 13, 20, 21, 28, 99 and 167.)

[18] R. Fischer, F. Kücükay, G. Jürgens, R. Najork, and B. Pollak, *The Automotive Transmission Book.* Springer International Publishing, 2015. (cited on pages 9, 10, 11, 12, 13, 14, 15, 20, 21, 74, 82, 83 and 102.)

[19] R. Falkensteiner, "Modelbased slip control of a torque converter lock-up clutch," Master's thesis, Graz University of Technology, 2017. (cited on page 9.)

[20] W. Ebner, "Ein modellbasierter Ansatz für die Auslegung und Regelung eines optimalen elektro-hydraulischen Systems für Automatikgetriebe," Ph.D. dissertation, Graz University of Technology, 2018. (cited on page 10.)

[21] J. Liu and H. Peng, "Modeling and control of a power-split," *IEEE Transactions on Control Systems Technology*, vol. 16, no. 6, pp. 1242–1251, 2008. (cited on page 13.)

[22] Y. Yang, X. Hu, H. Pei, and Z. Peng, "Comparison of power-split and parallel hybrid powertrain architectures with a single electric machine: Dynamic programming approach," *Applied Energy*, vol. 168, pp. 683–690, 2016. (cited on page 14.)

[23] D. Görke, *Untersuchungen zur kraftstoffoptimalen Betriebsweise von Parallelhybridfahrzeugen und darauf basierende Auslegung regelbasierter Betriebsstrategien*, ser. Wissenschaftliche Reihe Fahrzeugtechnik Universität Stuttgart. Springer Fachmedien Wiesbaden, 2016. (cited on page 15.)

[24] W. Wang, R. Song, M. Guo, and S. Liu, "Analysis on compound-split configuration of power-split hybrid electric vehicle," *Mechanism and Machine Theory*, vol. 78, no. 5988, pp. 272–288, 2014. (cited on pages 15 and 21.)

[25] S. Hüpkes, I. Steinberg, M. Leibbrandt, and R. Najork, "GETRAG boosted range extender - a highly flexible electric powertrain for maximum co2 reduction," in *Int. VDI-Kongress Getriebe in Fahrzeugen - Drivetrain for Vehicles*, vol. 2081. VDI Verlag, 2010, pp. 19–31. (cited on page 15.)

[26] U. Grebe, "GM's Voltec Antriebssystem - Elektrifizierung der Fahrzeuge auf neuem Niveau," in *21st Int. AVL Conf. Engine and Environment*. AVL, Graz, 2009. (cited on page 15.)

[27] L. W. Tsai and G. Schultz, "A motor-integrated parallel hybrid transmission," *Journal of Mechanical Design*, vol. 126, no. 5, p. 889, 2004. (cited on page 16.)

[28] R. Petersen, "Vario.Drive (Volkswagen AG): Novel active transmission (DHT) with high-performance electric motor and form-fitting coupling elements," Dec. 2017. (cited on pages 16 and 23.)

[29] F. Zhu, C. Yin, L. Chen, and C. Wang, "Design and analysis of a novel multi-mode transmission for a HEV using a single electric machine," *IEEE Trans. Veh. Technol.*, vol. 62, no. 3, pp. 1–9, 2013. (cited on pages 16, 19 and 21.)

[30] X. Zhang, C. T. Li, D. Kum, and H. Peng, "Prius+and Volt-: configuration analysis of power-split hybrid vehicles with a single planetary gear," *IEEE Transactions on Vehicular Technology*, vol. 61, no. 8, pp. 3544–3552, 2012. (cited on page 16.)

[31] A. Sciarretta, L. Serrao, P. C. Dewangan, P. Tona, E. N. Bergshoeff, C. Bordons, L. Charmpa, P. Elbert, L. Eriksson, T. Hofman, M. Hubacher, P. Isenegger, F. Lacandia, a. Laveau, H. Li, D. Marcos, T. Nüesch, S. Onori, P. Pisu, J. Rios, E. Silvas, M. Sivertsson, L. Tribioli, a. J. van der Hoeven, and M. Wu, "A control benchmark on the energy management of a plug-in hybrid electric vehicle," *Control Engineering Practice*, vol. 29, pp. 287–298, 2014. (cited on page 18.)

[32] L. Wang, Y. Zhang, C. Yin, H. Zhang, and C. Wang, "Hardware-in-the-loop simulation for the design and verification of the control system of a series-parallel hybrid electric city-bus," *Simulation Modelling Practice and Theory*, vol. 25, pp. 148–162, 2012. (cited on page 21.)

[33] R. Rajamani, *Vehicle Dynamics and Control*, ser. Mechanical Engineering Series. Springer US, 2011. (cited on page 21.)

[34] J. Rumetshofer, M. Stolz, M. Bachinger, and M. Horn, "A generic and modular modeling approach for automotive drivetrains using a coordinate partitioning method," *MATEC Web Conf.: International Conference on Mechanical, System and Control Engineering*, vol. 220, p. 02002, 2018. (cited on pages 27, 32, 40 and 56.)

[35] J. Rumetshofer, M. Bachinger, M. Stolz, and M. Horn, "A novel approach for model-based control of smooth and lossless gear shifts," *IEEE Transactions on Vehicular Technology*, vol. 67, no. 2, pp. 1012–1026, Feb 2018. (cited on pages 27, 46, 87, 89 and 107.)

[36] K. Janschek, *Systementwurf mechatronischer Systeme: Methoden – Modelle – Konzepte (german edition)*. Berlin Heidelberg: Springer, 2010. (cited on page 28.)

[37] S. E. Mattsson and G. Söderlind, "Index reduction in differential-algebraic equations using dummy derivatives," *SIAM Journal on Scientific Computing*, vol. 14, no. 3, pp. 677–692, 1993. (cited on page 28.)

[38] E. Hilding, M. Sven, and M. Otter, "Modelica — the new object-oriented modeling language," *The 12th European Simulation Multiconference*, 1998. (cited on page 28.)

[39] M. Tiller, *Introduction to Physical Modeling with Modelica*. Boston: Kluwer Academic Publishers, 2001. (cited on page 28.)

[40] N. Roberts, M. Dempsey, and A. Picarelli, "Detailed powertrain dynamics modelling in Dymola - Modelica," *IFAC Proceedings Volumes*, vol. 46, pp. 434–439, 2013. (cited on page 28.)

[41] K. J. Åström and H. E. S. Mattsson, "Evolution of continuous-time modeling and simulation," in *The 12th European Simulation Multiconference*. (cited on page 28.)

[42] W. Blajer, W. Schiehlen, and W. Schirm, "A projective criterion to the coordinate partitioning method for multibody dynamics," *Archive of Applied Mechanics*, vol. 64, no. 2, pp. 86–98, 1994. (cited on pages 28 and 41.)

[43] T. Kurz, M. Burkhardt, and P. Eberhard, "Systems with constraint equations in the symbolic multibody simulation software NEWEUL-M 2," *Multibody Dynamics 2011, ECCOMAS Thematic Conference*, 2011. (cited on pages 28 and 41.)

[44] S. S. Kim and M. J. Vanderploeg, "QR decomposition for state space representation of constrained mechanical dynamic systems 1," *Journal of Mechanism, Transmissions, and Automation in Design*, vol. 108, no. 85, 1986. (cited on page 28.)

[45] P. Pisu, K. Koprubasi, and G. Rizzoni, "Energy management and drivability control problems for hybrid electric vehicles," *Proceedings of the 44th IEEE Conference on Decision and Control*, pp. 1824–1830, 2005. (cited on page 28.)

[46] C. Schwarz, M. Bachinger, M. Stolz, and D. Watzenig, "Tool-driven design and automated parameterization for real-time generic drivetrain models," *4th International Conference on Advances in Mechanics Engineering, ICAME 2015, July 20, 2015 - July 21, 2015*, vol. 28, 2015. (cited on page 28.)

[47] M. Bachinger, M. Stolz, and M. Horn, "Fixed step clutch modeling and simulation for automotive real-time applications," in *Proceedings of the American Control Conference*, June 2014, pp. 2593–2599. (cited on page 29.)

[48] ——, "Fixed time-step drivetrain observer for embedded automotive applications," *Proc. 2014 IEEE Conf. on Control Applicat. (CCA)*, pp. 47–52, 2014. (cited on page 29.)

[49] ——, "A novel drivetrain modelling approach for real-time simulation," *Mechatronics*, vol. 32, pp. 67–78, 2015. (cited on page 29.)

[50] H. Goldstein, C. Poole, and J. Safko, *Classical Mechanics, 3rd Edition.* Addison-Wesley, 2002. (cited on page 34.)

[51] W. Schiehlen, "Multibody system dynamics: Roots and perspectives," *Multibody System Dynamics*, vol. 1, no. 2, pp. 149–188, 1997. (cited on page 34.)

[52] C. D. Meyer, Ed., *Matrix Analysis and Applied Linear Algebra.* Philadelphia, PA, USA: Soc. for Ind. and Appl. Math., 2000. (cited on pages 35 and 40.)

[53] A. A. Fogarasay and M. R. Mith, "A new simplified approach to the kinematic analysis and design of epicyclic gearboxes," *Proceedings of the Institution of Mechanical Engineers*, vol. 209, no. 3, pp. 49–53, 1995. (cited on page 37.)

[54] A. Kahraman, "Planetary gear train dynamics," *Journal of Mechanical Design*, vol. 116, no. 3, p. 713, 1994. (cited on page 37.)

[55] M. Stangl, "Methodik zur kinematischen und kinetischen Berechung mehrwelliger Planeten-Koppelgetriebe," Ph.D. dissertation, Technische Universität München, 2007. (cited on page 37.)

[56] H. Müller, W. Mannhardt, and J. Glover, *Epicyclic Drive Trains: Analysis, Synthesis, and Applications.* Detroit, MI: Wayne State University Press, 1982. (cited on page 38.)

[57] J. Rumetshofer, "Model-based control of a switching linear multibody system," Master's thesis, Graz University of Technology, 2015. (cited on pages 41 and 114.)

[58] K. Koprubasi, E. R. Westervelt, and G. Rizzoni, "Toward the systematic design of controllers for smooth hybrid electric vehicle mode changes," in *2007 American Control Conference*, July 2007, pp. 2985–2990. (cited on page 58.)

[59] C. Pelchen, C. Schweiger, and M. Otter, "Modeling and simulating the efficiency of gearboxes and of planetary gearboxes," in *2nd International Modelica Conference, Proceedings*, 2002, pp. 257–266. (cited on page 80.)

[60] M. Golkani, M. Steinberger, M. Bachinger, J. Rumetshofer, M. Stolz, and M. Horn, "Optimal gear shift strategy for dual clutch transmissions," in *Proceedings of the 20th World Congress of the International-Federation-of-Automatic-Control (IFAC)*, ser. IFAC-PapersOnLine, vol. 50. Elsevier B.V., 2017, pp. 4800–4805. (cited on page 83.)

[61] M. Yolga, "Robust 3-element gear shift for electrified powertrains," in *Proc. 2014 CTI Symposium Berlin*, Dec, 2014. (cited on page 83.)

[62] B. Morgan, "The synthesis of linear multivariable systems by state-variable feedback," vol. 9, no. 4, pp. 405–411, Oct. 1964. (cited on page 88.)

[63] P. L. Falb and W. A. Wolovich, "Decoupling in the design and synthesis of multivariable control systems," *NASA Technical Note D-4219*, Oct. 1967. (cited on page 88.)

[64] S. Saenger-Zetina, K. Neiss, R. Beck, and P. D.-I. D. Abel, "Optimal clutch control applied to a hybrid electric variable transmission with Kane equations," *IFAC Proceedings Volumes*, vol. 40, no. 10, pp. 87–94, 2007. (cited on page 99.)

[65] L. Chen, G. Xi, and J. Sun, "Torque coordination control during mode transition for a series–parallel hybrid electric vehicle," *IEEE Transactions on Vehicular Technology*, vol. 61, no. 7, pp. 2936–2949, 2012. (cited on page 99.)

[66] H. Zhang, Y. Zhang, and C. Yin, "Hardware-in-the-loop simulation of robust mode transition control for a series – parallel hybrid electric vehicle," *IEEE Transactions on Vehicular Technology*, vol. 65, no. 3, pp. 1059–1069, 2016. (cited on page 99.)

[67] R. Beck, F. Richert, a. Bollig, D. Abel, S. Saenger, K. Neil, T. Scholt, and K.-E. Noreikat, "Model predictive control of a parallel hybrid vehicle drivetrain," *Proceedings of the 44th IEEE Conference on Decision and Control*, pp. 2670–2675, 2005. (cited on page 99.)

[68] T. Pham, L. Bushnell, and S. Member, "Two-degree-of-freedom damping control of driveline oscillations caused by pedal tip-in maneuver," *Proceedings of the American Control Conference*, pp. 1425–1432, 2015. (cited on page 99.)

[69] D. Schwarzmann, *Nonlinear Internal Model Control with Automotive Applications*. Isd, 2008. (cited on pages 109, 110, 114, 119 and 130.)

[70] J. Lunenburg, "Inversion-based feedforward design for beyond rigid body systems: A literature survey," *DCT Report 2009.105*, no. November, p. 82, 2009. (cited on page 110.)

[71] J. M. Maciejowski, *Multivariable feedback design*. Addison Wesley, 1989. (cited on page 112.)

[72] J. Lunze, *Regelungstechnik 2: Mehrgrößensysteme, Digitale Regelung*, 9th ed., ser. Lehrbuch. Berlin: Springer Vieweg, 2016. (cited on pages 112, 127 and 129.)

[73] A. G. J. Macfarlane and N. Karcanias, "Poles and zeros of linear multivariable systems: a survey of the algebraic, geometric and complex-variable theory," *International Journal of Control*, vol. 24, no. 1, pp. 33–74, 1976. (cited on page 112.)

[74] C. E. Garcia and M. Morari, "Internal Model Control. 1. a unifying review and some new results," *Industrial and Engineering Chemistry Process Design and Development*, vol. 21, no. 2, pp. 308–323, 1982. (cited on page 119.)

[75] C. Q. Economou, M. Morari, and B. O. Palsson, "Internal model control: Extension to nonlinear system," *Industrial and Engineering Chemistry Process Design and Development*, vol. 25, no. 2, pp. 403–411, 1986. (cited on page 119.)

[76] M. Morari and E. Zafiriou, *Robust Process Control*. Prentice Hall, 1989. (cited on pages 119 and 174.)

[77] C. Westermaier, "Zeitdiskrete adaptive Regelung mit allgemeinem Referenzmodell bei instabilen Diskretisierungsnullstellen," Ph.D. dissertation, Technische Universität München, 2014. (cited on pages 127 and 128.)

[78] G. C. Goodwin, R. L. Leal, D. Q. Mayne, and R. H. Middleton, "Rapprochement between continuous and discrete model reference adaptive control," *Automatica*, vol. 22, no. 2, pp. 199–207, 1986. (cited on page 128.)

[79] J. Schäuffele and T. Zurawka, *Automotive Software Engineering: Grundlagen, Prozesse, Methoden und Werkzeuge effizient einsetzen*, ser. ATZ/MTZ-Fachbuch. Vieweg+Teubner Verlag, 2010. (cited on page 141.)

[80] L. Ljung, *System identification: theory for the user*, ser. Prentice-Hall information and system sciences series. Prentice-Hall, 1987. (cited on page 174.)

[81] N. Abe and K. Yamanaka, "Smith predictor control and internal model control- a tutorial," *Proceedings of SICE 2003 Annual Conference*, pp. 1383–1387, 2003. (cited on page 174.)